

# **An investigation into the influence of substituents and extended $\pi$ -conjugation on the substitution reactions of bifunctional platinum(II) complexes**

**By**

**Bongumusa Bucus Khusi**

**BSc. (Hons.) (UKZN)**

A thesis submitted in the fulfillment of the academic requirements for the  
degree of

**Master of Science**

in the college of Agriculture, Science and Engineering



UNIVERSITY OF  
KWAZULU-NATAL  
INYUVESI  
YAKWAZULU-NATALI

*School of Chemistry and Physics*

*University of KwaZulu-Natal, Pietermaritzburg*

**October 2015**

## **AUTHORSHIP DECLARATION**

I, Bongumusa Bucus Khusi declare that this thesis reports on research results of my own work carried out in the School of Chemistry and Physics, University of KwaZulu-Natal, Pietermaritzburg campus. Where use of work of others has been made, it is duly accredited through reference citation. This thesis has not been submitted for the award of a qualification award at any University.

.....

**B.B. Khusi**

We, hereby certify that this statement is correct, and as the supervisors of the candidate, we have approved the submission of this thesis.

.....

**Dr. A. Mambanda**

**(Supervisor)**

.....

**Prof. D. Jaganyi**

**(Co-supervisor)**

*Dedicated to my son, Asavela B. Khusi, with lots of love.*

*You never know how strong you are, until being strong is  
the only choice you have.*

-Cayla Mills-

# Acknowledgements

First and foremost, I would like to deeply thank my supervisors, Dr. A. Mambanda and Prof. D. Jaganyi for their guidance and help throughout this MSc work. Special thanks to **Dr. A. Mambanda** for the discussions on Pt(II) complexes which were synthesized and kinetically studied in this work, his trust in me on the execution of this project and allowing me to work independently. I thank him for fruitful discussions, helpful comments and unreserved advice on the write-up and arrangement of this thesis.

I also wish to express my sincere gratitude to:

- My parents, **Mrs. N.V. Khusi** and **Mr. B.R. Khusi** and my dear sisters, **Zibuyile, Sethembile, Ntandokazi** and **Mandisa Khusi**, for their love and motivation.
- **Thandeka A. Tshabalala** for her assistance and encouragement.
- All the members of the kinetic research group, Meshack Sitati, Asman Panyako and **Mthandi Mthiyane**.
- All technical staff in the school of chemistry and physics for their support. With special thanks to **Mr. Craig Grimmer** for his help with the NMR analysis and Mrs. Caryl Rensburg for her assistance with MS and elemental analysis.
- The University of KwaZulu-Natal for the financial support.

# Conference and publication contributions

## Publication

**Bongumusa B. Khushi**, Allen Mambanda and Deogratius Jaganyi, *The role of substituents in a bidentate N,N-chelating ligand on the substitution of aqua ligands from mononuclear Pt(II) complexes.*

This work has been accepted to Transition Metal Chemistry.

Manuscript ID: TMCH-D-15-00429

**Bongumusa B. Khushi**, Allen Mambanda and Deogratius Jaganyi, *The role of substituents and extended  $\pi$ -conjugation in a bidentate N,N-chelate on the substitution kinetics of aqua ligands from platinum(II) complexes.*

This work is on its final stage of preparation for publication.

## Poster presentation

SACI postgraduate colloquium 2014, University of KwaZulu-Natal, Pietermaritzburg campus, entitled: *Kinetic and Thermodynamic Studies on Stepwise Substitution of Aqua ligands from Bifunctional Platinum(II) Complexes.*

# List of Abbreviations

Å	Angström
T	temperature
K	Kelvin
kJ	kilojoule
g	gram
L	liter
mL	milliliter
M	molar, mol/L
R	gas constant, 8.3145 J K <sup>-1</sup> mol <sup>-1</sup>
h	Planck constant, 6.6261 x 10 <sup>-34</sup> J s
k <sub>B</sub>	Boltzmann constant, 1.3807 x 10 <sup>-23</sup> J K <sup>-1</sup>
ΔH <sup>‡</sup>	activation enthalpy
ΔS <sup>‡</sup>	activation entropy
ΔV <sup>‡</sup>	activation volume
<i>I</i>	ionic strength
DFT	density functional theory
DNA	deoxyribose nucleic acid
NMR	nuclear magnetic resonance
s, d, t, m (NMR)	singlet, doublet, triplet, multiplet
δ	chemical shift
ppm (NMR)	parts per million
MS	mass spectrometry
UV/vis	ultraviolet-visible
λ	wavelength
HOMO	highest occupied molecular orbital
LUMO	lowest unoccupied molecular orbital
NBO	natural bond orbital

# List of Figures and Schemes

<b>Figure 1.1</b>	Selected metal-based therapeutics and diagnostics that are used in the medical field. Cisplatin (a), sodium nitroprusside (b), auranofin (c) and cardiolite (d).	1
<b>Figure 1.2</b>	Schematic representation of the stages of cellular activation of cisplatin and possible biological consequences.	6
<b>Figure 1.3</b>	Different adducts formed from the interaction of cisplatin with DNA.	7
<b>Figure 1.4</b>	Second- and third-generation of anticancer drugs that have been approved for clinical use. Carboplatin (a), nedaplatin (b), heptaplatin (c), laboplatin (d) and oxaliplatin (e).	10
<b>Figure 1.5</b>	Mononuclear platinum(II) complexes with a trans geometry (a-e) and octahedral Pt(IV) complexes (f-g) that display anticancer activity.	12
<b>Figure 1.6</b>	Selected multinuclear platinum complexes that have promising anticancer agents.	14
<b>Figure 1.7</b>	Antitumour Ru(III) agents, KP1019 (a) and NAMI-A (b) with promising cytostatic properties.	16
<b>Figure 1.8</b>	Structures of pyrazole derivatives of cisplatin evaluated for anticancer activity.	18
<b>Figure 1.9</b>	Formulae of biologically active complexes evaluated against Hela cancer cell line. These compounds hold promise for anticancer treatment.	19
<b>Figure 1.10</b>	Platinum(II) terpy complexes studied by Jaganyi and co-workers.	21
<b>Figure 1.11</b>	Structures of bifunctional Pt(II) complexes with <i>N,N</i> -bidentate chelate and the nucleophiles used for kinetic investigations. The counter anions of the complexes are omitted for simplicity.	24
<b>Figure 2.1</b>	A representation of the direct attack by the entering ligand at the square planar Pt(II) centre below or above the plane. The nucleophile (Y) coordinates to give the trigonal bipyramidal intermediate species which loses the leaving group (X) with the retention of the stereochemistry.	33
<b>Figure 2.2</b>	The reaction-energy profile for the associative (A), associative interchange ( <i>I<sub>a</sub></i> ), dissociative interchange ( <i>I<sub>d</sub></i> ) and dissociative mechanism (D).	34



<b>Scheme 2.1</b>	Synthesis of the <i>cis</i> and <i>trans</i> isomers of [Pt(NH <sub>3</sub> ) <sub>2</sub> Cl <sub>2</sub> ].	43
<b>Scheme 2.2</b>	Synthesis of the <i>cis</i> and <i>trans</i> isomers of [Pt(NH <sub>3</sub> )(NO <sub>2</sub> )Cl <sub>2</sub> ] <sup>−</sup> .	44
<b>Figure 2.3</b>	Charge distribution and induced dipoles in the T–Pt–X coordinate.	44
<b>Figure 2.4</b>	The trigonal bipyramidal geometry of the transition state and the $\pi$ -back-bonding of the <i>trans</i> ligand.	45
<b>Figure 2.5</b>	Molecular orbital diagram of [PtCl <sub>4</sub> ] <sup>2−</sup> .	47
<b>Figure 2.6</b>	Trigonal bipyramidal transition state of the <i>cis</i> and <i>trans</i> isomers.	50
<b>Figure 3.1</b>	Schematic presentation of the fundamental approach in kinetic and mechanistic studies.	54
<b>Figure 3.2</b>	Schematic representation of a UV/Visible spectrophotometer.	66
<b>Figure 3.3</b>	Schematic representation of a stopped-flow spectrophotometric technique.	69
<b>Figure 4.1</b>	Chemical structures of the bifunctional Pt(II) complexes. The perchlorate (ClO <sub>4</sub> <sup>−</sup> ) counter ions are omitted for clarity.	74
<b>Scheme 4.1</b>	Synthesis of the (pyrazolylmethyl)pyridine ligands.	75
<b>Figure 4.2</b>	UV/visible spectra for the titration of 0.06 mM <b>Pt(dCH<sub>3</sub>Py)</b> with NaOH in the pH range 2-10 at <i>T</i> = 298.15 K. Insert: Boltzmann fit of the pH data at 305 nm.	81
<b>Scheme 4.2</b>	Proposed stepwise deprotonation of the diaqua Pt(II) complexes.	82
<b>Figure 4.3</b>	DFT-calculated HOMO and LUMO frontier molecular orbitals of Pt(II) complexes.	86
<b>Figure 4.4</b>	The effect of substituents on the pyrazole ring in the energies of HOMO and LUMO orbitals and the resultant LUMO-HOMO energy gap.	86
<b>Scheme 4.3</b>	The proposed stepwise substitution of aqua ligands from bifunctional Pt(II) complexes by thiourea nucleophiles.	87
<b>Figure 4.5</b>	typical kinetic trace for the first substitution step in a two-step reaction between <b>Pt(dCF<sub>3</sub>Py)</b> (0.133 mM) and TU (5.32mM) recorded at 310 nm, <i>T</i> = 298 K, pH = 2.0, <i>I</i> = 0.1 M (HClO <sub>4</sub> /NaClO <sub>4</sub> ) on the stopped-flow spectrophotometer.	88
<b>Figure 4.6</b>	<i>Pseudo</i> -first-order rate constants, <i>k</i> <sub>obs1</sub> and <i>k</i> <sub>obs2</sub> , plotted as a function of thiourea nucleophile concentration for the substitution of the first (a) and second (b) aqua ligand from <b>Pt(dCF<sub>3</sub>Py)</b> at pH = 2.0, <i>T</i> = 298 K and <i>I</i> = 0.1 M (HClO <sub>4</sub> /NaClO <sub>4</sub> ).	89

<b>Figure 4.7</b>	Plots of $\ln(k_2/T)$ versus $(1/T)$ for the substitution of the first (a) and second (b) aqua ligand from <b>Pt(dCH<sub>3</sub>Py)</b> by thiourea nucleophiles at varying temperatures.	91
<b>Figure 4.8</b>	<sup>1</sup> H NMR spectral arrays acquired during the reaction of <b>[Pt(H<sub>2</sub>Py)Cl<sub>2</sub>]</b> and 2 equiv. of TU in DMSO- <i>d</i> <sub>6</sub> at 303 K.	93
<b>Scheme 4.4</b>	Numbering scheme employed for the protons in <b>[Pt(H<sub>2</sub>Py)Cl<sub>2</sub>]</b> .	93
<b>Figure 4.9</b>	<sup>195</sup> Pt NMR spectra acquired during the reaction of <b>[Pt(H<sub>2</sub>Py)Cl<sub>2</sub>]</b> and 2 equiv. of TU in DMSO- <i>d</i> <sub>6</sub> at 303 K. Insert: <sup>195</sup> Pt NMR spectrum of <b>[Pt(H<sub>2</sub>Py)Cl<sub>2</sub>]</b> before the reaction.	95
<b>Figure SI 4.1a</b>	<sup>1</sup> H NMR spectrum of 2-(pyrazol-1-ylmethyl)pyridine ( <b>H<sub>2</sub>Py</b> ) in CDCl <sub>3</sub> .	108
<b>Figure SI 4.1b</b>	<sup>13</sup> C NMR spectrum of 2-(pyrazol-1-ylmethyl)pyridine ( <b>H<sub>2</sub>Py</b> ) in CDCl <sub>3</sub> .	108
<b>Figure SI 4.1c</b>	Low resolution ESI <sup>+</sup> mass spectrum of 2-(pyrazol-1-ylmethyl)-Pyridine ( <b>H<sub>2</sub>Py</b> ).	109
<b>Figure SI 4.2a</b>	<sup>1</sup> H NMR spectrum of [Pt{2-(3,5-dimethylpyrazol-1-ylmethyl)-Pyridine}Cl <sub>2</sub> ], <b>[Pt(dCH<sub>3</sub>Py)Cl<sub>2</sub>]</b> , in DMSO- <i>d</i> <sub>6</sub> .	109
<b>Figure SI 4.2b</b>	<sup>13</sup> C NMR spectrum of [Pt{2-(3,5-dimethylpyrazol-1-ylmethyl)-Pyridine}Cl <sub>2</sub> ], <b>[Pt(dCH<sub>3</sub>Py)Cl<sub>2</sub>]</b> , in DMSO- <i>d</i> <sub>6</sub> .	110
<b>Figure SI 4.2c</b>	<sup>195</sup> Pt NMR spectrum of [Pt{2-(3,5-dimethylpyrazol-1-ylmethyl)-Pyridine}Cl <sub>2</sub> ], <b>[Pt(dCH<sub>3</sub>Py)Cl<sub>2</sub>]</b> , in DMSO- <i>d</i> <sub>6</sub> .	110
<b>Figure SI 4.3</b>	UV/Visible spectra for the titration of 0.054 mM <b>Pt(dCF<sub>3</sub>Py)</b> with NaOH in the pH range 2-10 at <i>T</i> = 298.15 K. Inset: Absorbance versus pH plot at 295 nm for <b>Pt(dCF<sub>3</sub>Py)</b> complex.	111
<b>Figure SI 4.4</b>	Concentration dependence of plots of <i>k</i> <sub>obs1</sub> , s <sup>-1</sup> , for the displacement of the first aqua ligand of <b>Pt(H<sub>2</sub>Py)</b> (a) and <b>Pt(dCH<sub>3</sub>Py)</b> (b) by thiourea nucleophiles, pH = 2.0, <i>T</i> = 298 K, and <i>I</i> = 0.1 M (HClO <sub>4</sub> /NaClO <sub>4</sub> ).	115
<b>Figure SI 4.5</b>	Eyring plots for the substitution of the first aqua ligand of <b>Pt(H<sub>2</sub>Py)</b> (a) and <b>Pt(dCF<sub>3</sub>Py)</b> (b) by thiourea nucleophiles, pH = 2.0, and <i>I</i> = 0.1 M (HClO <sub>4</sub> /NaClO <sub>4</sub> ).	115
<b>Figure SI 4.6</b>	<sup>1</sup> H NMR spectrum of [Pt{2-[(3,5-bis(trifluoromethyl)pyrazol-1-ylmethyl)]pyridine}Cl <sub>2</sub> ], <b>[Pt(dCF<sub>3</sub>Py)Cl<sub>2</sub>]</b> in DMSO- <i>d</i> <sub>6</sub> .	116
<b>Figure SI 4.7</b>	<sup>13</sup> C NMR spectrum of [Pt{2-[(3,5-bis(trifluoromethyl)pyrazol-1-ylmethyl)]pyridine}Cl <sub>2</sub> ], <b>[Pt(dCF<sub>3</sub>Py)Cl<sub>2</sub>]</b> in DMSO- <i>d</i> <sub>6</sub> .	116
<b>Figure 5.1</b>	Chemical structures of the bifunctional Pt(II) complexes. Perchlorate counter ions (ClO <sub>4</sub> <sup>-</sup> ) are omitted for clarity.	120

<b>Scheme 5.1</b>	Proposed stepwise deprotonation for the pH dependence of mononuclear bifunctional Pt(II) system of complexes with different donors.	126
<b>Figure 5.2</b>	UV/Visible spectra for the titration of 0.050 mM <b>Pt(dCF<sub>3</sub>Qn)</b> with NaOH in the pH range 2-9 at $T = 298.15$ K. Insert: Boltzmann fit of Absorbance <i>vs.</i> pH at 275 nm for <b>Pt(dCF<sub>3</sub>Qn)</b> complex.	127
<b>Figure 5.3</b>	DFT-calculated HOMO and LUMO frontier molecular orbitals of Pt(II) complexes.	130
<b>Scheme 5.2</b>	The proposed stepwise substitution of diaqua ligand from bifunctional Pt(II) complexes by thiourea nucleophiles.	131
<b>Figure 5.4</b>	A typical kinetic trace for the first substitution step in a two-step reaction between <b>Pt(dCH<sub>3</sub>Qn)</b> (0.15 mM) and TU (6.0 mM) recorded at 290 nm, $T = 298$ K, pH = 2.0, $I = 0.1$ M (HClO <sub>4</sub> /NaClO <sub>4</sub> ) on the stopped-flow spectrophotometer.	132
<b>Figure 5.5</b>	UV/visible spectra recorded during a two-step reaction of 0.22 mM <b>Pt(H<sub>2</sub>Quin)</b> and 4.4 mM TU recorded at pH = 2, $T = 298$ K and $I = 0.1$ M (HClO <sub>4</sub> / NaClO <sub>4</sub> ). Insert: kinetic trace for the substitution of the second aqua ligand recorded at 293 nm.	133
<b>Figure 5.6</b>	<i>Pseudo</i> -first-order rate constants, $k_{\text{obs } 1/2}$ , plotted as a function of nucleophile concentration for the substitution of the first (a) and second (b) labile aqua ligand from <b>Pt(dCF<sub>3</sub>Qn)</b> at pH = 2.0, $T = 298$ K and $I = 0.1$ M (HClO <sub>4</sub> / NaClO <sub>4</sub> ).	135
<b>Figure 5.7</b>	Plots of $\ln(k_2/T)$ versus $(1/T)$ for the substitution of the first (a) and second (b) labile aqua ligand from <b>Pt(dCF<sub>3</sub>Qn)</b> by thiourea nucleophiles at varying temperatures.	136
<b>Figure SI 5.1a</b>	<sup>1</sup> H NMR spectrum of 2-(pyrazol-1-ylmethyl)quinoline ( <b>H<sub>2</sub>Qn</b> ) in CDCl <sub>3</sub>	148
<b>Figure SI 5.1b</b>	<sup>13</sup> C NMR spectrum of 2-[3,5-bis(trifluoromethyl)pyrazol-1-ylmethyl]quinoline, <b>dCF<sub>3</sub>Qn</b> in CDCl <sub>3</sub> .	148
<b>Figure SI 5.1c</b>	Low resolution ESI <sup>+</sup> mass spectrum of 2-(pyrazol-1-ylmethyl)quinoline ( <b>H<sub>2</sub>Qn</b> ).	149
<b>Figure SI 5.1d</b>	<sup>1</sup> H NMR spectrum of [Pt{2-[(3,5-bis(trifluoromethyl)-pyrazol-1-ylmethyl]quinoline}Cl <sub>2</sub> ], [ <b>Pt(dCF<sub>3</sub>Qn)</b> Cl <sub>2</sub> ] in DMSO-d <sub>6</sub> .	149
<b>Figure SI 5.1e</b>	<sup>13</sup> C NMR spectrum [Pt{2-[(3,5-bis(trifluoromethyl)-pyrazol-1-ylmethyl]quinoline}Cl <sub>2</sub> ], [ <b>Pt(dCF<sub>3</sub>Qn)</b> Cl <sub>2</sub> ] in DMSO-d <sub>6</sub> .	150
<b>Figure SI 5.1f</b>	<sup>1</sup> H NMR spectrum of [Pt{2-[(3,5-bis(trifluoromethyl)pyrazol-1-	150

	ylmethyl]quinoline}Cl <sub>2</sub> ], [ <b>Pt(dCF<sub>3</sub>Qn)Cl<sub>2</sub></b> ] in DMSO-d <sub>6</sub>	
<b>Figure SI 5.1g</b>	<sup>1</sup> H NMR spectrum of [Pt{(2-pyrazoly-1-ylmethyl)quinoline}Cl <sub>2</sub> ], [ <b>Pt(H<sub>2</sub>Qn)Cl<sub>2</sub></b> ] in DMSO-d <sub>6</sub> .	151
<b>Figure SI 5.2</b>	UV/visible scan for a trial run of the reaction between <b>Pt(H<sub>2</sub>Qn)</b> (written as PtL3) and 60-fold DMTU at different times.	151
<b>Figure SI 5.3</b>	UV/Visible spectra for the titration of 0.054 mM <b>Pt(dCH<sub>3</sub>Qn)</b> with NaOH in the pH range 2-10 at <i>T</i> = 298.15 K. Insert: Absorbance versus pH plot at 295 nm for <b>Pt(dCF<sub>3</sub>Qn)</b> complex.	152
<b>Figure SI 5.4</b>	Concentration dependence plots of <i>k<sub>obs</sub></i> , s <sup>-1</sup> , for the displacement of the first aqua ligand of <b>Pt(H<sub>2</sub>Qn)</b> (a) and <b>Pt(dCH<sub>3</sub>Qn)</b> (b) by thiourea nucleophiles, pH = 2.0, <i>T</i> = 298 K, and <i>I</i> = 0.1 M (HClO <sub>4</sub> /NaClO <sub>4</sub> ).	157
<b>Figure SI 5.5</b>	Eyring plot for the substitution of the first aqua ligand of <b>Pt(H<sub>2</sub>Qn)</b> (a) and <b>Pt(dCH<sub>3</sub>Qn)</b> (b) by thiourea nucleophiles, pH = 2.0, and <i>I</i> = 0.1 M (HClO <sub>4</sub> /NaClO <sub>4</sub> ).	157

# List of Tables

<b>Table 2.1</b>	The effect of different leaving groups on the rate of substitution of X in [Pt(dien)X] <sup>+</sup> complexes at 25°C.	38
<b>Table 2.2</b>	Solvent effect on chloride substitution (Equation 2.5) at 25 °C.	40
<b>Table 2.3</b>	<i>cis/trans</i> steric effects on the rate of chloride ligand substitution by pyridine in [Pt(PEt <sub>3</sub> ) <sub>2</sub> (L)Cl].	49
<b>Table 4.1</b>	Summary of p <i>K<sub>a</sub></i> data for the deprotonation of Pt-bound aqua ligands in the bifunctional Pt(II) complexes.	84
<b>Table 4.2</b>	DFT-calculated data for the bifunctional Pt(II) complexes.	87
<b>Table 4.3</b>	Summary of the second-order rate constants for the stepwise substitution of the aqua ligands by thiourea nucleophiles from diaqua Pt(II) complexes.	92
<b>Table 4.4</b>	Summary of the activation parameters for the stepwise substitution of aqua ligands from the diaqua Pt(II) complexes.	94
<b>Table SI 4.1a</b>	Summary of wavelengths (nm) used for monitoring the first substitution reactions between a series of bifunctional Pt(II) complexes and thiourea nucleophiles.	107
<b>Table SI 4.1b</b>	Summary of wavelengths (nm) used for monitoring the second substitution reactions between a series of bifunctional Pt(II) complexes and thiourea nucleophiles.	107
<b>Table SI 4.2a.</b>	Average observed rate constants, <i>k<sub>obs1</sub></i> , for the displacement of the first aqua ligand in <b>Pt(H<sub>2</sub>Py)</b> by thiourea nucleophiles, pH = 2.0, <i>T</i> = 298 K, <i>I</i> = 0.1 M (HClO <sub>4</sub> /NaClO <sub>4</sub> ).	111
<b>Table SI 4.2b</b>	Average observed rate constants, <i>k<sub>obs1</sub></i> , for the displacement of the first aqua ligand in <b>Pt(dCH<sub>3</sub>Py)</b> by thiourea nucleophiles, pH = 2.0, <i>T</i> = 298 K, <i>I</i> = 0.1 M (HClO <sub>4</sub> /NaClO <sub>4</sub> ).	111
<b>Table SI 4.2c</b>	Average observed rate constants, <i>k<sub>obs1</sub></i> , for the displacement of the first aqua ligand in <b>Pt(dCF<sub>3</sub>Py)</b> by thiourea nucleophiles, pH = 2.0, <i>T</i> = 298 K, <i>I</i> = 0.1 M (HClO <sub>4</sub> /NaClO <sub>4</sub> ).	112
<b>Table SI 4.2d</b>	Average observed rate constants, <i>k<sub>obs2</sub></i> , for the displacement of the second aqua ligand in <b>Pt(H<sub>2</sub>Py)</b> by thiourea nucleophiles, pH = 2.0, <i>T</i> = 298 K, <i>I</i> = 0.1 M (HClO <sub>4</sub> /NaClO <sub>4</sub> ).	112
<b>Table SI 4.2e</b>	Average observed rate constants, <i>k<sub>obs2</sub></i> , for the displacement of the second aqua ligand in <b>Pt(dCH<sub>3</sub>Py)</b> by thiourea nucleophiles, pH = 2.0, <i>T</i> = 298 K, <i>I</i> = 0.1 M (HClO <sub>4</sub> /NaClO <sub>4</sub> ).	112

<b>Table SI 4.2f</b>	Average observed rate constants, $k_{obs2}$ , for the displacement of the second aqua ligand in <b>Pt(dCF<sub>3</sub>Py)</b> by thiourea nucleophiles, pH = 2.0, $T = 298\text{ K}$ , $I = 0.1\text{ M}$ (HClO <sub>4</sub> /NaClO <sub>4</sub> ).	112
<b>Table SI 4.3a</b>	Temperature dependence of the second-order rate constants, $k_{2(1^{st})}$ , $\text{M}^{-1}\text{ s}^{-1}$ for the displacement of the first aqua ligand in <b>Pt(H<sub>2</sub>Py)</b> by thiourea nucleophiles, pH = 2.0, $I = 0.1\text{ M}$ (HClO <sub>4</sub> /NaClO <sub>4</sub> ).	113
<b>Table SI 4.3b</b>	Temperature dependence of the second-order rate constants, $k_{2(1^{st})}$ , $\text{M}^{-1}\text{ s}^{-1}$ for the displacement of the first aqua ligand in <b>Pt(dCH<sub>3</sub>Py)</b> by thiourea nucleophiles, pH = 2.0, $I = 0.1\text{ M}$ (HClO <sub>4</sub> /NaClO <sub>4</sub> ).	113
<b>Table SI 4.3c</b>	Temperature dependence of the second-order rate constants, $k_{2(1^{st})}$ , $\text{M}^{-1}\text{ s}^{-1}$ for the displacement of the first aqua ligand in <b>Pt(dCF<sub>3</sub>Py)</b> by thiourea nucleophiles, pH = 2.0, $I = 0.1\text{ M}$ (HClO <sub>4</sub> /NaClO <sub>4</sub> ).	113
<b>Table SI 4.3d</b>	Temperature dependence of the second-order rate constants, $k_{2(2^{nd})}$ , $\text{M}^{-1}\text{ s}^{-1}$ for the displacement of the first aqua ligand in <b>Pt(H<sub>2</sub>Py)</b> by thiourea nucleophiles, pH = 2.0, $I = 0.1\text{ M}$ (HClO <sub>4</sub> /NaClO <sub>4</sub> ).	114
<b>Table SI 4.3e</b>	Temperature dependence of the second-order rate constants, $k_{2(2^{nd})}$ , $\text{M}^{-1}\text{ s}^{-1}$ for the displacement of the first aqua ligand in <b>Pt(dCH<sub>3</sub>Py)</b> by thiourea nucleophiles, pH = 2.0, $I = 0.1\text{ M}$ (HClO <sub>4</sub> /NaClO <sub>4</sub> ).	114
<b>Table SI 4.3f</b>	Temperature dependence of the second-order rate constants, $k_{2(2^{nd})}$ , $\text{M}^{-1}\text{ s}^{-1}$ for the displacement of the first aqua ligand in <b>Pt(dCF<sub>3</sub>Py)</b> by thiourea nucleophiles, pH = 2.0, $I = 0.1\text{ M}$ (HClO <sub>4</sub> /NaClO <sub>4</sub> ).	114
<b>Table 5.1</b>	Summary of $\text{p}K_a$ values for the deprotonation of Pt-bound aqua ligands in bifunctional Pt(II) complexes studied.	127
<b>Table 5.2</b>	DFT-calculated data for bifunctional Pt(II) complexes.	129
<b>Table 5.3</b>	Summary of the second-order rate constants for the stepwise substitution of labile aqua ligands by thiourea nucleophiles in diaqua Pt(II) complexes.	134
<b>Table 5.4</b>	Summary of the activation parameters for the stepwise substitution of labile aqua ligands from the diaqua Pt(II) complexes.	137
<b>Table SI 5.1</b>	Summary of wavelength (nm) used for monitoring the first	147

substitution reactions between a series of bifunctional Pt(II) complexes and thiourea nucleophiles.

<b>Table SI 5.1b</b>	Summary of wavelength (nm) used for monitoring the second substitution reactions between a series of bifunctional Pt(II) complexes and thiourea nucleophiles	147
<b>Table SI 5.2a</b>	Average observed rate constants, $k_{obs1}$ , for the displacement of the first aqua ligand in <b>Pt(H<sub>2</sub>Qn)</b> by thiourea nucleophiles, pH = 2.0, $T = 298\text{ K}$ , $I = 0.1\text{ M}$ (HClO <sub>4</sub> /NaClO <sub>4</sub> ).	152
<b>Table SI 5.2b</b>	Average observed rate constants, $k_{obs1}$ , for the displacement of the first aqua ligand in <b>Pt(dCH<sub>3</sub>Qn)</b> by thiourea nucleophiles, pH = 2.0, $T = 298\text{ K}$ , $I = 0.1\text{ M}$ (HClO <sub>4</sub> /NaClO <sub>4</sub> ).	152
<b>Table SI 5.2c</b>	Average observed rate constants, $k_{obs1}$ , for the displacement of the first aqua ligand in <b>Pt(dCF<sub>3</sub>Qn)</b> by thiourea nucleophiles, pH = 2.0, $T = 298\text{ K}$ , $I = 0.1\text{ M}$ (HClO <sub>4</sub> /NaClO <sub>4</sub> ).	153
<b>Table SI 5.2d</b>	Average observed rate constants, $k_{obs1}$ , for the displacement of the first aqua ligand in <b>Pt(dCF<sub>3</sub>Py)</b> by thiourea nucleophiles, pH = 2.0, $T = 298\text{ K}$ , $I = 0.1\text{ M}$ (HClO <sub>4</sub> /NaClO <sub>4</sub> ).	153
<b>Table SI 5.2e.</b>	Average observed rate constants, $k_{obs2}$ , for the displacement of the second aqua ligand in <b>Pt(H<sub>2</sub>Qn)</b> by thiourea nucleophiles, pH = 2.0, $T = 298\text{ K}$ , $I = 0.1\text{ M}$ (HClO <sub>4</sub> /NaClO <sub>4</sub> ).	153
<b>Table SI 5.2f</b>	Average observed rate constants, $k_{obs2}$ , for the displacement of the second aqua ligand in <b>Pt(dCH<sub>3</sub>Qn)</b> by thiourea nucleophiles, pH = 2.0, $T = 298\text{ K}$ , $I = 0.1\text{ M}$ (HClO <sub>4</sub> /NaClO <sub>4</sub> ).	153
<b>Table SI 5.2g</b>	Average observed rate constants, $k_{obs2}$ , for the displacement of the second aqua ligand in <b>Pt(dCF<sub>3</sub>Qn)</b> by thiourea nucleophiles, pH = 2.0, $T = 298\text{ K}$ , $I = 0.1\text{ M}$ (HClO <sub>4</sub> /NaClO <sub>4</sub> ).	154
<b>Table SI 5.2h</b>	Average observed rate constants, $k_{obs2}$ , for the displacement of the second aqua ligand in <b>Pt(dCF<sub>3</sub>Py)</b> by thiourea nucleophiles, pH = 2.0, $T = 298\text{ K}$ , $I = 0.1\text{ M}$ (HClO <sub>4</sub> /NaClO <sub>4</sub> ).	154
<b>Table SI 5.3a</b>	Temperature dependence of the second-order rate constants, $k_{2(1^{st})}$ , $\text{M}^{-1}\text{ s}^{-1}$ for the displacement of the first aqua ligand in <b>Pt(H<sub>2</sub>Qn)</b> by thiourea nucleophiles, pH = 2.0, $I = 0.1\text{ M}$ (HClO <sub>4</sub> /NaClO <sub>4</sub> ).	154
<b>Table SI 5.3b</b>	Temperature dependence of the second-order rate constants, $k_{2(1^{st})}$ , $\text{M}^{-1}\text{ s}^{-1}$ for the displacement of the first aqua ligand in <b>Pt(dCH<sub>3</sub>Qn)</b> by thiourea nucleophiles, pH = 2.0, $I = 0.1\text{ M}$ (HClO <sub>4</sub> /NaClO <sub>4</sub> ).	154

<b>Table SI 5.3c</b>	Temperature dependence of the second-order rate constants, $k_{2(1^{st})}$ , $M^{-1} s^{-1}$ for the displacement of the first aqua ligand in <b>Pt(dCF<sub>3</sub>Qn)</b> by thiourea nucleophiles, pH = 2.0, $I = 0.1$ M (HClO <sub>4</sub> /NaClO <sub>4</sub> ).	155
<b>Table SI 5.3d</b>	Temperature dependence of the second-order rate constants, $k_{2(1^{st})}$ , $M^{-1} s^{-1}$ for the displacement of the first aqua ligand in <b>Pt(dCF<sub>3</sub>Py)</b> by thiourea nucleophiles, pH = 2.0, $I = 0.1$ M (HClO <sub>4</sub> /NaClO <sub>4</sub> ).	155
<b>Table SI 5.3e</b>	Temperature dependence of the second-order rate constants, $k_{2(2^{nd})}$ , $M^{-1} s^{-1}$ for the displacement of the first aqua ligand in <b>Pt(H<sub>2</sub>Qn)</b> by thiourea nucleophiles, pH = 2.0, $I = 0.1$ M (HClO <sub>4</sub> /NaClO <sub>4</sub> ).	155
<b>Table SI 5.3f</b>	Temperature dependence of the second-order rate constants, $k_{2(2^{nd})}$ , $M^{-1} s^{-1}$ for the displacement of the first aqua ligand in <b>Pt(dCH<sub>3</sub>Qn)</b> by thiourea nucleophiles, pH = 2.0, $I = 0.1$ M (HClO <sub>4</sub> /NaClO <sub>4</sub> ).	156
<b>Table SI 5.3g</b>	Temperature dependence of the second-order rate constants, $k_{2(2^{nd})}$ , $M^{-1} s^{-1}$ for the displacement of the first aqua ligand in <b>Pt(dCF<sub>3</sub>Qn)</b> by thiourea nucleophiles, pH = 2.0, $I = 0.1$ M (HClO <sub>4</sub> /NaClO <sub>4</sub> ).	156
<b>Table SI 5.3h</b>	Temperature dependence of the second-order rate constants, $k_{2(2^{nd})}$ , $M^{-1} s^{-1}$ for the displacement of the first aqua ligand in <b>Pt(dCF<sub>3</sub>Py)</b> by thiourea nucleophiles, pH = 2.0, $I = 0.1$ M (HClO <sub>4</sub> /NaClO <sub>4</sub> ).	156



# Table of Contents

<b>Chapter 1: The use of platinum and ruthenium complexes as anticancer therapeutic agents</b>	<b>1</b>
1.0 Metal complexes as potential therapeutics	1
1.1 Cancer and its treatment	2
1.2 Prospects of platinum and ruthenium complexes in cancer chemotherapy	3
1.2.1 The first generation of platinum anticancer drugs	3
1.2.2 Biochemical mechanism of action and resistance of cisplatin	4
1.2.2.1 The mechanism of action of cisplatin	4
1.2.2.2 The mechanism of resistance of cisplatin	7
1.2.3 General considerations for the development of new platinum anticancer drugs	8
1.2.4 The development of second and third generations of cisplatin.	9
1.2.5 New approaches in platinum drug development	11
1.2.5.1 Active platinum(II) complexes with a trans geometry	11
1.3 Platinum(IV) complexes as prodrugs	12
1.4 Development of polynuclear platinum complexes as anticancer agents	13
1.5 The anticancer activity of other metal complexes	15
1.6 Platinum(II) complexes with pyrazole-based ligands	17
1.6.1 Medical potential of pyrazole-based Pt(II) complexes	17
1.6.2 Cytotoxic studies of (pyrazolylmethyl)pyridine Pt(II) complexes	18
1.7 Mechanistic studies of Pt(II) complexes	20
1.7.1 The effect of substituents of a polydentate ligand on the rate of substitution	20
1.7.2 The role of an extended $\pi$ -conjugation in the ligand core on the rate of substitution	21
1.8 Role of kinetic data in the development of drugs	
1.9 Aims and objectives of the research	22
1.9.1 Pt(II) complexes with flexible (pyrazolylmethyl)pyridine and (pyrazolylmethyl)quinoline bidentate chelates	23
1.10 References	25
	26

<b>Chapter 2: Theoretical aspects on the substitution reactions in inorganic compounds focusing on platinum (II) complexes</b>	<b>31</b>
2.0 Introduction	31
2.1 Classification of Inorganic reaction mechanisms	31
2.1.1 Dissociative mechanism ( <i>D</i> -mechanism)	31
2.1.2 Associative mechanism ( <i>A</i> -mechanism)	32
2.1.3 Interchange mechanism ( <i>I</i> -mechanism)	34
2.2 Influence of the coordinated ligands around the metal centre on the mechanism of substitution	35
2.3 Ligand-exchange reactions at square-planar Pt(II) metal centre	36
2.4 Factors affecting the reactivity of square planar Pt(II) complexes	37
2.4.1 Effect of the leaving group	37
2.4.2 Effect of the entering ligand	38
2.4.3 Effect of the solvent	40
2.4.4 Effect of the non-leaving ligand	41
2.4.4.1 The trans-effect	41
2.4.4.2 The electrostatic polarization theory	44
2.4.4.3 The $\pi$ -bonding theory	45
2.4.4.4 The molecular orbital theory	46
2.4.4.5 The steric and electronic <i>cis</i> -effect	48
2.5 Dissociative mechanism in square planar Pt(II) complexes	51
2.6 References	52
 <b>Chapter 3: Kinetic theory and relevant techniques used for kinetic measurements</b>	 <b>55</b>
3.1 Introduction	55
3.2 The rate law	56
3.3 Integrated rate laws	57
3.3.1 First-order reactions	57
3.3.1.1 Irreversible first-order reactions	57
3.3.1.2 Reversible first-order reactions	58
3.3.2 second-order reactions	60
3.4 Measurements of activation parameters	63
3.5 Measurement of the activation volume	65
3.6 Techniques for studying chemical kinetics	66

3.6.1 UV/visible spectrophotometric technique	66
3.6.2 Stopped-flow technique	69
3.7 References	71
<b>Chapter 4: The role of substituents in a bidentate <i>N,N</i>-chelate on the substitution of aqua ligands from bifunctional Pt(II) complexes.</b>	<b>73</b>
4.0 Abstract	73
4.1 Introduction	74
4.2 Experimental	76
4.2.1 Chemicals	76
4.2.2 Synthesis of the ligands	77
4.2.3 Synthesis of Pt(II) complexes	79
4.2.4 Preparation of diaqua Pt(II) complexes	80
4.2.5 Instrumentation and physical measurements	80
4.2.6 Measurements of $pK_a$ values of the diaqua Pt(II) complexes	81
4.2.7 Kinetic measurements	82
4.2.8 Computational calculations	82
4.3 Results	83
4.3.1 Acid-base equilibrium of diaqua Pt(II) complexes	83
4.3.2 DFT-calculated optimised structures	86
4.3.3 Ligand substitution kinetics of the diaqua Pt(II) complexes	89
4.3.4 Activation parameters	93
4.4 NMR studies	94
4.5 Discussion	98
4.5.1 First substitution step	99
4.5.2 Second substitution step	100
4.5.3 Activation parameters and reactivity of the nucleophiles	102
4.6 Conclusion	102
4.7 References	104
4.8 Supporting information	107
<b>Chapter 5: The influence of substituents and extended <math>\pi</math>-conjugation in bidentate <i>N,N</i>-chelate on the substitution kinetics of aqua ligands from platinum(II) complexes</b>	<b>117</b>

5.0 Abstract	117
5.1 Introduction	118
5.2 Experimental	120
5.2.1 Chemicals and reagents	120
5.2.2 Preparation of the ligands	121
5.2.3 Synthesis of the platinum complexes	122
5.2.4 Preparation of diaqua Pt(II) complex and nucleophile solutions	124
5.2.5 Instrumentation and physical measurements	124
5.2.6 Kinetic measurements	125
5.2.7 Computational details	125
5.3 Results	126
5.3.1 Acidity of diaqua Pt(II) complexes	126
5.3.3 Kinetics of the substitution reactions with thiourea nucleophiles	131
5.4 Discussion	137
5.4.1 Acid-base equilibrium of diaqua Pt(II) complexes	137
5.4.2 DFT calculated optimised structures	138
5.4.3 Kinetic studies	138
5.4.3.1 First substitution	139
5.4.3.2 Second substitution	140
5.4.4 Activation parameters and reactivity of the nucleophiles	142
5.5 Conclusion	142
5.6 References	144
5.7 Supporting Information	147

# Abstract

The substitution rates of aqua ligands from bifunctional Pt(II) complexes were studied using biologically relevant thiourea nucleophiles *viz.*, thiourea (TU), *N,N*-dimethylthiourea (DMTU) and *N,N,N',N'*-tetramethylthiourea (TMTU). The reactions were studied in aqueous acidic media (pH 2) under *pseudo* first-order conditions as a function of nucleophile concentration and temperature, using conventional stopped-flow and UV/Visible spectrophotometric techniques.

Three of the Pt(II) complexes had a flexible (pyrazolylmethyl)pyridine core, differing on the 3,5-substituents ( $-H$ ,  $-CH_3$ ,  $-CF_3$ ) on the pyrazole ring. The other three complexes were structurally similar to the first but had a (pyrazolylmethyl)quinoline as the non-leaving ligand. Through a comparative approach, the two sets of Pt(II) complexes were designed to quantify the effect on the rate of substitution at the square-planar geometry when the substituents (electronic and steric properties) of the coordinated pyrazole ring are changed or when the strong  $\pi$ -acceptor pyridine ring is replaced with quinoline in the (pyrazolylmethyl)quinoline bidentate core.

The 3,5-substituents on the pyrazole ring as well as the replacement of a pyridine with a quinoline ring in the *N,N*-bidentate chelate both affected the electrophilicity of the Pt(II) centre. This in turn controlled the lability of the coordinated aqua ligands and hence the reactivity of the complexes. The inductive electron-donating groups ( $-CH_3$ ) on the pyrazole ring decreased the rate of substitution, whereas the inductive electron-withdrawing groups ( $-CF_3$ ) increased the rate of substitution. This is supported by the order of reactivity of **Pt(dCF<sub>3</sub>Py) > Pt(H<sub>2</sub>Py) > Pt(dCH<sub>3</sub>Py)** for the substitution of the aqua ligand *trans* to the pyrazole ring in the first series of the complexes. On the other hand, the lability of the aqua ligand *cis* to the pyrazole ring followed the order: **Pt(H<sub>2</sub>Py)  $\approx$  Pt(dCF<sub>3</sub>Py) > Pt(dCH<sub>3</sub>Py)**. This indicates that 3-substituent on the pyrazole ring causes a steric retardation on the lability of the aqua ligand in a *cis* position. In the second series of complexes, the complete order of reactivity for the first substitution was found to be **Pt(dCF<sub>3</sub>Py) > Pt(H<sub>2</sub>Qn) > Pt(dCF<sub>3</sub>Qn) > Pt(dCH<sub>3</sub>Qn)** and indicates an

interplay between steric and electronic effects, with the dominant factor controlling the rate. However, the reactivity trend for the substitution of the second aqua did not follow that of the first, and pointed out a steric retardation to the approach of the second incoming nucleophile due to the *cis*-positioned 3-substituent { either (  $-\text{CH}_3$ ) or (  $-\text{CF}_3$ ) } on the pyrazole ring.

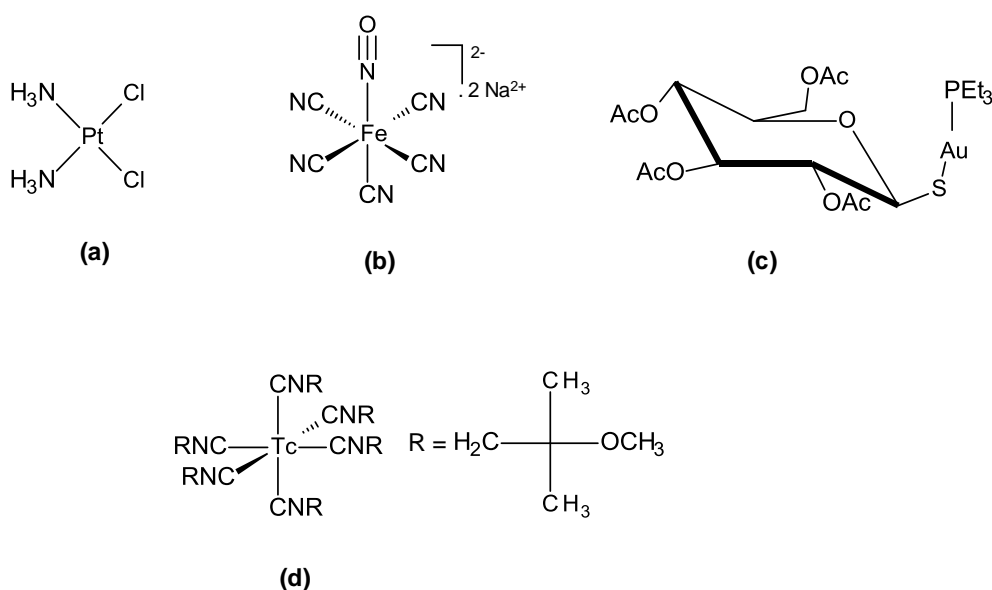
Further, the reactivity trends confirms that the quinoline substructure in the (pyrazolylmethyl)quinoline ligands acts as an apparent donor of electron density towards the metal centre rather than being a  $\pi$ -acceptor. This is contrary to what would be expected given its stabilized extended molecular orbitals, which should delocalise electron better than those of pyridine. The DFT and  $\text{p}K_a$  data both support the experimentally obtained kinetic data. The mechanism of substitution remains associative throughout.

# Chapter 1

## The use of platinum and ruthenium complexes as anticancer therapeutic agents

### 1.0 Metal complexes as potential therapeutics

The roles of metal ions in biological systems have stimulated the development of metal-based therapeutics. In particular coordination compounds of transition metals are important due to their enzymatic, homeostasis and transporting functions (e.g. oxygen transportation in the blood system by heme complexes which has four  $\text{Fe}^{2+}$  ions). The biochemical reactions of some inorganic compounds have long been known to treat certain diseases. For example complexes of platinum(II) are used for treating cancer, while gold(I) and iron(III) compounds are used to treat arthritis and cardiovascular diseases, respectively.<sup>1,2</sup> Furthermore, some coordination compounds have been used in biological systems as clinical diagnostics. Examples include radioactive technetium ( $^{99\text{m}}\text{Tc}$ ) tracers and complexes carrying fluorescent groups.<sup>1,2</sup> Some selected metal complexes that are currently used in clinical treatment and diagnostic are shown in **Figure 1.1**.



**Figure 1.1:** Selected metal-based therapeutic and diagnostic agents that are used in the medical field.<sup>2</sup> Cisplatin (a), sodium nitroprusside (b), auranofin (c) and cardiolite (d).

Knowledge of coordination and redox properties of metal ions also plays an important role in the development of modern medicinal inorganic chemistry.<sup>2</sup> Positively charged metal ions have a strong affinity for negatively charged biomolecules (e.g. constituents of proteins and nucleic acids) that provide perfect ligands for coordinative binding.<sup>2</sup> The pharmaceutical and medicinal applications of metals have an excellent future potential. As a result, the biological activities of numerous metal complexes have been investigated.<sup>2,3</sup> It is clear that mechanistic understanding of how metal complexes achieve their biological activities is essential for the design of new metal-based compounds with high efficiency and wide spectrum of activity.

### **1.1 Cancer and its treatment**

Cancer can be described as a group of diseases in which one or more cells display uncontrolled and accelerated cell growth leading to the formation of tumours.<sup>4</sup> The majority of cancers are stimulated by the mutation of specific genes.<sup>5,6</sup> The mutations may cause accelerated cell division or deactivation of important processes that control cell division in the cell cycle.<sup>6,7,8</sup> Uncontrolled and accelerated cell growth may ultimately cause benign or malignant tumour.<sup>9</sup> The latter is characterised by invasion of neighbouring tissues or other parts of the body. This creates a life-threatening condition since normal cells in the neighbourhood of the tumours are transformed to cancerous cells.<sup>10</sup>

Cancer can be treated by surgery, chemotherapy, radiotherapy, photodynamic therapy and biochemical therapies (e.g. immunotherapy and gene therapy). The treatment of localised solid tumours may primarily involve surgical removal of the tumour and nearby affected tissues. Modern clinical procedures generally combine several types of treatment (e.g. surgery and chemotherapy) for better effects. What makes cancer more complex is that each type of cancer has its own specific characteristics which are different from other types of cancers e.g. lung cancer is biologically different from colon cancer. As a result, there is no single treatment for cancer; the combination of clinical protocols used is based on the biological properties of a particular type of cancer. Radiation treatment and chemotherapy are



more effective against small tumours and leukaemia although treatment is associated with side effects such as hair loss, induced anaemia, as well as nausea and vomiting.<sup>11</sup>

## 1.2 Prospects of platinum and ruthenium complexes in cancer chemotherapy

### 1.2.1 The first generation of platinum anticancer drugs

The use of inorganic complexes in the treatment of cancer was unknown until the discovery of *cis*-diamminedichloroplatinum(II), commonly known as cisplatin (**Figure 1.1a**). This compound was first synthesized by Michele Pyrone in 1844. However its biological activity was serendipitously discovered by Barnett Rosenberg in 1969.<sup>12</sup> During his study on the effect of the electric field on the growth of *E.coli* bacteria using inert platinum electrodes, he observed that bacteria grew into long filaments, an indication that the division and replication of cells had been adversely affected by the electric field with no concomitant inhibition of bacterial cell growth. It was rationalised that ammonium chloride (NH<sub>4</sub>Cl) electrolyte had reacted with platinum ions from the inert electrode to form soluble platinum complexes. The two compounds which were capable of inducing filamentous growth in the absence of an electric field are *cis*-[Pt(NH<sub>3</sub>)<sub>2</sub>Cl<sub>2</sub>] (cisplatin) and *cis*-[Pt(NH<sub>3</sub>)<sub>2</sub>Cl<sub>4</sub>]. Subsequent evaluation of these compounds against the fast growing tumourous cells gave positive results leading to *cis*-Pt(NH<sub>3</sub>)<sub>2</sub>Cl<sub>2</sub> being registered as an anticancer drug in 1978.<sup>13,14</sup>

Cisplatin is currently the most established and valuable anticancer drug used to treat a number of cancers including; ovarian, testicular, skin, lung and blood cancer.<sup>13,14</sup> In a bid to better understand the mechanism of action of this new drug, its analogues were synthesised and forwarded for screening. These studies focussed on establishing the empirical relationship between the structure of a compound and its antitumour activity. Cleare and Hoeschele<sup>15</sup> came up with laid-down rules which they termed the structure-activity relationships (SARs) for anticancer activity of platinum complexes. They postulated that for a metal complex to have antitumor activity:

- it should have a *cis*-geometry and a general structural formula *cis*-[Pt(N)<sub>2</sub>X<sub>2</sub>], where N is an N-donor amine ligand and X is a labile leaving group. Transplatin, an isomer which has a *trans*-geometry was observed to be inactive against cancer cells propelling them to this conclusion.<sup>15</sup>
- its non-leaving ligand should have at least one N-H moiety, which was thought to be crucial for hydrogen bonding interactions with DNA. This would stabilize the Pt-DNA adducts.<sup>16</sup>
- its leaving group, X, should be an anionic ligand of moderate binding strength to the platinum metal ion (e.g. Cl<sup>-</sup> or SO<sub>4</sub><sup>2-</sup>). Such ligand would exhibit weak *trans*-effect to avoid labilization of the amine ligands.<sup>17</sup> Other leaving groups were found to be either highly toxic or inactive.
- it should be neutral so that it can easily pass through the cell membrane. Neutral compounds are found to be more lipophilic than charged species.<sup>18</sup>

A large number of new complexes that obeyed the empirical structure-activity rules were later synthesized.<sup>19</sup> Most of the platinum complexes that have entered clinical trials and practice adhere to a set of these empirical SAR rules. Later on, active complexes which did not obey the rules were synthesized, notably being the complexes of *trans*-geometry.<sup>20</sup>

## 1.2.2 Biochemical mechanism of action and resistance of cisplatin

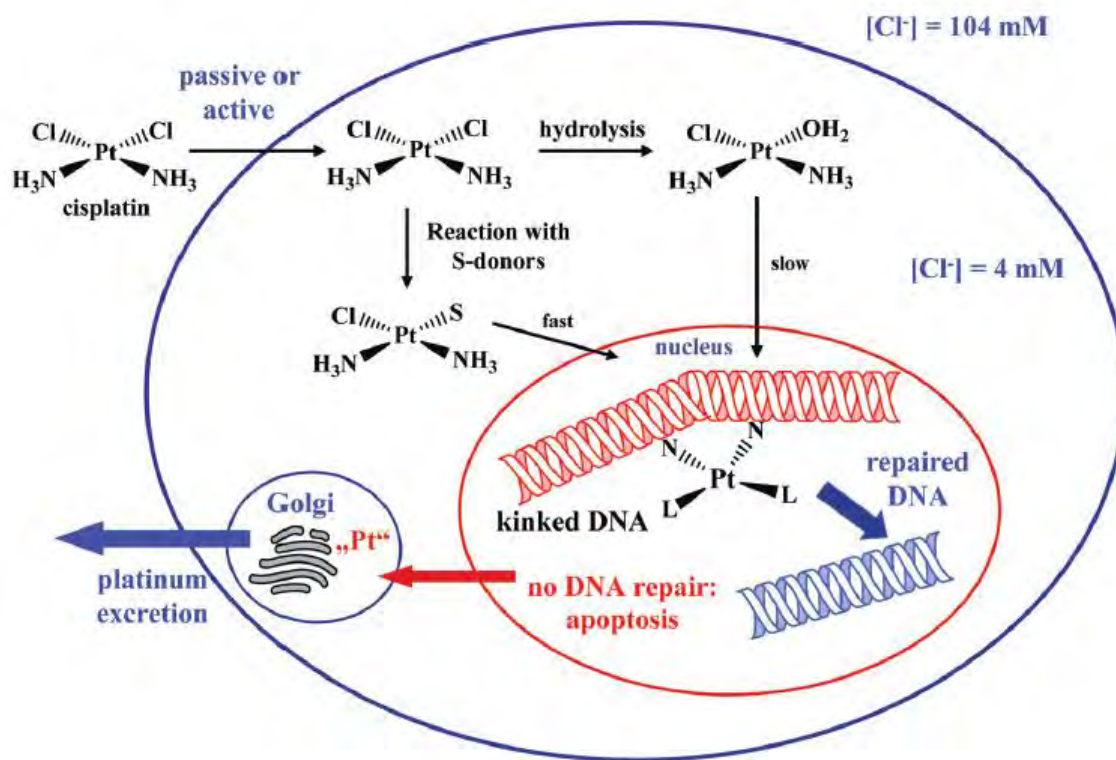
### 1.2.2.1 The mechanism of action of cisplatin

A wide range of low-molecular weight compounds of biological importance interact with DNA. The biological effect of these compounds may be associated with the alterations they cause in DNA and with the recognition of these changes by cellular constituents.<sup>21,22</sup> These compounds may therefore be used as probes in the studies of DNA properties and interactions. Some of these compounds are effective cross-linking agents that can form DNA-DNA or DNA-protein interactions showing remarkable antitumor and antiviral effects.<sup>21,22,23</sup> Platinum coordination complexes represent one class of such compounds. Several studies on cisplatin unravelled the mechanism of Pt(II) compounds and how they kill the cancer cells in the human

body. Consequently, it is widely accepted that the main target of cisplatin is the genomic DNA.<sup>24,25</sup>

Understanding the actual mechanism of cisplatin, and other platinum drugs has been essential for the development of improved anticancer drugs. Yet the actual mechanism of its biological activity is not fully understood, in spite of the large number of research initiatives in the past few decades.<sup>26,27</sup> However, considerable amount of data on how the drug induces the killing of certain cancers and how resistance develops have been reported. Compared to other metal complexes {e.g. Pd(II) and Ni(II)}, cisplatin is relatively kinetically inert. The substitution of its labile leaving groups follows an associative mechanism in many cases and is characterised by two independent reaction pathways i.e. solvent-assisted stepwise hydrolysis and direct attack by a nucleophile.<sup>17</sup>

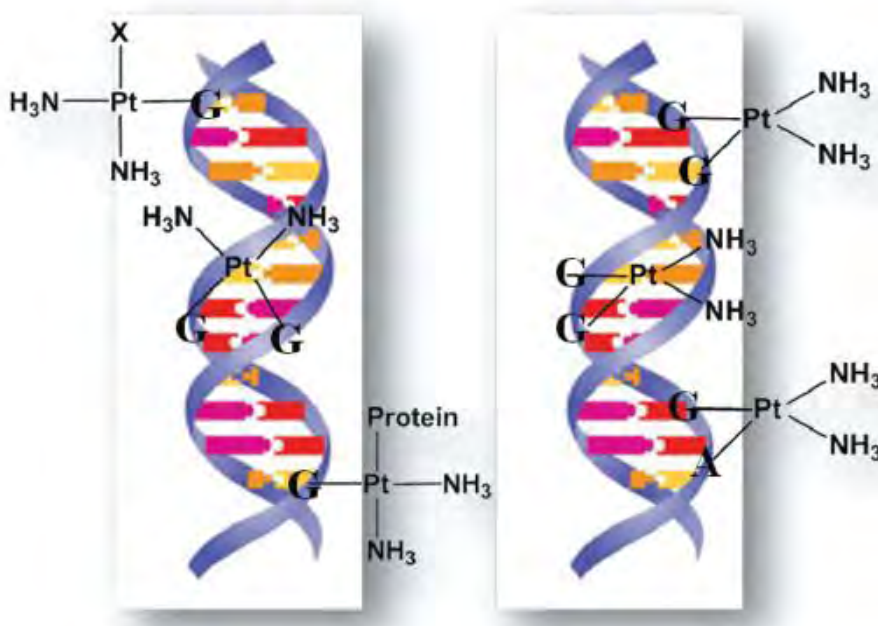
The two labile halide ligands are not susceptible to hydrolysis outside the cell due to elevated extracellular concentration of chloride ions (104 mM), thus cisplatin remains neutral before active uptake into the cells.<sup>17,28</sup> This is important in ameliorating toxicity. The neutral platinum compound diffuses across the cell membrane through active uptake, where it is gradually activated by a step-wise hydrolysis to generate positively charged aqua species,  $[\text{Pt}(\text{NH}_3)_2(\text{H}_2\text{O})\text{Cl}]^+$  and  $[\text{Pt}(\text{NH}_3)(\text{H}_2\text{O})_2]^{2+}$ . The first aquation step, for which the rate of DNA binding to form platinated-DNA adducts is dependent on, is very rapid due to low concentration of chloride (4 mM) inside the cell (**Figure 1.2**).<sup>11,29</sup> Upon hydrolysis, the platinum compound binds rapidly to DNA, since the water ligand is a better leaving group than the chloride ligand, and the resulting positively charged species are more reactive towards biomolecules.<sup>11,29</sup>



**Figure 1.2:** Schematic representation of the stages of cellular activation of cisplatin and possible biological consequences.<sup>28</sup>

DNA provides several nucleophilic sites in which the active  $[Pt(NH_3)_2(H_2O)_2]^{2+}$  can bind especially the nitrogen atoms of nucleobases. This form of complex can bind to DNA forming various intrastrand, interstrand and also DNA-proteins cross-links (**Figure 1.3**).<sup>28,30</sup> The cytostatic effect of this drug is widely accepted to occur through its interaction with the DNA in the nucleus of the cell, generating Pt-N adducts.<sup>31,32</sup> The major adducts produced are the 1,2-intrastrand cross-links between the adjacent N-7 atoms of guanine (G) residues.<sup>32,33</sup> Other nucleophilic sites of DNA e.g. N-7 atom of adenine and N-3 atom of cytosine are engaged in hydrogen bonding with the DNA framework, making G-N7 the most electron rich site. The binding of cisplatin to DNA induces significant distortions on the DNA helical structure and results in the inhibition of DNA replication and/or transcription.<sup>32,33,34</sup> Subsequently, this further persuades cell death through apoptosis and/or necrosis within the cancerous cells that form a tumoural mass.

Alternatively, active platinum complexes may interact with sulfur donors either in the blood plasma or inside the cell, since the sulphur atoms have high affinity for Pt(II) centres,<sup>35</sup> yielding kinetically inert or stable Pt-S adducts.<sup>36</sup> The presence of sulfur-containing amino acids or proteins may lead to potential deactivation of the platinum drug, which affects its pharmacokinetics or biodistribution.<sup>24,37</sup> Not only does this reduce the required platinated-DNA adducts and active drug accumulation, but also leads to toxic side effects.<sup>24,37,38</sup> Upon coordination to the Pt(II) complex, the *trans*-influence of the biological sulfur donors, can potentially de-coordinate the non-leaving amine groups, thereby suppressing the drug's actual mechanism of action that leads to cytotoxicity. This leads to the development of drug resistance.<sup>24</sup>



**Figure 1.3:** Different adducts formed from the interaction of cisplatin with DNA.<sup>39</sup>

### 1.2.2.2 The mechanism of resistance of cisplatin

Cisplatin has several drawbacks that restrict its use as an anticancer agent. It is applicable to narrow range of tumours and some sensitive ones develop resistance.<sup>40,41</sup> The resistance can either be intrinsic (i.e. when the tumours do not respond naturally to the drug) or acquired ( i.e. when tumours develop resistance to a drug which they were previously sensitive to its activity).<sup>40,42,43</sup> Drug resistance is closely related to the drug's bio-transformational pathways that compete for the bio-

availability of the drug to its target, DNA. Cross-resistance may develop between two or more drugs that exhibit similar inhibitory profiles. At least four biochemical pathways are thought to be responsible for the underlying mechanism of resistance to the cisplatin chemotherapy:<sup>44</sup>

- a) reduced active transport across the cell membrane.
- b) increased deactivation by plasma proteins in the extracellular bio-domain.
- c) intracellular irreversible binding to inactivating thiulates e.g. glutathione (GSH) and/or metallothionein (MT).
- d) enzymatic repair of platinated-DNA lesions (e.g excision repair).

Approximately 1% of the total intracellular platinum complex binds to DNA. The major causes for inadequate drug concentration reaching DNA include; the reduction in platinum drug uptake or its intracellular accumulation and increased cytoplasmic inactivation by GSH and MT. The resistance mechanisms that occur once the drug has bound to DNA include increased enzymatic repair of Pt-DNA adducts, and increased tolerance to high levels of DNA damage without simultaneously triggering downstream cellular mechanism that lead to programmed cell death.<sup>45</sup> The clarification of these major biochemical mechanisms of action and resistance is critical in the development of new platinum-based drugs with high efficiency and capability to evade drug resistance.

### **1.2.3 General considerations for the development of new platinum anticancer drugs**

In the past few decades, considerable amount of effort has been dedicated to establishing factors related to cytotoxicity properties of different platinum drugs. It has been shown that the development of new platinum drugs can be achieved by the variation of the carrier ligands and/or the leaving group. The carrier ligands are known to influence drug uptake, the reactivity of the metal centre and ultimate target selection. Lipophilic carrier ligands enhance the drug uptake, since the hydrophobic cell membrane is the first barrier that the drug encounters.<sup>28</sup> Several metal complexes with planar and intercalatory ligands have been shown to possess high affinity for DNA.<sup>27</sup>

Therefore, future development of platinum-based drugs should be informed by the following points:

- reactive platinum complexes may quickly bind to other biomolecules other than the targeted genomic DNA, causing severe toxic effects.
- the toxic side effects can be lowered using less labile leaving groups.
- replacing the non-leaving amine ( $\text{NH}_3$ ) ligand may also change the anticancer properties of the complexes through the formation of structurally different adducts with DNA.
- stable platinum complexes are less toxic, however, their tumour inhibiting properties are also reduced.
- lipophilic complexes diffuse quickly through the cell membrane and thus increase the intracellular drug uptake.

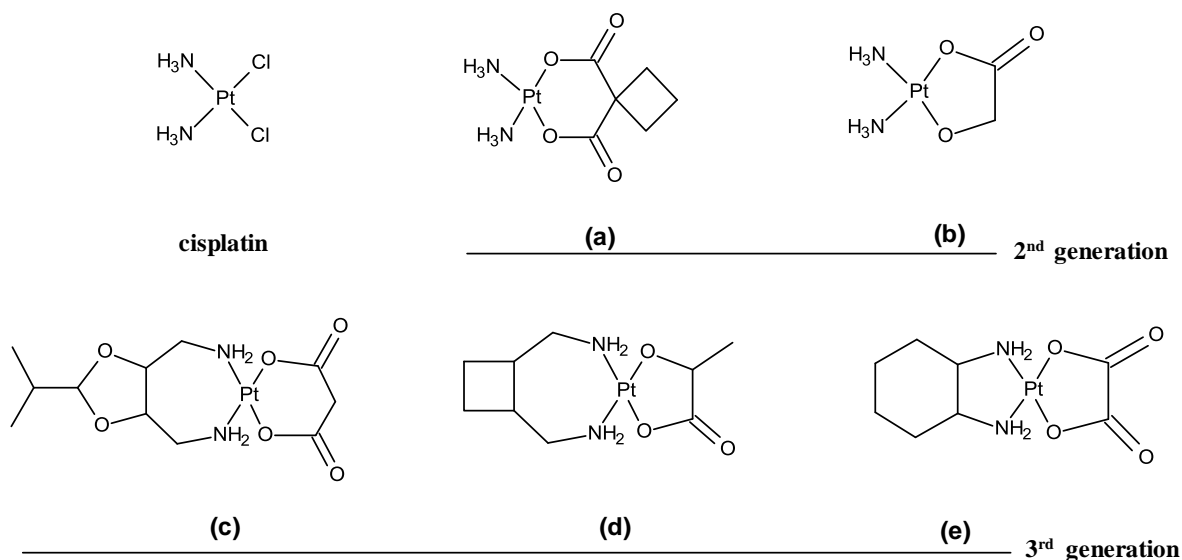
#### **1.2.4 The development of second and third generations of cisplatin.**

The applicability and effectiveness of cisplatin in cancer therapy has been thoroughly documented since its entry to clinical trials in the late 1970's.<sup>46</sup> The clinical success of cisplatin stimulated development of other new platinum complexes. This was necessitated because cisplatin was found to be highly toxic especially when administered in high dosage concentration despite its effectiveness in a variety of cancers.<sup>47</sup> The drug is also shrouded by intrinsic and acquired drug resistance.<sup>46,47</sup> In addition to these limitations, the use of cisplatin was noted to be accompanied by dose-limiting side effects including vomiting, nausea, hair loss and anaemia.<sup>47</sup> The side effects and systemic toxicities of cisplatin are, in part, associated with its poor specificity.

The limited efficiency and applicability of cisplatin caused a sustained momentum for the development of platinum-based anticancer drugs, with a common goal of finding new drugs with higher efficacy, lower toxicological profile and broader spectrum of anticancer activity. As a result, thousands of platinum complexes were synthesized and screened for anticancer activity.<sup>48,49,50</sup> However, only a few entered clinical trials, and most of these encountered pharmacokinetic difficulties.<sup>51,52,53</sup> Some examples of second and third generation of cisplatin derivatives that have been

prepared and approved for clinical use are shown in **Figure 1.4**. Today, carboplatin and oxaliplatin are commonly used anticancer drugs.<sup>52,53</sup> The structural modifications on the second- and third-generation of cisplatin analogues are based on replacing the halide leaving groups or changing the amine ligand, respectively. For example, carboplatin (second generation) has the chloride leaving group of cisplatin replaced by a less labile (or more kinetically inert) bidentate chelating dicarboxylate. This increases the intracellular and tissue distribution of the platinum drug due to limited susceptibility to deactivation. Therefore the drug may be administered at moderate to high dose concentration with no adverse effects. As a result, carboplatin has been widely used as a complementary drug to cisplatin in treating cancer.<sup>54</sup>

For oxaliplatin (third generation), the non-leaving amine ligands of cisplatin were replaced by a bulky diaminocyclohexane. This leads to the formation of stable Pt-DNA adducts which are believed to circumvent the recognition by repairing cellular proteins, thereby sustaining the activity of oxaliplatin in cisplatin resistant tumours.



**Figure 1.4:** Second- and third-generation of anticancer drugs that have been approved for clinical use.<sup>52</sup> Carboplatin (a), nedaplatin (b), heptaplatin (c), laboplatin (d) and oxaliplatin (e).

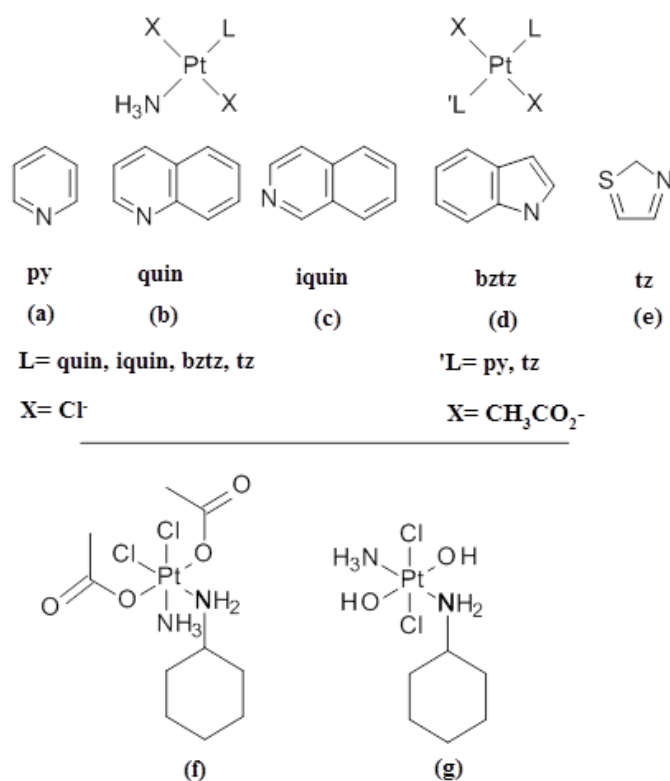


### 1.2.5 New approaches in platinum drug development

One of the main challenges in the rational design of metal-based chemotherapeutic agents is to enhance their cytotoxic activity while concurrently reducing toxicity.<sup>55</sup> Crucial progress includes the elucidation of drug resistance mechanisms, the development of combination therapeutic scheme and novel targeting strategies (e.g. nano-delivered drugs) and introduction of new platinum (IV) agents (e.g. satraplatin and picoplatin). Based on substantial expertise acquired on metal-based anticancer drugs in the past few decades, it is clear that carefully designed metal complexes structurally different from cisplatin and its related drugs (2<sup>nd</sup> and 3<sup>rd</sup> generation analogues) are prone to display an altered spectrum of clinical activity and toxicity, due to differences in biochemical mechanism for drug response.<sup>54</sup>

#### 1.2.5.1 Active platinum(II) complexes with a trans geometry

The early structure-activity relationship rules of Cleare and Hoeschele had stipulated that *trans*-diamminedichloroplatinum(II), transplatin and other *trans* platinum complexes lacked antitumour activity.<sup>56</sup> However, it was later shown that certain types of *trans*-Pt(II) complexes have antitumor activity comparable to that of cisplatin both *in vitro* and *in vivo*. It is known that the inactivity of transplatin is due to its kinetic instability or fast ligand kinetics and subsequent susceptibility to deactivation. Therefore new approaches have focused on the development of transplatin complexes using bulky ligands to reduce their kinetic reactivity. The hindering ligands retard the reactivity, thereby slowing down their inactivation by cellular components through ligand exchange reactions. Thus, higher concentration levels of the activated complex could reach its target, genomic DNA. The subclasses of *trans*-Pt(II) complexes that have shown significant *in vitro* antitumour activity include; *trans*-Pt(II) complexes bearing planar heterocyclic ligands such as pyridine, quinoline, isoquinoline, benzothiazole and thiazole (**Figure 1.5; a-e**).<sup>56</sup>



**Figure 1.5:** Mononuclear platinum(II) complexes with a *trans* geometry (a-e) and octahedral Pt(IV) complexes (f-g) that display anticancer activity.<sup>56</sup>

The cytotoxicity of the *trans* platinum complexes with bulky aromatic non-leaving groups were in some cases shown to be superior to cisplatin, and often better than the cytotoxicity of their respective *cis* analogues.<sup>56</sup> The *trans*-geometry complexes are characterised by a spectrum of activity different from cisplatin and often overcome resistance encountered by cisplatin. This is probably because these complexes generate different Pt-DNA adducts compared to cisplatin.

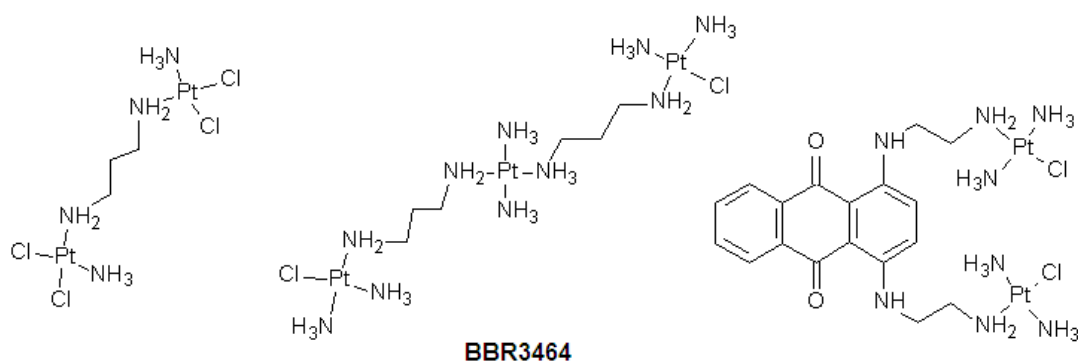
### 1.3 Platinum(IV) complexes as prodrugs

Most recently, kinetically inert Pt(IV) complexes have received much interest.<sup>57,58</sup> The structures of some of these complexes developed for anticancer activity are shown in **Figure 1.5 f-g**. Some of these complexes have lipophilic groups at the axial positions which facilitate the intestinal absorption of the drug, therefore making the oral administration possible.<sup>59</sup> The reduction of Pt(IV) to Pt(II) by extracellular or intracellular agents is necessary for the activation of the drug. Therefore these compounds are pro-drugs since chemical conversion by metabolic processes is required before the pharmacological agent reaches its site of action.

One of the most successful Pt(IV) complexes is bis(acetate)-amminedichlorido-(cyclohexylamine)platinum(IV), also known as satraplatin or JM216 (**Figure 1.5 f**). JM216 showed a great potential in phase I and II clinical stages of development.<sup>59</sup> It also represents the first platinum drug that was found to be suitable for oral administration due to its favourable pharmacokinetic properties. The phase II trial of this drug has been completed in hormone-refractory prostate cancer (HRPC), small lung cancer and ovarian cancer.<sup>60</sup> However, it was abandoned in phase III clinical trials due to variability in the drug uptake.<sup>58</sup> It has been suggested that the loss of lipophilic axial groups as a result of the reduction of the drug from Pt(IV) to Pt(II) in the bloodstream, accounts for the disparity in the activity between *in vitro* and *in vivo* systems.<sup>61</sup> JM216 also shows anticancer activity against various murine and human subcutaneous tumours comparable to the activity of cisplatin. It has a relatively low toxicological profile, being myelosuppression instead of dose-limiting nephrotoxicity in cisplatin.<sup>60</sup> Its analogous platinum(IV) complex with *trans* chloro labile groups (JM335, **Figure 1.5 g**) has shown similar and promising cytotoxic activity to that of JM216. Upon reduction, JM216 and JM335 form Pt(II) complexes with *cis*- and *trans*-geometry respectively. The specific activity of these compounds is thought to be associated with their ability to produce DNA-interstrand adducts that cannot be recognised or repaired by gene-specific repair enzymes.<sup>62</sup>

#### 1.4 Development of polynuclear platinum complexes as anticancer agents

Polynuclear platinum complexes represent a new and distinct class of anticancer agents, in terms of their DNA binding features and antitumour activity from their mononuclear counterparts, particularly cisplatin. Several polynuclear platinum complexes with two or more linked platinum centers have been developed in order to improve their DNA binding ability (**Figure1. 6**).<sup>63,64,65</sup> These compounds are characterised by innovative DNA interactions, producing additional long-range inter- and intra-strand crosslinks (e.g. 1,4-inter-strand and 1,6-inter-strand CLs) which are not available in conventional mononuclear platinum complexes. In general, polynuclear compounds display high cytotoxicity on both cisplatin sensitive and resistant cancer strains. The diversified nature of the DNA cross links of these agents is more likely to be responsible for their remarkable cytotoxicity.



**Figure 1.6:** Selected multinuclear platinum complexes that have promising anticancer agents.

A multinuclear platinum complex that has been shown to improve cross-resistance to cisplatin is an analogous trinuclear platinum(II) complex,<sup>65</sup> BBR3464 (**Figure 1.6**). This complex can bind to DNA with its two terminal monofunctional [*trans*-Pt(NH<sub>3</sub>)<sub>2</sub>] platinum units. The tetra-ammine platinum linker also contributes to DNA interactions through electrostatic and H-bonding. BBR3464 represents the first polynuclear platinum complex to enter the clinical trials. It has shown good cytostatic effects more so in several cisplatin-resistant cancers. The latter compound has recently undergone phase II clinical stage of development.<sup>63,64,65</sup> The activity of BBR3464 and other multinuclear platinum complexes against cisplatin-resistant cancer strains may be attributed to a distinctly different mode of binding to DNA. The HMG-protein domain that triggers DNA repair enzymes which shield Pt-DNA adducts of cisplatin cannot recognise Pt-DNA adducts of BBR3464 and other polynuclear platinum complexes.<sup>65</sup> Therefore, the resistance mechanism based on DNA-damage recognition and DNA repair by enzymes can be excluded. When compared to conventional platinum chemotherapeutics, polynuclear compounds show an increased cellular uptake and rapid formation of DNA adducts.<sup>66</sup> This is most likely due to their amphiphilic nature (lipophilic linker and hydrophilic platinum-ammine terminal) which enhances their membrane permeability compared to cisplatin or oxaliplatin.<sup>66</sup> As a result, preclinical and clinical tests have shown that polynuclear complexes are indeed more active than mononuclear analogues. However, their remarkable efficacy was found to be also tainted by acute toxicity as

was the problem with several mononuclear counterparts, prohibiting any further clinical tests on some of these potential candidate drugs.<sup>67</sup>

## 1.5 The anticancer activity of other metal complexes

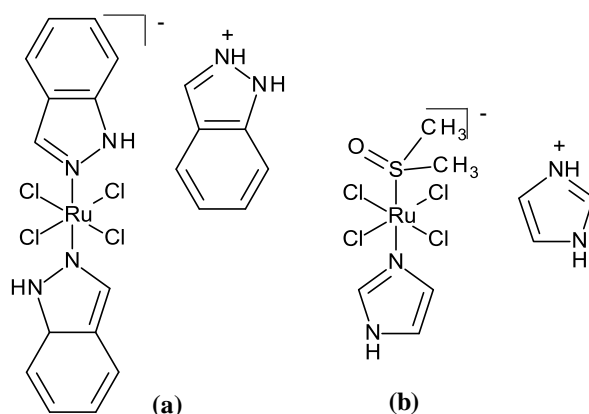
Preclinical and clinical studies have shown that the development of new metal complexes with improved biological and pharmacological properties is possible.<sup>68</sup> A few other metal complexes (including Fe, Co and Au) have been shown to exhibit promising cytostatic properties in preclinical studies, while those of Ti, Ru, and Ga were even evaluated in phase I and II clinical stage of development.<sup>68</sup> Metallocenes of Re, Mo, and Ni have also shown promising cytostatic properties *in vitro* and *in vivo*.<sup>68</sup> Although some of these compounds have been tested and proven to display anticancer activities, cisplatin and its analogues have by far displayed the best chemotherapeutic results.<sup>68</sup>

### 1.5.1 Ruthenium complexes as anticancer agents

This review will be limited to ruthenium-based anticancer chemotherapy, although a wide variety of other non-platinum containing metal complexes has been investigated for anticancer activities. Ruthenium(II) and ruthenium(III) exhibit relatively slow substitution reactions comparable to those of platinum(II) complexes. The slow ligand-exchange rates may prevent the deactivation of the drug, ensuring that the drug reaches its target without being modified. Under physiological conditions, various oxidation states (I, II and III) of ruthenium are accessible. Ru(II) complexes are usually less inert than their corresponding Ru(III) counterparts. As a result, Ru(III) complexes are thought to be prodrugs that undergo activation through reduction *in vivo*. The reduction of Ru(III) to Ru(II) is more favoured in tumours than in normal tissue, due to low oxygen content and low pH in tumour cells. Furthermore, extracellular reducing agents (such as glutathione (GSH)), and intracellular redox proteins may also enhance the reduction of Ru(III) to Ru(II).<sup>69</sup>

Various ruthenium complexes with monodentate heterocyclic ligands, amine or ammine have been synthesized for evaluation as anticancer agents.<sup>70</sup> Ru(III) complexes with the general formula  $[\text{RuCl}_4\text{L}_2](\text{HL})$ , where L is imidazole (im) or indazole (ind), have emerged as promising anticancer compounds.<sup>71</sup> The lead

compound,  $[\text{RuCl}_4(\text{ind})_2](\text{Hind})$  (KP1019; ind = indazole; **Figure 1.7 a**) displays anticancer activity against a number of cancer cell lines.<sup>71,72</sup> KP1019 has entered phase I clinical trial for anticancer activity, and is completely devoid of side effects.<sup>73</sup> KP1019 induces lethality at small dosages and has a higher therapeutic index than the imidazole derivative. Phase I clinical trial results have shown that the transferrin bound KP1019, as well as the apotransferrin modified  $[\text{RuCl}_4(\text{im})_2](\text{Him})$  exhibit superior anticancer activity compared to protein-free complexes.<sup>74</sup>



**Figure 1.7:** Antitumour Ru(III) agents, KP1019 (a) and NAMI-A (b) with promising cytostatic properties.

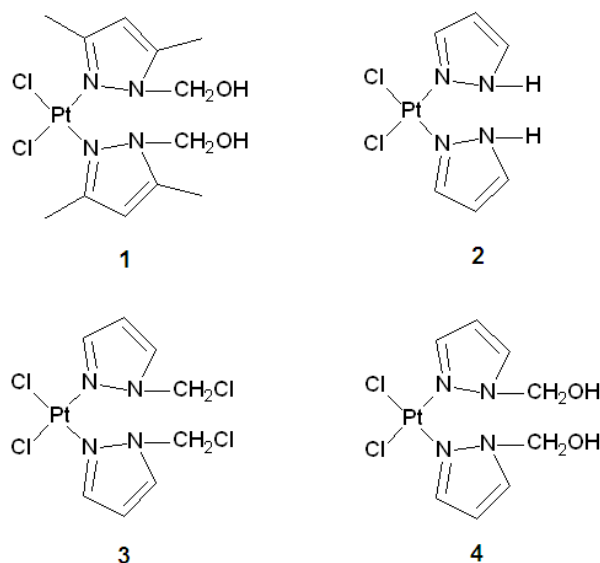
Another example is  $(\text{trans}-(\text{Him})[\text{RuCl}_4(\text{DMSO})(\text{H}_2\text{im})])$  (NAMI-A; **Figure 1.7 b**), which is the first Ru complex to accomplish phase I clinical trials and a recent evaluation candidate in phase II clinical trials.<sup>69,75</sup> Although this drug is inactive against tumour cells *in vitro*, it has shown significant efficiency against lung metastasis *in vivo*. NAMI-A is easily reduced to Ru(II) by bio-reducing agents under physiological conditions due to the labile S-bonded DMSO ligand.<sup>69</sup> Even though NAMI-A interacts with DNA *in vitro*, its anticancer activity does not appear to be related to DNA binding.<sup>76</sup> Instead, the anti-metastatic activity of this drug is related to its interaction with fibrous collagen of the lung and with the basement membrane of collagen type IV.<sup>76</sup> This significantly increases the thickness of the connective tissue around the tumour capsule and blood vessels, thereby blocking the blood flow to the tumour.<sup>76</sup>

## 1.6 Platinum(II) complexes with pyrazole-based ligands

### 1.6.1 Medical potential of pyrazole-based Pt(II) complexes

Complexes of pyrazole-based ligands are potential therapeutic agents and hold promise in medicine.<sup>77</sup> In particular, platinum complexes bearing N-donors have shown interesting biological activities in a wide range of diseases ranging from cancer to bacterial, viral and parasitic infections.<sup>77</sup> Pyrazole-metal based complexes have not been used extensively in medicine, compared to other metal complexes with N-donor atoms. A replacement of the inert amine non-leaving group (NH<sub>3</sub>) of cisplatin by N-containing heterocyclic ligands (e.g. pyridine and pyrazole) has been reported to afford complexes of decreased reactivity, leading to reduced toxicity.<sup>77</sup> Moreover, replacing the NH<sub>3</sub> group(s) of cisplatin with planar N-containing heterocyclic ligands does not considerably affect the DNA-binding ability of the complex and the formation of platinum-modified DNA.<sup>77</sup>

Thus, the rationale behind the improvement of the Pt-based drugs lies on the designing of kinetically inert platinum complexes, which have limited sensitivity towards deactivation by intracellular thiols, since this is thought to be responsible for the most severe side effects.<sup>41</sup> Ciesielka *et al.*<sup>78</sup> synthesized analogues of cisplatin in which the amine ligands of cisplatin were replaced with pyrazole. The cytotoxicity of the platinum complexes was evaluated against murine Leukemia cancer cell lines. The structures of the pyrazole Pt(II) complexes are shown in **Figure 1.8**. The cytotoxic properties of pyrazole-bearing analogues as well as their damages and modifications on DNA were compared to their respective parent compound, since DNA has been considered the major pharmacological target of cisplatin.



**Figure 1.8:** Structures of pyrazole derivatives of cisplatin evaluated for anticancer activity.<sup>78</sup>

The complexes displayed significant anticancer activity higher than the one for carboplatin, in terms of the IC<sub>50</sub> values, but relatively lower compared to the one for cisplatin. The cytotoxicity was dependent on the substituents introduced on the pyrazole ring. While complex (2) is an active anticancer agent, Sakai *et al.*<sup>79</sup> showed that its 3,5-dipyrazolecarboxylic acid analogue was inactive against human colorectal cancer cell line AGS and DLD-1. The carboxylic acids are known to be strong electron-withdrawing groups and would result in a diminished electron density on the coordinated pyrazole ring, which may be a possible explanation for the poor activity, since the complex may be pharmacokinetically unstable due to enhanced reactivity with other cellular nucleophiles. In spite of increased steric hindrance by substituents on the ligand system, complexes 1-4 (**Figure 1.8**) have the same electron density on the coordinated pyrazole moieties, and this accounts for similar cytotoxic properties.

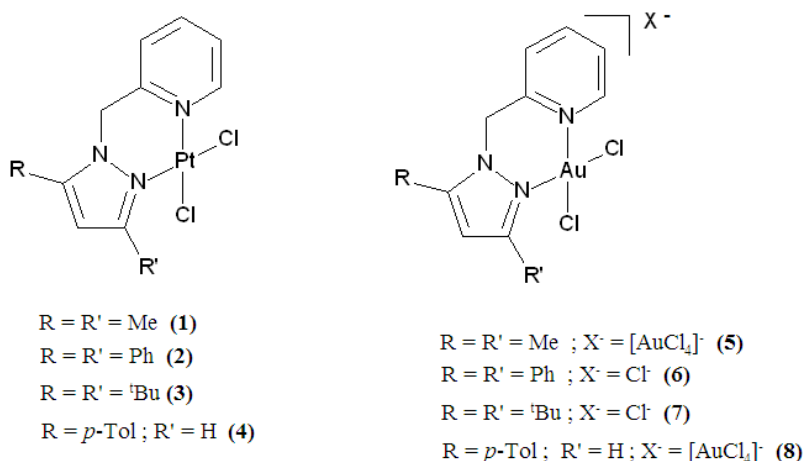
### 1.6.2 Cytotoxic studies of (pyrazolylmethyl)pyridine Pt(II) complexes

Since the discovery of the medical potential of pyrazole complexes, there has been a rapid growth in the synthesis of pyrazole derivatives for applications as anticancer, antiviral and anti-inflammatory agents.<sup>77</sup> Pyrazolyl ligands are easily modulated or fine-tuned to achieve the desired electronic and steric effects, which are necessary in



controlling the thermodynamic and kinetic properties of their respective metal complexes.

The (pyrazolylmethyl)pyridine Pt(II) complexes with bidentate ligands are more stable than their monodentate counterparts, because of the chelate effect. The (pyrazolylmethyl)pyridine coordinate to the metal centre *via* N-donors of pyrazole and pyridine forming a stable six-membered chelate ring. The methylene linker of the two rings confers moderate flexibility at the (pyrazolylmethyl)pyridine ligand. Segapelo *et al.*<sup>80</sup> evaluated the cytotoxicity of (pyrazolylmethyl)pyridine ligands and their respective Pt(II) and Au(III) complexes (**Figure 1.9**). All the complexes were active against Hela cancer cell line. The activities of the Pt(II) and Au(III) complexes were within the range of 10-20 times lower than cisplatin and also exhibited low tumor specificity. Growth inhibition of normal human lymphocytes cells (PBMC) were tested under the same experimental conditions. It was found that the complexes exhibit poor selectivity, indiscriminately killing both normal and cancerous cells. However, these complexes have superior activity than carboplatin, a widely used anticancer drug. Compared to platinum complexes, gold complexes displayed even lower cytotoxicity when tested against Hela cancer cell line. The low cytotoxicity of gold complexes is probably due to low stability of Au(III) which is usually reduced to Au(I).



**Figure 1.9:** Formulae of biologically active complexes evaluated against Hela cancer cell line.<sup>80</sup> These compounds hold promise for anticancer treatment.

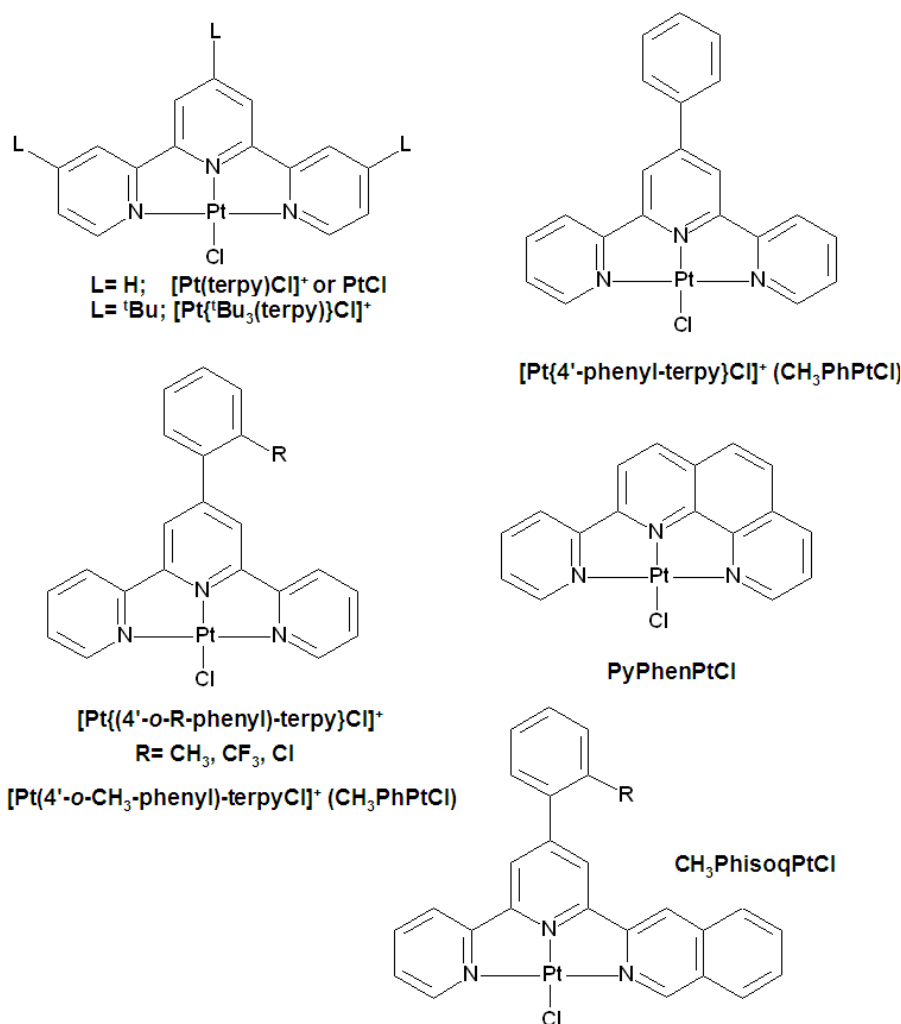
## 1.7 Mechanistic studies of Pt(II) complexes

### 1.7.1 The effect of substituents of a polydentate ligand on the rate of substitution

The influence of chelate substituents on the ligand substitution reactions was extensively studied by Jaganyi *et al.*<sup>81,82,83</sup> A series of platinum(II) complexes (**Figure 1.10**) were studied using neutral and ionic nucleophiles, *viz.* TU, DMTU, TMTU and  $I^-$  and  $SCN^-$ , respectively. The results have shown that the chloride ligand substitution is controlled by the electrophilicity of the Pt(II) centre, which is in turn dependent on the electronic properties of the non-leaving terpy ligand. The electron-donating groups decelerated the substitution reaction by reducing the  $\pi$ -back-bonding ability of the terpy fragment. On the other hand, electron-withdrawing groups increased the reactivity by enhancing the extent of  $\pi$ -back-bonding of the terpy fragment.<sup>81,82</sup> These observations are true when the substitution rate constants for  $[Pt\{tBu_3\text{-terpy}\}Cl]^+$  and  $[Pt(terpy)Cl]^+$  are compared.<sup>81b</sup> The slower reactivity of the former complex is due to the electron-donating *tert*-butyl groups on the terpy ligand, which reduce the  $\pi$ -acceptability of the ligand and hence reduce the electrophilicity of the metal centre. The same is true for  $[Pt\{4'\text{-phenyl-terpy}\}Cl]^+$  with the electron-donating phenyl ring at the 4' position of terpy, reducing the reactivity of the complex compared to  $[Pt(terpy)Cl]^+$ .

The presence of ancillary substituents on the *ortho* position of the 4'-phenyl ring attached to the terpy ligand also control the reactivity of the complexes by either reducing or enhancing the  $\pi$ -back-bonding of the terpy, depending on the electronic properties of the ancillary substituent. The presence of an electron-withdrawing trifluoromethyl ( $-CF_3$ ) group on the *ortho* position of the 4'-phenyl ring in  $[Pt\{4'-(o\text{-}CF_3\text{-phenyl})\text{-terpy}\}Cl]^+$  increases the  $\pi$ -back-bonding ability of the terpy ring. This increases the electrophilicity of the metal centre which in turn increases the rate of substitution compared to  $[Pt\{4'\text{-phenyl-terpy}\}Cl]^+$ . The opposite is true for  $[Pt\{4'-(o\text{-}CH_3\text{-phenyl})\text{-terpy}\}Cl]^+$ , which has an electron-donating methyl ( $-CH_3$ ) group on the *ortho* position of the 4'-phenyl ring. The reactivity of the complexes is therefore dependent on the electron-donating or electron-withdrawing strength of the substituents. The complexes with the strongest electron-withdrawing substituents

are more reactive, whereas those with the best electron-donating substituents are less reactive.



**Figure 1.10:** Platinum(II) terpy complexes studied by Jaganyi and co-workers.<sup>81,82,83</sup>

### 1.7.2 The role of an extended $\pi$ -conjugation in the ligand core on the rate of substitution

Most recently, the  $\pi$ -acceptor effect of N-donor tridentate ligands on the reactivity of platinum(II) complexes has been studied.<sup>81,82,83</sup> The extended  $\pi$ -conjugation in which pyridine formed part of the aromatic ring system has been shown to enhance the extent of  $\pi$ -back-bonding due to a favourable overlap of ligand  $\pi^*$ -orbitals with  $d\pi$ -orbitals of the metal.<sup>84</sup> Jaganyi and Ongoma<sup>83</sup> studied a series of mononuclear Pt(II) complexes bearing isoquinolyl and phenanthrolyl groups as part of the tridentate ligand. Their structures are labeled as **CH<sub>3</sub>PhisoqPtCl**) and **PyPhenPtCl**, respectively, in **Figure 1.10**.

It was found that the increase in the  $\pi$ -conjugation at the *cis/trans* position as in **PyPhenPtCl** (when compared to **PtCl**) strengthen the extent of  $\pi$ -back-bonding of the chelate backbone making the platinum centre more electrophilic. This accelerates the rate of chloride ligand substitution. However, the extended  $\pi$ -conjugation in the *cis* position as in **CH<sub>3</sub>PhisoqPtCl** (when compared to **CH<sub>3</sub>PhPtCl**) retards the substitution process, contrary to what was expected. The increase in the number of fused rings around the metal centre was expected to be accompanied by an efficient transfer of electron density from the *d*-orbitals of the metal ion into the extended and easily accessible molecular orbitals of the fused rings, leading to rapid substitution of the leaving group. The decreased rate of substitution was due to a more dominant *cis*  $\sigma$ -effect of the isoquinoline ring that facilitates the accumulation of the electron density on the Pt(II) center, reducing its electrophilicity.

### 1.8 Role of kinetic data in the development of drugs

While cisplatin is one of the most developed inorganic compounds and successful anticancer agent, it shows limited activity against the most common and recalcitrant forms of cancers such as those of the colon and breast. The clinical success of cisplatin is also limited by significant side effects, drug resistance (intrinsic and acquired), poor water solubility and intravenous administration. Therefore, much attention is still directed towards the designing of new platinum compounds with carrier groups that target tumour cells with high specificity, improving and expanding the range of antitumor activity spectrum. Recent cytotoxicity studies came up with new platinum complexes which exhibit remarkable anticancer activity against many cancer cell lines.<sup>77-80</sup> Some of these Pt(II) complexes are endowed with superior anticancer activity compared to cisplatin.

Since the understanding of the mechanistic pathways and the reactivity of metal complexes both *in vitro* and *in vivo* is vital for the rational design of new compounds with improved potency, kinetic studies on these new and improved potential drugs should be carefully undertaken. It is known that the reactivity of platinum complexes can be systematically tuned through steric and electronic properties to achieve the desired thermodynamic and kinetic properties. The data from such

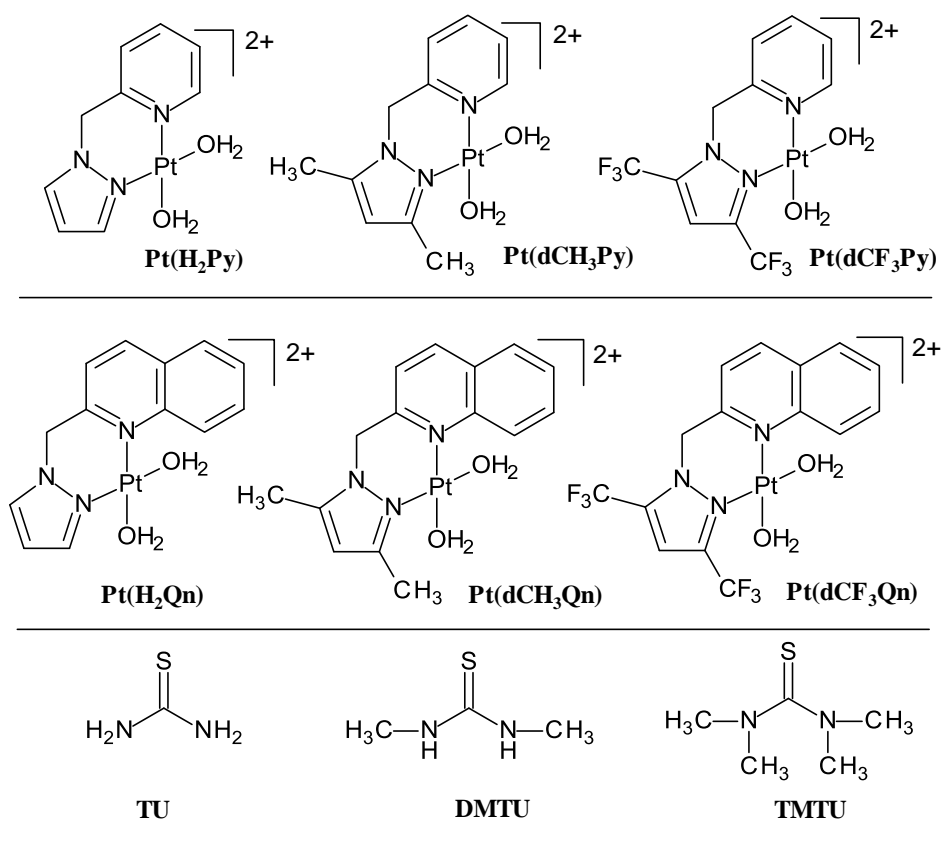
studies is crucial in understanding drug metabolism, chemo-protection as well as the influence of intrinsic reactivity on the mechanism of action. Kinetic data including mechanism of product formation from the substitution reactions of Pt(II) and model nucleophiles such as iodides, bromides, thiocyanate as well as nitrogen- and sulphur-donor nucleophiles such as azoles and thioureas are important in understanding the fate of the drug after administration.

### 1.9 Aims and objectives of the research

Recent work by Jaganyi *et al.*<sup>81,83,85</sup> has concentrated on the modification of the tridentate N-donor ligands by either varying the number of  $\pi$ -accepting pyridine rings and through direct substitution of the pyridine ring with an electron-donating or electron-withdrawing group, in order to modulate the reactivity of the Pt(II) centre by controlling the extent of  $\pi$ -back-bonding. The anomalous decrease in the rate of substitution with an increase in the  $\pi$ -conjugation has caught our interest in this study.<sup>83,84,86</sup> Jaganyi and Kinunda<sup>87</sup> have most recently reported the effect of the extended  $\pi$ -conjugation of a quinoline ring positioned *cis* to the leaving group on the reactivity of the tridentate Pt(II) complexes. The observed trend in the reactivity was contrary to the expected higher reactivity based on the increase in  $\pi$ -conjugation as reported elsewhere in the literature.<sup>81,84,85</sup>

There is a limited information on the influence of the  $\pi$ -conjugation of a coordinated bidentate ligand on the reactivity of bifunctional Pt(II) complexes. In order to extend our understanding of the role of substituents on the core ligand in controlling the extent of  $\pi$ -back-bonding, part of this study was to look into the effect of introducing electron-donating and electron-withdrawing groups in the 3,5-positions of the pyrazole ligand in bifunctional Pt(II) complexes endowed with *N,N*-(pyrazolylmethyl)pyridine/quinoline chelates. Therefore this work enables the investigation of the competing effect of the  $\sigma$ -donor or  $\pi$ -acceptor strength of the pyrazole ligand positioned *cis* or *trans* to the aqua leaving groups, on the rate of substitution reaction in a series of bifunctional Pt(II) complexes. The structures of the Pt(II) complexes and the nucleophiles studied are shown in **Figure 1.11**. It will also report on the effect of the  $\pi$ -conjugation incorporated into the (pyrazolylmethyl)-

quinoline by making a direct comparison with one of the (pyrazolylmethyl)pyridine analogue.



**Figure 1.11:** Structures of bifunctional Pt(II) complexes with *N,N*-bidentate chelate and the nucleophiles used for kinetic investigations. The counter anions of the complexes are omitted for simplicity.

Sulphur-containing bio-relevant nucleophiles i.e. thiourea (TU), *N,N'*-dimethylthiourea (DMTU), and *N,N,N',N'*-tetramethylthiourea (TMTU) will be used as substituting nucleophiles. The choice of nucleophiles was made based on their difference in nucleophilicity, steric hindrance and binding properties. TU and its derivatives have a combination of thiolates ( $\pi$ -donor) and thioether ( $\sigma$ -donor and  $\pi$ -acceptor) ligand properties similar to those found in biological nucleophiles.<sup>88</sup> In addition, TU and other sulphur-containing molecules (e.g. cysteine and glutathione) are used as protective agents against nephro- and neuro-toxicity following cisplatin administration.<sup>88</sup> Therefore understanding how Pt(II) complexes interact with S-

containing bio-relevant molecules is of vital importance from the medicinal and biological point of view.

### **1.9.1 Pt(II) complexes with flexible (pyrazolylmethyl)pyridine and (pyrazolylmethyl)quinoline bidentate chelates**

This study was divided into two parts with different but interrelated aims and specific objectives. This thesis will report on the:

- synthesis and characterization of dichloro bifunctional Pt(II) complexes with flexible and versatile 2-(3,5-disubstituted-pyrazolylmethyl)quinoline and 2-(3,5-disubstituted-pyrazolylmethyl)pyridine chelates as well as their respective unsubstituted analogues .
- preparation of their respective diaqua complexes in solution and determination of the  $pK_a$  values of the coordinated aqua ligands as a measure of their electrophilicity and hence the reactivity of the Pt(II) centre.
- effect of replacing the  $\pi$ -acceptor pyridine ring with a quinoline in a flexible bidentate chelate on the reactivity of the complex by following the substitution of the coordinated aqua ligands by S-containing nucleophiles *viz.* TU, DMTU and TMTU.
- effect of modulating the donicity of the substituted pyrazole ring on the reactivity of the complex by bringing in electron donating or withdrawing ancillary groups on the ring, while maintaining the pyridine or quinoline ring constant.
- data from computational modelling of the diaqua complexes to understand the low energy structural geometries of the complexes and how it supports observed trends in reactivity.
- on how electronic and steric properties of the synthesised complexes can be used to modulate their reactivity.

## 1.10 References

---

1. D. E. Reichert, J. S. Lewis, C. J. Anderson. *Coord. Chem. Rev.*, 999, **184**, 3.
2. C. Xin Zhang and S. J. Lippard, *Current Opinions in Chem. Biol.*, 2003, **7**, 481.
3. P. C. A. Bruijninx, P. J. Sadler. *Curr. Opinions In Chemistry and Biology.*, 2000, **12**, 197.
4. S. P. Gupta, *Chem. Rev.*, 1994, **94**, 1507.
5. K. B. Burck, E. T. Liu, J. W. Larrick, *Oncogenes: An Introduction to The Concept of Cancer Genes*, Springer-Verlag, New York, 1988.
6. B. Alberts, D. Bray, J. Lewis, N. Raff, K. Roberts, J.D. Watson, *Molecular Biology of The Cell*, Garland publishing, Inc., New York, 3<sup>rd</sup> edn., 1994.
7. J. B. Weiltzman, M. Yaniv, *Nature*, 1999, **400**, 401.
8. W. C Hahn, C.M. Counters, A. S. Lundburg, R. L. Beijersbergen, M. W. Brooks, R. A. Weiburg, *Nature*, 1999, **400**, 464.
9. A. W. Murray, *Nature*, 1992, **359**, 599.
10. L. H. Hartwell, M. B. Kastan, *Sciences*, 1994, **266**, 1821.
11. J. Reedijk, *Chem. Commun.*, 1996, 801.
12. B. Rosenberg, L. Van Camp, J. E. Trosko and V. H. Mansour, *Nature*, 1969, **222**, 385.
13. B. K. Klepper, *Metal Complexes in Cancer Chemotherapy*, VCH, New York, 1993.
14. E. Wong, C.M. Giandromenico, *Chem. Rev.*, 1999, 4251.
15. M. J. Cleare and J.D. Hoeschele. *Bioinorg. Chem.*, 1973, **2**, 187.
16. M. J. Cleare and J.D. Hoeschele, *Plat. Met. Rev.*, 1973, **17**, 3.
17. C. J. Jones and J. R. Thornback, *Medical Applications of Coordination Chemistry*, Cambridge, 2007, p 1, 218-257.
18. P. S. Singupta, R. S. Sinha, S. K. Bera and G.S. De, *Ind. J. Chem., Sect.A.*, 2002, **41(A)**, 712.
19. A. Bakalova. *Journal of the University of Chemical Technology and Metallurgy*, 2006, **41(2)**, 119.
20. W. Zhan, T.C. Link, M. P. O' Connor, A. Reed, R. Parker, S. B. Howell and V. Bohr, *Mol. Cell. Biol.*, 1992, **12**, 3689.



21. X. Wan, Z. Guo. *Chem. Soc. Rev.*, 2013, **42**, 202.
22. T. W. Hambley, *Coord. Chem. Rev.*, 1997, **166**, 181.
23. C. M. Sorenson and A. Eastman, *Cancer Rev.*, 1988, **48**, 4484.
24. S. E. Crider, R. J. Holbrook and R.J. Franz, *Metallomics.*, 2010, **7**, 19.
25. (a) X. Wang, and Z. Guo, *Anti-Cancer Agents Med. Chem.*, 2007, **7**, 19. (b) J. Vinje and E. Sletten, *Anti-Cancer Agents Med. Chem.*, 2007, **7**, 35.
26. N. A. Kas'yanenko, E. E. E. Aia, A. A. Bogdanov, Y.V. Kosmotynskaya and K. I. Yakovlev, *Mol. Biol.*, 2002, **36**, 745.
27. A. A. Tulub and V. E. Stefanov, *Int. J. Biol. Macromol.*, 2001, **28**, 191.
28. J. Bogojeski, Ž. D. Bugarčić, R. Puchta, R. van Eldik. *Eur. J. Inorg. Chem.*, 2010, 5439.
29. J. Kozelka, F. Longendre, F. Reeder, J.-C. Chottard, *Chem. Rev.*, 1999, **61**, 190.
30. V. Brabec *et al.* *Biochem. Pharm.*, 2007, **73**, 1887.
31. J. Reedijk, *Chem. Commun.*, 1996, 801.
32. E. R. Jamieson, S. J. Lippard, *Chem. Rev.*, 1999, **99**, 2467.
33. S. M. Cohen and S. J. Lippard. *Prog. Nucleic Acid Res. Mol. Biol.*, 2001, **67**, 93.
34. M. Kartalon, J. M. Essigmann. *Mutat. Res.*, 2001, **487**, 1.
35. J.-M. Teuben, M. R. Zubiri, J. Reedijk, *J. Chem. Soc., Dalton Trans.*, 2000, 369.
36. Ž. D. Bugarčić, B. V. Diordević, *Monatshefte für Chemie.*, 1998, 1267.
37. T. Peleng-Shulman, Y. Najajreh, D. Gibson, *J. Inorg. Biochem.*, 2002, **91**, 306.
38. A. Pasini and C. Fiore, *Inorg. Chim. Acta.*, 1999, **285**, 249.
39. V. Capeda, M. A. Fuertes, J. Castilla, C. Alonso, C. Quevedo, J. M Perez, *Anti-cancer Agents In Med. Chem.*, 2007, **7**, 3.
40. N. Farell, *Cancer Invest.*, 1993, **11**, 578.
41. E. Wong, C. M. Giandomenico. *Chem. Rev.*, 1999, **99**, 2451.
42. S. Komeda, S. Bombard, S. Perrier, J. Reedijk, J. Kozelka, *J. Inorg. Biochem.*, 2003, **96**, 357.
43. S. Komeda, G. V. Kalayda, M. Luts, A. L. Spek. Y. Yamanaka, T. Sato, T. Chikuma, J. Reedijk, *J. Med. Chem.*, 2003, **46**, 1210.
44. C. H. Versantvoort, H. J. Broterman, T. R. Badrij. J. Scheper and P. R. Twentyman, *J. Cancer*, 1995, **72**, 82.

45. P. J. Sadler and Z. Guo, *Pure & Appl. Chem.*, 1998, **70**(4), 863.
46. R. B. Weiss, M. C. Christian. *Drugs*, 1993, **46**, 360.
47. L. S. Hollis, W. I. Sundquist, J. N. Burstyn, *et al.*, *Cancer Res.*, 1991, **51**, 1866.
48. J. C. Dabrowiak, W. T. Bradner. *Prog. Med. Chem.*, 1987, **24**, 129.
49. M. K. Anderson, D. A. Quagliato, *et al.*, *Cancer Treat. Rep.*, 1986, **70**, 997.
50. A. Rahman, J. K. Roh, M. K. Wolpert-deFilippes, A. Golden, *et al.*, *Cancer Rev.*, 1988, **48**, 1745.
51. L. S. Hollins, W. I. Sundquist, J.N. Burstyn, *et al.*, *Cancer Rev.*, 1991, **51**, 187.
52. A. S Abu-Surrah, M. Kettunen. *Curr. Med. Chem.*, 2006, **13**, 1337.
53. D. Lebowhl, R. Canitta. *Eur. J. Cancer*, 1998, **34**, 1522.
54. J. Reedijk, *Platinum Metals Rev.*, 2008, **52**(1), 2.
55. P. J. Dyson and G. Sava, *Dalton Trans.*, 2006, **16**, 1929.
56. (a) N. Farrell, *Met. Ions Biol. Sys.*, 1996, **32**, 603. (b) N. Farrell, *Eur. J. Inorg.*, 2009, 1293.
57. M. A. Jakupec, M. Glanski, B. K. Klepper, *Rev. Physiol. Biochem. Pharmacol.*, 2003, **146**, 1.
58. M. D. Hall, T. W. Hambley, *Coord. Chem. Rev.*, 2002, **232**, 49.
59. L. R. Kelland, G. Abel, M. J. McKeage, M. Jones, D. M. Goddard, M. Valenti, B. A. Murrer, K. R. Harrap, *Cancer Res.*, 1993, **53**, 2581.
60. E. M. Bengtson, J. R. Rigas, *Drugs*, 1999, **58**, 57.
61. M. J. Mc Keage, F. Raynaud, J. Ward, C. Berry, D. Odell, L. R. Kellard, B. Murrer, B. Santabarabara, K. R. Harrap, I. R. Judson, *J. Clin. Oncol.*, 1997, **15**, 2691.
62. J. Holford, S.Y. Sharp, B. A. Murrer, M. Abams, L. R. Kelland, *Br. J. Cancer*, 1998, **77**, 360.
63. V. Brabec, J. Kasparkaova, O. Novakava, *Biochem.*, 1999, **38**, 6781.
64. N. J. Wheate, J. G. Collins. *Curr. Med. Anticancer Agents*, 2005, **5**, 267.
65. T. Banerjee, N. Dubey, R. Mukhopadhyay. *Biochemie*, 2005, **92**, 846.
66. C. Billecke, S. Finnis, L. Tahash, C. Miller, T. Mikkelsen, N. P. Farrell, O. Böglér, *Neuro-Oncology*, 2006, **8**, 215.

67. P. P. Calvert, M. S. Highley, A. N. Hughes, E. R. Plummer, A. S. Azzabi, M. G. Camboni, E. Verdi, A. Bernareggi, M. Zucchetti, and A. M. Robinson. *Clin. Cancer Res.*, 1999, **5**, 3796.
68. I. Ott and R. Gust. *Arch. Pharm*, 2007, **340**(3), 117.
69. G. Sava, A. Bergamo, S. Zorzet, B. Gava, C. Casarse, M. Cocchietto, M. Furlani, V. Scacia, B. Serli, E. Iengo, E. Alessio, G. Mestroni, *Eur. J. Cancer*, 2002, **38**, 427.
70. M. J. Clarke, *Coord. Chem. Rev.*, 2003, **236**, 209.
71. M. H. Seeling, M. R. Berger, B. K. Keppler, *J. Coord. Res. Clin. Oncol.*, 1992, **118**, 195.
72. B. Keppler, M. Hartmann, *Metal-Based Drugs*, 1994, **1**, 145.
73. M. R. Beger, F. T. Garzon, B. K. Keppler, D. Schemahl, *Anticancer Res.*, 1989, **9**, 761.
74. F. Kratz, B. K. Keppler, M. Hartmann, L. Messori, M. R. Berger, *Metal-Based Drugs*, 1996, **3**, 15.
75. E. Alessio, G. Mestroni, A. Bergamo, G. Sava, *Metal Ions in Biological Systems*, 2004, **42**, 323.
76. F. K. Keter, J. Darkwa, *Biometals*, 2012, **25**(9), 9.
77. S. Zorzet, A. Bergamo, M. Cocchietto, A. Sorc, B. Gava, E. Alessio, E. Iengo, G. Sava, *J. Pharmacol. Exp. Ther.*, 2000, **295**, 927.
78. E. Ciesielska, A. Szulawska, K. Studzia, J. Ochocki, K. Malinowska, K. Kik, L. Szmigiero, *J. Inorg. Biochem.*, 2006, **100**, 1579.
79. S. Sakai, Y. Tomita, T. Ue, K. Goshima, M. Ohminato, T. Tshubomuna, K. Matsumoto, K. Ohmura, K. Kawakami, *Inorg. Chem. Acta.*, 2000, **297**, 64.
80. T. V. Segapelo, I. A. Guzei, L. C. spencer, W. E. Van Zyl, J. Darkwa, *Inorganica Chemica Acta*, 2009, **362**, 3314.
81. (a) D. Jaganyi, D. Reddy, J. Gertenbach, A. Hofmann, and R. van Eldik, *Dalton Trans.*, 2004, 299. (b) D. Jaganyi and D. Reddy, *Dalton Trans.*, 2008, 6724.
82. D. Jaganyi, K.-L. De Boer, J. Gertenbach, J. Perils, *Int. J. Chem. Kinet.*, 2008, 808.
83. P. Ongoma and D. Jaganyi, *Dalton Trans.*, 2012, **41**, 10724.
84. A. Shaira, D. Reddy and D. Jaganyi, *Dalton Trans.*, 2013, **42**, 8426.

85. A. Hofmann, D. Jaganyi, O. Q. Munro, G. Liehr, and R. van Eldik, *Inorg. Chem.*, 2003, **42**, 1688.
86. D. Reddy, K. Akerman, M.P. Akerman, D. Jaganyi, *Transition Met. Chem.*, 2011, **36**, 593.
87. G. Kinunda and D. Jaganyi, *Transition Met. Chem.*, 2014, **39**, 451.
88. (a) W. C. Schiessl, N.K. Summa, C. F. Weber, S. Gubo, C. Dücker-Benfer, R. Puchta, N. T. van Eikema Hommea, and R. van Eldik, *Z. Anorg. Chem.*, 2005, **631**, 2812. (b) M. T. Ashby, *Comments Inorg. Chem.*, 1990, **10**, 297.

# Chapter 2

---

## Theoretical aspects on the substitution reactions of inorganic compounds focusing on platinum (II) complexes

### 2.0 Introduction

Substitution reactions are single-replacement reactions of a functional group by another group. Inorganic substitution reactions include the displacement of the ligand from a coordination complex by another. The substitution reactions in inorganic chemistry can be classified as Lewis acid-base reactions in which a positively charged metal ion can act as a Lewis acid and the coordinated ligand acts as a Lewis base. Mechanisms for such reactions have been studied for  $d^8$  Pt(II) square planar complexes as well as for complexes of other metal ions such as Pd(II), Au(II), Ni(II), Ir(I) and Rh(I).<sup>3,4</sup> Ligand substitution reactions involving complexes of these metal ions play a fundamental role in homeostasis, anticancer therapy and homogeneous catalysis. For example, in the treatment of tumours, metallo-drugs such as cisplatin are designed to inhibit tumour growth by replacing the chloride ligand with guanosine base of DNA.<sup>1,2</sup>

This chapter covers the general mechanistic pathways for substitution reactions of  $d^8$  square-planar Pt(II) complexes i.e. classification of reaction mechanisms as well as other factors that affect the reactivity of these complexes.

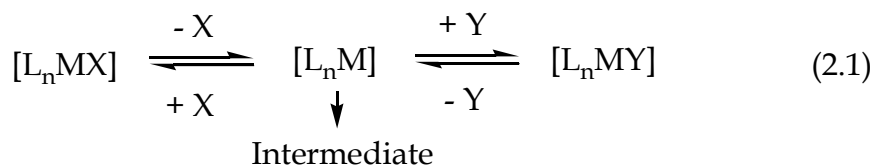
### 2.1 Classification of Inorganic reaction mechanisms

In an attempt to classify inorganic substitution reactions based on their mechanistic schemes, Langford and Grey<sup>5</sup> introduced the stoichiometric mechanism of substitution which exists in three forms; associative, dissociative and interchange mechanism.

#### 2.1.1 Dissociative mechanism (*D*-mechanism)

This reaction pathway involves the formation of an intermediate with a reduced coordination number as the reaction proceeds. The intermediate is generated through the bond breaking of the leaving group (X) prior to the attachment of the

entering group (Y) to the coordination sphere (M). The reaction scheme for this mechanism can be summarised as follows;

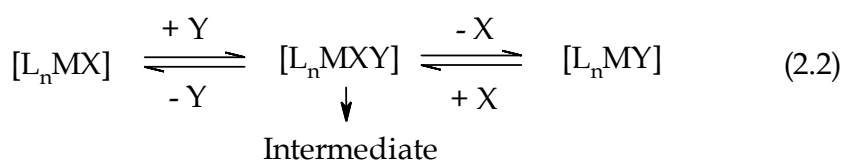


The rate of the reaction is dependent on the bond breaking step and is insensitive to the nature of the entering group. Since the breaking of the bond between the metal and the leaving group also affects the rate determining step; the nature of the leaving group affects the rate of its substitution from the metal ion.

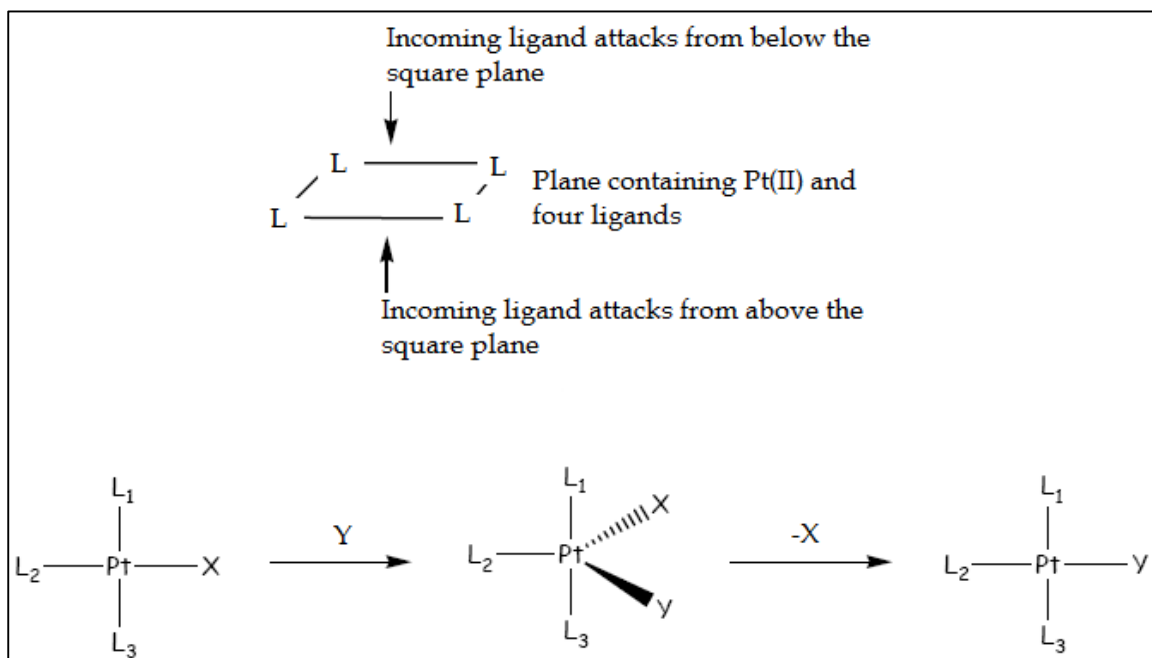
*D*-mechanism of substitution is common in octahedral metal complexes of the first transition metal series because they are coordinatively saturated i.e. they have reached their maximum stable coordination number of six. In square-planar complexes, the *D*-mechanistic pathway leads to the formation of a 14-electron, T-shaped transition state. For square planar complexes, the dissociative mechanism will only occur when very bulky spectator ligands or good leaving groups are coordinated to the metal centre in the presence of a strongly coordinating solvent.<sup>6</sup> Bulky ligands will destabilise the ground state energy as well as obstruct the approach of a nucleophile. On the other hand, a good leaving group will enhance the bond breaking between itself and the metal centre. When this dominates over the approach of an incoming nucleophile, the dissociative mechanism is favoured.

### 2.1.2 Associative mechanism (A-mechanism)

This reaction pathway is characterised by the formation of an intermediate with an increase in the coordination number.<sup>7</sup> The intermediate is formed between the metal centre and the entering group prior to the displacement of the leaving group. The reaction scheme for this mechanism can be summarised as follows;



The bond formation between the metal centre and the entering group is the rate-determining step, and therefore the rate of the reaction is dependent on the entering group. The rate of the reaction is not very sensitive to the leaving group. The associative mechanism of substitution is the most common mechanism for coordinatively unsaturated metal complexes especially for  $d^8$  square-planar complexes. The mechanism usually proceeds *via* the formation of a 5-coordinate transition state intermediate with a trigonal bipyramidal geometry (**Figure 2.1**). In the transition state, the entering nucleophile (Y), the leaving group (X) and the ligand *trans* to the leaving group ( $L_2$ ) occupy the trigonal plane, while the other two non-labile groups ( $L_1$  and  $L_3$ ) that were formerly coordinated in a *cis* position to the leaving group occupy the axial positions. Throughout the substitution, the spatial arrangement of the groups in the transition state is maintained, thus leading to the substitution process with a retained configuration. Associative mechanistic pathways are also characterised by an increase in the micro-static order of arrangement of species in the transition state. This is because A-mechanism proceeds *via* a contracted transition state with a greater extent of bond making.

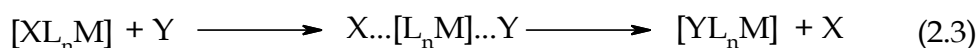


**Figure 2.1:** A representation of the direct attack by the entering ligand at the square planar Pt(II) centre below or above the plane. The nucleophile (Y) coordinates to give the trigonal bipyramidal intermediate species which loses the leaving group (X) with the retention of the stereochemistry.

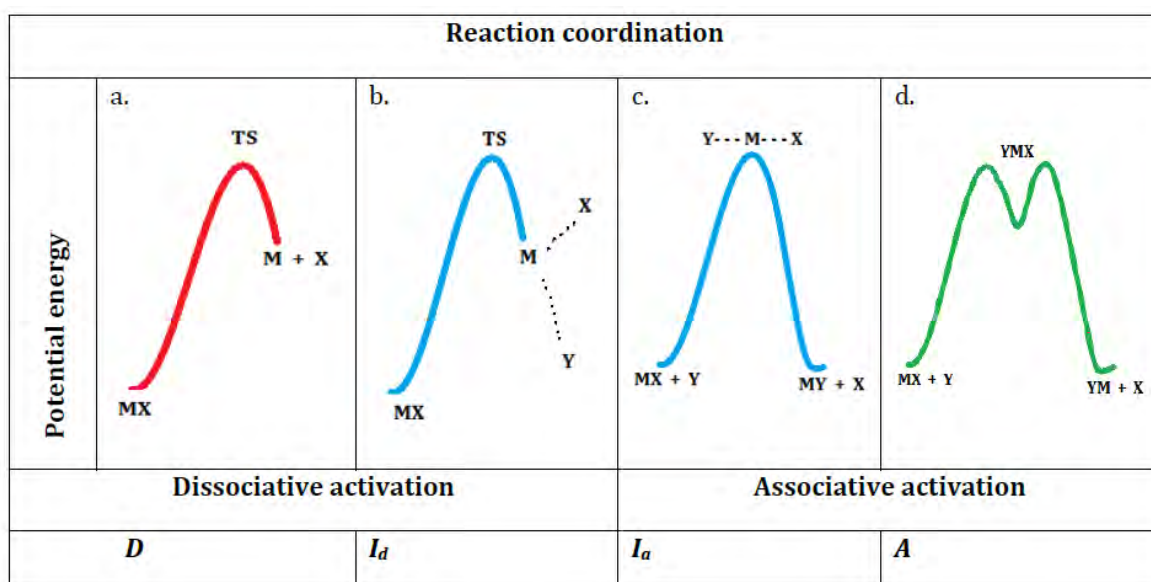
This corresponds to a decrease in both volume and entropy of activation of the activated complex compared to the ground states of the reactants. Thus, the change in the volume of activation ( $\Delta V^\ddagger$ ) is negative since the coordinative partial volume of the transition state is smaller compared to the volume of the complex and the nucleophile before the substitution reaction. The change in entropy of activation ( $\Delta S^\ddagger$ ) is also negative, indicative of the more ordered microstates for the substitution process at the transition state.<sup>8</sup>

### 2.1.3 Interchange mechanism (I-mechanism)

For this reaction pathway, bond formation between the metal centre and the entering group as well as the bond breaking between the metal centre and the leaving group occur at the same time.<sup>9</sup> As a result, there is no observable intermediate during the reaction. The reaction scheme for this mechanism can be summarised as follows;



The energy-reaction coordinate diagrams illustrating dissociative, associative and interchange processes and respective intermediates formed are shown in **Figure 2.2**, where X= leaving group and Y= entering group.



**Figure 2.2:** The reaction-energy profiles for the associative (*A*), associative interchange (*I<sub>a</sub>*), dissociative interchange (*I<sub>d</sub>*) and dissociative mechanism (*D*).<sup>5</sup>



The interchange reaction mechanism may be divided into two other reaction pathways according to various transition states formed:<sup>5</sup>

- **associatively activated interchange reaction mechanism ( $I_a$ -mechanism)** is the one in which the transition state consists of substantial bonding of the metal centre to both the leaving and the entering group. Usually the bond formation between the incoming ligand and the metal centre dominates over the bond breaking with the leaving group, and the rate of the reaction shows sensitivity on the nature and concentration of the entering ligand. The rate of this reaction is insensitive to the concentration of leaving group.
- **dissociatively activated interchange mechanism ( $I_d$ -mechanism)** is the one in which a transition state consists only of very weak bonding from the metal centre to both the leaving and the entering group. On the other hand, if the bond breaking dominates over bond formation, and the rate of the reaction is influenced by the leaving group, the mode of activation becomes dissociatively interchange mechanism ( $I_d$ ). The rate of this reaction is not affected by the nature and concentration of the entering group.

## **2.2 Influence of the coordinated ligands around the metal centre on the mechanism of substitution**

Both ground and transition state geometries of the coordination compounds are controlled by electronic and steric factors of the coordinated ligands around the central atom. Various factors determine the changes from the ground state to the transition state. For example, the observed mechanism of substitution may be dependent on the number of ligands coordinated around the central atom. The more ligands surrounding the central atom, the more difficult it is for the next ligand to attach on the metal centre. Logically, metal centres with large number of ligands coordinated should favour a dissociative mechanism, while centres with few ligands coordinated should favour an associative mechanism.

### 2.3 Ligand-exchange reactions at square-planar Pt(II) metal centre

Theoretically, substitution reactions of square-planar complexes would be expected to proceed most readily by an increase in the coordination number due to the attachment of the entering group to the coordination sphere.<sup>10,11</sup> For electronic and steric reasons, these reactions are also expected to favour biomolecular nucleophilic substitution or an associative reaction mechanism. The metal complex is susceptible to nucleophilic attack above and below its plane as there is no obstruction of the incoming ligand in both positions (**Figure 2.3**). The expansion of the coordination number readily occurs as complexes of more than four coordinated groups around the central atom are common. Furthermore, the low-spin  $d^8$  system of a central atom comprises a vacant  $p_z$ -orbital of relatively low energy that may accommodate a pair of electrons donated by the incoming ligand.

Pt(II) complexes are favoured when studying square-planar substitution reactions because they are generally thermodynamically stable and insensitive to oxidative addition.<sup>11</sup> Moreover, they also display moderate to slow kinetic lability (slow reactivity) in their ligand-exchange reactions.<sup>12</sup> In contrast to Pt(II) complexes, analogous complexes derived from metal ions with +2 oxidation state {e.g. Pd(II) or Ni(II)} or other  $d^8$  metal ions {e.g. Ir(I), Rh(I) or Ru(III)} are thermodynamically unstable, sensitive to oxidative addition and undergo rapid ligand-exchange reactions.<sup>13,14</sup> A relatively low reactivity or kinetic stability and stable redox behaviour of Pt(II) complexes lead to simple, easily monitored and interpreted kinetics. As a result, extensive research has been done on mechanistic and kinetic behaviour of ligand-exchange reactions on Pt(II) complexes.<sup>12-14</sup>

In spite of their differences in kinetic stability and redox behaviour, data gathered for Pt(II) complexes can also be applied to analogous square-planar complexes due to similarities in their reaction mechanism.<sup>10,15</sup> For example, ligand-exchange behaviour of Pd(II) complexes is known to be very similar to that of Pt(II) complexes often with reaction rates of five orders of magnitude faster than Pt(II) analogue.<sup>11,15</sup> Like Pt(II) complexes, analogous Au(III) complexes are also effective as anticancer agents, however, they are usually thermodynamically unstable and are readily

reduced to Au(I) and Au(0).<sup>15,16</sup> This analysis indicates that a continued study on ligand-exchange reactions of Pt(II) complexes remains an essential area in rational drug design and synthesis. Parameters such as electronic and steric effects may be used to modulate the reactivity and solubility of the metal complexes. Particularly for platinum-based anticancer drugs, these parameters may be used to ameliorate the drug potency as well as widen the anticancer activity spectrum.

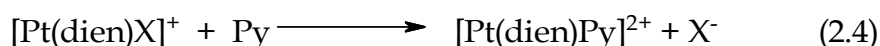
Ligand substitution reaction kinetics on square-planar Pt(II) complexes and mechanistic investigations are important in understanding how Pt-based drugs achieve their desired anticancer activity. Structural attributes using model compounds could be systematically investigated both thermodynamically and kinetically to unveil the underlying mechanism for the interaction of these drugs with their target material *viz.* genomic DNA and bio-competing deactivating species such as plasma proteins (cysteine and methionine) and other intracellular bio-regulating thiols such as glutathione.

## 2.4 Factors affecting the reactivity of square-planar Pt(II) complexes

### 2.4.1 Effect of the leaving group

The effect of the leaving group is more significant in the substitution reactions that follow dissociative pathway compared to the ones in which the reaction pathway is associative. The type and nature of the leaving group has a remarkable influence on the rates of ligand-exchange reactions on square planar complexes.

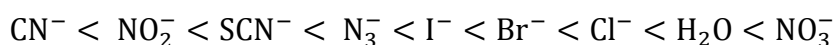
The extent of this influence is determined by the degree in which bond breaking between the metal centre and the leaving group occurs. A classic example elaborating on the influence of the leaving group on the square planar substitution reactions is the reaction of [Pt(dien)X]<sup>+</sup> with pyridine (*Equation 2.4*).<sup>17,18</sup> The kinetic data is reproduced in **Table 2.1**.



**Table 2.1** The effect of different leaving groups on the rate of substitution of X in  $[\text{Pt}(\text{dien})\text{X}]^+$  complexes at 25°C.<sup>17,18</sup>

Ligand X	$k_{\text{obs}} / 10^6 \text{ s}^{-1}$
$\text{NO}_3^-$	Very fast
$\text{H}_2\text{O}$	1900
$\text{Cl}^-$	35
$\text{Br}^-$	23
$\text{I}^-$	10
$\text{N}_3^-$	0.83
$\text{SCN}^-$	0.30
$\text{NO}_2^-$	0.05
$\text{CN}^-$	0.017

It was found that the rate of substitution reaction increased in the order;



for the displacement of X by the pyridine ligand. Generally, it is much easier to displace the ligands which are less nucleophilic than those which are more nucleophilic. Although the reactivity of square-planar complexes strongly depends on the nature of the incoming group, this data shows a clear dependence of the rate of substitution on the leaving group.<sup>17,18</sup> This shows that the strength of the Pt–X bond influences the rate of dissociation in the transition state. Further insight on the effect of the leaving group on the reactivity of square planar complexes could be obtained from the activation parameters e.g. activation volume, enthalpy and entropy. This could provide evidence for the extent of bond breaking in the transition state.

#### 2.4.2 Effect of the entering ligand

The incoming ligand is markedly important when dealing with the substitution reactions that follow an associative pathway. The magnitude of the second-order rate constants ( $k_2$ ) quantifies the rate at which the incoming ligand substitutes the

leaving group. The rate of the substitution reaction is dependent on the nucleophilicity of the incoming ligand. The nucleophilicity is a measure of how readily the nucleophile is able to attack an electron deficient centre (Pt(II) metal centre). Therefore, the stronger the nucleophile the faster the rate of substitution of a particular Pt(II) complex. The nucleophilicity of the ligand is usually characterised by the following several factors:<sup>7,10,16</sup>

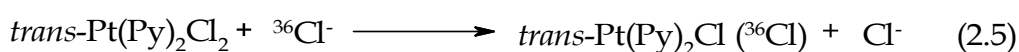
- a) basicity            The basicity of the ligand is usually characterised by its  $pK_a$  values and is directly proportional to the nucleophilicity of the ligand towards the metal centre.
- b) oxidizability    Ligands that are strongly oxidized (strong reducing agents) are considered good nucleophiles. The oxidizability of the ligand can be identified from their electron reduction potential.
- c) polarizability    The polarization of the ligand is better explained by the Pearson's Hard Soft Acid Base (HSAB) theory which stated that hard acids<sup>1</sup> prefer hard bases and soft acids prefer soft bases. An increase in the polarizability increases the effectiveness of the entering group in attacking the metal centre by increasing its electron donor ability.
- d) solvation energy    Ligands that are strongly solvated are considered weak nucleophiles because energy is required to remove the bound solvent molecules or to free the ligand before it coordinate to the metal centre.
- e) metal centre      An increase in the polarizability of the metal centre also increases the effectiveness of the attacking nucleophile. Heavier metals are better polarised in the transition state, therefore the corresponding rate of substitution follow the trend  $Ni(II) \gg Pd(II) \gg Pt(II)$ .

---

<sup>1</sup> Hard acids are metal ions that are highly charged and bear the valence electron shell that is not easily distorted ( $Li^+$  &  $Mg^{2+}$ ). Similarly, soft acids are metal ions that have a low charge, and bear a valence electron shell that easily distorted ( $Pt^{2+}$  &  $Pd^{2+}$ ).

### 2.4.3 Effect of the solvent

Since the solvent is the medium in which the reaction takes place and is usually provided in excess, it can potentially substitute the labile group rendering a rate law that is independent on the entering nucleophile. The established two-term rate law common for an associative pathway for the substitution of square-planar complexes, consists of a term that is independent of the concentration of the nucleophile.<sup>19</sup> This may be ascribed to the parallel solvolysis pathway i.e. the mechanism in which the solvent displaces the leaving group prior to substitution by the entering nucleophile. The contribution of the solvent to the overall rate of the reaction depends on its coordinating ability.<sup>20</sup> For this process, the bond formation between the metal and the solvent in the transition state is imperative and the rate of substitution can be expected to increase proportionally with the coordinating ability of the solvent. Data showing the solvent effect on the substitution is shown in **Table 2.2** for the reaction of *trans*-Pt(Py)<sub>2</sub>Cl<sub>2</sub> and <sup>36</sup>Cl<sup>-</sup> (Equation 2.5).<sup>7,10,19</sup>



**Table 2.2** Solvent effect on chloride substitution (Equation 2.5) at 25 °C.<sup>7,10,19</sup>

Strongly Coordinating solvents	$k_{-2}/10^{-5} \text{ s}^{-1}$	Weakly Coordinating solvent	$k_2/\text{M}^{-1} \text{ s}^{-1}$
DMSO	380	CCl <sub>4</sub>	10 <sup>4</sup>
H <sub>2</sub> O	3.5	C <sub>6</sub> H <sub>6</sub>	10 <sup>2</sup>
CH <sub>3</sub> NO <sub>2</sub>	3.2	<i>i</i> -BuOH	10 <sup>-1</sup>
EtOH	1.4	Me <sub>2</sub> CO	10 <sup>-2</sup>
PrOH	0.4	DMF	10 <sup>-3</sup>

The results show that for strongly coordinating solvents, the reaction proceeds predominantly through the solvolytic pathway which is independent of the chloride concentration, while the opposite is true for weakly coordinating (or non-

coordinating) solvents. The values of  $k_{-2}$  (measuring the solvolytic pathway) were found to decrease in the order of the coordinating strength of the solvent;



where DMSO is the strongest coordinating solvent and PrOH the weakest. The second-order rate constants ( $k_2$ ) for the direct nucleophilic substitution were found to be higher in non-polar solvents (e.g.  $\text{CCl}_4$ ) than in polar solvents (e.g. DMF) because of poor solvating abilities of the non-polar solvents. Linear free energy relationships between a number of common parameters that are used to describe the Lewis acidity of the solvent and the reactivity were found to depend strongly on the solvation of the anionic nucleophile.

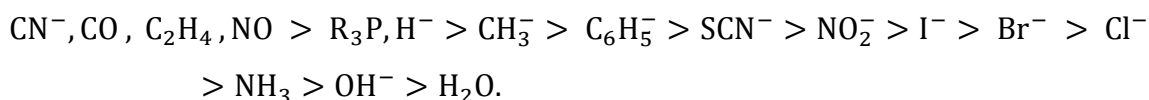
#### 2.4.4 Effect of the non-leaving ligand

Apart from the influence of the entering and leaving ligand, the substitution reactions on square planar Pt(II) complexes are also affected by the nature of the non-leaving group. The penta-coordinate transition state of an associative mechanism typical for square-planar Pt(II) complexes comprises of a trigonal bipyramidal intermediate with the *trans* ligand, the leaving group and the entering group in a trigonal plane and the two *cis* ligands in the axial positions.<sup>3,4</sup> The effect exerted by the *trans* ligand on the leaving group is different from the one of the *cis* ligand. Numerous studies have reported on the effect of the non-leaving ligands *cis* and *trans* to the leaving group, on the reactivity of the Pt(II) complexes.<sup>21,22</sup> The effect that the non-leaving ligand has on the coordinated labile ligand in a *trans* and *cis* positions is referred to as the *trans*- and *cis*-effect respectively. The effect on the reactivity of Pt(II) complexes from the non-leaving ligand *trans* to the labile leaving group is more prominent compared to the one in the *cis* position<sup>23</sup> i.e. the *trans*-effect is stronger than the *cis*-effect.

##### 2.4.4.1 The *trans*-effect

The *trans*-effect is the effect exerted by the non-leaving ligand on the rate of substitution of the labile ligand *trans* to it.<sup>4,20</sup> Kinetic data reported on the ability of

the non-leaving ligand to directing an entering group on a position *trans* to it using several nucleophiles has established a general order of labilization to be:<sup>4,10,16</sup>

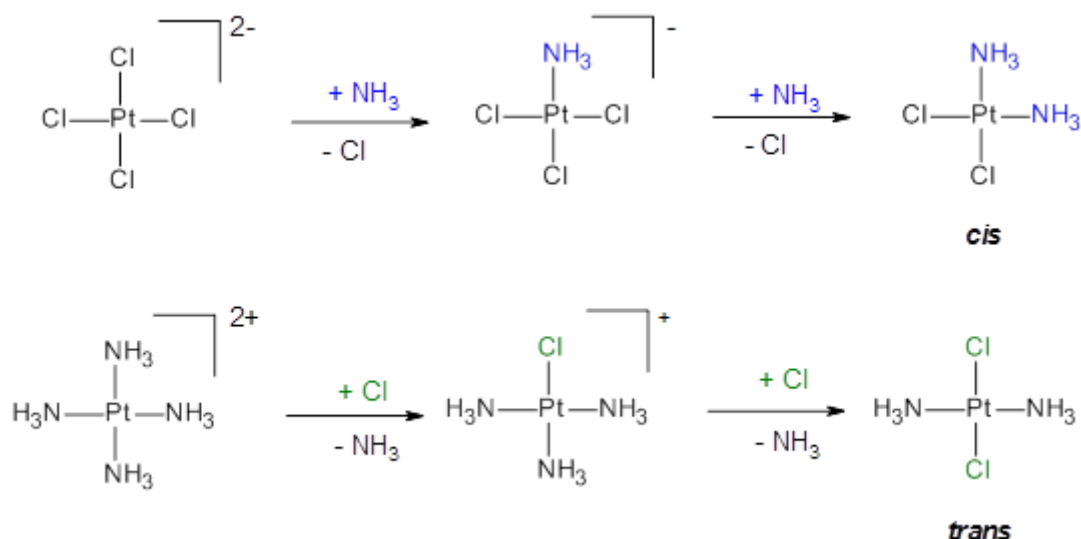


A ligand high up in the *trans*-effect series (strong *trans*-ligand) enhances the rate of substitution of the leaving group *trans* to itself e.g.  $\text{CN}^-$  has a stronger *trans*-effect than  $\text{SCN}^-$ . This is due to the fact that  $\text{CN}^-$  has both  $\sigma$ -donor and  $\pi$ -acceptor properties, which contribute to the ground state destabilization and transition state stabilization, respectively. Thus, the relative stabilities of both ground state and transition state are relevant in determining the overall magnitude of the *trans*-effect. These two factors accelerate the rate of substitution by reducing the activation energy barrier necessary to activate the reactants to the transition state. Therefore, the *trans*-effect is a kinetic phenomenon.

A characteristically different but closely related concept to the *trans*-effect is the *trans*-influence. This is the influence of the non-leaving ligand on the strength of the metal-to-ligand bond *trans* to it. Therefore, the *trans*-influence is a thermodynamic effect that affects the ground state properties of the metal complex. Experimental evidence of the *trans*-influence has been shown through the use of X-ray analysis, nuclear magnetic resonances and infrared spectroscopy confirming the elongation of the bond between the metal and the leaving group.<sup>10,20</sup>

The *trans*-effect plays a significant role in the synthesis of desired Pt(II) complexes with a specific geometry.<sup>4,23</sup> Examples showing the role of the *trans*-effect rule in the synthesis of geometric isomers of  $[\text{Pt}(\text{NH}_3)_2\text{Cl}_2]$  are shown in **Scheme 2.1**.

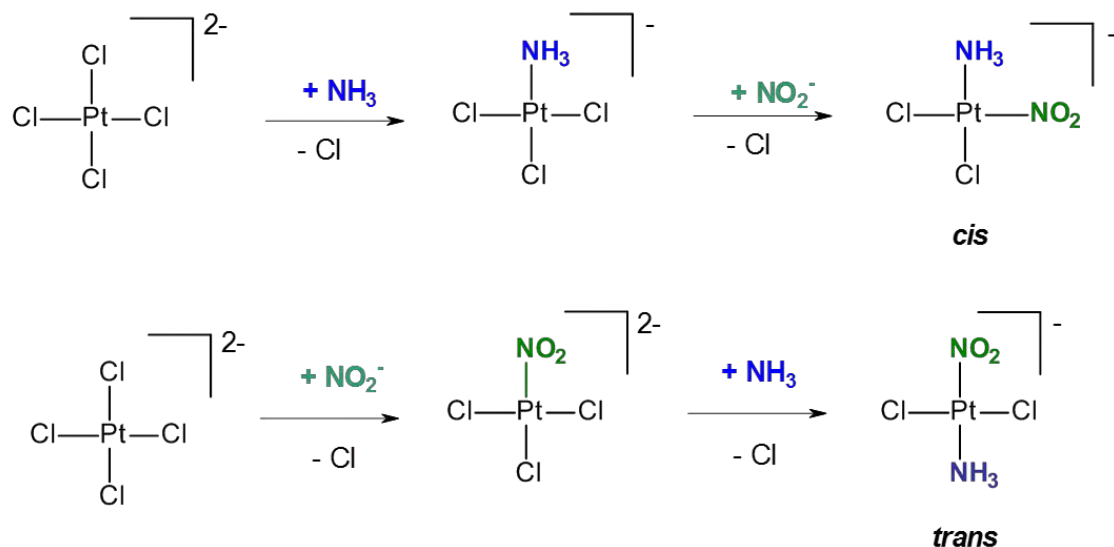




**Scheme 2.1:** Synthesis of the *cis* and *trans* isomers of  $[\text{Pt}(\text{NH}_3)_2\text{Cl}_2]$ .

Theoretically, *cis*- $[\text{Pt}(\text{NH}_3)_2\text{Cl}_2]$  can be prepared by a stepwise reaction of  $[\text{PtCl}_4]^{2-}$  with two mole equivalents of ammonia ( $\text{NH}_3$ ). The success of this reaction is dependent on the strong *trans*-directing effect of the chloride ion compared to ammonia, which ensures that the second ammonia coordinates at the *cis* position. Therefore, the least reactive chloride ligand in the  $[\text{Pt}(\text{NH}_3)\text{Cl}_3]^-$  intermediate is the one *trans* to the ammonia ligand. On one hand, *trans*- $[\text{Pt}(\text{NH}_3)_2\text{Cl}_2]$  is prepared by a stepwise reaction of the tetraamine Pt(II) complex,  $[\text{Pt}(\text{NH}_3)_4]^{2+}$ , with two mole equivalents of a chloride ( $\text{Cl}^-$ ) ligand. Upon the coordination of the first chloride ligand, the second chloride ligand replaces the most labile ammonia ligand from  $[\text{Pt}(\text{NH}_3)_3\text{Cl}]^+$ , in a *trans* position. Therefore, the strong *trans*-effect of the chloride ligand directs the substitution of the ammonia ligand *trans* to it.

Another example is shown in **Scheme 2.2** for the stepwise synthesis of *cis*- and *trans*- $[\text{Pt}(\text{NH}_3)(\text{NO}_2)\text{Cl}_2]^-$ . Reversing the order at which the ligands are introduced to  $[\text{PtCl}_4]^{2-}$  results into the formation of different isomers.<sup>4,24</sup> The *trans*-directing effect of nitrite is greater than that of chloride, thus directs the incoming  $\text{NH}_3$  group to the position *trans* to itself. Therefore, the *trans*-labilizing effect of the ligands follow the order  $\text{NO}_2 > \text{Cl} > \text{NH}_3$ .<sup>4,24</sup>

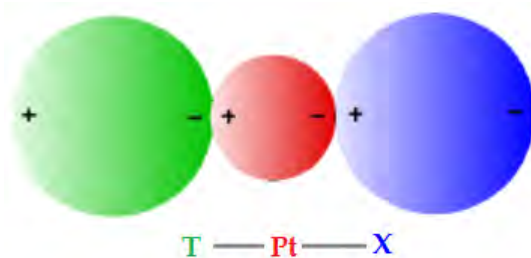


**Scheme 2.2:** Synthesis of the *cis* and *trans* isomers of  $[\text{Pt}(\text{NH}_3)(\text{NO}_2)\text{Cl}_2]^-$ .

Several theories have been used to explain the *trans*-effect. The three most prominent ones include the electrostatic polarization,  $\pi$ -bonding and molecular orbital (MO) theory.

#### 2.4.4.2 The electrostatic polarization theory

This theory was first proposed by Grinberg<sup>25</sup> using the charge distributions of induced dipoles along the  $T\text{--Pt--X}$  coordinate within a square-planar complex, where  $T$  is a *trans* ligand and  $X$  is the leaving group (**Figure 2.3**).

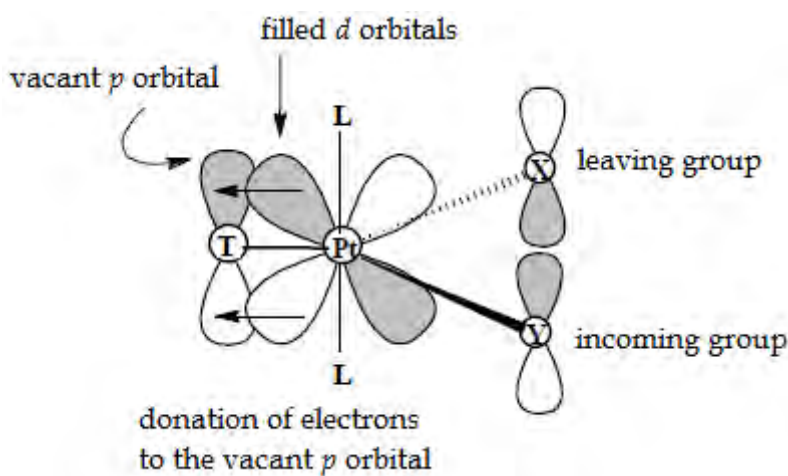


**Figure 2.3:** Charge distribution and induced dipoles in the  $T\text{--Pt--X}$  coordinate.

The charge on the Pt(II) metal ion induces the primary dipole in the *trans* ligand ( $T$ ), which in turn induces the secondary dipole to the metal ion. The orientation of the secondary dipole on the Pt(II) metal ion repels the negative charge on the leaving group ( $X$ ), thereby weakening or lengthening the  $\text{Pt--X}$  bond.

#### 2.4.4.3 The $\pi$ -bonding theory

This theory suggests that the  $\pi$ -bonding ligands such as CO, C<sub>2</sub>H<sub>2</sub>, and R<sub>3</sub>P are able to stabilise the transition state and therefore are high in the *trans*-effect series.<sup>3,10</sup> The  $\pi$ -bond is formed when the filled *d*-orbitals of the Pt(II) metal overlap with the empty  $\pi^*$ -orbitals of the ligand. On the other hand, the  $\sigma$ -bond is formed from the donation of a pair of electrons from the ligand to the metal centre. It would appear that withdrawal of electrons from the metal centre through  $\pi$ -back-bonding would strengthen the bond between the Pt(II) metal and the *trans* ligand in the ground state, instead of weakening the bond between the metal centre and the leaving group.<sup>20</sup> Therefore, the destabilization of the *trans* bond in the ground state cannot be used to adequately account for the effect of good *trans* activators.<sup>3,10,20</sup> As a result, Chatt *et al.*<sup>26</sup> and Orgel *et al.*<sup>27,28</sup> proposed that the explanation of the *trans*-effect has to involve the stabilization of the transition state. The intermediate is assumed to have a trigonal bipyramidal geometry as shown in **Figure 2.4**.



**Figure 2.4:** The trigonal bipyramidal geometry of the transition state and the  $\pi$ -back-bonding of the *trans* ligand.

Chatt *et al.*<sup>26</sup> highlighted that the removal of electrons from the metal centre through  $\pi$ -back-bonding of the *trans* ligand (T) will enhance the addition of the entering ligand (Y), thus increasing the rate of substitution. Orgel *et al.*<sup>27</sup> highlighted that the observed higher substitution rate is due to the stabilization of the transition state because of the reduced accumulation of the electron density in the T–Pt and Pt–X coordinate, through  $\pi$ -back-bonding.

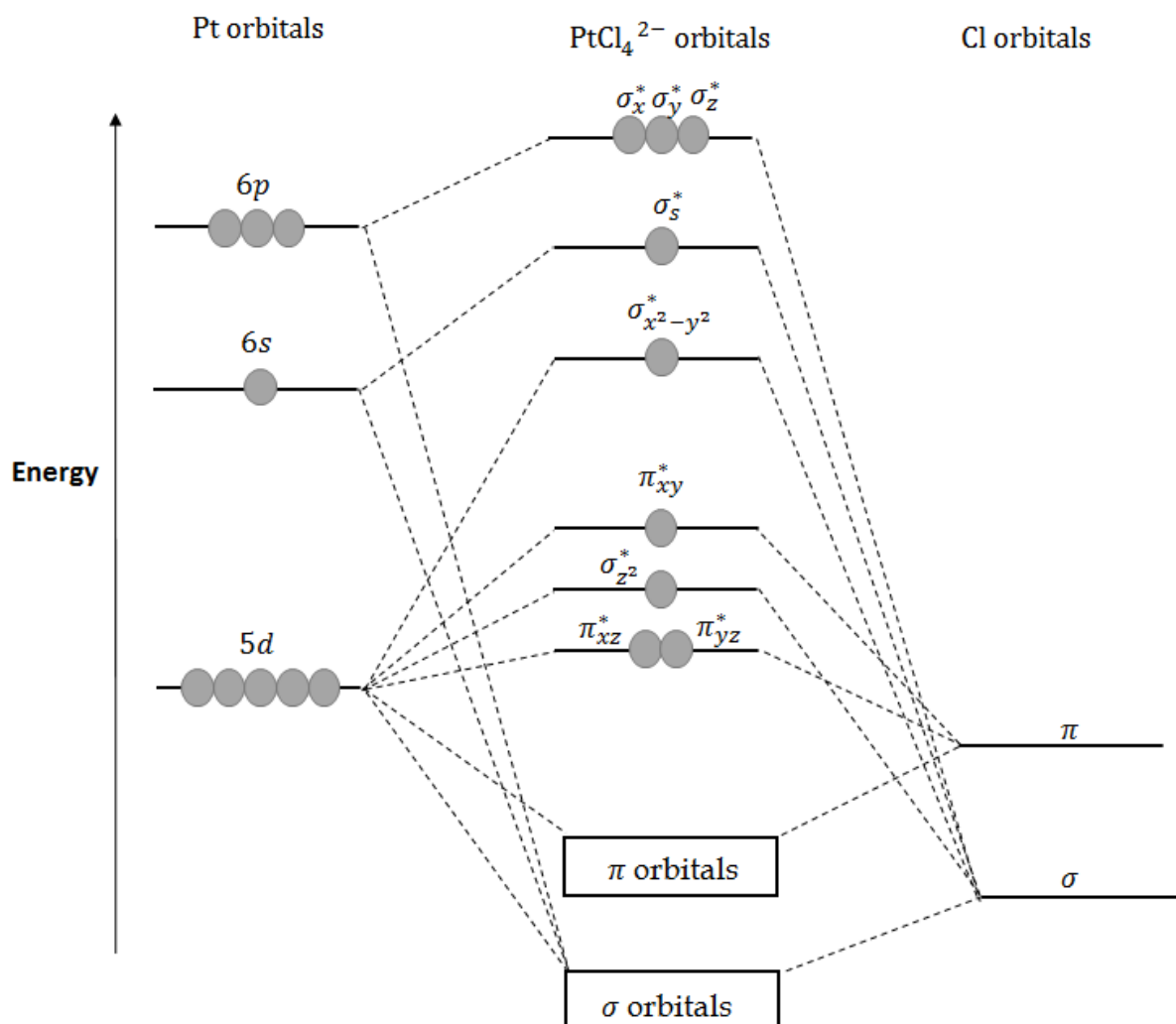
#### 2.4.4.4 The molecular orbital theory

The  $\sigma/\pi$ -trans effect is also supported by the molecular orbital (MO) theory.

##### a) The $\sigma$ -trans effect

A simplified MO diagram for an exemplary square planar  $[\text{PtCl}_4]^{2-}$  complex is shown in **Figure 2.5**. It can be seen from the diagram that the most stable orbitals are the  $\sigma$ -bonding atomic orbitals which are primarily located on the chloride ligands. These are followed by the  $\pi$ -bonding molecular orbitals as well as their anti-bonding partners,  $\pi_{xz}^*, \pi_{yz}^*, \pi_{z^2}^*, \sigma_{z^2}^*, \pi_{xy}^*$ , which are relatively stable. These orbitals are derived from the  $5d$  atomic orbitals of the Pt(II) metal. The  $\sigma_{x^2-y^2}^*$  orbitals are located at a higher energy and are comparatively unstable and inaccessible. The anti-bonding  $\sigma$ -orbitals,  $\sigma_s^*, \sigma_x^*$  and  $\sigma_y^*$  as well as the valence  $p_z$  orbital which is not involved in the  $\sigma$ -bonding, are the least stable.

Considering the geometry of the four valence atomic orbitals of the Pt(II) metal ( $d_{x^2-y^2}, s, p_x$  and  $p_y$ ) which are used for  $\sigma$ -bonding in the square planar complex, only  $p_x$  and  $p_y$  orbitals have the *trans* directional properties.<sup>20,24</sup> Therefore, in *trans*- $\text{PtL}_2\text{TX}$ , the *trans* ligand (T) and leaving group (X), must share the same  $\sigma_x$  orbital in the overall MO arrangement.<sup>20</sup> When strong  $\sigma$ -donor ligands such as  $\text{H}^-$  and  $\text{CH}_3^-$  are positioned *trans* to the leaving group, they contribute a greater share of the electron density to the  $\sigma_x$  orbital of the metal, thereby increasing the  $\sigma$ -bond strength. This will repel the electrons of the leaving group leading to the weakening of the Pt–X bond. This leads to an increase in the rate of displacement of the leaving group irrespective of the mechanism of substitution. This is true for the reactions in which ground state destabilization of the *trans* bond is operational in the reactivity of the complex. However, for the associative mode of action, the strong  $\sigma$ -donating ligand may result in the destabilization of the electron-rich penta-coordinate transition state, resulting into a decrease in the rate of substitution.<sup>22</sup>



**Figure 2.5:** Molecular orbital diagram of [PtCl<sub>4</sub>]<sup>2-</sup>.<sup>20,24</sup>

### b) The $\pi$ -*trans* effect

Good *trans* activators such as C<sub>2</sub>H<sub>4</sub>, CN<sup>-</sup> and CO, stabilize the square planar complex through strong  $\pi$ -back-donation from the filled *d*-orbitals of the metal with an appropriate  $\pi$ -symmetry, to the  $\pi^*$ -orbitals of the ligand.<sup>20</sup> Out of five *d*-orbitals in the Pt(II) complex, only three have a suitable symmetry for  $\pi$ -bonding, i.e.  $\pi_{xy}^*$ ,  $\pi_{xz}^*$ ,  $\pi_{yz}^*$ . Upon the coordination of the entering ligand and the formation of a trigonal bipyramidal intermediate, the number of molecular orbitals with the appropriate  $\pi$ -symmetry increases to four (including  $\pi_{x^2-y^2}^*$ ). These orbitals are shared in the  $\pi$ -interaction with the *trans* ligand, *T*, the entering group, *Y*, and the leaving group, *X*, in the trigonal plane. Therefore, the trigonal bipyramidal transition state will be stabilised more by the *trans* ligand with low energy lying vacant  $\pi$ -orbitals since their

interaction with the  $d$ -orbitals of the metal centre delocalises the excess electron density on the metal centre donated by the other three coordinated ligands thereby lowering the activation energy. The transition state is stabilised relative to the ground state, since it has more  $\pi^*$ -orbitals. Thus, strong  $\pi$ -acceptor ligands occupying a *trans* position enhance the addition of the entering group, leading to an accelerated rate of substitution. Consequently, facile substitution kinetics have been reported for Pt(II) complexes with good  $\pi$ -acceptor ligands.<sup>22</sup>

#### 2.4.4.5 The steric and electronic *cis*-effect

Steric effect is one of the most widely used concepts in chemistry.<sup>29</sup> It originates from the fact that each atom in a free molecule has a specific spatial size. It is a space-filling effect categorised as steric hindrance or steric bulk. When atoms are brought closer together, mutual repulsion between bonded and non-bonded electrons occurs. If an atom is bonded to bulk groups, its accessibility to attack by other groups is limited due to steric hindrance. In ligand substitution reactions, steric hindrance refers to the shielding of the central metal atom from the direct attack by the entering nucleophile. The magnitude of the resulting steric effect is directly proportional to the space occupied by the substituents that causes it. Therefore, the steric effect depends on:<sup>10,16,29</sup>

- a) the spatial size or space occupied by the bonded atoms and substituents.
- b) relative spatial configuration or orientation of the bonded substituents with respect to the targeted metal centre.
- c) the spatial position of steric imparting substituents with respect to the leaving group.

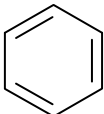
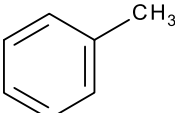
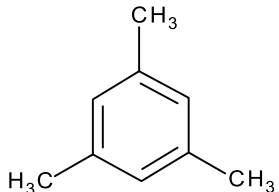
Since an associative pathway's transition state is characterised by an increase in the coordination number, due to bond formation between the metal centre and the incoming ligand, steric effects due to substituent (non-leaving) hindrance is increased in the transition state. This destabilises the transition state, thereby slowing down the rate of substitution. The steric influence on the rate of the substitution reaction can be either due to the steric bulk in the spectator ligand or in the incoming nucleophile. Generally, the larger the incoming ligand the slower is the

rate of a reaction. It is also rationalised that an increase in the steric bulk of the spectator ligand usually decrease the rate of the reaction.

The steric effects of spectator ligands may influence the lability of the leaving group in *trans* or *cis* position differently. When the steric imparting substituent is located in a *cis* position to the leaving group, the retardation on the rate of substitution on square-planar complexes is more prominent rather than in the *trans* position.<sup>3,7,10</sup> This was demonstrated in the chloride substitution from *cis/trans*-[Pt(Et<sub>3</sub>P)(L)Cl] by pyridine (Equation 2.6). The reported data is reproduced in **Table 2.3**.

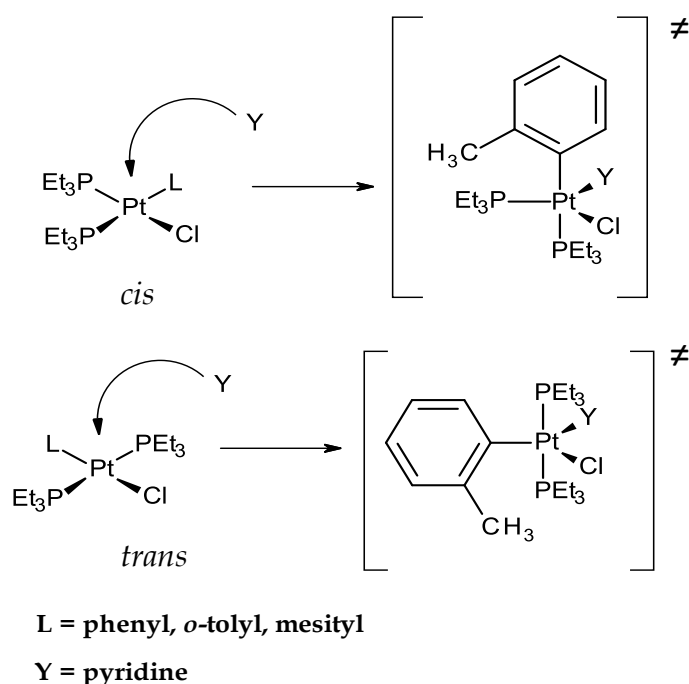


**Table 2.3** *cis/trans* steric effects on the rate of chloride ligand substitution by pyridine in [Pt(PEt<sub>3</sub>)<sub>2</sub>(L)Cl].<sup>3,7,10</sup>

Ligand, L	$k_{obs}/s^{-1}$	
	<i>Cis</i> -[Pt(PEt <sub>3</sub> ) <sub>2</sub> (L)Py (0 °C)	<i>trans</i> -[Pt(PEt <sub>3</sub> ) <sub>2</sub> (L)Py (25 °C)
 <b>Phenyl</b>	$8.0 \times 10^{-2}$	$1.2 \times 10^{-4}$
 <b>O-tolyl</b>	$2.0 \times 10^{-4}$	$1.7 \times 10^{-5}$
 <b>Mesityl</b>	$1.0 \times 10^{-6}$ (25 °C)	$3.4 \times 10^{-6}$

The introduction of one or more methyl substituents on the coordinated phenyl ring retards the reactivity of the complex. The retardation in the rate of substitution due to *cis* steric effect was more prominent than the corresponding *trans* steric effect. The larger decrease in the substitution rates for the *cis* complexes can be explained in

terms of their trigonal bipyramidal transition state with both the leaving group and the entering nucleophile in the equatorial positions as shown in **Figure 2.6**.



**Figure 2.6:** Trigonal bipyramidal transition state of the *cis* and *trans* isomers.<sup>7</sup>

In the transition state of the *cis*-isomer, the *o*-tolyl group occupies an axial position and interacts with the leaving group at the angle of 90°. This causes greater repulsion between the *ortho*-methyl substituent, the leaving group and the entering ligand. In the *trans*-isomer, the *o*-tolyl group is in the equatorial position and interacts with the leaving group at 120 ° angle which is further apart. As a result, the repulsions between the *ortho*-methyl substituent, the leaving group and the entering ligand are reduced.

A distinctive *cis*-electronic effect similar in effect to the steric effect occurs for substitution reactions on a square planar complex. The presence of the  $\sigma$ -donor ligand *cis* to the leaving group usually retards the reactivity of the Pt(II) complexes through the accumulation of electron density on the metal centre thereby decreasing its electrophilicity.<sup>30,31</sup> This further repel the approach of a nucleophile through transition state destabilization thereby decreasing the rate of substitution.<sup>30,31</sup> This explanation fits to what is known as a *cis*  $\sigma$ -effect.<sup>22,30,31</sup> Both steric *cis*-effect and



electronic  $\sigma$  *cis*-effect have the same net effect on the reactivity of the Pt(II) complexes. On the other hand, the presence of the strong  $\pi$ -accepting ligand in a *cis* position suppresses the transition state destabilization by withdrawing the  $\pi$ -electron density from the metal centre. This leads to a more electropositive metal centre and a simultaneous increase in its reactivity. This effect is called the  $\pi$ -*cis* effect. Therefore, the  $\sigma$ -*cis* effect and the  $\pi$ -*cis* effect have the opposite net effect on the rate of substitution.

## 2.5 Dissociative mechanism in square planar Pt(II) complexes

Dissociative mechanism of substitution is not very common for square planar Pt(II) complexes, owing to the instability of the 14-electron three coordinate transition state. However, some studies have reported the mechanistic changeover from associative to dissociative mode of action for square planar Pt(II).<sup>3,6,32</sup> Dissociative mechanism has also been reported for some Pt(II) complexes with strong *cis*  $\sigma$ -donor atoms such as carbon, sulfur or phosphorous.<sup>33-35</sup> Some examples of the complexes that undergo the mechanistic changeover are *cis*-[Pt(Me)<sub>2</sub>R<sub>2</sub>] and *cis*-[Pt(Ph)<sub>2</sub>R<sub>2</sub>], where R = DMSO or thioether.<sup>35</sup> However, when one of the thioether groups is replaced by a strong  $\pi$ -accepting CO ligand, the substitution reaction followed an associative mode of action. The strong  $\pi$ -accepting ligand reduces the electron density on the metal centre and hence favours the formation of an 18-electron-rich 5-coordinate transition state. It will also destabilize the formation of the 14-electron 3-coordinate transition state.

## 2.6 References

---

1. S. H. van Ritj, P.J. Sadler, *Drug Discovery Today*, 2009, **114**, 1089.
2. (a) J. Reedijk, *Chem. Rev.*, 1999, **99**, 2499. (b) C. Meljer, N. H. Mulder, H. Timmer-Bossch, W. J. Sluiter, G. J. Meersma, E. G. de Vries, *Cancer Res.*, 1992, **52**(24), 6885. (c) N. Fox, J. J. Roberts, *Cancer Metastasis Rev.*, 1987, **6**(3), 261.
3. M.L. Tobe, J. Burgess, *Inorganic Reaction Mechanism*, Addison Wesley Longman, Ltd. Essex, 1999, p. 30-43, 70-112.
4. R.G. Wilkins, *Kinetics and Mechanism of Reactions of Transition Metal Complexes*, 2nd Ed. VCH, Weinheim, 1991, p. 199-205, 221-242.
5. C. H. Langford, H. B. Gray, *Ligand Substitution Dynamics*, Benjamin, New York, 1965, p. 18 – 48.
6. (a) M. Rashidi, S. M. Nabavizadeh, A. Zare, S. Jamali and R. J. Puddephatt, *Inorg.Chem.*, 2010, **49**, 8435; (b) S. Choi, L. Vastag, C.-H. Leung, A. M. Beard, D. E. Knowles, and J. A. Larrabee, *Inorg. Chem.*, 2006, **45**(25), 10108; (c) R. Van Eldik, D. A. Palmer, H. Kelm, *Inorg. Chem.*, 1979, **18**(3), 572.
7. R. B. Jordan, *Reaction mechanisms of Inorganic and Organometallic Systems*, New York, Oxford, 1991, p. 23-30, 47-60, 140-153
8. R. Logan, *Fundamental of Chemical Kinetics*, Longman, Essex, 1996, p. 1-27.
9. R. A. Henderson, *The Mechanisms of Reactions at Transition Metal Sites*, Oxford University Press, Oxford, 1993, p. 1-22.
10. J. D. Atwood, *Inorganic and Organic Reaction Mechanisms*, 2nd Ed., Wiley- VCH Inc., New York, 1997, p. 32-34, 43-61, 747-771.
11. R. K. Murmann, R. T. M. Fraser and J. Bauman, *Mechanisms of Inorganic Reactions*, American Chemical Society, Washington, D. C, 1965, p. 20-23, 81-97.
12. N. De Barrios, G. González, A. Grandas, M. Martinez and V. Moreno, *Inorganic Reaction Mechanisms*, 1999, **1**, 205.
13. D. S. Gill, In *Platinum Coordination Complexes in Cancer Chemotherapy*, M. P. Hacker, E. B. Douple, I. H. Krakoff Eds., Martinus Nijhoff Publishing, Boston MA, 1984, 267.
14. J. Reedijk, *Eur. J. Inorg. Chem.*, 2009, 1303.

15. A. Peloso, *Coord. Chem. Rev.*, 1973, **10**, 123.
16. S. Ašperger, *Chemical Kinetics and Inorganic Reaction Mechanisms*, 2nd Ed., Kluwer Academic/Plenum Publisher, New York, 2003, p. 38-39, 105- 106 , 140-153.
17. F. Basolo, J. Chatt, H. B. Gray, R. G. Pearson and B. L. Shaw, *J. Chem. Soc.*, 1961, 2207.
18. H. B. Gray and R. J. Olcott, *Inorg. Chem.*, 1962, **1**, 481.
19. R. G. Pearson, H. B. Gray, F. Basolo, *J. Am. Chem. Soc.*, 1960, **82**, 787.
20. F. Basolo and R. G. Pearson, *Mechanisms of Inorganic Reactions*, 2nd Ed., Wiley, New York, 1967, p. 193-195, 351-356, 369- 400.
21. (a) D. Jaganyi, A. Hofmann, R. van Eldik, *Angew. Chem. Int. Ed. Engl.* 2001, **40**, 1680; (b) A. Hofmann, D. Jaganyi, O. Q. Munro, G. Liehr, R. van Eldik, *Inorg. Chem.* 2003, **42**, 1688; (c) A. Mambanda; D. Jaganyi, *Dalton Trans.* 2011, **40**, 79; (d) A. Mambanda, D. Jaganyi, *Dalton Trans.* 2012, **41**, 908; (e) D. Reddy, D. Jaganyi, *Int. J. Chem. kinet.* 2011, **43**, 161; (f) P. O. Ongoma, D. Jaganyi, *Dalton Trans.* 2013, **42**, 2724.
22. (a) D. Jaganyi, K-L. De Boer, J. Gertenbsch, J. Perils, *Int. J. Chem. Kinet.*, 2008, **40**, 808. (b) D. Reddy, K. J. Akerman, M. P. Akerman, D. Jaganyi, *Transition Met. Chem.*, 2011, **36**, 593.
23. L. Cattalini, *Progr. Inorg. Chem.*, 1970, **13**, 263.
24. U. Belucco, *Organometallic and Coordination Chemistry of Platinum*, Academic press, London, 1974, p. 138-160.
25. A. A. Grinberg, *Acta Physicochim*, 1935, **3**, 573.
26. J. Chatt, L. A. Duncanson and L. M. Venanzi, *J. Chem. Soc*, 1955, 1955.
27. L. E. Orgel, *J. Inorg. Nucl. Chem*, 1956, **2**, 137.
28. J. Chatt, G. A. Gamlen and L. E Orgel, *J. Am. Chem. Soc*, 1959, 486.
29. S. Lui, *J. Chem. Phys.*, 2007, **126**, 244103
30. A. Hofmann, L. Dahlenburg and R. van Eldik, *Inorg. Chem.*, 2003, **42**, 6528.
31. D. Jaganyi, D. Reddy, J. A. Gertenbach, A. Hofmann and R. van Eldik, *Dalton Trans.*, 2004, 299.

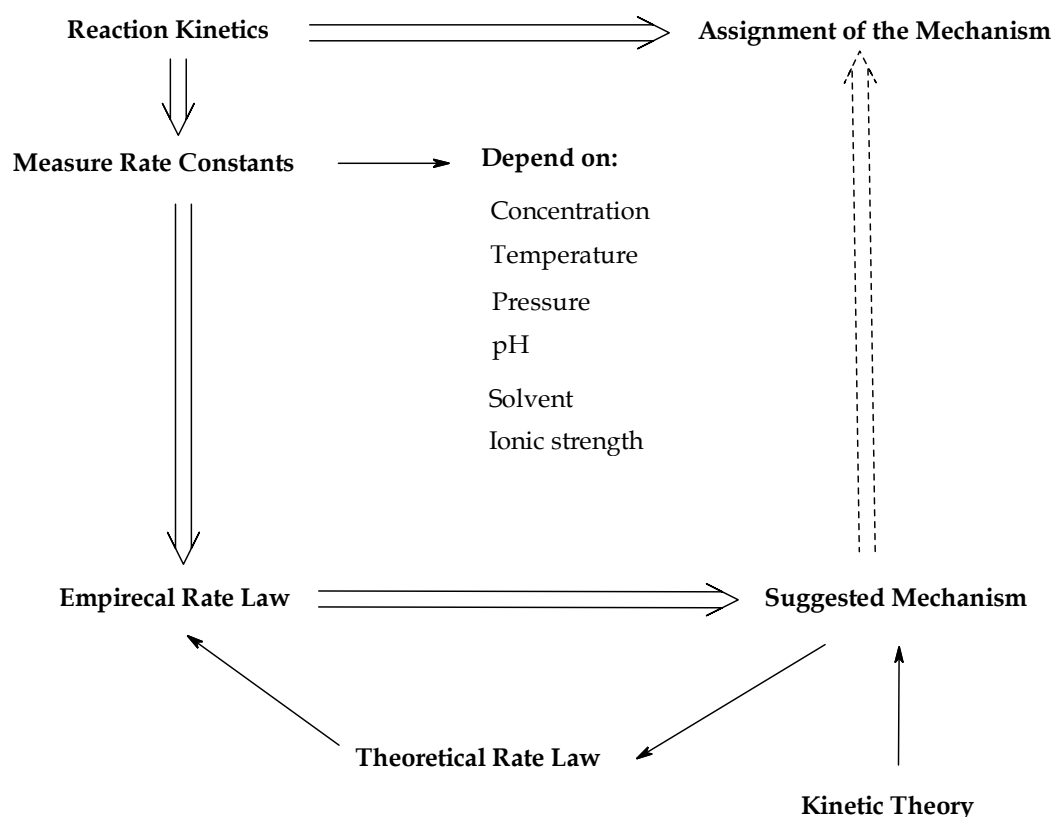
32. R. Romeo, L. M. Scolaro, M. R. Plutino, F. F. De Biani, G. Bottari and A. Romeo, *Inorg. Chim. Acta*, 2003, **350**, 143.
33. S. Lanza, D. Minniti, P. Moore, J. Sachinidis, R. Romeo and M. L. Tobe, *Inorg. Chem.*, 1984, 23, 4428.
34. M. R. Plutino, L. M. Scolaro, R. Romeo and A. Grassi, *Inorg. Chem.*, 2000, **39**, 2712.
35. R. Romeo, A. Grassi and L. M. Scolaro, *Inorg. Chem.*, 1992, **31**, 4383.

# Chapter 3

## Kinetic theory and relevant techniques used for kinetic measurements

### 3.0 Introduction

The reactivity of metal complexes can only be quantified by a kinetic approach. It is important to gather as much as possible information from the empirical rate law, activation parameters, evidence of intermediates from the studied systems, and the theoretical analysis of the suggested mechanism and proposed transition states, in order to come as close as possible to the “real” mechanism. **Figure 3.1** depicts schematic presentation of the fundamental approach in kinetic-mechanistic studies. The application of thermodynamic and kinetic techniques can reveal crucial information of the assignment of mechanism for ligand exchange reactions.



**Figure 3.1:** Schematic presentation of the fundamental approach in kinetic and mechanistic studies.<sup>1</sup>

In addition to proper knowledge of electronic and geometrical structures, a detailed knowledge of thermodynamics and kinetics is essential to address issues of structure, reactivity and stability in metal coordination compounds. In some cases, a ligand is displaced at a faster rate from metal complexes whose M-L bonds are of the same thermodynamic strength.<sup>2</sup> Therefore the kinetic stability of molecules must be considered in addition to their thermodynamic stability.

In this chapter, a brief summary of relevant rate laws and experimental techniques used in the kinetic measurements will be given.

### 3.2 The rate law

The rate of a reaction can be expressed as the change in the concentration of reactants or products per unit time (*Equation. 3.1*).<sup>3,4</sup>

$$\text{Rate} = -\frac{d[\text{reactant}]}{dt} = \frac{d[\text{product}]}{dt} \quad (3.1)$$

The negative sign in the above equation signifies that the rate of a reactant decreases with time. The rate of a chemical reaction can therefore be expressed in  $\text{mol dm}^{-3} \text{ s}^{-1}$ .<sup>5</sup> On the other hand, the rate law is an expression based on the experimentally measured data, which shows the relationship between the rate of a chemical reaction and the concentrations of all species involved in the turnover of the reactants to products. Considering the following chemical reaction;



where the chemical compounds are represented by capital letters and the stoichiometric coefficients are represented by lower case letters. Using the concentrations of all the components of the reaction, the rate can be expressed as;<sup>3</sup>

$$\text{Rate} = -\frac{1}{a} \cdot \frac{d[A]}{dt} = -\frac{1}{b} \cdot \frac{d[B]}{dt} = \frac{1}{c} \cdot \frac{d[C]}{dt} = \frac{1}{d} \cdot \frac{d[D]}{dt} \quad (3.3)$$

Alternatively, the rate law can be written as;

$$\text{Rate} = -k[A_i]^{\alpha_i}[X_j]^{\beta_j} \quad (3.4)$$

where  $k$  is a rate constant,  $A_i$  is a reactant and  $X_j$  is any other species such as a catalyst that may affect the rate of the reaction, while  $\alpha$  and  $\beta$  are the rate orders with respect to  $A_i$  and  $X_j$ , respectively, which are determined experimentally and are independent on the stoichiometric coefficients. The magnitude of the rate constant ( $k$ ) is a direct measure of how fast or slow a chemical reaction is. The sum of  $\alpha$  and  $\beta$  represent the overall order of the reaction.

### 3.3 Integrated rate laws

Integrated rate laws are used to determine how the concentrations of reactants (or products) are related with time. A brief overview of the theory underlying the integrated rate law will be discussed in the following sub-headings.

#### 3.3.1 First-order reactions

For first-order reactions, only one species is involved in the rate determining step. The concentration profiles of such reactions follow an exponential decay or growth. These reactions can either be reversible or irreversible, depending on the factors that affect the rate of a reaction.

##### 3.3.1.1 Irreversible first-order reactions

For an irreversible first-order reaction below (*Equation. 3.5*),



the rate law can be written as;

$$Rate = -\frac{d[A]}{dt} = k[A] \quad (3.6)$$

rearranging *Equation 3.6* gives;

$$-\frac{d[A]}{dt} = k_1 dt \quad (3.7)$$

Integrating from  $t = 0$  ( $[A]_0$ ) to  $t = t$  ( $[A]_t$ ) gives;

$$\int_{[A]_0}^{[A]_t} \frac{d[A]}{[A]} = -k_1 \int_0^t dt \quad (3.8)$$

$$\ln \frac{[A]_t}{[A]_0} = -k_1 t \quad (3.9)$$

or

$$\ln[A]_t = -k_1 t + \ln[A]_0 \quad (3.10)$$

where  $[A]_t$  and  $[A]_0$  are concentrations of a reactant at time  $t = t$  and  $t = 0$ , respectively.

From Equation 3.10, a plot of  $\ln[A]_t$  against time ( $t$ ), yields a straight line which passes through the intercept,  $\ln[A]_0$ , and has a negative slope from which the first-order rate constant ( $k_1$ ) is obtained.

Equation 3.10 can also be written as;

$$\frac{[A]_t}{[A]_0} = e^{-k_1 t} \quad (3.11)$$

which rearranges to

$$[A]_t = [A]_0 e^{-k_1 t} \quad (3.12)$$

The above equations indicate that the plot of  $[A]_t$  against time ( $t$ ) follows an exponential decay or growth.

### 3.3.1.2 Reversible first-order reactions

Reversible first-order reactions that attain equilibrium can be represented by the following equation;



with the rate law;

$$Rate = \frac{-d[B]}{dt} = \frac{-d[A]}{dt} = -k_1[A]_t - k_{-1}[B]_t \quad (3.14)$$

At time  $t = 0$ ,  $[B]_0 = 0$  and  $[A]_t = [A]_0$ , the concentration of  $B$  at time  $t$  ( $[B]_t$ ) can be written as;

$$[B]_t = [A]_0 - [A]_t \quad (3.15)$$

Substitution of Equation 3.15 into Equation 3.14 gives;

$$\frac{-d[A]}{dt} = k_1[A]_t - k_{-1}([A]_0 - [A]_t) \quad (3.16)$$

At equilibrium, there is no overall reaction, thus

$$\frac{-d[A]}{dt} = 0 \quad (3.17)$$

Therefore applying Equation 3.17 to Equation 3.14 gives;



$$k_1[A]_{eq} = k_{-1}[B]_{eq} = k_{-1}([A]_0 - [A]_{eq}) \quad (3.18)$$

or

$$[A]_0 = \frac{k_1 + k_{-1}}{k_{-1}} [A]_{eq} \quad (3.19)$$

Substituting  $[A]_0$  from Equation 3.19 to Equation 3.16 yields;

$$-\frac{d[A]}{dt} = (k_1 + k_{-1})[A] - (k_1 + k_{-1})[A]_{eq} \quad (3.20)$$

Separations of variables and integrating from time  $t = 0$  ( $[A]_0$ ) to  $t = t$  ( $[A]_t$ ) leads to;

$$\int_{[A]_0}^{[A]_t} \frac{d[A]}{([A]_t - [A]_{eq})} = -(k_1 + k_{-1}) \int_0^t dt \quad (3.21)$$

or

$$\ln \frac{[A]_0 - [A]_{eq}}{[A]_t - [A]_{eq}} = -(k_1 + k_{-1})t \quad (3.22)$$

Rearranging Equation 3.22 affords;

$$\ln([A]_t - [A]_{eq}) = -(k_1 + k_{-1})t + \ln([A]_0 - [A]_{eq}) \quad (3.23)$$

A plot of  $\ln([A]_t - [A]_{eq})$  against time ( $t$ ) will produce a straight line with a slope of  $-(k_1 + k_{-1})$ . Experimentally, the observed rate constant,  $k_{obs}$ , can be used to determine the individual rate constants,  $k_1$  and  $k_{-1}$ , for the forward and backward reaction using Equation 3.24.

$$k_{obs} = k_1 + k_{-1} \quad (3.24)$$

It is crucial to also consider the equilibrium constant,  $K_{eq}$ , since the above equation has two unknowns. Thus, Equations 3.24 and 3.25 can be solved simultaneously to determine the individual rate constants of the forward and backward reaction.<sup>3,6</sup>

$$K_{eq} = \frac{[B]_{eq}}{[A]_{eq}} = \frac{k_1}{k_{-1}} \quad (3.25)$$

### 3.3.2 second-order reactions

For second-order reactions, the rate of the reaction depends on both reactant species, i.e. both reactant species are involved in the rate-determining step. Depending on the contribution of the reverse reaction, second-order reactions can be either reversible or irreversible.<sup>7</sup> The reaction is irreversible when there is no significant contribution from the reverse reaction, otherwise it is reversible as shown in *Equation 3.26*.



The rate law of this reaction can be written as;

$$-\frac{d[A]}{dt} = -\frac{d[B]}{dt} = \frac{d[C]}{dt} = k_2 [A]_t [B]_t - k_{-2} [C]_t \quad (3.27)$$

Assuming that the stoichiometric ratio of all species involved in a reaction is 1:1:1, application of the mass balance at time,  $t$ , affords;

$$[A]_t = [A]_0 - [C]_t \text{ and } [B]_t = [B]_0 - [C]_t \quad (3.28)$$

At equilibrium, the above expressions can be written as;

$$[A]_{eq} = [A]_0 - [C]_{eq} \text{ and } [B]_{eq} = [B]_0 - [C]_{eq} \quad (3.29)$$

At equilibrium, the rate of a forward reaction is equal to the one for a reverse reaction, as shown in *Equation 3.30*.

$$-\frac{d[A]}{dt} = k_2 [A]_{eq} [B]_{eq} - k_{-2} [C]_{eq} = 0 \quad (3.30)$$

Hence,

$$k_2 [A]_{eq} [B]_{eq} = k_{-2} [C]_{eq} \quad (3.31)$$

Substituting the expression of  $[C]_{eq}$  from *Equation 3.29* into *Equation 3.31* yield;

$$k_2 [A]_{eq} [B]_{eq} = k_{-2} ([A]_{eq} - [A]_0) \quad (3.32)$$

This simplifies to;

$$k_{-2} [A]_0 = k_2 [A]_{eq} [B]_{eq} + k_{-2} [A]_{eq} \quad (3.33)$$

Substituting the expression of  $[C]_t$  from Equation 3.28 into Equation 3.27 gives;

$$-\frac{d[A]}{dt} = k_2 [A]_t [B]_t - k_{-2} ([A]_0 - [A]_t) \quad (3.34)$$

This simplifies to;

$$k_2 [A]_t [B]_t - k_{-2} [A]_0 + k_2 [A]_t \quad (3.35)$$

Combining Equation 3.35 and Equation 3.33 affords;

$$-\frac{d[A]}{dt} = k_2 [A]_t [B]_t - k_2 [A]_{eq} [B]_{eq} - k_{-2} [A]_{eq} + k_{-2} [A]_t \quad (3.36)$$

Under *pseudo*-first order conditions,<sup>3,6</sup> where  $[B]_0 \gg [A]_0$ , Equation 3.36 becomes;

$$\begin{aligned} -\frac{d[A]}{dt} &= k_2 [A]_t [B]_0 - k_2 [A]_{eq} [B]_0 - k_{-2} [A]_{eq} + k_{-2} [A]_t \\ &= (k_2 [B]_0 + k_{-2}) ([A]_t - [A]_{eq}) \end{aligned} \quad (3.37)$$

Separation of variable and integrating from time = 0 ( $[A]_0$ ) to time =  $t$  ( $[A]_t$ ) gives;

$$\int_{[A]_0}^{[A]_t} \frac{d[A]}{([A]_t - [A]_{eq})} = -(k_2 [B]_0 + k_{-2}) \int_0^t dt \quad (3.38)$$

This results in;

$$\ln \left( \frac{[A]_t - [A]_{eq}}{[A]_0 - [A]_{eq}} \right) = -(k_2 [B]_0 + k_{-2})t = -k_{obs}t \quad (3.39)$$

where

$$k_{obs} = k_2 [B]_0 + k_{-2} \quad (3.40)$$

A plot of  $k_{obs}$  vs.  $[B]_0$  is linear with a slope of  $k_2$  and the y-intercept of  $k_{-2}$ . According to the above Equation, second-order rate constants,  $k_2$ , can be determined by measuring the observed *pseudo*-first order rate constants,  $k_{obs}$ , as a function of nucleophile concentration (in this case  $[B]_0$ ).

Some reactions do not establish equilibrium between the reactants and the formed products but instead go to completion. These reactions are known as irreversible second-order reactions and can be represented by *Equation 3.41*.



The rate law of this reaction can be written as;

$$Rate = \frac{d[C]}{dt} = -\frac{d[A]}{dt} = -\frac{d[B]}{dt} = k [A]_t [B]_t \quad (3.42)$$

Considering the initial concentrations of reactants at time  $t = 0$  as  $[A]_0$  and  $[B]_0$ , after a particular time,  $t$ , the concentration of reactants will be reduced to  $([A]_0 - x)$  and  $([B]_0 - x)$ , respectively, where  $x$  is the amount of reactants that has reacted to form the product. Therefore the rate of the reactions can be expressed as;

$$-\frac{d[A]}{dt} = k_2([A]_0 - x)([B]_0 - x) \quad (3.43)$$

Since  $[A]_t = [A]_0 - x$ , it follows that  $-\frac{dx}{dt} = -\frac{d[A]}{dt}$ , thus the rate law in *Equation 3.43* can be written as;

$$\frac{dx}{dt} = k_2([A]_0 - x)([B]_0 - x) \quad (3.44)$$

Separation of variable and intergrating from  $x = 0$  to  $x = x$  and  $t = 0$  to  $t = t$ , yields;

$$\int_0^x \frac{dx}{([A]_0 - x)([B]_0 - x)} = k_2 \int_0^t dt \quad (3.45)$$

Provided  $[A]_0 \neq [B]_0$  *Equation 3.45* can also be written as;

$$\frac{1}{[A]_0 - [B]_0} \ln \frac{[B]_0 ([A]_0 - x)}{[A]_0 ([B]_0 - x)} = k_2 t \quad (3.46)$$

This expression can be simplified to;

$$\frac{1}{[A]_0 - [B]_0} \ln \frac{[B]_0 [A]_t}{[A]_0 [B]_t} = k_2 t \quad (3.47)$$

From Equation 3.47, the second-order rate constant can only be determined if one knows the instantaneous concentrations of the reactants, i.e.  $[A]_t$  and  $[B]_t$ . However, this is very complicated and inconvenient.<sup>8-10</sup> As a result, second order rate constants are usually studied under adjusted experimental conditions which simplify the kinetics to first-order. This is achieved by providing one of the reagents in large excess such that its concentration remains constant during the reaction. These experimental conditions are known as *pseudo* first-order conditions. For instance if  $[B]_0 \gg [A]_0$  then the rate law in Equation 3.42 can be expressed as;

$$-\frac{d[A]}{dt} = k_2 [A]_t [B]_t = (k_2 [B]_0) [A]_t = k_{obs} [A]_t \quad (3.48)$$

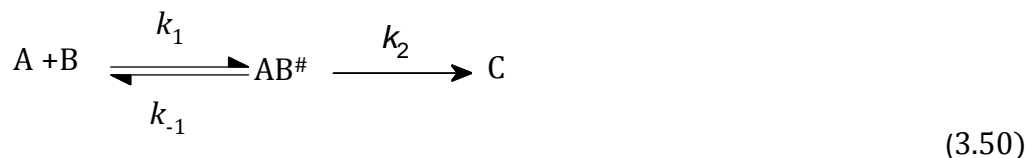
where,

$$k_{obs} = k_2 [B]_0 \quad (3.49)$$

A plot of  $k_{obs}$  vs.  $[B]_0$  will give a straight line passing through the origin, with a slope of  $k_2$ . For square planar complexes, the value of  $k_2$  measures a direct attack of the incoming nucleophile to the metal centre.

### 3.4 Measurements of activation parameters

Apart from the rate law, the magnitude of activation parameters also helps in the elucidation of the mechanism of action in which inorganic substitution reactions proceed. The enthalpy, entropy and volume of activation can be determined by measuring the second-order rate constant as a function of temperature and pressure, respectively.<sup>11</sup> The mechanism can be assigned based on the magnitudes and signs of the values of these parameters. These parameters are formulated on the transition theory.<sup>3,6</sup> This theory works on the assumption that a reaction between the metal complex (A) and the incoming nucleophile (B) passes through the transition state where it forms an activated complex ( $AB^\ddagger$ ) before it converts to product (C).<sup>12-13</sup> This reaction pathway can be represented as;



The rate of this reaction at a particular temperature can be written as;

$$-\frac{d[A]}{dt} = \frac{k_b T}{h} K^\ddagger [A]_{eq} [B]_{eq} \quad (3.51)$$

where  $k_b$  = Boltzmann's constant ( $1.38 \times 10^{-23}$  J/K),  $h$  = Plank's constant ( $6.626 \times 10^{-34}$  J/s),  $T$  = Temperature in Kelvin and  $K^\ddagger$  = Equilibrium constant.<sup>12</sup>

It is known that the equilibrium constant is related to the experimental second-order rate constant according to *Equation 3.52*.

$$k_{2(exp)} = \frac{k_b T}{h} K^\ddagger \quad (3.52)$$

The Gibb's free energy,  $\Delta G^\ddagger$ , is also related to the equilibrium constant according to *Equation 3.53*.

$$\Delta G^\ddagger = -RT \ln K^\ddagger = \Delta H^\ddagger - T\Delta S^\ddagger \quad (3.53)$$

Substituting *Equation 3.53* into *Equation 3.52* yields the following expression;

$$k_{2(exp)} = \frac{k_b T}{h} e^{(-\frac{\Delta G^\ddagger}{RT})} = e^{(-\frac{\Delta H^\ddagger}{RT})} e^{(-\frac{\Delta S^\ddagger}{R})} \quad (3.54)$$

Taking the natural logarithm on both sides of *Equation 3.54* yields;

$$\ln \left( \frac{k_{2(exp)}}{T} \right) = \frac{-\Delta H^\ddagger}{R} \cdot \frac{1}{T} + \left( \ln \frac{k_b}{h} + \frac{\Delta S^\ddagger}{R} \right) \quad (3.58)$$

Therefore a plot of  $\ln \left( \frac{k_{2(exp)}}{T} \right)$  against  $\frac{1}{T}$ , known as the Eyring plot,<sup>5,13,14</sup> is a straight line with a slope of  $\frac{-\Delta H^\ddagger}{R}$  and the intercept of  $\ln \frac{k_b}{h} + \frac{\Delta S^\ddagger}{R}$  from which the enthalpy of activation ( $\Delta H^\ddagger$ ) and the entropy of activation ( $\Delta S^\ddagger$ ) can be determined, respectively.

In an associatively-activated ligand substitution reaction mechanism, the magnitude of the  $\Delta H^\ddagger$  values are small while the values of  $\Delta S^\ddagger$  are large and negative

compared to a dissociatively-activated mechanism of action whose  $\Delta H^\ddagger$  and  $\Delta S^\ddagger$  values are usually large and positive.<sup>14,15</sup>

### 3.5 Measurement of the activation volume

The values of entropy of activation are not totally reliable especially when they are too small because of the errors associated with the determination of these values from the y-intercept by extrapolating to infinite temperatures.<sup>15,16</sup> The most powerful and reliable parameter that can be used to supplement the entropy of activation data is the volume of activation,  $\Delta V^\ddagger$ .<sup>3,6,15</sup> This can be determined from a series of experiments in which the second-order rate constant,  $k_2$ , is recorded as a function of pressure in an isothermal system. Therefore, these measurements are of great interest in ligand substitution reactions since they allow for precise assignment of the underlying mechanism.<sup>15,17</sup> The principle on which the volume of activation is based on is outlined from the thermodynamic equation below;

$$\Delta V = \left( \frac{\delta \Delta G}{\delta P} \right)_T \quad (3.59)$$

Substituting the expression of Gibb's free energy (*Equation 3.53*) in *Equation 3.59* followed by rearranging the equation simplifies it to;

$$\left( \frac{d \ln k_2}{dp} \right) = - \frac{\Delta V}{RT} \quad (3.60)$$

where  $\Delta V$  = the change in partial molar volume between products and reactants.

In the transition state, *Equation 3.60* can be used to write the expression for the volume of activation,  $\Delta V^\ddagger$ .

$$\left( \frac{d \ln k_2}{dp} \right) = - \frac{\Delta V^\ddagger}{RT} \quad (3.61)$$

Integrating this equation from  $P = 0$  to  $P = P$  to gives;

$$\ln k_2 = - \frac{\Delta V^\ddagger}{RT} P + \ln(k_2)_0 \quad (3.62)$$

where  $(k_2)_0$  = second-order rate constant at zero pressure

A plot of  $\ln k_2$  against  $P$  is linear and the activation volume can be calculated from the slope of the graph. Positive values of  $\Delta V^\ddagger$  signify a dissociative mechanism whereas negative  $\Delta V^\ddagger$  values indicate an associative mechanism. Therefore, the volume of activation changes with the mechanism in the same way as the entropy of activation.

### 3.6 Techniques for studying chemical kinetics

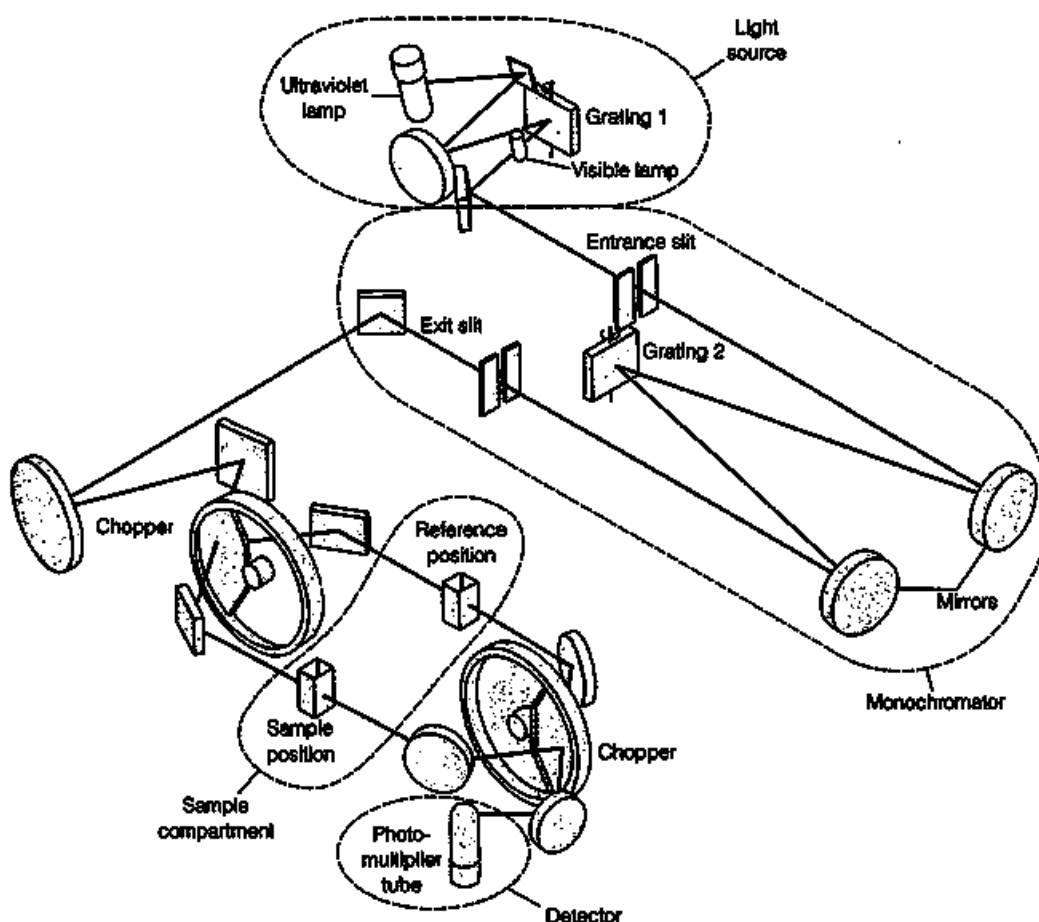
Kinetic investigations are normally accomplished by monitoring the dependence of some physical variables (e.g. absorbance) which are proportional to the concentration of the reactants or products as a function of time. The experimental technique selected for kinetic measurements depends on how fast or slow the reaction is. For example, fast reactions that complete within time range from  $10^{-14}$  s to 60 s require a specialised instrumentation for rapid mixing of the reactants and rapid data collection.<sup>18</sup> Under such conditions, the instrument used to collect the kinetic data must be programmed to continuously record the concentration profiles of a reaction over time. For slow reactions, the reaction kinetics can be studied using conventional techniques.<sup>16,19</sup>

Various experimental techniques have been developed to study reaction kinetics. These include flow methods (e.g. stopped-flow analysis), UV/visible spectrophotometry, pulse methods and nuclear magnetic resonance (NMR) spectroscopy.<sup>3,13</sup> Despite the number of techniques available, only UV/visible and stopped-flow spectrophotometric methods will be briefly reviewed in this thesis.

#### 3.6.1 UV/visible spectrophotometric technique

UV/visible spectrophotometer is used to monitor reactions which take longer than 16 minutes to complete.<sup>20</sup> It is a sensitive technique which can detect sample concentrations within the optimum range of  $10^{-4}$  to  $10^{-6}$  mol/dm<sup>3</sup>.<sup>20</sup> The instrument consists of key components (**Figure 3.2**) including two light sources, one in the visible region (800-400 nm; Tungsten lamp) and another one in the ultraviolet region (400-200 nm; deuterium lamp), monochromator, detector, data processor and internal or external temperature control unit.<sup>19,21</sup>





**Figure 3.2:** Schematic representation of a UV/Visible spectrophotometer.<sup>21</sup>

Photomultiplier tube is the detector commonly used in the UV/visible spectrophotometer which measures transmitted radiation as photons. This detector comprises of a photoemittive cathode that emits electrons when struck by photons from the UV/visible radiation. A cascade of electrons produced is amplified at the dynodes before they are collected at the anode, resulting in a current that is amplified and measured. Transparent tandem cuvettes made up of quartz are used for initiating the reaction. These cuvettes have two separate compartments that allow for reactants to be pre-equilibrated at a required temperature before manually mixing them to start the reaction.

The light passing through the sample (transmittance) can be represented as;

$$T = \frac{I_0}{I} \quad (3.63)$$

where  $I_0$  is the intensity of the incident light obtained from the solvent reference cell and  $I$  is the transmitted light from the power source passing through the sample cell.

This is related to the absorbance according to the following equation;

$$A = -\log T \quad (3.64)$$

For dilute solutions, absorbance is also related to the concentration according to the Beer's Law (*Equation 3.65*).<sup>19</sup>

$$A = \epsilon cl \quad (3.65)$$

where  $A$  is the absorbance,  $\epsilon$  is the molar absorptivity ( $\text{dm}^3 \text{ mol}^{-1} \text{ cm}^{-1}$ ),  $c$  is the concentration ( $\text{mol}/\text{dm}^3$ ) and  $l$  is the path length (cm).

For a first-order reaction,



the absorbance at any time  $t$  can be written as;

$$A_t = \epsilon_X[X] + \epsilon_Y[Y] \quad (3.67)$$

where  $\epsilon_X$  and  $\epsilon_Y$  = molar absorptivity of X and Y, respectively.

Once the reaction has gone to completion, the absorbance can be represented as;

$$A_\infty = \epsilon_X[X]_0 + \epsilon_Y[Y]_0 \quad (3.68)$$

where  $A_\infty$  = the absorbance at the end of the reaction and  $[X]_0$  &  $[Y]_0$  = initial concentration of X and Y, respectively.

The integrated rate law of the absorbance expressions (*Equations 3.67 and 3.68*), shown in *Equation 3.69* can be used for kinetic analysis.

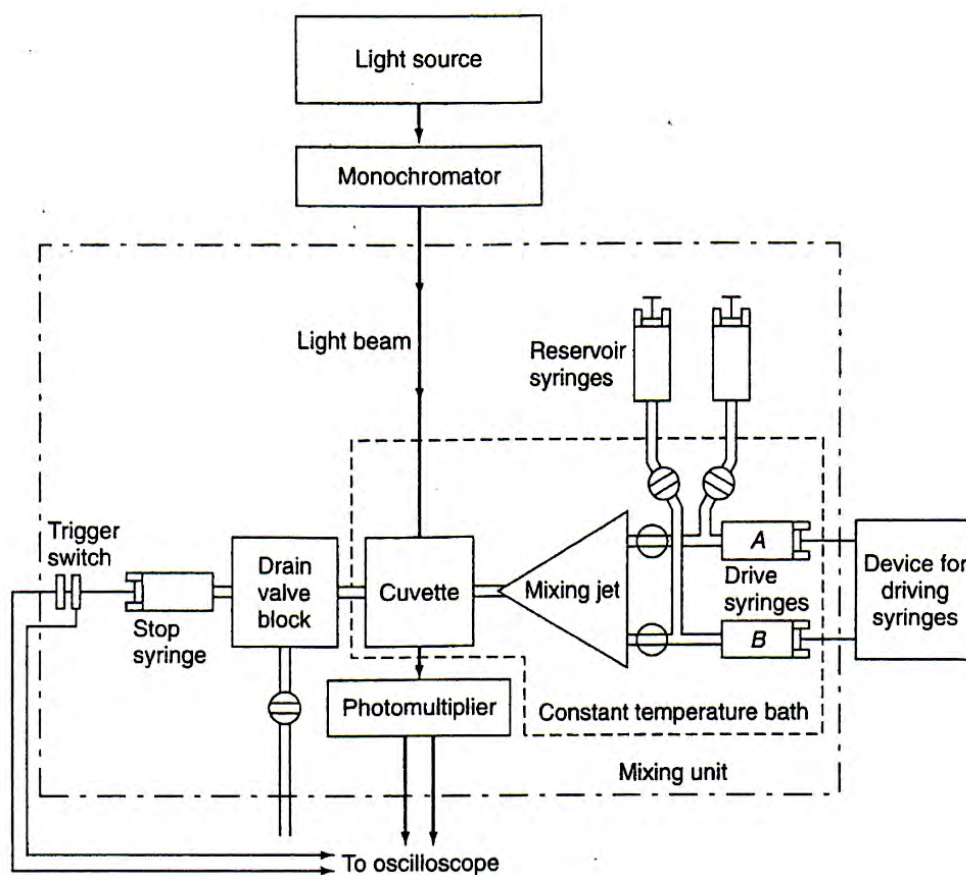
$$\ln \frac{[X]_0}{[X]_t} = \ln \left( \frac{A_0 - A_\infty}{A_t - A_\infty} \right) = k_{\text{obs}} t \quad (3.69)$$

From the above equation, a least-squares fit of the absorbance versus time at a specific wavelength can be used to determine the observed rate constant ( $k_{\text{obs}}$ ). By

monitoring the reaction at different concentrations, second-order rate constants can be determined. The reactions can also be performed at different temperatures and constant concentration to determine the activation parameters.

### 3.6.2 Stopped-flow technique

Some chemical reactions occur too fast to be monitored by conventional UV/visible spectrophotometer. Such reactions require shorter sampling and mixing times. Stopped-flow technique is a commonly used tool for investigating kinetic processes that go to completion in the time range of milliseconds to hundreds of seconds.<sup>22</sup> Schematic diagram of the stopped-flow analyser is shown in **Figure 3.3**. In the stopped-flow analyser, the two reactants are mixed rapidly from the syringes by a compressed gas-driven piston (800 kPa) into a mixing jet or a reaction chamber (**Figure 3.3**). The mixing takes approximately  $10^{-3}$  s then the resultant solution is driven into the cuvettes. The solution mixture is then allowed to rest at a fixed time interval. The reactive species is monitored and detected spectrophotometrically during the rest period. The reaction is monitored at a pre-determined constant temperature from the injection point to the reaction stage at the mixing chamber. Once the reaction is initiated, transmitted light is converted to an electric current in a photomultiplier unit then a signal is sent to a computer at an appropriate time interval. The data acquisition system promptly records absorbance-time resolved kinetic trace at a specific wavelength.



**Figure 3.3:** Schematic representation of a stopped-flow spectrophotometric analyser.<sup>13</sup>

### 3.7 References

---

1. R. van Eldik. *Coord. Chem. Rev.*, 2007, **251**,1649.
2. Reedijk. *Platinum Metals Rev.*, 2008, **52**:1, 2.
3. J. D. Atwood, *Inorganic and Organic Reaction Mechanisms*, 2nd Ed., Wiley- VCH Inc., New York, 1997, p. 1-32.
4. E. L. King, *How Chemical Reactions Occur: An Introduction to Chemical Kinetics and Reaction Mechanisms*, W. A. Benjamin, Inc, New York, 1964, p. 1.
5. J. W. Moore and R. G. Pearson, *Kinetics and Mechanism*, 3rd Ed., John Wiley and Sons, New York, 1981, p. 12-19.
6. R. B. Jordan, *Reaction Mechanisms of Inorganic and Organometallic Systems*, Oxford University Press New York, 1991, p. 1 - 17.
7. P. Atkins, J. de Paula Atkins, *Physical Chemistry*, 8th Ed. Oxford University Press, Oxford, 2006, p. 791-829.
8. S. E. Sherman, S. J. Lippard, *J. Chem. Rev.*, 1987, **50**, 147.
9. B.L. Rosenberg van Champ, J.E. Trosko, V. H. Mansour, *Nature*, 1969, **22**, 385.
10. S. Ašpergér, *Chemical Kinetics and Inorganic Reaction Mechanisms*, 2nd Ed. Kluwer Academic/Plenum Publishers, New York, 2003 (**3**), p. 14-23.
11. R. Van Eldik, *High Pressure Molecular Science*, 1999, **358**, 267.
12. R. Chang, *Physical chemistry for Biosciences*, USA, University Science Books, 2005, p. 338-342.
12. P. W. Atkins, *Physical Chemistry*, 6th ed., Oxford University Press, Oxford, 1998, p. 761-830.
13. K. J. Laidler, J. H. Meiser and B. C. Sanctuary, *Physical Chemistry*, 4th Ed., Houghton Mifflin Company, New York, 2003, p. 374-379, 390-393.
14. H. Eyring, *J. Chem. Phys.*, 1935, **3**, 107.
15. L. Helm, A.E. Merbach, *Dalton. Trans.*, 2002, 633.
16. S. R. Logan, *Fundamentals of Chemical Kinetics*, Longman, Essex, 1996, p. 1-30.
17. G. Jenner, *J. Phys. Org. Chem.* 2002, **15**, 1.
18. J. H. Espenson, *Chemical Kinetic and Reaction Mechanisms*, 2nd Ed., McGraw-Hill, New York, 1995, p. 1-80,155-159,161-162, 253-256.

19. D. A. Skoog, D. M. West, F. J. Holler and S. R. Crouch, *Fundamentals of Analytical Chemistry, 8th edition*, Brooks/Cole-Thomson Learning, Inc., United States, 2004, p. 718 - 734, 771 - 775, 878 - 894.
20. D. Katakis, G. Gordon, *Mechanisms of Inorganic Reactions*, John Wiley & Sons, New York, 1987, p. 99.
21. D. C. Harris, *Quantitative Chemical Analysis*, 4th Ed., W. H. Freeman and Company, New York, 1995, p. 480.
22. R-Y. Wang, *Application of Physical methods in Inorganic and Bioinorganic Chemistry*, Edited by R. A. Scott and C. M. Lukehart, 2007, John Wiley & Sons, Ltd. ISBN978-0-470-032176.

# Chapter 4

---

## The role of substituents in a bidentate *N,N*-chelate on the substitution of aqua ligands from bifunctional Pt(II) complexes

### 4.0 Abstract

The rate of substitution of aqua ligands from three bifunctional Platinum(II) complexes, *viz.*, [Pt{2-(pyrazol-1-ylmethyl)pyridine}(H<sub>2</sub>O)<sub>2</sub>](ClO<sub>4</sub>)<sub>2</sub>, [Pt(H<sub>2</sub>Py)], [Pt{2-(3,5-dimethylpyrazol-1-ylmethyl)pyridine}(H<sub>2</sub>O)<sub>2</sub>](ClO<sub>4</sub>)<sub>2</sub>, [Pt(dCH<sub>3</sub>Py)], and [Pt{2-[(3,5-bis(trifluoromethyl)pyrazol-1-ylmethyl)pyridine}(H<sub>2</sub>O)<sub>2</sub>](ClO<sub>4</sub>)<sub>2</sub>, [Pt(dCF<sub>3</sub>Py)], by three neutral sulfur donor nucleophiles, *viz.*, thiourea (TU), *N,N*-dimethylthiourea (DMTU), and *N,N,N',N'*-tetramethylthiourea (TMTU), were studied in aqueous perchloric acid medium of constant ionic strength. The substitution reactions were investigated under *pseudo*-first order conditions as a function of nucleophile concentration and temperature using UV/visible and stopped-flow spectrophotometries. The observed *pseudo*-first order rate constants,  $k_{obs(1/2)}$ , for the step-wise substitution of the first and second aqua ligands obeyed the rate laws:  $k_{obs(1/2)} = k_{2(1st/2nd)}[Nu]$ . The first substitution reaction takes place *trans* to the pyrazole ligand, while the second entering nucleophile is stabilised on the reaction site *trans* to the pyridine ligand. The order of reactivity: **Pt(dCF<sub>3</sub>Py) > Pt(H<sub>2</sub>Pyrd) > Pt(dCH<sub>3</sub>Py)** was found for the first aqua substitution, while that of a second aqua was **Pt(H<sub>2</sub>Py) ≈ Pt(dCF<sub>3</sub>Py) > Pt(dCH<sub>3</sub>Py)**. Spectrophotometric acid-base titrations were performed to determine the  $pK_a$  values of the coordinated aqua ligands. Lower  $pK_a$  values were recorded for the aqua ligands *trans* to the pyridine ring, when compared to  $pK_a$  values which were observed for the aqua ligand *trans* to the pyrazole ring. Density functional theoretical (DFT) calculations were performed to support the interpretation and discussion of the experimentally obtained kinetic and thermodynamic results.

## 4.1 Introduction

The antitumor activity of cisplatin initiated extensive investigations on platinum coordination compounds.<sup>1</sup> Cisplatin is still one of the most used anticancer drugs on the market.<sup>2</sup> However, it has a narrow spectrum of activity and its clinical use is accompanied by severe side effects, including ototoxicity, neurotoxicity, nephrotoxicity, myelosuppression, nausea and vomiting.<sup>3</sup> To overcome these limitations, considerable efforts have been made on designing new drugs with a potential to display improved therapeutic properties, through understanding their ligand exchange reactions which are thought to be responsible for cytotoxicity.<sup>3</sup>

Early kinetic studies on the mechanism of action of cisplatin and its analogues, established the empirical relationships between the structures of the platinum complexes and their activity which Cleare and Hoeschele termed the structure-activity relationships (SARs).<sup>4,5</sup> A *cis*-geometry on the complex of the form *cis*-[Pt(*N*-*N*)X<sub>2</sub>], where *N* = nitrogen donor ligands and *X* = labile group, was postulated as the basic requirement for the anticancer activity. This *cis*-geometry is still of interest in the search for effective antitumour drugs.

The conformational instability of the helical structure of DNA, caused by the binding of Pt(II) drugs is now known as one of the mechanisms responsible for cytotoxicity.<sup>6</sup> However, there are many other competing biomolecules that can react with the Pt(II) complexes such as peptides, proteins and enzymes.<sup>7</sup> In particular, sulfur-containing biomolecules have a high affinity for Pt(II) drugs. Their reactions are associated with nephrotoxicity and neurotoxicity.<sup>7,8</sup> It remains unclear how Pt(II) drugs reach their target (genomic DNA), despite their stronger affinity for binding to S-containing nucleophiles known to be ubiquitous in the blood serum and cytoplasm.<sup>8,9</sup> A plausible hypothesis is that S-containing nucleophiles initially bind to the Pt(II) metal centre to form stable intermediates which subsequently convert to thermodynamically more stable Pt-DNA adducts in the nucleus.<sup>3,6</sup> These Pt-Sulfur adducts have been regarded as Pt(II) drug reservoirs.

Understanding the mechanistic pathways and the reactivity of Pt(II) complexes both *in vitro* and *in vivo* is vital in the rational design of new compounds with improved potency.<sup>6-9</sup> Tailoring the steric and electronic properties of the non-leaving ligands



around Pt(II) ions can be a useful tool for optimising cytotoxicity and circumvention of drug resistance.<sup>10</sup>

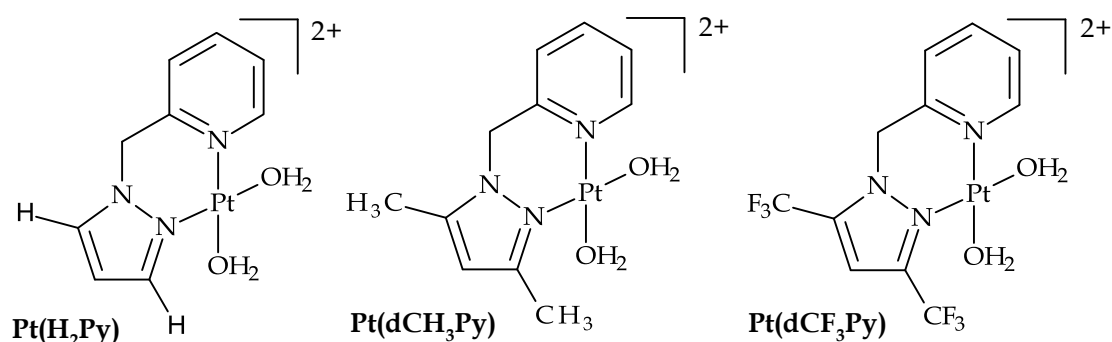
Recent studies have shown that  $\pi$ -acceptors increase the electrophilicity of the Pt(II) centre due to  $\pi$ -back-bonding, resulting in an increase in the rate of nucleophilic substitution.<sup>11</sup> van Eldik and co-workers<sup>12</sup> systematically studied the effect of different *N*-donor non-leaving ligands on the reactivity of diaqua Pt(II) complexes of the type  $cis-[Pt(N-N)(H_2O)_2]^{2+}$ , where *N-N* = ethylenediamine (en), diaminocyclohexane (dach), aminomethylpyridine (amp) and bipyridine (bpy). These complexes have one (amp) or two (bpy)  $\pi$ -accepting pyridine rings coordinated to the Pt(II) centre. Reactivity of the complexes increased in a proportional manner with an increase in  $\pi$ -accepting rings.

In a related study of Pt(II) complexes with *N-N/N-S* bidentate ligands *viz.*  $cis-[Pt(NH_3)_2Cl_2]$ ,  $cis-[Pt(en)Cl_2]$ ,  $cis-[Pt(dach)Cl_2]$  and  $cis-[Pt(SCM)Cl_2]^-$  (where SCM = S-methyl-L-cysteine), the lability of the chloride was found to depend on both steric and electronic effects of the non-leaving group.<sup>13</sup> The rate of substitution followed the order:  $[Pt(dach)Cl_2] < [Pt(en)Cl_2] < cis-[Pt(NH_3)_2Cl_2] < [Pt(SCM)Cl_2]^-$ . High reactivity of  $[Pt(SCM)Cl_2]^-$  was attributed to the strong *trans*-labilization effect of the coordinated sulphur donor, as evidenced by the elongation of the Pt-Cl bond in a *trans* position.  $[Pt(dach)Cl_2]$  was the least reactive complex because of the steric congestion due to the diaminocyclohexane group which also imparts some positive inductive effect to the Pt(II) centre, making it less electrophilic.<sup>13</sup>

To further our understanding on the role of *cis* and *trans*  $\sigma/\pi$ -effects as well as the steric influence on the thermodynamic and kinetic properties of Pt(II) complexes, three Pt(II) complexes with flexible (pyrazolylmethyl)pyridine ligands (**Figure 4.1**) were synthesised and their substitution kinetics were studied. The (pyrazolylmethyl)pyridine ligand was altered by incorporating either methyl or trifluoromethyl groups in 3,5-positions of the pyrazole ring. Sulfur-containing nucleophiles, *viz.* thiourea (TU), *N,N*-dimethylthiourea (DMTU), and *N,N,N',N'*-tetramethylthiourea (TMTU) were used to substitute the two aqua labile ligands.

Thiourea nucleophiles were chosen because of their neutral character, good solubility, high nucleophilicity, and biological relevance.<sup>3,14</sup> Thiourea is used as a

protective agent to minimise nephrotoxicity, following cisplatin treatment.<sup>3</sup> In addition, thioureas combine ligand properties of thiolates ( $\sigma$ -donors) and thioethers ( $\sigma$ -donors and  $\pi$ -acceptors) which are present in the biological systems.<sup>15</sup> The substitution kinetics of the diaqua complexes was undertaken, since they are considered to be reactive species in the crucial step of the binding of cisplatin to DNA.<sup>11</sup> The density functional theoretical (DFT) calculations were used to support the experimentally obtained thermodynamic ( $pK_a$  values) and kinetic results (rate constants).



**Figure 4.1:** Chemical structures of the bifunctional Pt(II) complexes. The perchlorate ( $\text{ClO}_4^-$ ) counter ions are omitted for clarity.

## 4.2 Experimental

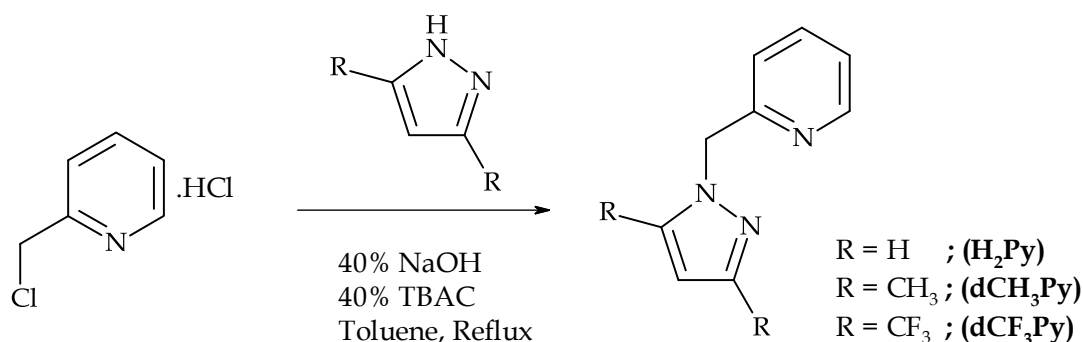
### 4.2.1 Chemicals

All synthetic manipulations of the ligands were carried out in air, whereas the coordination of the ligands to the platinum metal was performed under inert atmosphere of nitrogen using standard Schlenk techniques. The ligand precursors, 2-(chloromethyl)pyridine hydrochloride (98%), pyrazole (98%), 3,5-dimethylpyrazole (99%), 3,5-bis(trifluoromethyl)pyrazole (99%) as well as the metal salts, potassium tetrachloroplatinate ( $\text{K}_2\text{PtCl}_4$ , 99+%) and sodium perchlorate monohydrate ( $\text{NaClO}_4 \cdot \text{H}_2\text{O}$ , 98%) were all purchased from Aldrich and used without further purification. Silver perchlorate ( $\text{AgClO}_4$ , 99+%, Aldrich) was stored under nitrogen and used as received. Perchloric acid ( $\text{HClO}_4$ , 70% solution) and hydrochloric acid ( $\text{HCl}$ , 32% solution) were obtained from Saarchem and used as supplied. The nucleophiles thiourea (TU, 99%), *N,N*-dimethylthiourea (DMTU, 99%) and *N,N,N',N'*-tetramethylthiourea (TMTU, 98%) were also obtained from Aldrich and

used without further purification. Ultrapure water (MODULAB purification system) was used for all aqueous reactions. All other chemicals and solvents were of reagent grade and used as received.

#### 4.2.2 Synthesis of the ligands

Three ligands, namely 2-(pyrazol-1-ylmethyl)pyridine (**H<sub>2</sub>Py**), 2-(3,5-dimethylpyrazol-1-ylmethyl)pyridine (**dCH<sub>3</sub>Py**) and 2-[(3,5-bis(trifluoromethyl)pyrazol-1-ylmethyl)]pyridine (**dCF<sub>3</sub>Py**) were prepared *via* a phase transfer catalysed *N*-alkylation reaction of either pyrazole, 3,5-dimethylpyrazole or 3,5-bis(trifluoromethyl)pyrazole with 2-(chloromethyl)pyridine hydrochloride in a biphasic medium (**Scheme 4.1**) following a method described by Steel *et al.*<sup>16</sup> Copious amount of water was used to completely remove tetrabutylammonium chloride (TBAC) from the organic phase. All ligands were obtained in moderate to high yields (63-90%) and collected as either yellow or brown oils of sufficient purity for subsequent use in platinum coordination. The purity of the ligands was confirmed by <sup>1</sup>H NMR, <sup>13</sup>C NMR, TOF-MS-ESI<sup>+</sup> and CHN elemental analysis.



**Scheme 4.1:** Synthesis of the (pyrazolylmethyl)pyridine ligands.

#### 2-(pyrazol-1-ylmethyl)pyridine (**H<sub>2</sub>Py**)

A mixture of 2-(chloromethyl)pyridine hydrochloride (2.72 g; 16.6 mmol) and pyrazole (1.13 g; 16.6 mmol) was dissolved in toluene (50 mL), to which 25 mL of 40% aqueous NaOH and 10 drops of 40% aqueous tetrabutylammonium chloride (TBAC) was added. The mixture was refluxed for 24 h after which the organic phase was extracted with dichloromethane (CH<sub>2</sub>Cl<sub>2</sub>) and evaporated under reduced pressure to yield a brown-yellow oil. The crude product was re-dissolved in CH<sub>2</sub>Cl<sub>2</sub>,

washed with water (3 x 50 mL), and then further purified by column chromatography, using a short-column of aluminium oxide and CH<sub>2</sub>Cl<sub>2</sub> as an eluent. The organic extracts were dried over anhydrous MgSO<sub>4</sub> and evaporated under *vacuo* to afford an analytically pure bright yellow oil of **H<sub>2</sub>Py**.

Yield = 2.379 g (90 %). <sup>1</sup>H NMR (400 MHz: CDCl<sub>3</sub>): δ<sub>H</sub> (ppm); 5.37 (s, 2H, -CH<sub>2</sub>-), 6.22-6.23 (t, 1H, pz), 6.87-6.89 (d, 1H, py), 7.07-7.09 (t, 1H, py), 7.44-7.45 (t, 1H, py), 7.48-7.53 (m, 2H, pz), 8.46-8.47 (d, 1H, py). <sup>13</sup>C NMR (100 MHz: CDCl<sub>3</sub>): δ<sub>C</sub> (ppm); 57.40, 106.13, 121.59, 122.65, 129.94, 136.99, 139.84, 149.31, 156.66. TOF MS-ESI<sup>+</sup> *m/z*: 160.0873, 100% (M+1). Anal. calculated for C<sub>9</sub>H<sub>9</sub>N<sub>3</sub>: C, 67.90; H, 5.70, N, 26.40%. Found: C, 67.26; H, 5.35; N, 26.54%.

Ligands **dCH<sub>3</sub>Py** and **dCF<sub>3</sub>Py** were prepared following the same procedure for **H<sub>2</sub>Py**, with 3,5-dimethylpyrazole and 3,5-bis(trifluoromethyl)pyrazole used instead of unsubstituted pyrazole, respectively. All ligands were stored under nitrogen until their subsequent platination.

#### **2-(3,5-dimethylpyrazolyl-1-ylmethyl)pyridine (dCH<sub>3</sub>Py)**

Yield = 1.917 g (77 %, bright-yellow oil). <sup>1</sup>H NMR (400 MHz: CDCl<sub>3</sub>): δ<sub>H</sub> (ppm); 2.10 (s, 3H, CH<sub>3</sub>, pz), 2.19 (s, 3H, CH<sub>3</sub>, pz), 5.28 (s, 2H, -CH<sub>2</sub>-), 5.82 (s, 1H, pz), 6.72-6.74 (d, 1H, py), 7.04-7.07 (t, 1H, py), 7.47- 7.51 (t, 1H, py), 8.45-8.46 (d, 1H, py). <sup>13</sup>C NMR (100 MHz: CDCl<sub>3</sub>): δ<sub>C</sub> (ppm); 10.97, 13.49, 54.32, 105.65, 120.89, 122.29, 128.25, 136.95, 139.59, 149.17, 157.39. TOF MS-ESI<sup>+</sup> *m/z*: 188.1185, 100% (M+1). Anal. calculated for C<sub>11</sub>H<sub>13</sub>N<sub>3</sub>: C, 70.56; H, 7.00, N, 24.44%. Found: C, 70.09; H, 6.81; N, 22.69%.

#### **2-[(3,5-bis(trifluoromethyl)pyrazolyl-1-ylmethyl)pyridine (dCF<sub>3</sub>Py)**

Yield= 1.483 (63%, light brown oil). <sup>1</sup>H NMR (400 MHz: CDCl<sub>3</sub>): δ<sub>H</sub> (ppm); 5.68 (s, 2H, -CH<sub>2</sub>-), 6.95-6.97 (d, 1H, py), 7.00 (s, 1H, pz), 7.26-7.30 (t, 1H, py), 7.68- 7.73 (t, 1H, py), 8.61-8.62 (d, H, py). <sup>13</sup>C NMR (100 MHz: CDCl<sub>3</sub>): δ<sub>C</sub> (ppm); 57.08, 106.57, 117.73, 120.41, 120.97, 123.13, 133.91, 137.07, 142.64, 149.64, 154.35. TOF MS-ESI<sup>+</sup> *m/z*: 296.057, 100% (M+1). Anal. calculated for C<sub>11</sub>H<sub>7</sub>N<sub>3</sub>F<sub>6</sub>: C, 44.76; H, 2.39, N, 14.24%. Found: C, 44.42; H, 2.46; N, 14.41%.

#### 4.2.3 Synthesis of Pt(II) complexes

The complexes, *viz.*, [Pt{2-(pyrazol-1-ylmethyl)pyridine}Cl<sub>2</sub>], [Pt(H<sub>2</sub>Py)Cl<sub>2</sub>], [Pt{2-(3,5-dimethylpyrazol-1-ylmethyl)pyridine}Cl<sub>2</sub>], [Pt(dCH<sub>3</sub>Py)Cl<sub>2</sub>], and [Pt{2-[(3,5-bis(trifluoromethyl)pyrazol-1-ylmethyl)]pyridine}Cl<sub>2</sub>], [Pt(dCF<sub>3</sub>Py)Cl<sub>2</sub>], were synthesised following a common method adopted from Rauterkus *et al.*<sup>17</sup> with minor modifications. K<sub>2</sub>PtCl<sub>4</sub> (0.20 g; 0.48 mmol) was stirred for about 10 min in ultrapure water (35 mL). To this solution the ligand (0.48 mmol) dissolved in a small amount of CH<sub>2</sub>Cl<sub>2</sub> was added in a drop-wise manner. The reaction mixture was stirred under reflux for 24 h (in the dark) and then cooled to room temperature. The resulting yellow precipitate was collected by filtration and sequentially washed with small amounts of water, methanol and diethyl ether. It was then thoroughly dried under vacuum to get a fine yellow powder of the neutral complex. For the formation of the complex, [Pt(dCF<sub>3</sub>Py)Cl<sub>2</sub>], 0.01 M HCl solution was used instead of ultrapure water. The purity was confirmed by <sup>1</sup>H NMR, <sup>13</sup>C NMR, <sup>195</sup>Pt NMR, elemental analysis, TOF MS-ESI<sup>+</sup> and infrared (IR) spectroscopy.

[Pt(H<sub>2</sub>Py)Cl<sub>2</sub>]. Yield: 154 mg (75 %). <sup>1</sup>H NMR (400 MHz: DMSO-d<sub>6</sub>): δ<sub>H</sub> (ppm); 5.81 (s, 2H, -CH<sub>2</sub>-), 6.56-6.57 (t, 1H, pz), 7.59-7.63 (t, 1H, py), 7.75-7.78 (d, 1H, py), 7.88- 7.89 (d, 1H, py), 8.17-8.24 (dd, 2H, pz), 9.14-9.16 (d, 1H, py). <sup>13</sup>C NMR (100 MHz: DMSO-d<sub>6</sub>): δ<sub>C</sub> (ppm); 57.72, 107.67, 126.55, 126.76, 134.36, 141.03, 141.39, 151.96, 153.84. <sup>195</sup>Pt NMR (107 MHz: DMSO-d<sub>6</sub>): δ<sub>Pt</sub> (ppm); -2189.72. TOF MS-ESI<sup>+</sup> *m/z*: 390.028 (M-Cl)<sup>+</sup>. IR (KBr) cm<sup>-1</sup>: 451, 617, 702, 759, 1078, 1155, 1273, 1421, 1611, 2852, 2922. Anal. calculated for C<sub>9</sub>H<sub>9</sub>N<sub>3</sub>PtCl<sub>2</sub>: C, 25.42; H, 2.13, N, 9.88%. Found: C, 25.56; H, 2.60; N, 9.97%.

[Pt(dCH<sub>3</sub>Py)Cl<sub>2</sub>]. Yield: 186 mg (86%). <sup>1</sup>H NMR (400 MHz: DMSO-d<sub>6</sub>): δ<sub>H</sub> (ppm); 2.42 (s, 3H, CH<sub>3</sub>, pz), 2.44 (s, 3H, CH<sub>3</sub>, pz), 5.61-5.65 (d, 1H, -CH<sub>2</sub>-, AB-spin system), 5.81-5.84 (d, 1H, -CH<sub>2</sub>-, AB-spin system), 6.14 (s, 1H, pz), 7.55-7.58 (t, 1H, py), 7.92-7.94 (d, 1H, py), 8.11-8.22 (d, 1H, py), 8.94-9.14 (d, 1H, py). <sup>13</sup>C NMR (100 MHz: DMSO-d<sub>6</sub>): δ<sub>C</sub> (ppm); 11.63, 14.34, 53.06, 108.14, 126.15, 126.63, 140.91, 142.90, 151.41, 152.97, 153.93. <sup>195</sup>Pt NMR (107 MHz: DMSO-d<sub>6</sub>): δ<sub>Pt</sub> (ppm); -2158.67. TOF MS-ESI<sup>+</sup> *m/z*: 418.060 (M-Cl)<sup>+</sup>. IR (KBr) cm<sup>-1</sup>: 454, 601, 675, 780, 800, 1154, 1225, 1278, 1418, 1471,

1552, 1605, 2163, 2853, 2919. Anal. calculated for  $C_{11}H_{13}N_3PtCl_2$ : C, 29.14; H, 2.89, N, 9.27%. Found: C, 28.99; H, 3.28; N, 9.20%.

[Pt(dCF<sub>3</sub>Py)Cl<sub>2</sub>]. Yield: 170 mg (63%). <sup>1</sup>H NMR (400 MHz: DMSO-d<sub>6</sub>): δ<sub>H</sub> (ppm); 5.89-5.93 (d, 1H, -CH<sub>2</sub>-, AB-spin system), 6.39 (s, 1H, pz), 6.49-6.53 (d, 1H, -CH<sub>2</sub>-, AB-spin system), 7.61-7.65 (d, 1H, py), 7.93- 7.98 (t, 1H, py), 8.15-8.19 (t, 1H, py), 8.91-8.92 (d, 1H, py). <sup>13</sup>C NMR (100 MHz: DMSO-d<sub>6</sub>): δ<sub>C</sub> (ppm); 57.04, 107.93, 122.08, 123.76, 124.03, 137.73, 141.51, 149.86, 154.61, 154.92, 15.92. <sup>195</sup>Pt NMR (107 MHz: DMSO-d<sub>6</sub>): δ<sub>Pt</sub> (ppm); -2888.75. TOF MS-ESI<sup>+</sup> *m/z*: 525.979 (M-Cl)<sup>+</sup>. IR (KBr) cm<sup>-1</sup>: 469, 778, 829, 976, 1045, 1095, 1129, 1227, 1275, 1384, 1599, 1643, 2741, 2922. Anal. calculated for  $C_{11}H_7N_3PtCl_2F_6$ : C, 23.54; H, 1.26, N, 7.49%. Found: C, 23.70; H, 1.30; N, 7.54%.

#### 4.2.4 Preparation of diaqua Pt(II) complexes

The solutions of diaqua Pt(II) complexes Pt(H<sub>2</sub>Py), Pt(dCH<sub>3</sub>Py) and Pt(dCF<sub>3</sub>Py) (Figure 4.1), were prepared as described in the literature.<sup>18</sup> Accurately weighed dichloro Pt(II) complex and AgClO<sub>4</sub> (1.98 molar ratio) were suspended in 0.01 M HClO<sub>4</sub> and the mixture was vigorously stirred at 50 °C for 24 h in the dark. The white precipitate of silver chloride (AgCl) was filtered off through 0.45 µm nylon membrane using a Millipore filtration setup. The clear and colourless filtrate was diluted with 0.01 M HClO<sub>4</sub> in a volumetric flask to make the required concentration of the complex in solution. An acidic medium (pH = 2) was necessary to ensure that only diaqua complexes and not the mixture of aqua/hydroxo complexes, were present in solution once the metathesis reaction was complete. The adjustment of *I* = 0.10 M with NaClO<sub>4</sub> was done to ensure a constant ionic strength throughout the kinetic measurements.

#### 4.2.5 Instrumentation and physical measurements

NMR spectra of the ligands and complexes were recorded on the Bruker Avance DRX 400 or DRX 500. Low resolution electrospray ionization (ESI<sup>+</sup>) mass spectra of the ligands and the complexes were recorded on a time-of-flight (TOF) micromass spectrometer. Infrared (IR) spectra were acquired using KBr discs on a Perkin Elmer Spectrum One FTIR spectrometer. Elementary composition of all synthesised

compounds was determined on FLASH 2000 CHN analyser. Kinetic measurements of fast reactions were monitored using an Applied Photophysics (v4.33) SX.18 MV stopped-flow spectrophotometer coupled to an online data acquisition system. The temperature of the instrument was controlled to within  $\pm 0.1$  °C for all measurements. Spectrophotometric pH titrations, preliminary wavelength searching experiments as well as kinetic measurements for the slow reactions were recorded on a Cary 100 Bio UV-visible spectrophotometer equipped with a Varian Peltier temperature thermostat with an accuracy of  $\pm 0.05$  °C. The pH measurements were determined on a Jenway 4330 pH meter equipped with a 4.5  $\mu$ m glass electrode. The microelectrode was calibrated at 25 °C using the standard buffer solutions (Merck) at pH 4.0, 7.0 and 10.0.  $pK_a$  titration curves and time-dependent kinetic traces were graphically analysed using Origin 7.5® software package.<sup>19</sup>

#### **4.2.6 Measurements of $pK_a$ values of the diaqua Pt(II) complexes**

Spectrophotometric pH titrations of diaqua Pt(II) complexes were performed in the pH range of 2-10, using NaOH as a base. To minimise dilution effects due to the addition of the titrant, and hence the shifting of the baseline, a large volume (300 mL) of the metal complex solution was used for titration and small amounts of crushed NaOH pellets were used within the pH range of 2-3. Dilute NaOH and HClO<sub>4</sub> solutions of decreasing concentrations were used in the manner that ensured as many evenly distributed points were obtained on the rising or falling parts of the titration curve. Upon the addition of HClO<sub>4</sub> as a titrant, the reversibility of the titration reaction was observed with the baseline remaining intact. Small vials were used for sampling out 2 mL aliquots of the complex solution for pH measurements. These aliquots were then discarded after each measurement to avoid the *in situ* contamination of the complex solution by chloride ions which may be released from the electrode. Following each titrant addition, the solution was allowed to stir before its pH and respective absorbance spectrum were acquired. Sample aliquots from each absorbance measurements were returned to the stock solution of the complex for re-use.

#### 4.2.7 Kinetic measurements

All substitution reactions were performed under *pseudo* first-order conditions, as a function of nucleophile concentration and temperature. The nucleophile concentration was provided in at least 20-fold excess over that of a bifunctional Pt(II) complex. This afforded a 10-fold excess of the nucleophile concentration for each of the two coordinated leaving groups, which is sufficient to force the reactions to go to completion. A pH of 2.0 was maintained throughout the kinetic runs to guarantee the presence of only diaqua complexes (based on the  $pK_a$  results; **Table 4.1**). Slow reactions were initiated by manually mixing equal volumes of the complex and nucleophile solutions manually in a Suprasil tandem cuvette. For fast reactions, equal amounts of pre-equilibrated complex and nucleophile solutions were mixed through a pressure-driven cross-plunging technique in the chamber of the stopped-flow analyser. Suitable wavelengths at which kinetic measurements were performed were established spectrophotometrically by monitoring spectral changes (absorbance *vs.* wavelength) due to mixing of the Pt(II) metal complex and nucleophile solutions. These are summarised in **Table SI 4.1** (supporting information).

#### 4.2.8 Computational calculations

In an effort to gain insight into the experimental data as well as to understand the electronic differences of the bifunctional Pt(II) complexes, computational calculations were performed. The ground state electronic structures of **Pt(H<sub>2</sub>Py)**, **Pt(dCH<sub>3</sub>Py)** and **Pt(dCF<sub>3</sub>Py)** were optimized at the Density Functional Theoretical (DFT) level, to identify energy-minimized structures based on B3LYP/LanL2DZ (Los Alamos National Laboratory 2 Double  $\zeta$ ) level of theory.<sup>20</sup> B3LYP refers to Becke's three parameter functional hybrid exchange with functional correlation gradient of Lee, Yang and Parr basis set.<sup>21,22</sup> This method is suitable for gaseous simulations of compounds containing heavy atoms such as platinum. The aqua complexes were each modelled at +2 with respect to their total charge. A singlet state was assumed due to low electronic spin of Pt(II) complexes. Gaussian09 suite of programs was used for all computational analysis.<sup>23</sup>

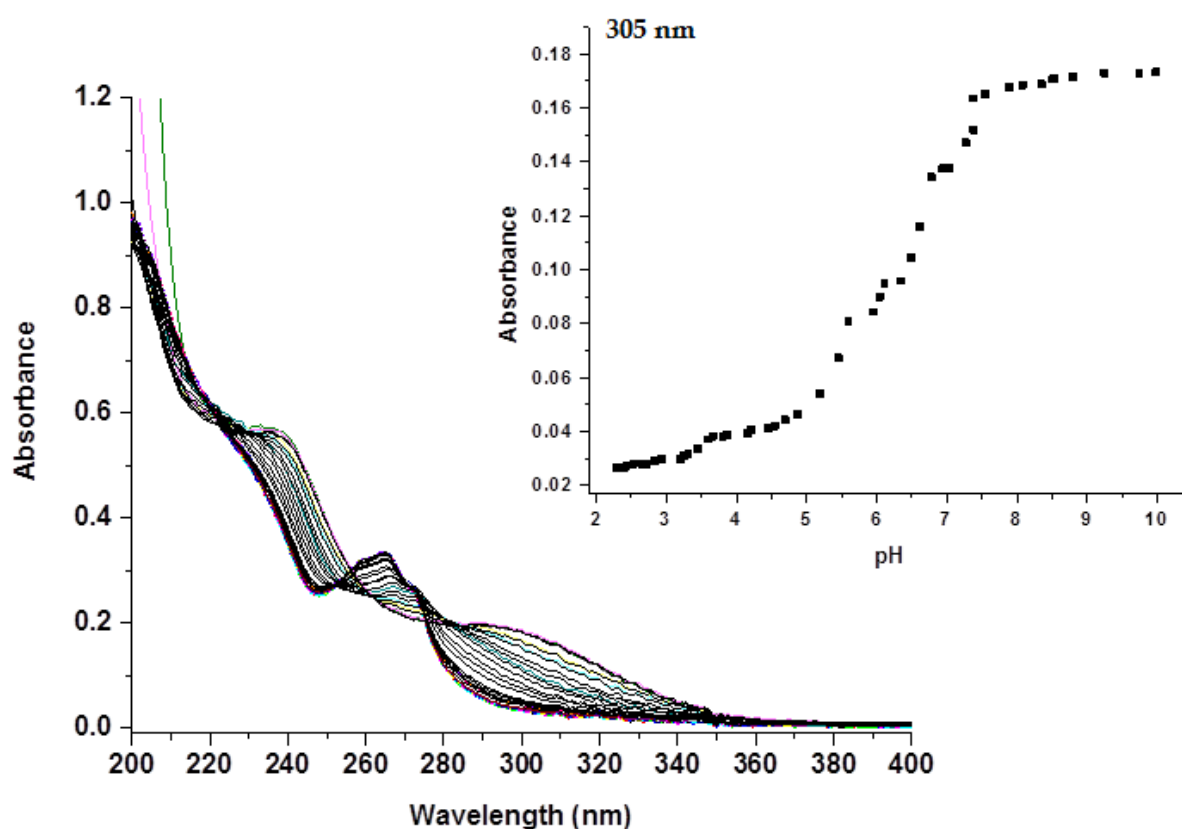


### 4.3 Results

In order to investigate the electronic and steric effects of the non-leaving ligands, three bifunctional Pt(II) complexes with (pyrazolylmethyl)pyridine ligands (**Figure 4.1**) were synthesised, characterised and their ligand substitution reactions studied kinetically and thermodynamically. The ligands were altered by introducing substituents on the 3,5-positions of the pyrazole ring.

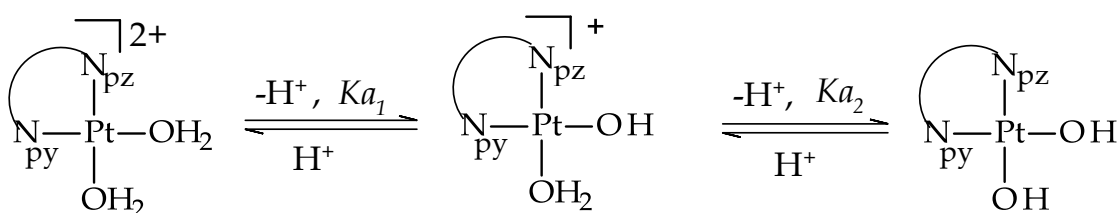
#### 4.3.1 Acid-base equilibrium of diaqua Pt(II) complexes

Representative spectral changes in absorbance recorded as a function of wavelength during the pH titration of **Pt(dCH<sub>3</sub>Py)** with NaOH are shown in **Figure 4.2**. The  $pK_a$  value of each coordinated aqua ligand was determined by plotting the absorbance as a function of pH at a suitable wavelength. A typical example is presented as an inset in **Figure 4.2**. The resulting  $pK_a$  values of the coordinated aqua ligands were obtained by fitting the data to two concerted sigmoidal function (Boltzman) using origin 7.5® software.<sup>19</sup>



**Figure 4.2:** UV/visible spectra for the titration of 0.06 mM **Pt(dCH<sub>3</sub>Py)** with NaOH in the pH range 2-10 at  $T = 298.15$  K. Insert: Boltzmann fit of the pH data at 305 nm.

All diaqua Pt(II) complexes exhibited three different absorbance maxima, which shifted towards higher wavelengths with increasing pH (also see **Figure SI 4.3**). This suggests the presence of three different species in solution as a function of pH *viz.* diaqua, aqua-hydroxo and dihydroxo complexes. This is also supported by the presence of three isosbestic points. In addition, the absorbance *versus* pH plots for all diaqua complexes exhibited two *quasi*-inflection points, which is a clear indication of two concerted deprotonation steps with equilibrium constants,  $K_{a1}$  and  $K_{a2}$  as shown in **Scheme 4.2**.



**Scheme 4.2:** Proposed stepwise deprotonation of the diaqua Pt(II) complexes.

**Table 4.1** summarises the  $pK_a$  values for diaqua Pt(II) complexes. Included for comparison purposes are the  $pK_a$  values of [Pt(aminomethylpyridine)(H<sub>2</sub>O)<sub>2</sub>]<sup>2+</sup> **Pt(amp)** and [Pt(*N,N'*-bipyridine)(H<sub>2</sub>O)<sub>2</sub>]<sup>2+</sup>, **Pt(bpy)**.<sup>12</sup>

**Table 4.1.** Summary of  $pK_a$  data for the deprotonation of Pt-bound aqua ligands in the bifunctional Pt(II) complexes

	<b>Pt(H<sub>2</sub>Py)</b>	<b>Pt(dCH<sub>3</sub>Py)</b>	<b>Pt(dCF<sub>3</sub>Py)</b>	<b>Pt(amp)</b>	<b>Pt(bpy)</b>
<b>p<i>K</i><sub>a1</sub></b>	4.85 ± 0.06	5.29 ± 0.10	4.76 ± 0.05	5.82 <sup>a</sup>	4.80 <sup>a</sup>
<b>p<i>K</i><sub>a2</sub></b>	6.30 ± 0.02	6.32 ± 0.14	6.27 ± 0.02	6.83 <sup>a</sup>	6.32 <sup>a</sup>

<sup>a</sup>  $pK_a$  value of related bifunctional Pt(II) complexes extracted from ref.12

van Eldik and co-workers,<sup>12,24,25</sup> investigated a set of similar bifunctional Pt(II) complexes with bidentate nitrogen-donor ligands. A distinction between the first and second deprotonation site was made. They proposed the first step to occur at an aqua *trans* to the pyridine ring. Because of the similarity of their complexes to those investigated in this work, we also postulate that the first deprotonation step occurs

to the aqua ligand *trans* to the pyridine ring, followed by the one *trans* to pyrazole ring as indicated in **Scheme 4.1**. The electron density on the Pt(II) centre and the coordinated hydroxo ligands are stabilised by the electron-withdrawing ability of the  $\pi$ -accepting pyridine ring, which leads to lower  $pK_a$  values.<sup>24,25</sup> The pyrazole ring has a stronger  $\sigma$ -donor strength than pyridine, making the bond between aqua ligand positioned *trans* to this group weaker due to its strong *trans*-influence in the ground state.<sup>24,25</sup> This is evidenced by a longer Pt–OH<sub>2</sub> (1) bond *trans* to the pyrazole ring compared to the Pt–OH<sub>2</sub> (2) bond *trans* to the pyridine ring (**Table 4.2**). Consequently, a higher  $pK_a$  value is obtained for the aqua ligand *trans* to the pyrazole ring, compared to the one *trans* to pyridine (**Table 4.1**).

Previous studies have shown that the  $pK_a$  values of aqua Pt(II) complexes decrease as the  $\pi$ -accepting capacity of the core ligand increases due to an increased acidity of the coordinated aqua ligand.<sup>11,25,26</sup> However, the enhancement of the  $\sigma$ -donor strength of the ligand leads to a higher  $pK_a$  value due to the increased basicity of the coordinated aqua ligand.<sup>24,26,27</sup> Similarly, the introduction of electron-donating methyl groups to the pyrazole ring as in **Pt(dCH<sub>3</sub>Py)** increase the  $\sigma$ -donor strength of the coordinated pyrazole resulting in a moderate increase in the  $pK_{a(1/2)}$  values for this complex compared to **Pt(H<sub>2</sub>Py)**. Alternatively, the introduction of an electron-withdrawing trifluoromethyl groups to the pyrazole ring as in **Pt(dCF<sub>3</sub>Py)** results into a decrease in the  $pK_{a(1/2)}$  values due to an increased  $\pi$ -acceptability and decreased  $\sigma$ -donor capacity of the pyrazole ring. It is also noted that the formation of dihydroxo species from the aqua/hydroxo species occurs at a higher pH than the first deprotonation step. This has been reported before in related bifunctional Pt(II) complexes,<sup>12,25</sup> and is attributed to a decrease in the overall charge from +2 to +1 on forming the hydroxo species. Since the  $pK_a$  values depend on the electrophilicity of the metal centre,<sup>11,26,27</sup> the introduction of different substituents on the pyrazole ligand has a significant influence on the lability of the coordinated aqua ligands in the bifunctional Pt(II) complexes.

#### 4.3.2 DFT-calculated optimised structures

The geometry-optimised structures for the bifunctional Pt(II) complexes and the calculated data are shown in **Figure 4.3** and **Table 4.2**, respectively. The (pyrazolymethyl)pyridine ligand coordinates to the metal centre *via* its two nitrogen donors, forming a six-membered chelate ring which can exist in either chair or boat conformation due to the flexibility of the methylene ( $-\text{CH}_2-$ ) linker between pyrazole and pyridine rings. The two aqua ligands complete the coordination spheres resulting in the slightly distorted square planar geometry around the metal centre.

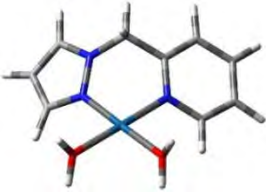

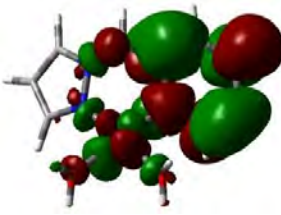
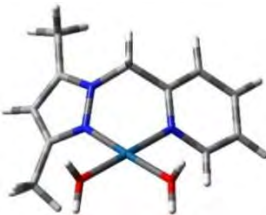
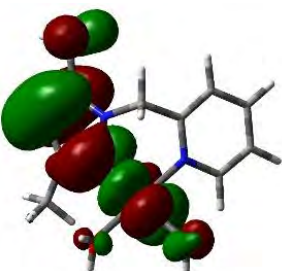
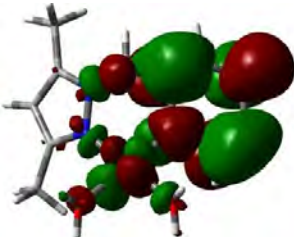
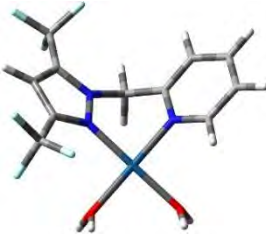
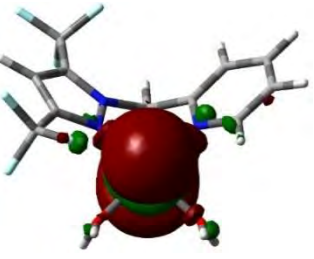
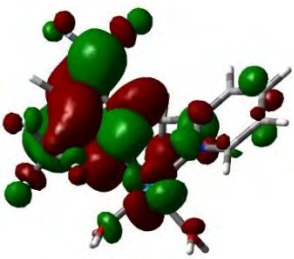
This is shown by the magnitude of bond angles,  $a$  and  $d$  ( $\sim 90^\circ$ ) as well as nearly linear arrangement of the atoms:  $\text{N}_{\text{pz}}-\text{Pt}-\text{OH}_2$  (1) and  $\text{N}_{\text{py}}-\text{Pt}-\text{OH}_2$  (2) (see **Table 4.2**). The mapping of the frontier orbitals indicate that the HOMOs are concentrated directly above and below the Pt(II) ion for **Pt(H<sub>2</sub>Py)** and **Pt(dCF<sub>3</sub>Py)**, with no significant contribution from the ligand and the leaving groups. The HOMO for **Pt(dCH<sub>3</sub>Py)**, is delocalised on 3,5-dimethylpyrazole, metal centre as well as on the aqua ligand in the *trans* axis. The 3,5-methyl groups donate electrons into the pyrazole ring coordinated to the metal centre, thereby labilising the aqua ligands in the ground state.

In **Pt(H<sub>2</sub>Py)** and **Pt(dCH<sub>3</sub>Py)**, the LUMOs are delocalised on the metal centre and the pyridine ring with no significant contribution from the pyrazole ring. Thus, the electron density on the metal can be back-donated into low-energy  $\pi^*$ -orbitals of the pyridine ring. The location of the LUMOs in **Pt(H<sub>2</sub>Py)** and **Pt(dCH<sub>3</sub>Py)** also indicates that the extent of  $\pi$ -backbonding between the metal centre and the pyrazole is very weak, which is consistent with pyridine being a better  $\pi$ -acceptor than pyrazole. However, for **Pt(dCF<sub>3</sub>Py)** the LUMOs are mainly localised on 3,5-bis(trifluoromethyl)pyrazole, with moderate contributions from the metal centre and pyridine nitrogen. The 3,5-trifluoromethyl ( $-\text{CF}_3$ ) substituents withdraw electron density from pyrazole ring. This activates its  $\pi$ -acceptor strength and enhances back-donation of the electron density from the metal centre. This is another confirmation that the  $\sigma$ -donor or  $\pi$ -acceptor strength of pyrazole can be controlled by introducing substituents in its 3,5-positions.

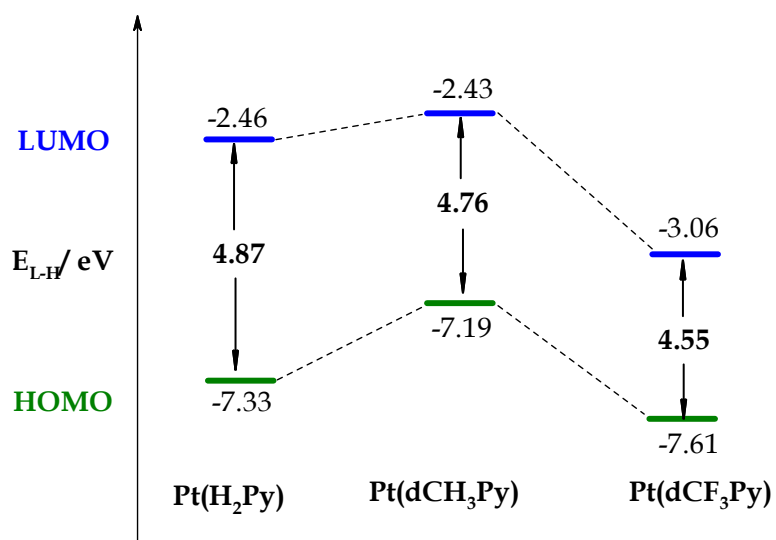
**Table 4.2.** DFT-calculated data for the bifunctional Pt(II) complexes.

<p style="text-align: center;"> <math>R = \begin{matrix} \text{H} \\ \text{CH}_3 \\ \text{CF}_3 \end{matrix}</math> </p>			
Property	Pt(H <sub>2</sub> Py)	Pt(dCH <sub>3</sub> Py)	Pt(dCF <sub>3</sub> Py)
<b>MO Energy (eV)</b>			
LUMO	-2.46	-2.43	-3.06
HOMO	-7.33	-7.19	-7.61
$\Delta E_{L-H}$	4.87	4.76	4.55
<b>NBO charges</b>			
Pt	0.950	0.913	0.991
<b>Bond lengths (Å)</b>			
<i>d</i> Pt–N <sub>py</sub>	2.020	2.016	2.018
<i>d</i> Pt–N <sub>pz</sub>	1.990	2.000	2.010
<i>d</i> Pt–OH <sub>2</sub> (1)	2.103	2.103	2.094
<i>d</i> Pt–OH <sub>2</sub> (2)	2.100	2.101	2.078
<b>Bond angles (°)</b>			
< <sup>1</sup> N <sub>pz</sub> –Pt–OH <sub>2</sub> (1)	179.0	178.5	177.8
< <sup>1</sup> N <sub>py</sub> –Pt–OH <sub>2</sub> (2)	179.6	179.2	179.9
< <i>a</i>	90.3	92.1	91.1
< <i>b</i>	89.3	88.3	88.8
< <i>c</i>	90.2	90.5	90.2
< <i>d</i>	90.2	89.1	89.9

<sup>1</sup> N<sub>py</sub> is the coordinated N-donor atom in the pyridine ring (py) and N<sub>pz</sub> is the coordinated N-donor atom in the pyrazole ring (pz)

Complex	Structure	HOMO Map	LUMO Map
Pt(H <sub>2</sub> Py)			
Pt(dCH <sub>3</sub> Py)			
Pt(dCF <sub>3</sub> Py)			

**Figure 4.3:** DFT-calculated HOMO and LUMO frontier molecular orbitals of Pt(II) complexes.

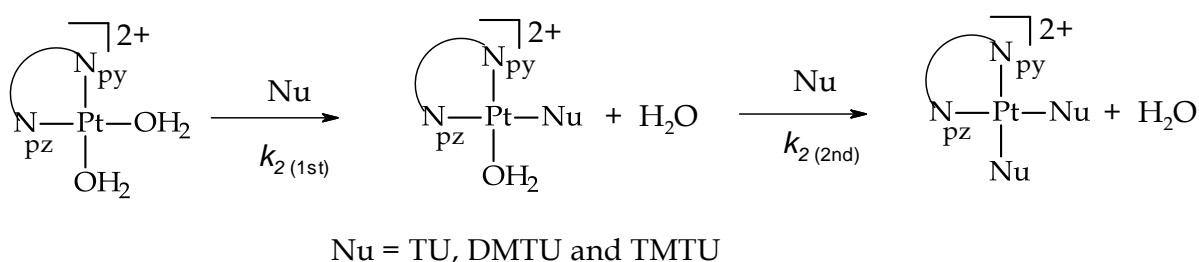


**Figure 4.4:** The effect of substituents on the pyrazole ring in the energies of HOMO and LUMO orbitals and the resultant LUMO-HOMO energy gap.

Because of the location of the HOMO and LUMO, electron donation into the metal centre has an expected effect of raising the energy level of the HOMO and destabilise the LUMO as shown in **Figure 4.4** for **Pt(dCH<sub>3</sub>Py)**. The opposite is observed for **Pt(dCF<sub>3</sub>Py)** which bears an electron-withdrawing group on the coordinated pyrazole ring. What is more intriguing is that the electron-withdrawal effect of the –CF<sub>3</sub> groups convert the pyrazole ring into a stronger  $\pi$ -acceptor, possibly better than the pyridine ring, by stabilising its LUMO frontier orbitals. This lowers the HOMO-LUMO energy gap, leading to a more reactive Pt(II) metal centre.

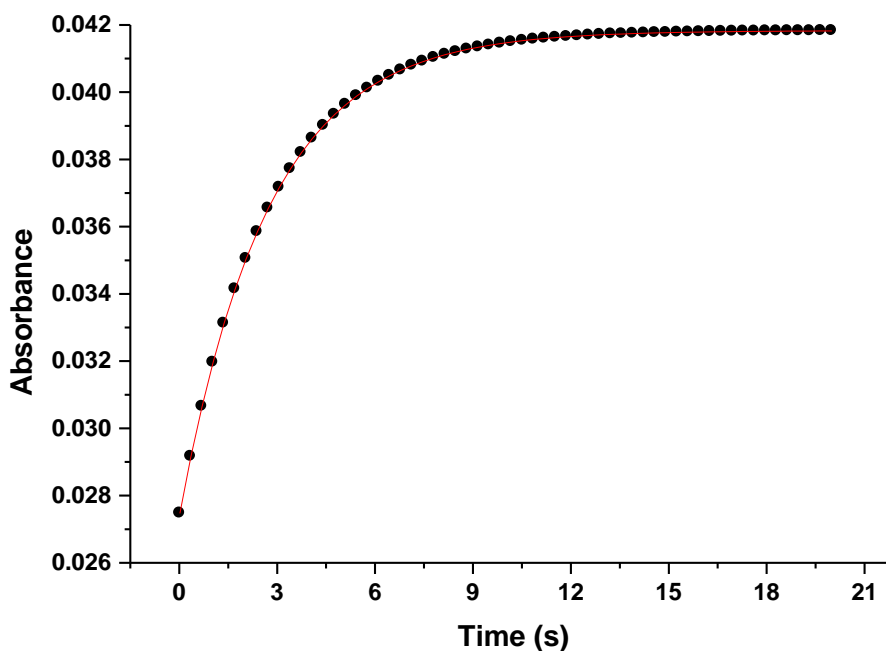
### 4.3.3 Ligand substitution kinetics of the diaqua Pt(II) complexes

The substitution reactions of all diaqua Pt(II) complexes with thiourea nucleophiles (TU, DMTU and TMTU) occurred in two consecutive steps as shown in **Scheme 4.3**.



**Scheme 4.3:** The proposed stepwise substitution of aqua ligands from bifunctional Pt(II) complexes by thiourea nucleophiles.

The two steps are characterised by the second-order rate constants,  $k_{2(1\text{st})}$  and  $k_{2(2\text{nd})}$ . Each step represents the substitution of one of the coordinated aqua leaving groups. Two different substitution steps were expected due to different *trans*-labilization effect of the pyridine and pyrazole rings. The substitution of the first aqua ligand was monitored by the stopped-flow technique while the slower and second substitution step was followed by UV/visible spectrophotometry. A representative time-dependent kinetic trace for the first substitution step in the two-step reaction between **Pt(dCF<sub>3</sub>Py)** and 40-fold TU is shown in **Figure 4.5**.



**Figure 4.5:** A typical kinetic trace for the first substitution step in a two-step reaction between **Pt(dCF<sub>3</sub>Py)** (0.133 mM) and TU (5.32mM) recorded at 310 nm,  $T = 298$  K, pH = 2.0,  $I = 0.1$  M (HClO<sub>4</sub>/NaClO<sub>4</sub>) on the stopped-flow spectrophotometer.

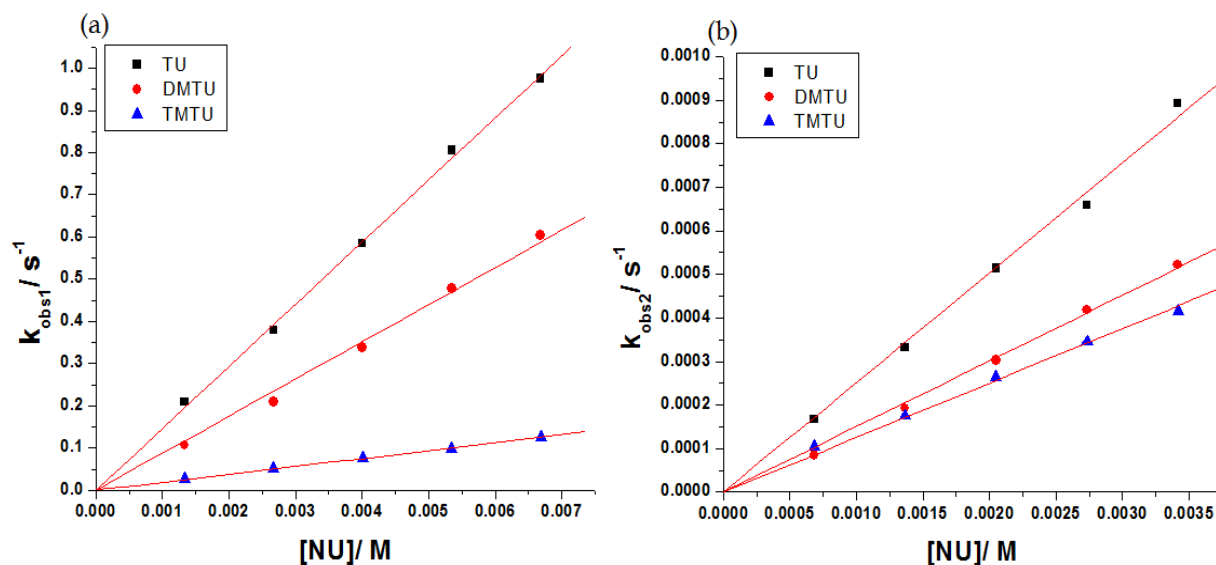
The kinetic traces of the ligand substitution reactions for the diaqua Pt(II) complexes gave excellent fits to a single exponential function used to generate the *pseudo* first-order rate constants,  $k_{obs(1)}$  and  $k_{obs(2)}$  at specific nucleophile concentration and temperature, for the first and second substitution steps, respectively. The values of  $k_{obs(1/2)}$  considered in subsequent analysis are averages of 8-10 independent kinetic runs from the stopped-flow analyser and duplicate runs from UV/visible spectrophotometer, respectively.

The observed *pseudo*-first order rate constants,  $k_{obs(1/2)}$ , were found to vary linearly with the concentration of the nucleophile, according to the rate laws described by equations (4.1).<sup>28</sup>

$$k_{obs(1/2)} = k_{2(1st/2nd)} [Nu] + k_{-1(1st/2nd)} \approx k_{2(1st/2nd)} [Nu] \quad (4.1)$$

Representative plots displaying a linear dependence of  $k_{obs(1/2)}$  on the concentration of the entering nucleophiles are shown in **Figure 4.6** (also see **Figures SI 4.4**).

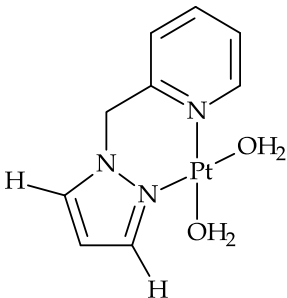
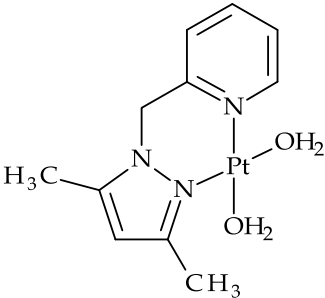
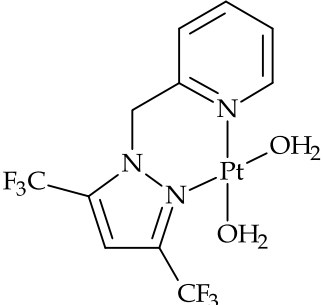




**Figure 4.6:** Pseudo-first-order rate constants,  $k_{obs1}$  and  $k_{obs2}$ , plotted as a function of thiourea nucleophile concentration for the substitution of the first (a) and second (b) aqua ligand from  $Pt(dCF_3Py)$  at pH = 2.0,  $T = 298$  K and  $I = 0.1$  M ( $HClO_4/NaClO_4$ ).

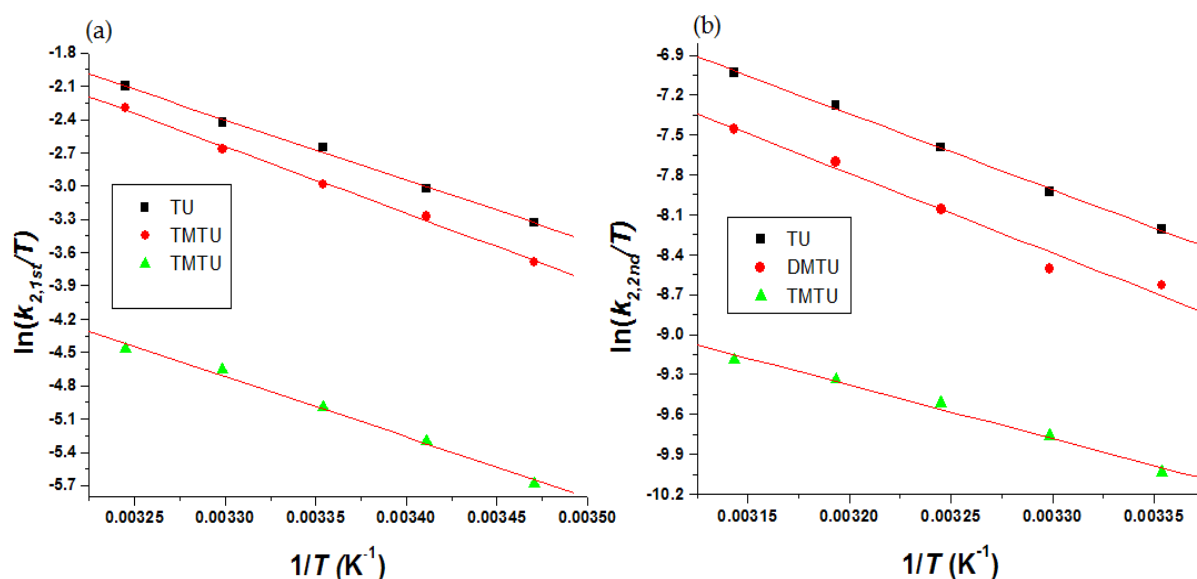
All linear regression plots pass through the origin, suggesting the insignificance or absence of the solvolytic or reverse reaction pathways.<sup>29</sup> The second-order rate constants,  $k_{2(1st/2nd)}$  were calculated from the slopes of  $k_{obs(1/2)}$  vs. nucleophile concentration plots. The values are summarised in **Table 4.3**.

**Table 4.3.** Summary of the second-order rate constants for the stepwise substitution of the aqua ligands by thiourea nucleophiles from diaqua Pt(II) complexes

Complex	Nu	$k_2$ (1st)/ $\text{M}^{-1} \text{s}^{-1}$	$k_2$ (2nd)/ $10^{-1} \text{M}^{-1} \text{s}^{-1}$
<b>Pt(H<sub>2</sub>Py)</b> 	TU	$30.2 \pm 0.4$	$2.65 \pm 0.01$
	DMTU	$29.2 \pm 0.4$	$1.55 \pm 0.05$
	TMTU	$19.7 \pm 0.2$	$0.74 \pm 0.01$
<b>Pt(dCH<sub>3</sub>Py)</b> 	TU	$20.7 \pm 0.2$	$0.82 \pm 0.01$
	DMTU	$15.4 \pm 0.2$	$0.52 \pm 0.01$
	TMTU	$2.1 \pm 0.1$	$0.16 \pm 0.03$
<b>Pt(dCF<sub>3</sub>Py)</b> 	TU	$147 \pm 1$	$2.52 \pm 0.05$
	DMTU	$88.0 \pm 2$	$1.51 \pm 0.02$
	TMTU	$18.8 \pm 0.1$	$0.26 \pm 0.03$

#### 4.3.4 Activation parameters

The temperature dependence of the second-order rate constants,  $k_{2\text{ (1st/2nd)}}$ , was investigated over the temperature range of 15 - 45 °C at the increments of 5 °C. Typical Eyring plots<sup>30</sup> are shown for the reactions of **Pt(dCH<sub>3</sub>Py)** and thiourea nucleophiles in **Figure 4.7** {also see **Figure SI 4.5** for the reactions of **Pt(H<sub>2</sub>Py)** and **Pt(dCF<sub>3</sub>Py)** with thiourea nucleophiles}. The calculated values for the change in activation enthalpy ( $\Delta H_{1/2}^\ddagger$ ) and activation entropy ( $\Delta S_{1/2}^\ddagger$ ) are summarised in **Table 4.4**.



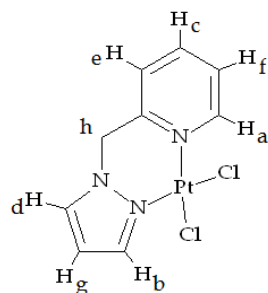
**Figure 4.7:** Plots of  $\ln(k_2/T)$  versus  $(1/T)$  for the substitution of the first (a) and second (b) aqua ligand from **Pt(dCH<sub>3</sub>Py)** by thiourea nucleophiles at varying temperatures.

**Table 4.4.** Summary of the activation parameters for the stepwise substitution of aqua ligands from the diaqua Pt(II) complexes.

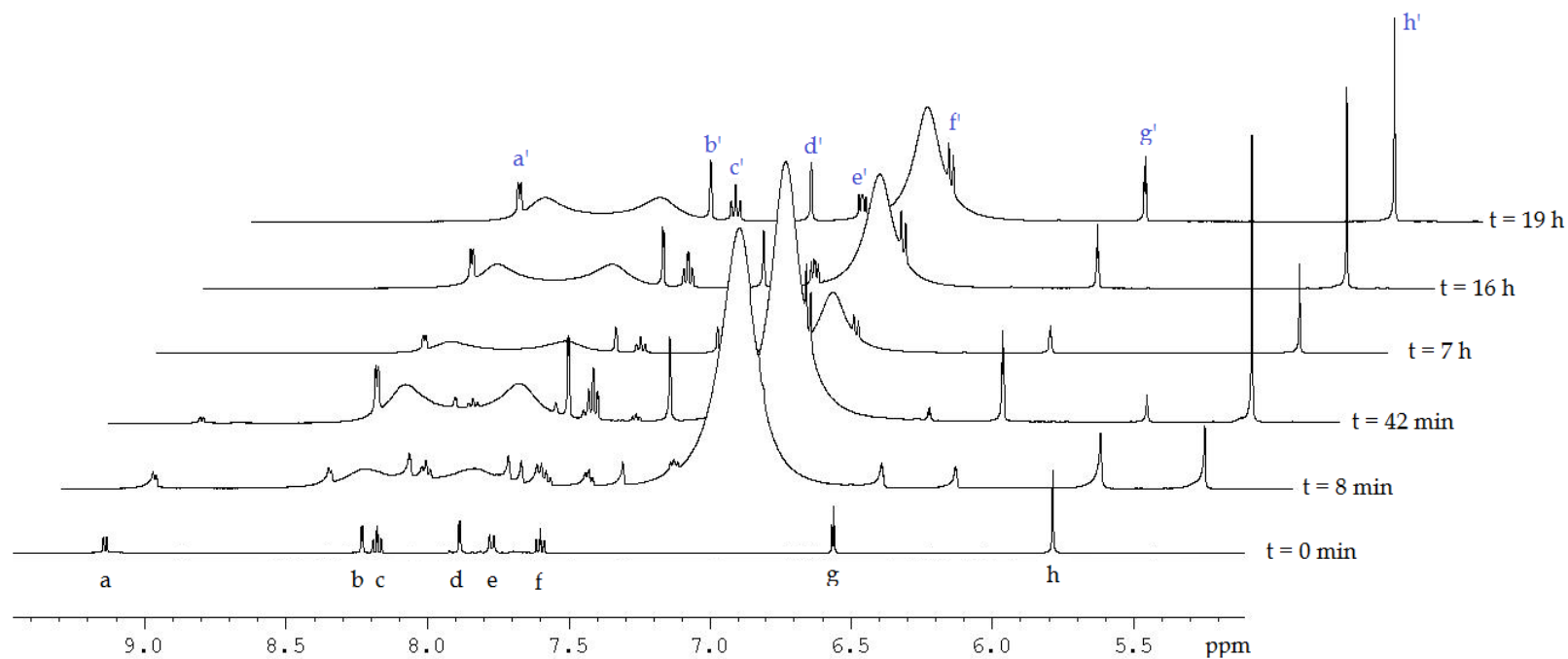
Complex	Nu	$\Delta H_1^\ddagger /$ $\text{kJ mol}^{-1}$	$\Delta H_2^\ddagger /$ $\text{kJ mol}^{-1}$	$\Delta S_1^\ddagger /$ $\text{J mol}^{-1}\text{K}^{-1}$	$\Delta S_2^\ddagger /$ $\text{J mol}^{-1}\text{K}^{-1}$
<b>Pt(H<sub>2</sub>Py)</b>	TU	39 ± 1	17 ± 1	- 85 ± 2	- 210 ± 3
	DMTU	38 ± 2	31 ± 1	- 89 ± 8	- 163 ± 1
	TMTU	40 ± 2	46 ± 2	- 86 ± 6	- 112 ± 8
<b>Pt(dCH<sub>3</sub>Py)</b>	TU	45 ± 1	47 ± 1	- 69 ± 4	- 107 ± 4
	DMTU	50 ± 2	56 ± 5	- 55 ± 6	- 82 ± 2
	TMTU	49 ± 1	37 ± 2	-75 ± 4	- 159 ± 8
<b>Pt(dCF<sub>3</sub>Py)</b>	TU	41 ± 2	46 ± 2	- 67 ± 3	- 101 ± 7
	DMTU	45 ± 2	48 ± 2	- 58 ± 6	- 101 ± 7
	TMTU	36 ± 2	58 ± 3	- 101 ± 7	- 121 ± 1

#### 4.4 NMR studies

Due the asymmetrical nature of bidentate ligands of the Pt(II) complexes, the aqua ligands are susceptible to substitution at a different rate. Their reactions with the nucleophiles therefore proceed *via* a stepwise mechanism as shown in **Scheme 4.3**. To test this assumption, we followed the substitution reaction of [Pt(H<sub>2</sub>PyCl<sub>2</sub>)] and thiourea (TU) for 19 h using <sup>1</sup>H NMR spectroscopy. The complex, [Pt(H<sub>2</sub>Py)Cl<sub>2</sub>], dissolved in DMSO-*d*<sub>6</sub> was reacted with two mole equivalents of TU at 303 K. An array of the <sup>1</sup>H NMR spectra recorded during the substitution process is shown in **Figure 4.8**. The numbering scheme employed for the protons in [Pt(H<sub>2</sub>Py)Cl<sub>2</sub>] is presented in **Scheme 4.4**. Pyridyl and pyrazolyl protons labelled H<sub>a</sub> and H<sub>b</sub>, respectively, were used to monitor the progress of the reaction since they are closest to the N-donor atoms coordinated to the Pt(II) centre at which the substitution occurs.



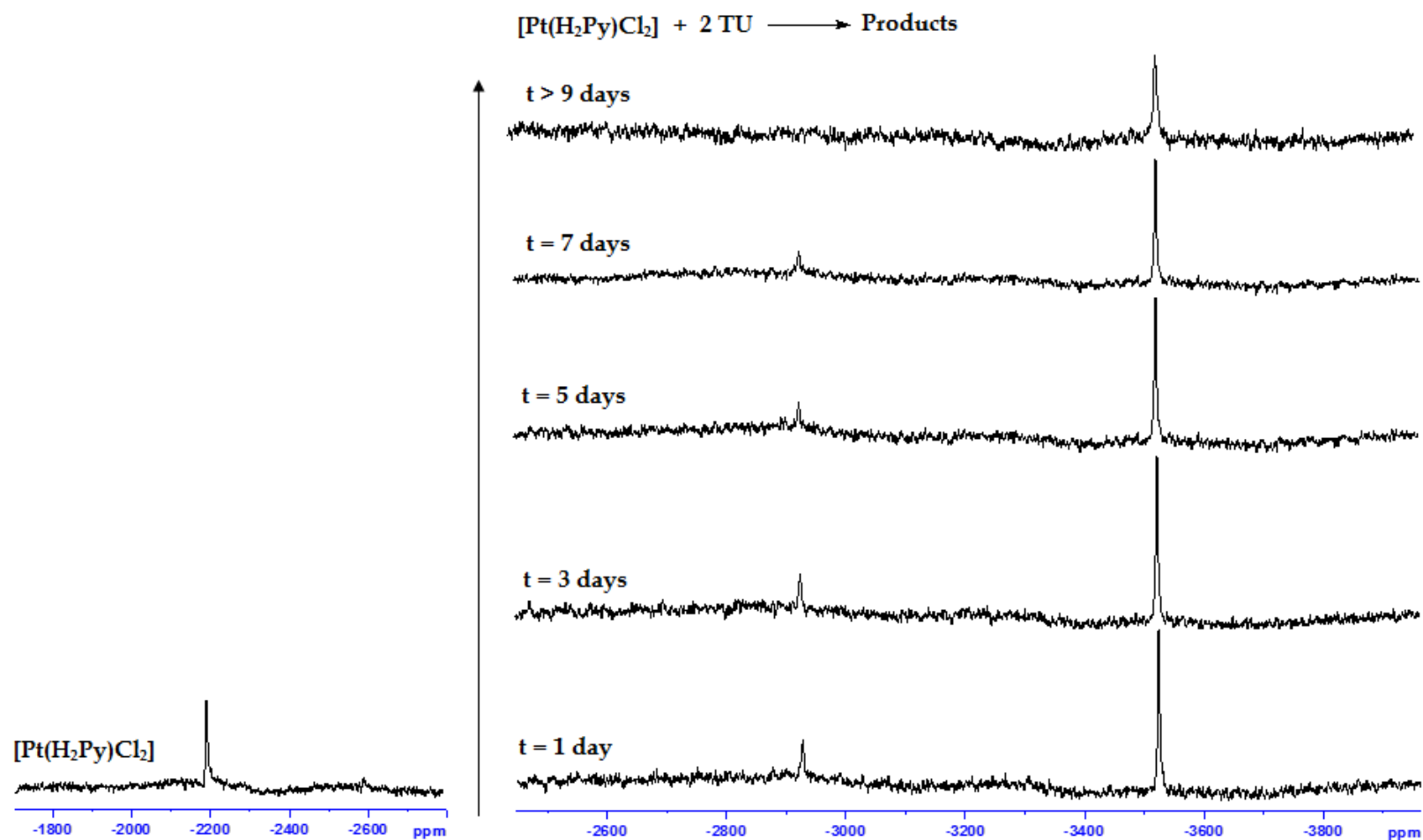
**Scheme 4.4:** Numbering scheme employed for the protons in  $[\text{Pt}(\text{H}_2\text{Py})\text{Cl}_2]$ .



**Figure 4.8:**  $^1\text{H}$  NMR spectral arrays acquired during the reaction of  $[\text{Pt}(\text{H}_2\text{Py})\text{Cl}_2]$  and 2 equiv. of TU in  $\text{DMSO-}d_6$  at 303 K.

These protons resonate at  $\delta(H_a) = 9.14$  ppm and  $\delta(H_b) = 8.26$  ppm, respectively, in an unreacted  $[\text{Pt}(\text{H}_2\text{Py})\text{Cl}_2]$  complex (**Figure 4.8**;  $t = 0$  min). The  $\delta(H_{a'}) = 8.35$  ppm and  $\delta(H_{b'}) = 7.70$  ppm resonances are shifted upfield ( $t = 8$  min), due to the replacement of a more electronegative chloride ligand by sulphur donor, indicating the formation of the TU-coordinated intermediate i.e.  $[\text{Pt}(\text{H}_2\text{Py})(\text{TU})\text{Cl}]^+$ . During the reaction,  $H_{a'}$  and  $H_{b'}$  resonance of the intermediate product formed on the onset ( $t = 8$  min) further grew, while the corresponding resonances of the unreacted  $[\text{Pt}(\text{H}_2\text{Py})\text{Cl}_2]$  complex ( $H_a$  and  $H_b$ ) decreased accordingly. The  $H_a$  and  $H_b$  resonances disappeared after 45 min, indicating that the first and fast substitution reaction has gone to completion. Subsequent snaps of the  $^1\text{H}$  NMR spectra (7-19 h), do not indicate that these resonances ( $H_{a'}$  and  $H_{b'}$ ) vanish within the timeframe of the reaction.

$^{195}\text{Pt}$  NMR spectroscopy is an effective method to determine the coordination details of complexes, since the chemical shift of  $^{195}\text{Pt}$  resonance is influenced by the type of donor atoms coordinated to the platinum centre. In this respect, the reaction between  $[\text{Pt}(\text{H}_2\text{Py})\text{Cl}_2]$  and two equivalents of TU was also monitored by  $^{195}\text{Pt}$  NMR spectroscopy for a much longer time, to confirm the proposed stepwise mechanism (**Scheme 4.3**). An evolution of the  $^{195}\text{Pt}$  NMR spectra during the substitution reaction is presented in **Figure 4.9**. The peak at  $\delta(^{195}\text{Pt}) = -2189$  ppm (shown as an inset of **Figure 4.9**) corresponds to resonance due to the unreacted  $[\text{Pt}(\text{H}_2\text{Py})\text{Cl}_2]$  complex. During the substitution process, new peaks at  $\delta(^{195}\text{Pt}) = -2930$  ppm and  $\delta(^{195}\text{Pt}) = -3535$  ppm are observed, suggesting the formation of two new species in solution. It is well-known from literature<sup>31</sup> that the  $^{195}\text{Pt}$  NMR chemical shift within the range of -2750 to -3150 ppm corresponds to the  $[\text{PtN}_2\text{SCl}]$  coordination sphere, whereas the one for  $[\text{PtN}_2\text{S}_2]$  resonate within the range of -3150 to -3550 ppm. Therefore, the two peaks observed at  $\delta(^{195}\text{Pt}) = -2930$  ppm and  $\delta(^{195}\text{Pt}) = -3535$  ppm correspond to  $[\text{Pt}(\text{H}_2\text{Py})(\text{TU})\text{Cl}]^+$  and  $[\text{Pt}(\text{H}_2\text{Py})(\text{TU})_2]^+$  species, respectively. The resonance peaks of the intermediate decrease while those of the final product increase.



**Figure 4.9:**  $^{195}\text{Pt}$  NMR spectra acquired during the reaction of  $[\text{Pt}(\text{H}_2\text{Py})\text{Cl}_2]$  and 2 equiv. of TU in  $\text{DMSO-}d_6$  at 303 K. Insert:  $^{195}\text{Pt}$  NMR spectrum of  $[\text{Pt}(\text{H}_2\text{Py})\text{Cl}_2]$  before the reaction.

In addition, there was no evidence observed for the de-coordination of the (pyrazolylmethyl)pyridine (**H<sub>2</sub>Py**) as would be evidenced by a  $\delta(^{195}\text{Pt})$  peak within -3800 to -4000 ppm for [PtS<sub>4</sub>] coordination sphere.<sup>31,32</sup> Thus, despite the strong nucleophilicity of thiourea, the non-leaving ligand, **H<sub>2</sub>Py** remains coordinated to the metal centre. This does not exclude the possibility of de-coordination or decomposition of a non-leaving group at longer reaction times. This observation suggests that the increase in the steric hindrance and reduced electrophilicity imparted by the coordination of two thiourea nucleophiles at the metal centre, retards de-coordination or decomposition of **H<sub>2</sub>Py** from the metal centre. Therefore, it can be concluded that the final product is a bifunctional Pt(II) complex with two thiourea nucleophiles coordinated to the metal centre and that the substitution mechanism is a sequential process as represented in **Scheme 4.3**.

## 4.5 Discussion

By introducing the inductive electron-donating or electron-withdrawing substituents at the 3,5-positions of the pyrazole ring, it is possible to quantify their electronic and steric influence on the reactivity of bifunctional Pt(II) complexes. For all complexes, the substitution of the aqua ligands by thiourea nucleophiles involves two reaction steps differing by a factor of at least two orders of magnitude. The large difference in the rate constants between the first and the second substitution step is ascribed to an increased steric hindrance around the metal centre arising from the incorporation of the first thiourea nucleophile as well as a decreased electrophilicity of the Pt(II) metal centre due to  $\sigma$ -donor capacity of the coordinated thiourea nucleophile. These two factors retard the aerial approach of the nucleophile at the transition state, thereby decreasing the rate of substitution.

For structurally similar types of complexes with different N-donors,<sup>12-13,24-25</sup> the two steps were ascribed to stepwise substitution of each of the aqua ligand coordinated to the Pt(II) centre. In order to address the question of which aqua ligand is substituted first, as well as to clarify the trends in the lability of each of the coordinated aqua ligands, a key structural differences in the donor properties of the (pyrazolylmethyl)pyridine core ligand should be highlighted. The coordinated



ligands consist of two different types of donors, i.e. a pyridine ring with a strong  $\pi$ -accepting ability and a pyrazole ring with a strong  $\sigma$ -donor capacity. These electronic properties may compete with each other during substitution.

Theoretically, the first substitution step should take place *trans* to pyrazole ring, whereas the second substitution step should take place *trans* to pyridine ring, with both steps dependent on the electronic nature of the 3,5-substituents of the pyrazole ring. Consistent with this view is that the length of the Pt–OH<sub>2(1)</sub> bond *trans* to pyrazole which is marginally longer than the one *trans* to pyridine (Pt–OH<sub>2(2)</sub>), **Table 4.2**) for all complexes. This aqua ligand is substituted first. The sensitivity of the Pt(II) centre towards the 3,5-substituents on the pyrazole ring is shown by the difference in NBO charges and the HOMO-LUMO energy gaps of the complexes (**Table 4.2** and **Figure 4.4**). The experimentally obtained thermodynamic and kinetic data, i.e. the trends in the  $pK_a$  values and the second-order rate constants respectively, are also in good agreement with the DFT-calculated parameters.

#### 4.5.1 First substitution step

In comparing the rate of substitution of the first aqua ligand,  $k_{2(1st)}$ , data in **Table 4.3** shows that the reactivity of the bifunctional Pt(II) complexes follow the trend **Pt(dCF<sub>3</sub>Py) > Pt(H<sub>2</sub>Py) > Pt(dCH<sub>3</sub>Py)**. If the reactivity of **Pt(dCH<sub>3</sub>Py)** with TU is taken as a reference, the ratio of reactivity is 7.1: 1.5: 1.0, respectively for **Pt(dCF<sub>3</sub>Py): Pt(H<sub>2</sub>Py): Pt(dCH<sub>3</sub>Py)**. The difference in the reactivity can be accounted for, in terms of the nature of the 3,5-substituents on the pyrazole ring. If we assume that the first substitution site occurs to the aqua ligand *trans* to the pyrazole ring, the results of **Table 4.3** corroborates that the two methyl (–CH<sub>3</sub>) substituents at the 3,5-positions enhance the *trans*  $\sigma$ -effect of the pyrazole ring more in the transition state than in the ground state. The electron-donating –CH<sub>3</sub> groups in **Pt(dCH<sub>3</sub>Py)** inductively donate electron density to the pyrazole ring coordinated to the metal centre. This causes the accumulation of the electron density at the metal centre, and decelerates the substitution process by making the Pt(II) centre less electrophilic or more electronegative.<sup>33,34</sup> Not only does the  $\sigma$ -inductive effect repel the approach of the nucleophile towards the metal centre, but it also suppresses the stabilization of the

18-electron-rich 5-coordinate transition state, thereby retarding the rate of aqua ligand substitution by the thiourea nucleophiles. The trifluoromethyl ( $-\text{CF}_3$ ) groups at the 3,5-positions of the coordinated pyrazole ring withdraw electron density from the ring, switching it from a net  $\sigma$ -donor to a  $\pi$ -acceptor. This makes the Pt(II) atom more electrophilic or electropositive and thus accelerates the rate of ligand substitution by increasing the affinity of the metal centre for an entering nucleophile. The reduced accumulation of electron density on the Pt(II) centre also facilitates facile substitution of the aqua ligands by stabilising the 18-electron-rich 5-coordinate transition state. The increased electrophilicity and reactivity of **Pt(dCF<sub>3</sub>Py)** is supported by relatively lower  $\text{p}K_a$  values, a small HOMO-LUMO energy gap as well as a large and positive NBO charge value of the platinum centre. Therefore, it can be concluded that the lability of the aqua ligand in the first substitution step is dependent on the  $\sigma$ -donor and  $\pi$ -acceptor strength of the substituents on the pyrazole ring.

The reactivity of the complexes decreases with an increase in the  $\sigma$ -donor capacity of the pyrazole ring or alternatively increases with an increase in its  $\pi$ -acceptor strength. Experimental data obtained in this study supports the conclusions drawn by Jaganyi and co-workers<sup>35,36</sup> for monofunctional Pt(II) complexes with electron donating- or electron-withdrawing groups in the ancillary positions of the polypyridyl tridentate (NNN/NNC) ligand framework. A moderate decrease in the reactivity of the metal centre was noted upon the addition of the electron-donating *tert*-butyl<sup>33,34a</sup> or methyl groups,<sup>34</sup> while the placement of electron-withdrawing trifluoromethyl groups<sup>34</sup> led to an increased reactivity of the metal centre.

#### 4.5.2 Second substitution step

Data in Table 3 shows that the rate of substitution of the second aqua ligand,  $k_2$  (2nd), follows the order: **Pt(H<sub>2</sub>Py)**  $\approx$  **Pt(dCF<sub>3</sub>Py)** > **Pt(dCH<sub>3</sub>Py)**. Taking the second substitution step with TU as a reference, the reactivity of the Pt(II) complexes decrease in the order:  $\{(2.65 \pm 0.01) \approx (2.52 \pm 0.05) > (0.82 \pm 0.01)\} \times 10^{-1} \text{ M}^{-1} \text{ s}^{-1}$  for **Pt(H<sub>2</sub>Py)**, **Pt(dCF<sub>3</sub>Py)** and **Pt(dCH<sub>3</sub>Py)**, respectively. However, **Pt(dCF<sub>3</sub>Py)** was expected to be much faster than **Pt(H<sub>2</sub>Py)** due the electron-withdrawing  $-\text{CF}_3$

substituents as reflected by the increased positive charge of the metal centre (NBO charge) and the corresponding decrease in the separation of the frontier orbitals ( $\Delta E_{L-H}$ ; Table 4.2). This suggests that there is a combination of electronic and steric influence imparted by the substituents, on the lability of the aqua ligand *cis* to the 3,5-substituted pyrazole ring. These two properties are working *anti* to each other, and the net effect is that rate constants for **Pt(H<sub>2</sub>Py)** is approximately equal to that of **Pt(dCF<sub>3</sub>Py)** as a result of a more dominant steric effect in the latter complex.

The replacement of a hydrogen (H) atom by either a –CH<sub>3</sub> or –CF<sub>3</sub> group at the 3-position of the pyrazole ring causes a steric hindrance to the approach of the second nucleophile which overrides the *cis*  $\sigma$ - or  $\pi$ -electronic effect, thereby slowing down the rate of the reaction. This is contrary to the substitution of the first aqua ligand (i.e. *trans* to the 3,5-disubstituted pyrazole) where the substituent on the 3-position has limited steric influence on the rate of reaction. The effect of steric crowding in the *cis* position on the rate of substitution has been well documented for Pt(II)/Pd(II) complexes.<sup>37,38</sup> It is known that increasing the steric bulk of the *cis* ligand decelerates the rate of an associative substitution reaction, due to an increase in steric hindrance in the 5-coordinate transition state.<sup>35-39</sup> This steric *cis*-effect reduces the reactivity more than the corresponding steric *trans*-effect.<sup>35-37</sup>

The data also shows that the substitution rate constant of the second aqua ligand  $k_2$  (2nd), decrease in the order: **Pt(dCF<sub>3</sub>Py)** > **Pt(dCH<sub>3</sub>Py)**, with the former complex reacting three times faster than the latter when TU is used as a reference. This is despite the –CF<sub>3</sub> group being more bulk than the –CH<sub>3</sub> group. However, both **Pt(dCF<sub>3</sub>Py)** and **Pt(dCH<sub>3</sub>Py)** complexes have a relatively larger steric bulk substituents on their core ligands compared to **Pt(H<sub>2</sub>Py)**. Therefore, between these two complexes, the rate of substitution of the second and *cis* aqua ligand can be ascribed entirely to the difference in the electronic effects of the 3,5-substituents of the pyrazole ring. The electron-withdrawing –CF<sub>3</sub> substituents in **Pt(dCF<sub>3</sub>Py)** withdraw the electrons from the pyrazole ring *via*  $\pi$ -back bonding, thereby increasing the electrophilicity of the metal centre (*vide supra*). This increases the rate of substitution. The electron-donating –CH<sub>3</sub> substituents in **Pt(dCH<sub>3</sub>Py)**, increase the  $\sigma$ -donor strength of the pyrazole ring through positive inductive effects, thereby

decreasing the lability of the second aqua ligand. Thus, for these complexes, the *cis*  $\pi$ -effect is greater than the *cis*  $\sigma$ -effect.

#### 4.5.3 Activation parameters and reactivity of the nucleophiles

The activation parameters in **Table 4.4** support an associative mechanism, with relatively low enthalpies of activation ( $\Delta H_{1/2}^\ddagger$ ), signifying how it is energetically favourable to form a bimolecular transition state. In addition, the entropies of activation ( $\Delta S_{1/2}^\ddagger$ ) are large and negative, indicating a highly ordered and more compact transition state compared to the micro-states of the reactants or products. All this confirms that the nucleophilic substitution reactions proceed *via* an associative mechanism.<sup>11,34,36</sup>

The substitution of the aqua ligands depends on the steric hindrance of the entering nucleophiles, with the less sterically hindered thiourea (TU) nucleophile having the highest rate of substitution, while the most sterically hindered nucleophile, *N,N,N',N'*-tetramethylthiourea (TMTU) is reacting significantly slower (**Table 4.3**). Not only does the more bulk nucleophile find it increasingly difficult to approach the Pt(II) centre,<sup>33</sup> but also upon coordination suppresses the stabilization of the 5-coordinate transition state,<sup>37</sup> thereby decreasing the substitution rate.

#### 4.6 Conclusion

The introduction of the substituents in the 3,5-positions of the pyrazole ring in the *N,N*-bidentate chelate influences its  $\sigma$ -donicity and  $\pi$ -acceptibility. Consequently, this controls the electrophilicity of the Pt(II) centre, which in turn affects the lability of the two coordinated aqua leaving groups. The first substitution step takes place *trans* to the pyrazole ring. The  $\sigma$ -donation effect of the coordinated pyrazole ring causes the second entering nucleophile to be stabilised on the reaction site *trans* to the pyridine ring. The inductive electron-donating  $-\text{CH}_3$  substituents decrease the rate of substitution whereas the inductive electron-withdrawing  $-\text{CF}_3$  substituents increase the rate of substitution. This is supported by the order of reactivity of **Pt(dCF<sub>3</sub>Py) > Pt(H<sub>2</sub>Py) > Pt(dCH<sub>3</sub>Py)** for the substitution of the aqua ligand *trans* to the pyrazole ring. On the other hand, the lability of the aqua ligand *cis* to the

pyrazole ring followed the order:  $\text{Pt}(\text{H}_2\text{Py}) \approx \text{Pt}(\text{dCF}_3\text{Py}) > \text{Pt}(\text{dCH}_3\text{Py})$ . This indicates that 3-substituent on the pyrazole ring causes a steric retardation on the lability of the aqua ligand in a *cis* position. Therefore, the steric of the 3-pyrazole substituent is stronger than the expected electronic *cis*  $\sigma/\pi$ -effect. The comparison of the complexes with 3,5-disubstituted pyrazole ring on the lability of the *cis* aqua ligand, indicates that the *cis*  $\pi$ -effect is stronger than the *cis*  $\sigma$ -effect. The DFT and  $\text{p}K_a$  data both support the experimentally obtained kinetic data. The mode of action remains associative throughout.

## 4.7 References

---

1. B. Rosenberg, L.V. Camp, *Nature*, 1965, **205**, 698.
2. (a) alzani, A. Juris, N. Venture, S. Campagna, S. Serroni, *Chem. Rev.*, 1996, **96**, 759. (b) E. Wong, C. M. Giandomenico, *Chem. Rev.*, 1999, **99**, 2451. (c) E. R. Janeison and S. J. Lippard, *Chem. Rev.*, 1999, **99**, 2467. (d) T. Storr, K. H. Thomson, C. Orvig, *Chem. Soc. Rev.*, 2006, **35**, 534.
3. (a) J. Reedijk, *Chem. Rev.*, 1999, **99**, 2499. (b) C. Meljer, N. H. Mulder, H. Timmer-Bossch, W. J. Sluiter, G. J. Meersma, E. G. de Vries, *Cancer Res.*, 1992, **52**(24), 6885. (c) N. Fox, J. J. Roberts, *Cancer Metastasis Rev.*, 1987, **6**(3), 261.
4. (a) A. S. Abu-Surrah, M. Kettunen, *Current Medical Chemistry*, 2006, **13**, 1337. (b) S. P. Gupta, *Chem. Rev.*, 1994, **94**, 1507. (c) H. D. H. Showalter, J. L. Johnson, J. M. Hoftiezer, W. R. Turner, L. M. Werbel, W. R. Leopold, J. L. Shills, R. C. Jackson, E. F. Elslager, *J. Med. Chem.*, 1987, **30**, 121.
5. M. J. Cleare and J. D. Hoeschele, *Bioinorg. Chem.*, 1973, **2**, 187.
6. S. H. van Ritj, P.J. Sadler, *Drug Discovery Today*, 2009, **114**, 1089.
7. (a) L. A. S. Costa, W.R. Rocha, W. B. De Almeida, H. F. Dos Santos, *Chem. Phys. Lett.*, 2004, **387**, 182-187. (b) M. A. Jakubec, M. Galanski, B. K. Keppler, *Rev. Physiol. Biochem. Pharmacol.*, 2003, **146**, 1.
8. J. Zhao, S. Gou, F. Liu, Y. Sun, C. Gao, *Inorg. Chem.*, 2013, **52**, 8163.
9. Y. Jung, S. J. Lippard, *Chem. Rev.*, 2007, **107**, 1387.
10. (a) A. G. Quiroga, *Current Topics in Medicinal Chemistry*, 2011, **11**, 2613. (b) G. Mamekov, A. Bakalova, M. Karaivanova, *Current Medicinal Chemistry*, 2005, 2197.
11. (a) A. Hofmann, D. Jaganyi, O. Q. Munro, G. Lier, R. van Eldik, *Inorg. Chem.*, 2003, **42**, 1688. (b) A. Hofmann, D. Jaganyi, O. Q. Munro, G. Lier, R. van Eldik, *Angew. Chem. Int. Ed.*, 2001, **40**(2), 1680.
12. N. Summa, W. Schiessl, R. Putcha, N. van Eikema Hommes, R. van Eldik, *Inorg. Chem.*, 2006, **45**, 2948.
13. J. Bogojeski, Ž. D. Bugarčić, R. Puchta, R. van Eldik, *Eur. J. Inorg. Chem.*, 2010, 5439.

14. S. G. Murray, and F. R. Hartley, *Chem. Rev.*, 1981, **81**, 365.
15. (a) W. C. Schiessl, N. K. Summa, C. F. Weber, S. Gubo, C. Dücker-Benfer, R. Puchta, N. T. van Eikema Hommea, and R. van Eldik, *Z. Anorg. Chem.*, 2005, **631**, 2812.. (b) M. T. Ashby, *Comments Inorg. Chem.*, 1990, **10**, 297.
16. (a) D. A. House, P. J. Steel, A. A. Watson, *Inorg. Chim. acta.*, 1987, **130**, 169. (b) D.A. House, P. J. Steel, A.A. Watson, *Aust. J. Chem.*, 1986, **39**, 1525.
17. (a) M. J. Rauterkus, S. Fakih, C. Mock, I. Puscasu, B. Krebs, *Inorganica Chimica Acta*, 2003, **350**, 355. (b) I. Puscasu, C. Mock, M. Rauterkus, A. Röndings, G. Tallen, S. Gangopadhyay, J. E. A. Wolff, B. Krebs, *Z. Anorg. Allg. Chem.*, 2001, **627**, 1292.
18. Ž. D. Bugarčić, B. V. Petrović, R. Jelić, *Transition Met. Chem.*, 2001, **26**, 668.
19. Origin 7.5™ SRO, v7.5714 (B5714), Origin Lab Corporation, Northampton, One, Northampton, MA, 01060, USA, 2003.
20. (a) P. J. Hay and W. R. Wadt, *Chem. Phys.*, 1985, **82**, 270. (b) A. D. Becke, *J. Chem Phys.*, 1993, **98**, 5648.
21. C. Lee, W. Yang, G. R. Parr, *Phys. Rev. B.*, 1988, **37**, 785.
22. B. Miehlich, A. Savin, H. Stoll and H. Preuss, *Chem. Phys. Lett.*, 1989, **157**, 200.
23. Gaussian 09, Revision A. I, M. J. Frisch, G. W. Trucks, H. B. Schlegel, G. E. Scuseria, M. A. Robb, J. R. Cheeseman, G. Scalmani, V. Barone, B. Mennucci, G. A. Petersson, H. Nakatsuji, M. Caricato, X. Li, H. P. Hratchian, A. F. Izmaylov, J. Bloino, G. zheng, J. L. Sonnenberg, M. Ehara, K. Toyota, R. Fukuda, J. Hasegawa, M. Ishida, T. Nakajima, Y. Honda, O. Kitao, H. Nakai, T. Vreven, J. A. Montgomery, Jr., J. E. Peralta, F. Ogliaro, M. Bearpark, J. J. Heyd, E. Brothers, K. N. Kudin, V. N. Staroverov, R. Kobayashi, J. Normand, K. Raghavachari, A. Rendell, J. C. Burant, S. S. Iyengar, J. Tomasi, M. Cossi, N. Rega, J. M. Millam, M. Klene, J. E. Knox, J. B. Cross, V. Bakken, C. Adamo, J. Jaramillo, R. Gomperts, R. E. Stratmann, O. Yazyvev, A. J. Austin, R. Cammi, C. Pomelli, J. W. Ochterski, R. L. Martin, K. Morokuma, V. G. Zakrzewski, G. A. Voth, P. Salvador, J. J. Dannenberg, S. Dapprich, A. D. Daniels, O. Farkas, J. B. Foresman, J. V. Ortiz, J. Cioslowski and D. J. Fox, Gaussian, Inc., Wallingford CT, 2009.

24. S. Hochreuther, R. Puchta, R. van Eldik, *Inorg. Chem.*, 2011, **50**, 8984.
25. S. Hochreuther, S. T. Nandibewoor, R. Putcha, R. van Eldik, *Dalton Trans.*, 2012, **40**, 512.
26. A. Hofmann, R. van Eldik, *Dalton Trans.*, 2003, 2979.
27. M. Schmülling, D.M. Grove, G. van Koten, R. van Eldik, N. Veldman, A. L. Spek, *Organometallics*, 1996, **15**, 1384.
28. R. B. Jordan, *Reaction Mechanisms of Inorganic and Organometallic Systems*, Oxford University Press Inc., New York, 1991.
29. H. B. Grey, R. J. Olcott, *Inorg. Chem.*, 1962, **1**, 481.
30. J. D. Atwood, *Inorganic and Organometallic Reaction Mechanisms*, Wiley-VCH Inc., New York, 2<sup>nd</sup> edn, 1997.
31. J. R. L. Priqueler, I. S. Butler, F. D. Rochon, *Applied Spectroscopy Reviews*, 2006, **41**, 185.
32. P. O. Ongoma, D. Jaganyi, *Dalton Trans.*, 2013, **42**, 2724.
33. P. O. Ongoma, D. Jaganyi, *Dalton Trans.*, 2012, **41**, 10724.
34. A. Shaira, D. Reddy, D. Jaganyi, *Dalton Trans.*, 2013, **42**, 8426.
35. D. Reddy and D. Jaganyi, *Dalton Trans.*, 2008, 6724.
36. (a) D. Jaganyi, K-L. De Boer, J. Gertenbsch, J. Perils, *Int. J. Chem. Kinet.*, 2008, **40**, 808. (b) D. Reddy, K. J. Akerman, M. P. Akerman, D. Jaganyi, *Transition Met. Chem.*, 2011, **36**, 593.
37. M. Kotowski and R. van Eldik, *Inorganic High Pressure Chemistry*, Eds., Elsevier Science Publisher: New York, 1986, **7**, 219.
38. M. L. Tobe, J. Burgess, *Inorganic Reaction Mechanisms*, Addison-Wesley Longman: Essex, England, 1999.
39. A. Hofmann, L. Dahlenburg, and R. van Eldik, *Inorg. Chem.*, 2003, **42**, 6528.



## 4.8 Supporting information

---

**Table SI 4.1a.** Summary of wavelengths (nm) used for monitoring the first substitution reactions between a series of bifunctional Pt(II) complexes and thiourea nucleophiles.

Complex	Nucleophile	Wavelength (nm)
Pt(H <sub>2</sub> Py)	TU	289
	DMTU	280
	TMTU	335
Pt(dCH <sub>3</sub> Py)	TU	300
	DMTU	300
	TMTU	330
Pt(dCF <sub>3</sub> Py)	TU	310
	DMTU	300
	TMTU	340

**Table SI 4.1b.** Summary of wavelengths (nm) used for monitoring the second substitution reactions between a series of bifunctional Pt(II) complexes and thiourea nucleophiles.

Complex	Nucleophile	Wavelength (nm)
Pt(H <sub>2</sub> Py)	TU	278
	DMTU	275
	TMTU	320
Pt(dCH <sub>3</sub> Py)	TU	292
	DMTU	315
	TMTU	280
Pt(dCF <sub>3</sub> Py)	TU	305
	DMTU	305
	TMTU	289

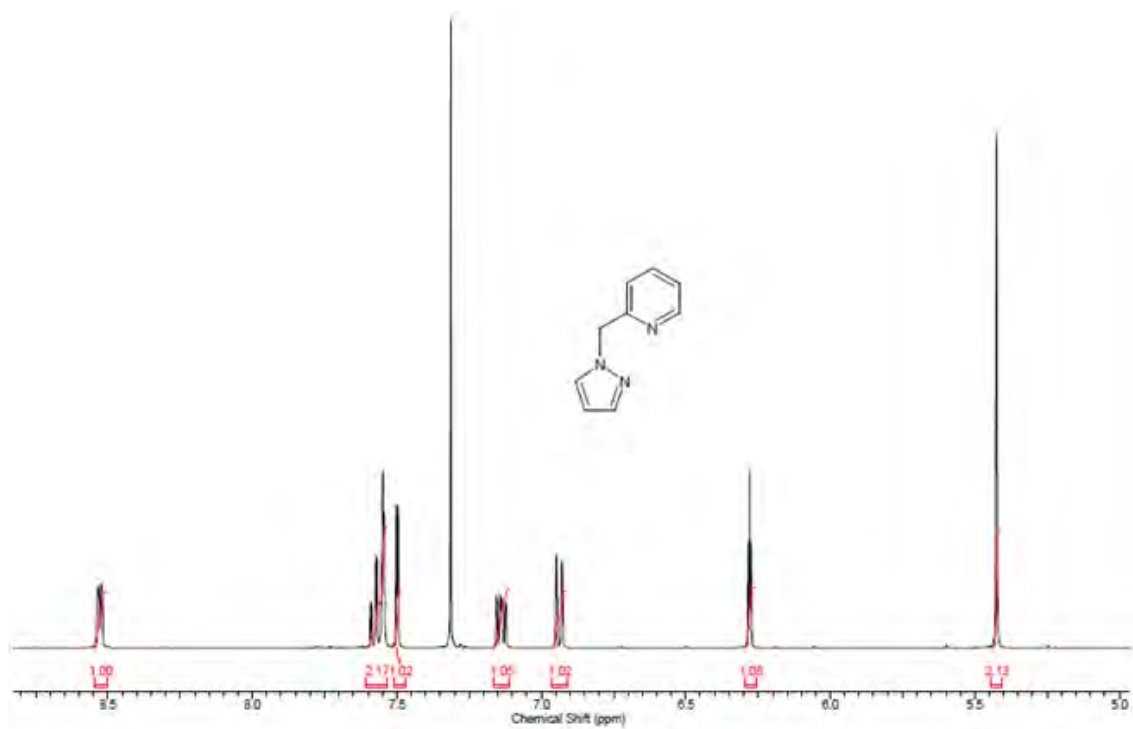


Figure SI 4.1a:  $^1\text{H}$  NMR spectrum of 2-(pyrazol-1-ylmethyl)pyridine ( $\text{H}_2\text{Py}$ ) in CDCl<sub>3</sub>.

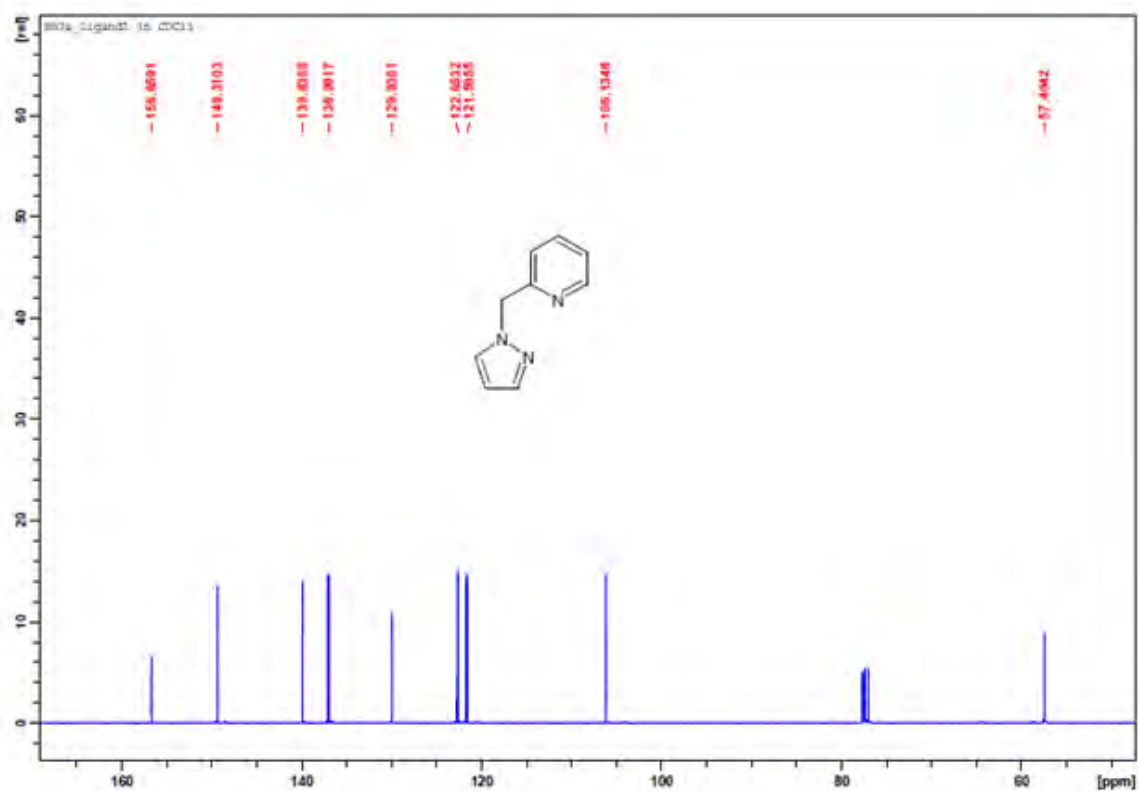


Figure SI 4.1b:  $^{13}\text{C}$  NMR spectrum of 2-(pyrazol-1-ylmethyl)pyridine ( $\text{H}_2\text{Py}$ ) in CDCl<sub>3</sub>.

## Single Mass Analysis

Tolerance = 50.0 PPM / DBE: min = -1.5, max = 50.0

Element prediction: Off

Number of isotope peaks used for i-FIT = 3

Monoisotopic Mass, Even Electron Ions

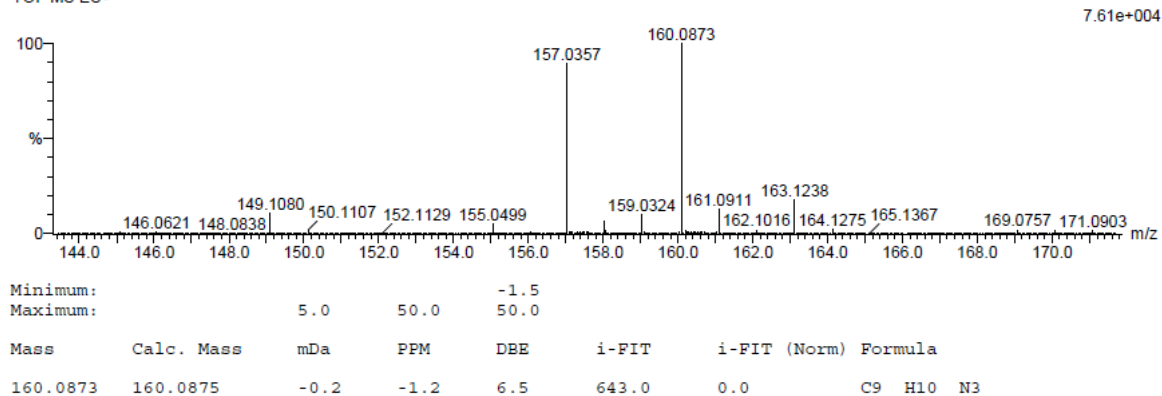
4 formula(e) evaluated with 1 results within limits (up to 50 best isotopic matches for each mass)

Elements Used:

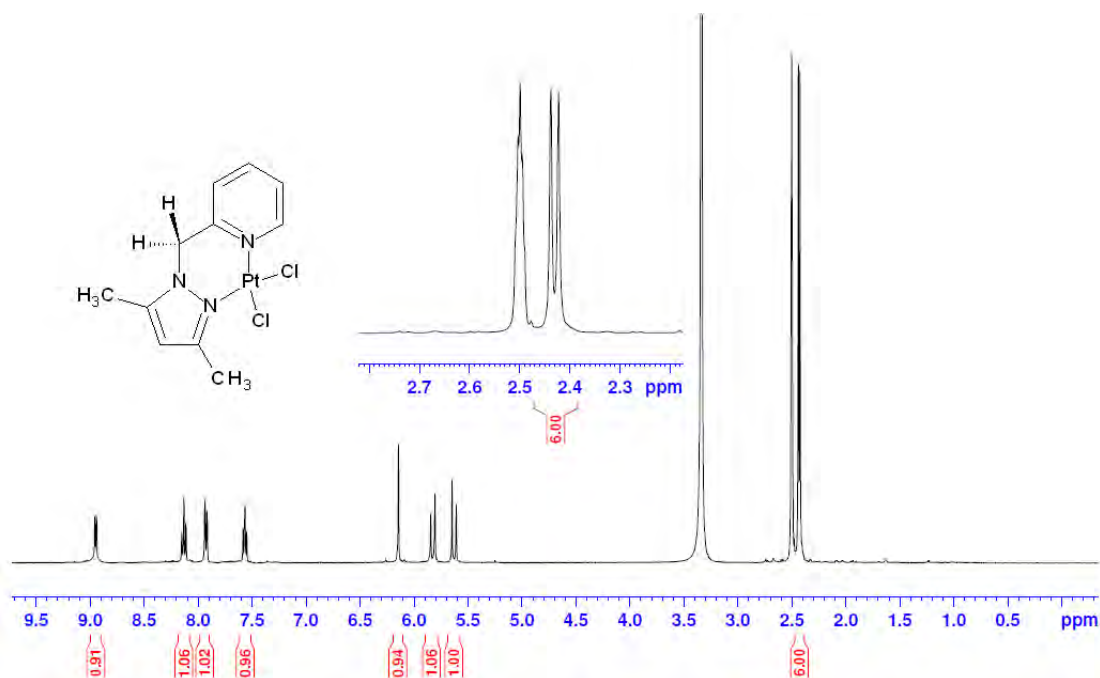
C: 5-10 H: 5-10 N: 0-5

Ligand 1 K 19 (0.307) Cm (1:31)

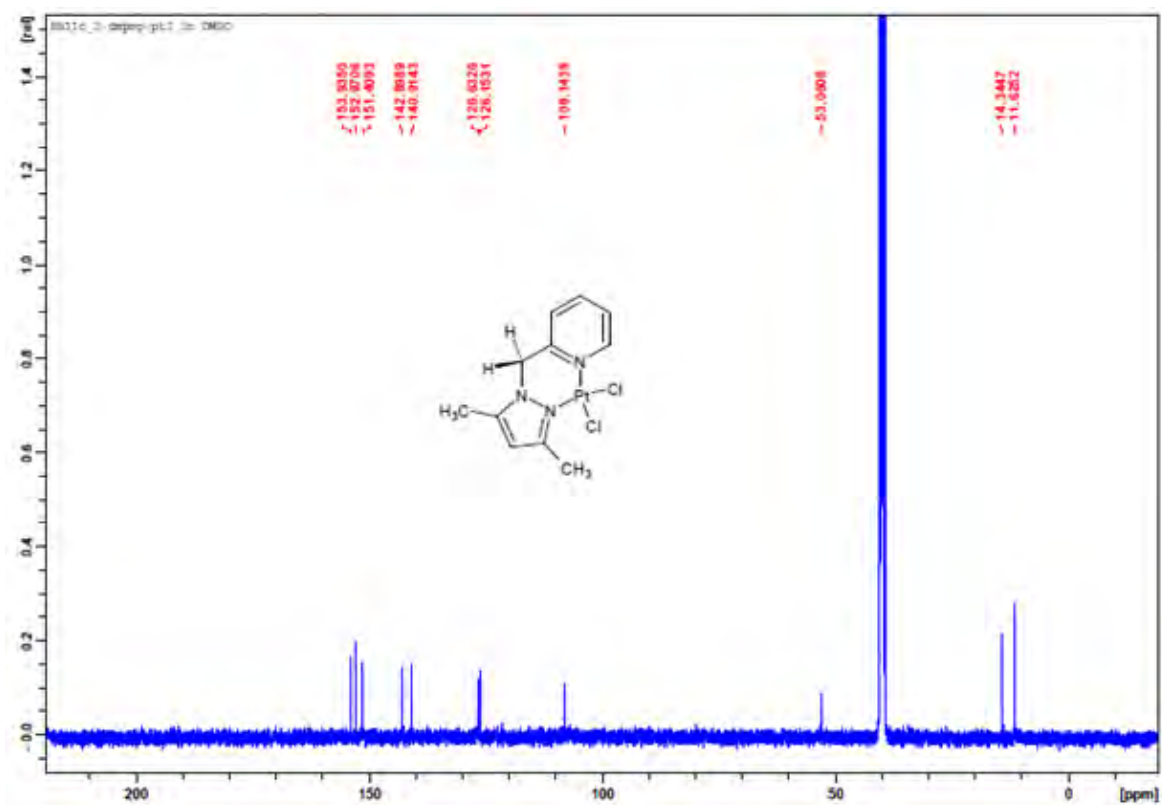
TOF MS ES+



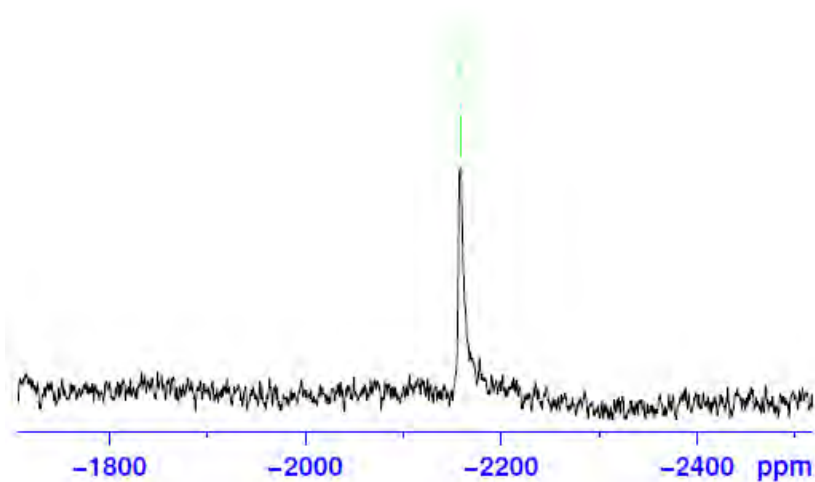
**Figure SI 4.1c:** Low resolution ESI<sup>+</sup> mass spectrum of 2-(pyrazol-1-ylmethyl)pyridine (**H<sub>2</sub>Py**).



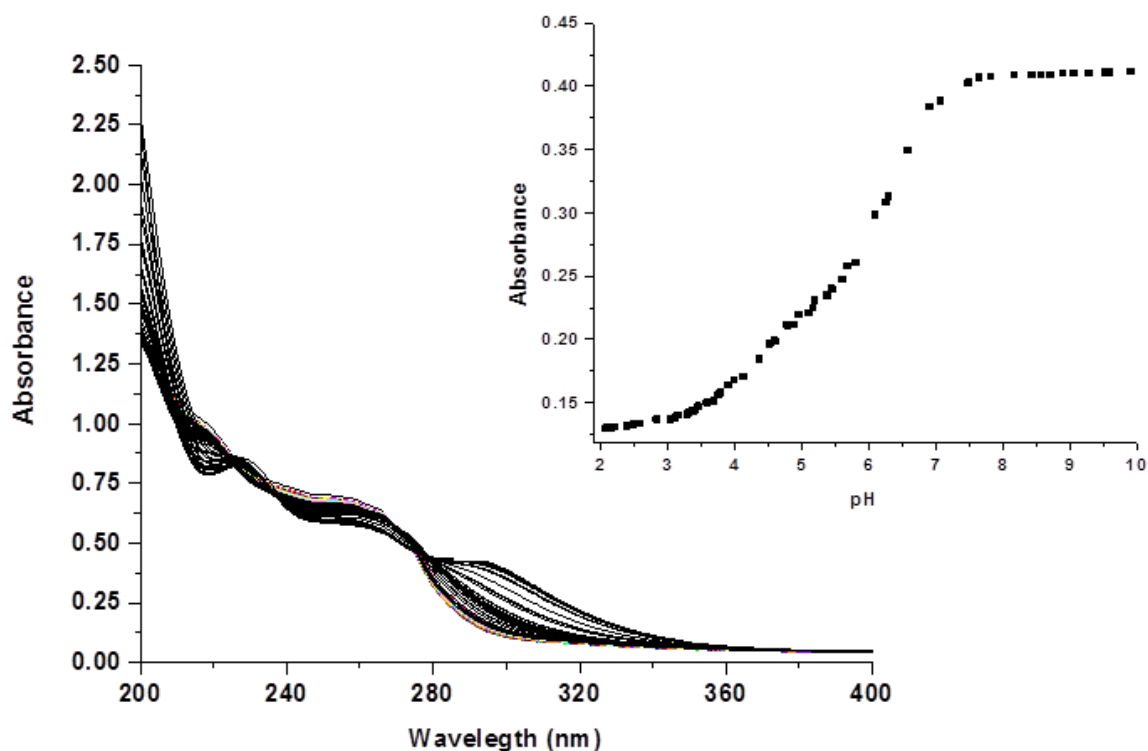
**Figure SI 4.2a:** <sup>1</sup>H NMR spectrum of [Pt{2-(3,5-dimethylpyrazol-1-ylmethyl)pyridine}Cl<sub>2</sub>], [**Pt(dCH<sub>3</sub>Py)**Cl<sub>2</sub>] in DMSO-d<sub>6</sub>.



**Figure SI 4.2b:** <sup>13</sup>C NMR spectrum of [Pt{2-(3,5-dimethylpyrazol-1-ylmethyl)pyridine}Cl<sub>2</sub>], [Pt(dCH<sub>3</sub>Py)] in DMSO-d<sub>6</sub>.



**Figure SI 4.2c:** <sup>195</sup>Pt NMR spectrum of [Pt{2-(3,5-dimethylpyrazol-1-ylmethyl)pyridine}Cl<sub>2</sub>], [Pt(dCH<sub>3</sub>Py)Cl<sub>2</sub>] in DMSO-d<sub>6</sub>.



**Figure SI 4.3:** UV/Visible spectra for the titration of 0.054 mM  $\text{Pt}(\text{dCF}_3\text{Py})$  with NaOH in the pH range 2-10 at  $T = 298.15$  K. Inset: Absorbance versus pH plot at 295 nm for  $\text{Pt}(\text{dCF}_3\text{Py})$  complex.

**Table SI 4.2a.** Average observed rate constants,  $k_{\text{obs}1}$ , for the displacement of the first aqua ligand in  $\text{Pt}(\text{H}_2\text{Py})$  by thiourea nucleophiles, pH = 2.0,  $T = 298$  K,  $I = 0.1$  M ( $\text{HClO}_4/\text{NaClO}_4$ ).

[TU]/ M	$k_{\text{obs}1}/ \text{S}^{-1}$	[DMTU]/ M	$k_{\text{obs}1}/ \text{S}^{-1}$	[TMTU]/ M	$k_{\text{obs}1}/ \text{S}^{-1}$
0.001764	0.0532998	0.001764	0.060781	0.001764	0.03839121
0.003528	0.0968539	0.003528	0.101665	0.003528	0.07085705
0.005292	0.1602171	0.005292	0.156104	0.005292	0.10713093
0.007056	0.2161881	0.007056	0.207837	0.007056	0.13684907
0.008820	0.2685696	0.008820	0.254593	0.008820	0.17279378

**Table SI 4.2b.** Average observed rate constants,  $k_{\text{obs}1}$ , for the displacement of the first aqua ligand in  $\text{Pt}(\text{dCH}_3\text{Py})$  by thiourea nucleophiles, pH = 2.0,  $T = 298$  K,  $I = 0.1$  M ( $\text{HClO}_4/\text{NaClO}_4$ ).

[TU]/ M	$k_{\text{obs}1}/ \text{S}^{-1}$	[DMTU]/ M	$k_{\text{obs}1}/ \text{S}^{-1}$	[TMTU]/ M	$k_{\text{obs}1}/ \text{S}^{-1}$
0.0016548	0.031694	0.0024822	0.034991	0.0049644	0.0086561
0.0033096	0.064188	0.0049644	0.071305	0.0097880	0.0186228
0.0049644	0.104314	0.0074466	0.112241	0.0148932	0.0301868
0.0066192	0.139097	0.0099288	0.155755	0.0198576	0.0412438
0.0082740	0.171279	0.0124110	0.193079	0.0248220	0.0525051

**Table SI 4.2c.** Average observed rate constants,  $k_{obs1}$ , for the displacement of the first aqua ligand in **Pt(dCF<sub>3</sub>Py)** by thiourea nucleophiles, pH = 2.0,  $T = 298$  K,  $I = 0.1$  M (HClO<sub>4</sub>/NaClO<sub>4</sub>).

[TU]/ M	$k_{obs1}/ S^{-1}$	[DMTU]/ M	$k_{obs1}/ S^{-1}$	[TMTU]/ M	$k_{obs1}/ S^{-1}$
0.0013365	0.209136	0.0013365	0.1062663	0.0013365	0.02589553
0.0026730	0.379717	0.0026730	0.2088192	0.0026730	0.05136792
0.0040095	0.584138	0.0040095	0.3379142	0.0040095	0.07594849
0.0053460	0.805353	0.0053460	0.4778034	0.0053460	0.09938629
0.0066825	0.975599	0.0066825	0.6032466	0.0066825	0.12552738

**Table SI 4.2d.** Average observed rate constants,  $k_{obs2}$ , for the displacement of the second aqua ligand in **Pt(H<sub>2</sub>Py)** by thiourea nucleophiles, pH = 2.0,  $T = 298$  K,  $I = 0.1$  M (HClO<sub>4</sub>/NaClO<sub>4</sub>).

[TU]/ M	$k_{obs2}/ S^{-1}$	[DMTU]/ M	$k_{obs2}/ S^{-1}$	[TMTU]/ M	$k_{obs2}/ S^{-1}$
0.00176	9.18814E-05	0.00176	5.98523E-05	0.00176	0.000133622
0.00352	0.000438506	0.00352	0.000229481	0.00352	0.000253572
0.00528	0.000932244	0.00528	0.000472197	0.00528	0.000364966
0.00704	0.001428284	0.00704	0.000744978	0.00704	0.000515384
0.00880	0.001930135	0.00880	0.001047522	0.00880	0.000669135

**Table SI 4.2e.** Average observed rate constants,  $k_{obs2}$ , for the displacement of the second aqua ligand in **Pt(dCH<sub>3</sub>Py)** by thiourea nucleophiles, pH = 2.0,  $T = 298$  K,  $I = 0.1$  M (HClO<sub>4</sub>/NaClO<sub>4</sub>).

[TU]/ M	$k_{obs2}/ S^{-1}$	[DMTU]/ M	$k_{obs2}/ S^{-1}$	[TMTU]/ M	$k_{obs2}/ S^{-1}$
0.0016548	0.000114145	0.0016548	0.000104634	0.0016548	1.05835E-05
0.0033096	0.000265083	0.0033096	0.000175988	0.0033096	3.41050E-05
0.0049644	0.000402572	0.0049644	0.000264663	0.0049644	6.47261E-05
0.0066192	0.000541993	0.0066192	0.000345894	0.0066192	9.09161E-05
0.0082740	0.000685695	0.0082740	0.000414915	0.0082740	0.000117287

**Table SI 4.2f.** Average observed rate constants,  $k_{obs2}$ , for the displacement of the second aqua ligand in **Pt(dCF<sub>3</sub>Py)** by thiourea nucleophiles, pH = 2.0,  $T = 298$  K,  $I = 0.1$  M (HClO<sub>4</sub>/NaClO<sub>4</sub>).

[TU]/ M	$k_{obs2}/ S^{-1}$	[DMTU]/ M	$k_{obs2}/ S^{-1}$	[TMTU]/ M	$k_{obs2}/ S^{-1}$
0.0006833	0.000166531	0.0006833	8.56831E-05	0.0013665	3.1800E-05
0.0013666	0.000332366	0.0013666	0.000192329	0.0027330	7.3600E-05
0.0020499	0.000514252	0.0020499	0.000303338	0.0040995	1.0900E-04
0.0027332	0.000658979	0.0027332	0.000418477	0.0054660	1.4000E-04
0.0034165	0.000892367	0.0034165	0.000521954	0.0068325	1.7700E-04

**Table SI 4.3a.** Temperature dependence of the second-order rate constants,  $k_{2\text{ (1st)}}$ ,  $\text{M}^{-1} \text{s}^{-1}$  for the displacement of the first aqua ligand in **Pt(H<sub>2</sub>Py)** by thiourea nucleophiles, pH = 2.0,  $I = 0.1 \text{ M}$  ( $\text{HClO}_4/\text{NaClO}_4$ ).

TU		DMTU		TMTU	
$1/T, \text{K}^{-1}$	$\ln(k_2/T)$	$1/T, \text{K}^{-1}$	$\ln(k_2/T)$	$1/T, \text{K}^{-1}$	$\ln(k_2/T)$
0.003470415	-2.85341	0.003470415	-2.81901	0.003470415	-3.31794393
0.003411223	-2.58079	0.003411223	-2.53794	0.003411223	-2.98925905
0.003354016	-2.28726	0.003354016	-2.31327	0.003354016	-2.68974123
0.003298697	-2.02887	0.003298697	-2.09197	0.003298697	-2.48454498
0.003245173	-1.79451	0.003245173	-1.75174	0.003245173	-2.20686541

**Table SI 4.3b.** Temperature dependence of the second-order rate constants,  $k_{2\text{ (1st)}}$ ,  $\text{M}^{-1} \text{s}^{-1}$  for the displacement of the first aqua ligand in **Pt(dCH<sub>3</sub>Py)** by thiourea nucleophiles, pH = 2.0,  $I = 0.1 \text{ M}$  ( $\text{HClO}_4/\text{NaClO}_4$ ).

TU		DMTU		TMTU	
$1/T, \text{K}^{-1}$	$\ln(k_2/T)$	$1/T, \text{K}^{-1}$	$\ln(k_2/T)$	$1/T, \text{K}^{-1}$	$\ln(k_2/T)$
0.003470415	-3.32996	0.003470415	-3.683904	0.003470415	-5.67997962
0.003411223	-3.02483	0.003411223	-3.274142	0.003411223	-5.30077158
0.003354016	-2.65248	0.003354016	-2.984706	0.003354016	-4.99109667
0.003298697	-2.42749	0.003298697	-2.666791	0.003298697	-4.65832806
0.003245173	-2.09758	0.003245173	-2.296801	0.003245173	-4.47252569

**Table SI 4.3c.** Temperature dependence of the second-order rate constants,  $k_{2\text{ (1st)}}$ ,  $\text{M}^{-1} \text{s}^{-1}$  for the displacement of the first aqua ligand in **Pt(dCF<sub>3</sub>Py)** by thiourea nucleophiles, pH = 2.0,  $I = 0.1 \text{ M}$  ( $\text{HClO}_4/\text{NaClO}_4$ ).

TU		DMTU		TMTU	
$1/T, \text{K}^{-1}$	$\ln(k_2/T)$	$1/T, \text{K}^{-1}$	$\ln(k_2/T)$	$1/T, \text{K}^{-1}$	$\ln(k_2/T)$
0.003470415	-1.94020813	0.003470415	-1.82993478	0.003470415	-3.33277200
0.003411223	-1.24929178	0.003411223	-1.52737825	0.003411223	-3.05254003
0.003354016	-0.71612601	0.003354016	-1.26347124	0.003354016	-2.75620791
0.003298697	-0.40161104	0.003298697	-0.93898081	0.003298697	-2.55663744
0.003245173	-0.14142259	0.003245173	-0.60713315	0.003245173	-2.36156920

**Table SI 4.3d.** Temperature dependence of the second-order rate constants,  $k_{2\text{ (2nd)}}$ ,  $\text{M}^{-1} \text{s}^{-1}$  for the displacement of the first aqua ligand in **Pt(H<sub>2</sub>Py)** by thiourea nucleophiles, pH = 2.0,  $I = 0.1 \text{ M}$  ( $\text{HClO}_4/\text{NaClO}_4$ ).

TU		DMTU		TMTU	
$1/T, \text{K}^{-1}$	$\ln(k_2/T)$	$1/T, \text{K}^{-1}$	$\ln(k_2/T)$	$1/T, \text{K}^{-1}$	$\ln(k_2/T)$
0.003470415	-7.76273	0.003470415	-8.65780	0.003354016	-8.37174311
0.003411223	-7.65076	0.003411223	-8.42840	0.003298697	-8.03141772
0.003354016	-7.56529	0.003354016	-8.22820	0.003245173	-7.67855270
0.003298697	-7.44832	0.003298697	-8.02290	0.003193358	-7.44099524
0.003245173	-7.27691	0.003245173	-7.81510	0.003143171	-7.20103030

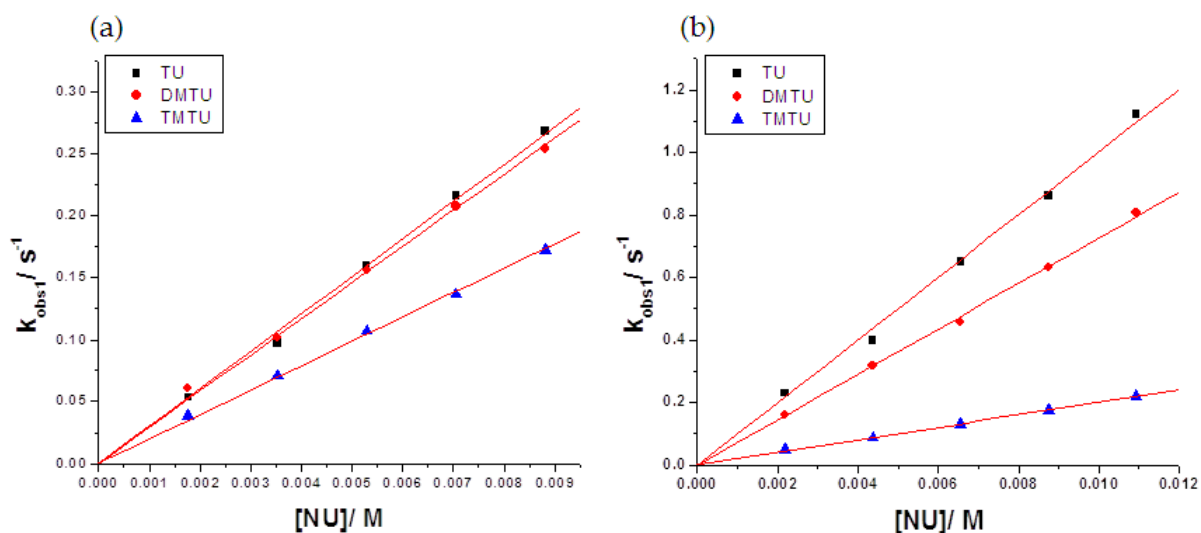
**Table SI 4.3e.** Temperature dependence of the second-order rate constants,  $k_{2\text{ (2nd)}}$ ,  $\text{M}^{-1} \text{s}^{-1}$  for the displacement of the first aqua ligand in **Pt(dCH<sub>3</sub>Py)** by thiourea nucleophiles, pH = 2.0,  $I = 0.1 \text{ M}$  ( $\text{HClO}_4/\text{NaClO}_4$ ).

TU		DMTU		TMTU	
$1/T, \text{K}^{-1}$	$\ln(k_2/T)$	$1/T, \text{K}^{-1}$	$\ln(k_2/T)$	$1/T, \text{K}^{-1}$	$\ln(k_2/T)$
0.003354016	-8.20977099	0.003354016	-8.62918677	0.003354016	-10.0374808
0.003298697	-7.92752219	0.003298697	-8.50688154	0.003298697	-9.76256976
0.003245173	-7.59254944	0.003245173	-8.05662456	0.003245173	-9.51511435
0.003193358	-7.27852335	0.003193358	-7.70298613	0.003193358	-9.33516011
0.003143171	-7.03205966	0.003143171	-7.45585711	0.003143171	-9.19287380

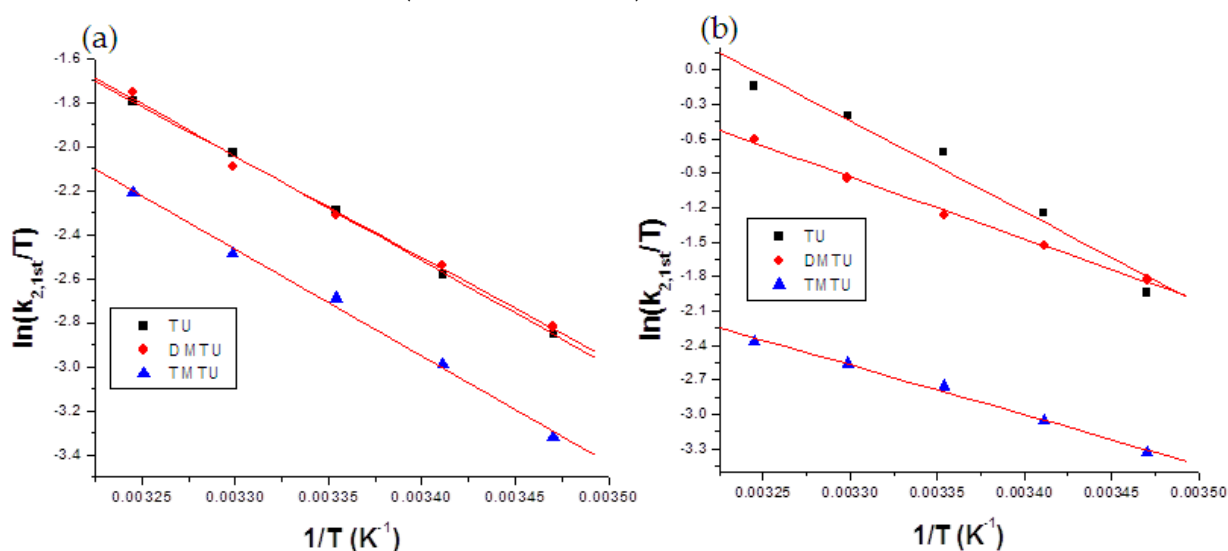
**Table SI 4.3f.** Temperature dependence of the second-order rate constants,  $k_{2\text{ (2nd)}}$ ,  $\text{M}^{-1} \text{s}^{-1}$  for the displacement of the first aqua ligand in **Pt(dCF<sub>3</sub>Py)** by thiourea nucleophiles, pH = 2.0,  $I = 0.1 \text{ M}$  ( $\text{HClO}_4/\text{NaClO}_4$ ).

TU		DMTU		TMTU	
$1/T, \text{K}^{-1}$	$\ln(k_2/T)$	$1/T, \text{K}^{-1}$	$\ln(k_2/T)$	$1/T, \text{K}^{-1}$	$\ln(k_2/T)$
0.003354016	-7.08042913	0.003354016	-7.60829774	0.003354016	-9.32225342
0.003298697	-6.82076324	0.003298697	-7.22648780	0.003298697	-8.89819742
0.003245173	-6.45131890	0.003245173	-6.91286531	0.003245173	-8.57414989
0.003193358	-6.16827619	0.003193358	-6.65181158	0.003193358	-8.28614497
0.003143171	-5.93919625	0.003143171	-6.38318238	0.003143171	-7.99989456

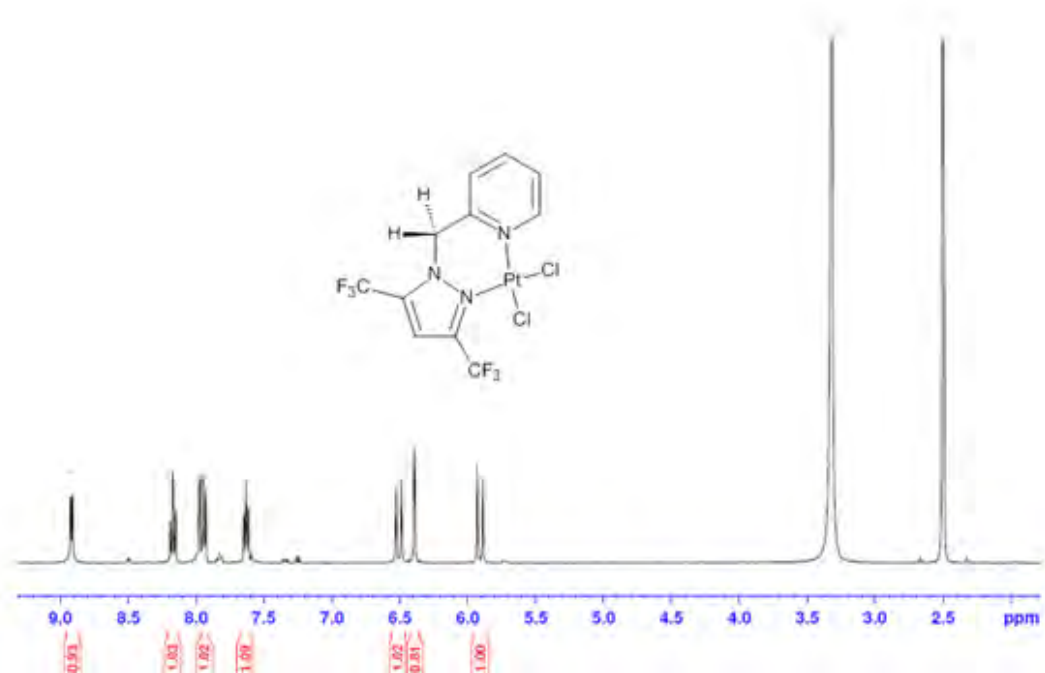




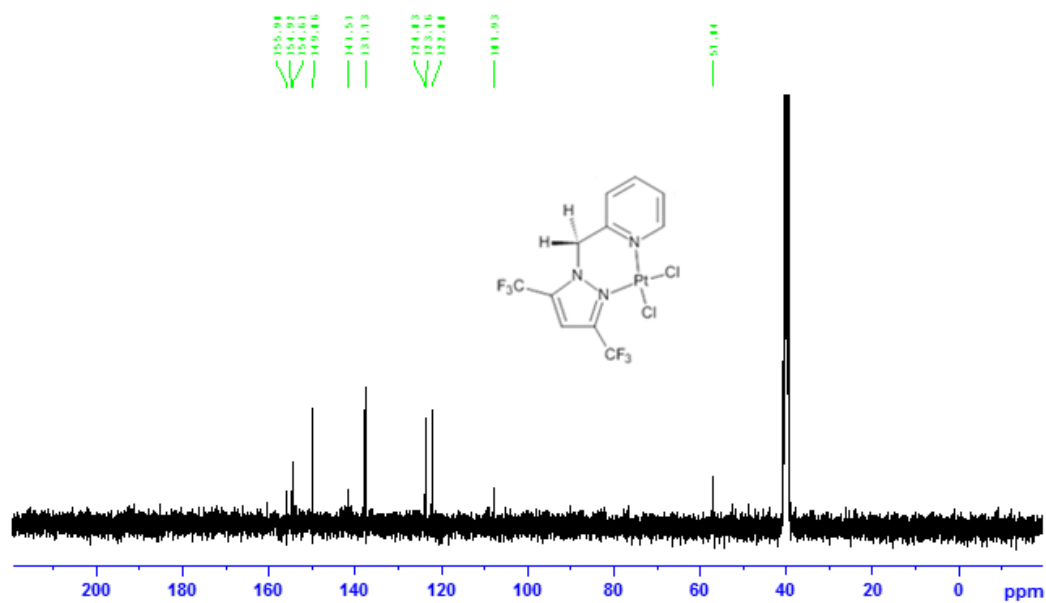
**Figure SI 4.4:** Concentration dependence plots of  $k_{obs1}$ , s<sup>-1</sup>, for the displacement of the first aqua ligand of Pt(H<sub>2</sub>Py) (a) and Pt(dCH<sub>3</sub>Py) (b) by thiourea nucleophiles, pH = 2.0, T = 298 K, and I = 0.1 M (HClO<sub>4</sub>/NaClO<sub>4</sub>).



**Figure SI 4.5:** Eyring plots for the substitution of the first aqua ligand of Pt(H<sub>2</sub>Py) (a) and Pt(dCF<sub>3</sub>Py) (b) by thiourea nucleophiles, pH = 2.0, and I = 0.1 M (HClO<sub>4</sub>/NaClO<sub>4</sub>).



**Figure SI 4.6:**  $^1\text{H}$  NMR spectrum of  $[\text{Pt}\{2-[(3,5\text{-bis(trifluoromethyl)pyrazol-1-yl)methyl]pyridine}\}\text{Cl}_2]$ ,  $[\text{Pt}(\text{dCF}_3\text{Py})\text{Cl}_2]$  in  $\text{DMSO-d}_6$ .



**Figure SI 4.7:**  $^{13}\text{C}$  NMR spectrum of  $[\text{Pt}\{2-[(3,5\text{-bis(trifluoromethyl)pyrazol-1-yl)methyl]pyridine}\}\text{Cl}_2]$ ,  $[\text{Pt}(\text{dCF}_3\text{Py})\text{Cl}_2]$  in  $\text{DMSO-d}_6$ .

# Chapter 5

---

## The influence of substituents and extended $\pi$ -conjugation in bidentate *N,N*-chelate on the substitution kinetics of aqua ligands from platinum(II) complexes

### 5.0 Abstract

Substitution reactions of aqua ligands from four bifunctional Pt(II) complexes, namely, [Pt{2-(pyrazol-1-ylmethyl)quinoline}(H<sub>2</sub>O)<sub>2</sub>](ClO<sub>4</sub>)<sub>2</sub>, [Pt(H<sub>2</sub>Qn)], [Pt{2-(3,5-dimethylpyrazol-1-ylmethyl)quinoline}(H<sub>2</sub>O)<sub>2</sub>](ClO<sub>4</sub>)<sub>2</sub>, [Pt(dCH<sub>3</sub>Qn)], [Pt{2-[(3,5-bis(trifluoromethyl)pyrazol-1-ylmethyl)quinoline}(H<sub>2</sub>O)<sub>2</sub>](ClO<sub>4</sub>)<sub>2</sub>, [Pt(dCF<sub>3</sub>Qn)], and [Pt{2-[(3,5-bis(trifluoromethyl)pyrazol-1-ylmethyl)pyridine}(H<sub>2</sub>O)<sub>2</sub>](ClO<sub>4</sub>)<sub>2</sub>, [Pt(dCF<sub>3</sub>Py)], with three sulphur donor nucleophiles, *viz.*, thiourea (TU), *N,N*-dimethylthiourea (DMTU), *N,N,N',N'*-tetramethylthiourea (TMTU), were studied. The reactions were followed under *pseudo* first-order conditions as a function of nucleophile concentration and temperature, using stopped-flow and UV/visible spectrophotometry. The second-order rate constants for the lability of the aqua ligands in the first substitution step increased in the order of Pt(dCH<sub>3</sub>Qn) < Pt(dCF<sub>3</sub>Qn) < Pt(H<sub>2</sub>Qn) < Pt(dCF<sub>3</sub>Py), while that of the second substitution step was Pt(dCH<sub>3</sub>Qn) < Pt(dCF<sub>3</sub>Qn) < Pt(dCF<sub>3</sub>Py) < Pt(H<sub>2</sub>Qn). The observed substitution steps were ascribed to a sequential substitution of the labile aqua ligands. The reactivity trend confirms that quinoline substructure in the (pyrazolylmethyl) quinoline ligands acts as an apparent donor of electron density towards the metal centre rather than being a  $\pi$ -acceptor. Measured  $pK_a$  values from spectrophotometric acid-base titrations were respectively, Pt(H<sub>2</sub>Qn) ( $pK_{a1}$  = 4.56;  $pK_{a2}$  = 6.32), Pt(dCH<sub>3</sub>Qn) ( $pK_{a1}$  = 4.88;  $pK_{a2}$  = 6.31), Pt(dCF<sub>3</sub>Qn) ( $pK_{a1}$  = 4.07;  $pK_{a2}$  = 6.35), and Pt(dCF<sub>3</sub>Py) ( $pK_{a1}$  = 4.76;  $pK_{a2}$  = 6.27). The activation parameters from the temperature dependence of the second-order rate constants support an associative mechanism of substitution.

## 5.1 Introduction

Complexes of pyrazole-based ligands hold a great promise in medicine.<sup>1</sup> In particular, platinum(II) complexes with pyrazole ligands have shown interesting biological activities including anticancer, antibacterial and anti-inflammatory properties.<sup>1</sup> Pt(II) complexes display a wide range of anticancer properties owing to their ability to bind covalently or through intercalation to the nucleophilic sites of DNA.<sup>2,3</sup> This alters the conformational structure of DNA, resulting into apoptotic death of cancerous cells.<sup>2,4</sup> In this respect, mechanistic studies of Pt(II) complexes with biologically relevant nucleophiles should be explored to provide a detailed insight into specific kinetic and thermodynamic properties that control the reactivity of such complexes.

The rate of substitution in chelated square-planar Pt(II) complexes can be controlled by varying the electronic and steric factors of the coordinated non-leaving ligand. These factors can be either cooperative or antagonistic depending on the electronic properties as well as spatial orientation of the non-leaving ligand.<sup>5,6,7</sup> A substructure within the ligand which donates electron density *trans* to the leaving group usually increase the rate of substitution *via* its *trans*-influence on the ground state properties of the complex. This is also true for  $\pi$ -acceptors, especially those with extended molecular orbital within the substructure which withdraw electron density at the metal centre thereby increasing the electrophilicity of the metal centre in the transition state. These two are termed the *trans*-effect.<sup>8-14</sup>

However, when the donation of the electron density occurs *cis* to the leaving group, it retards the rate due to an increase in electron density at the metal centre which repels the incoming nucleophile in the transition state. This is termed the *cis*-effect.<sup>8-14</sup> It is generally assumed to be much weaker than the *trans*-effect.<sup>11,13</sup> This assumption has not been fully validated and the experimental results are somehow contradictory.<sup>10,11,12</sup> For example, in a study by Romeo,<sup>15</sup> the rate of substitution decreased when a chelated  $\pi$ -acceptor ligand had a strong  $\sigma$ -donor moiety coordinated *cis* to the leaving group. The electron-donating effect dominated over the electron-withdrawing of the rest of the chelate ligand. In a related study, the rate of substitution was higher for a complex with a *cis*  $\pi$ -accepting moiety than that with

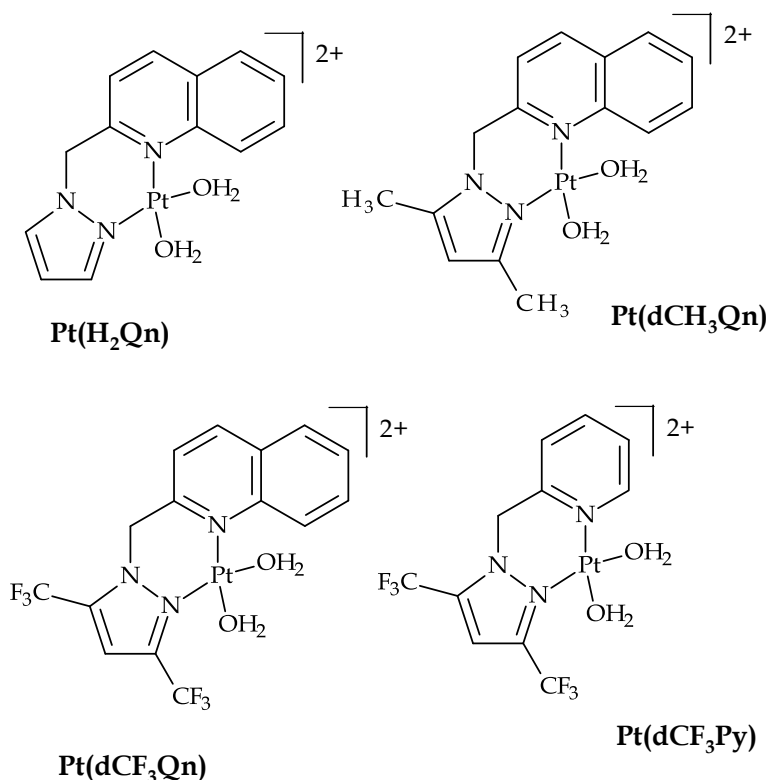
same moiety on the *trans* position.<sup>10</sup> Therefore, if the ligand contains both  $\sigma$ -donor and  $\pi$ -acceptor properties, the observed overall *cis*-effect is dependent on whichever effect is stronger, since the latter accelerates while the former decelerates the reaction. Jaganyi *et al.* have studied in detail the effect on the rate of changing the  $\pi$ -acceptability of tridentate popyridyl nitrogen-donor ligands by varying the number of pyridine rings or attaching electron-withdrawing or electron-donating substituents on the ligand framework.<sup>16,17,18</sup> A somehow surprising result to what has been reported elsewhere in literature was that,<sup>21,22</sup> when a quinoline or isoquinoline formed part of the tridentate ligand in the *cis* position to the leaving group, an anomalous decrease in the reactivity was observed.<sup>17,19,20</sup> This was ascribed to a weaker back-bonding between the quinoline moiety and the metal centre which weakens the  $\pi$ -acceptability of the whole ligand.

Equally important about the structure of the non-leaving ligand are its steric effects on reactivity and cytotoxicity. The effects can be due to spatial size (steric demand) and/or due to spatial orientation (steric hindrance) relative to the leaving group. An advantageous consequence on antitumour activity of Pt(II) complexes due to steric hindrance by a non-leaving ligand is revealed on the relative cytotoxicity indices of two isomeric complexes *cis*-[Pt(NH<sub>3</sub>)<sub>2</sub>(2-methylpyridine)Cl]<sup>+</sup> and *cis*-[Pt(NH<sub>3</sub>)<sub>2</sub>(4-methylpyridine)Cl]<sup>+</sup>.<sup>8,9</sup> The former complex was found to be more active due to its reduced rates of deactivation by sulphur nucleophiles caused by an aerial block to substitution by the *ortho*-methyl substituent.

The steric influence on reactivity imposed onto an incoming nucleophile especially if it is *cis*-positioned (steric *cis*-effect) to the leaving group is usually strong and can dominate over its electronic contribution.<sup>11,13</sup> It was demonstrated in Chapter 4 that an increase in the  $\pi$ -accepting capacity of an *N,N*-bidentate chelate incorporating a 3,5-bis(trifluoromethyl)pyrazole moiety is counteracted by a steric retardation to the substitution rate of the aqua ligand in the *cis* position. The 3-positioned trifluoromethyl substituent of pyrazole shields the leaving group, thus slowing down the rate of substitution.

To further our understanding on the influence on the rate of substituents of an *N,N*-bidentate core, four Pt(II) complexes bearing (pyrazolylmethyl)quinoline/pyridine

ligands (see **Figure 5.1**) were synthesized and their substitution kinetics were studied. The choice of complexes was based on impressive cytotoxic data reported for structurally similar Pt(II) complexes.<sup>23</sup> Biologically relevant sulfur-containing nucleophiles *viz.*, thiourea (TU), *N,N*-dimethylthiourea (DMTU) and *N,N,N',N'*-tetramethylthiourea (TMTU) were used as substituting nucleophiles. Density functional theoretical (DFT) calculations were used to aid the interpretation of the experimentally obtained kinetic data.



**Figure 5.1:** Chemical structures of the bifunctional Pt(II) complexes. Perchlorate counter ions ( $\text{ClO}_4^-$ ) are omitted for clarity.

## 5.2 Experimental

### 5.2.1 Chemicals and reagents

All synthetic manipulations of the ligands were carried out in air, whereas the coordination of the ligands to the platinum metal was performed under inert atmosphere of nitrogen using standard Schlenk techniques. The ligand precursor 2-(chloromethyl)quinoline hydrochloride (97%) was purchased from Aldrich and used

without further purification. All other chemical were purchased from suppliers as already described in Chapter 4, section 4.2.1.

### 5.2.2 Preparation of the ligands

Three (pyrazolylmethyl)quinoline ligands and one (pyrazolylmethyl)pyridine ligand, namely, 2-(pyrazol-1-ylmethyl)quinoline (**H<sub>2</sub>Qn**), 2-(3,5-dimethylpyrazol-1-ylmethyl)quinoline (**dCH<sub>3</sub>**), 2-[(3,5-bis(trifluoromethyl)pyrazol-1-ylmethyl)]quinoline (**dCF<sub>3</sub>Qn**), and 2-[(3,5-bis(trifluoromethyl)pyrazol-1-ylmethyl)]pyridine (**dCF<sub>3</sub>Py**) were prepared using the same procedure described for the ligand used in Chapter 4, section 4.2.2. However, 2-(chloromethyl)quinoline was used instead of 2-(chloromethyl)pyridine for synthesizing the quinolone bearing ligands. All ligands were obtained in moderate yields (59-61%) and collected as brown oils of sufficient purity for subsequent use in platinum coordination. The purity of the ligands was confirmed by <sup>1</sup>H NMR, <sup>13</sup>C NMR, TOF-MS-ESI<sup>+</sup> and elemental analysis.

#### 2-(pyrazol-1-ylmethyl)quinoline (**H<sub>2</sub>Qn**)

Yield = 0.7131 g (60%). <sup>1</sup>H NMR (400 MHz: CDCl<sub>3</sub>): δ<sub>H</sub> (ppm); 5.66 (s, 2H, -CH<sub>2</sub>-), 6.35-6.36 (t, 1H, pz), 7.11-7.13 (d, 1H, py), 7.54-7.58 (dd, 2H, pz), 7.62- 7.63 (t, 1H, ph), 7.73-7.77 (t, 1H, ph), 7.80-7.82 (d, 2H, ph), 8.08-8.13 (dd, 2H, py, ph). <sup>13</sup>C NMR (100 MHz: CDCl<sub>3</sub>): δ<sub>C</sub> (ppm); 57.60, 79.63, 106.23 , 119.94, 127.02, 127.42, 128.33, 130.37, 137.58, 139.95, 139.95, 147.37, 157.97. TOF MS-ESI<sup>+</sup> *m/z*: 210.027, 100% (M+1). Anal. calculated for C<sub>13</sub>H<sub>11</sub>N<sub>3</sub>: C, 74.62; H, 5.30, N, 20.08%. Found: C, 74.29; H, 5.36; N, 19.67%.

#### 2-(3,5-dimethylpyrazolyl-1-ylmethyl)quinoline (**dCH<sub>3</sub>Qn**)

Yield = 0.797 g (59%). <sup>1</sup>H NMR (400 MHz: CDCl<sub>3</sub>): δ<sub>H</sub> (ppm); 2.19 (s, 3H, CH<sub>3</sub>), 2.30 (s, 3H, CH<sub>3</sub>), 5.54 (s, 2H, -CH<sub>2</sub>-), 5.91 (s, 1H, pz), 6.96-6.98 (d, 1H, py), 7.52-7.56 (t, 1H, ph), 7.71-7.776 (t, 1H, ph), 7.79- 7.81 (d, 1H, ph), 8.06-8.10 (dd, 2H, ph, py). <sup>13</sup>C NMR (100 MHz: CDCl<sub>3</sub>): δ<sub>C</sub> (ppm); 11.14, 13.56, 55.39, 105.94, 118.85, 126.46, 127.35, 127.63, 129.01, 129.78, 137.30, 139.92, 147.55, 148.14, 157.76. TOF MS-ESI<sup>+</sup> *m/z*: 238.134, 100% (M+1)<sup>+</sup>. Anal. calculated for C<sub>15</sub>H<sub>15</sub>N<sub>3</sub>: C, 75.92; H, 6.37, N, 17.71%. Found: C, 75.05; H, 6.13; N, 17.98%.

## 2-[3,5-bis(trifluoromethyl)pyrazol-1-ylmethyl]quinoline (dCF<sub>3</sub>Qn)

Yield = 1.10 g (56%). <sup>1</sup>H NMR (400 MHz: CDCl<sub>3</sub>): δ<sub>H</sub> (ppm); 5.84 (s, 2H, -CH<sub>2</sub>-), 7.01 (s, 1H, pz), 7.04-7.06 (d, 1H, py), 7.56-7.59 (t, 1H, ph), 7.73- 7.77 (t, 1H, ph), 7.82-7.89 (d, 1H, ph), 8.05-8.03 (d, 1H, py), 8.15-8.17 (d, 1H, ph). <sup>13</sup>C NMR (100 MHz: CDCl<sub>3</sub>): δ<sub>C</sub> (ppm); 57.78, 106.66, 118.18, 121.71, 126.98, 127.44, 127.60, 129.34, 130.08, 134.08, 137.46, 142.32, 142.71, 147.64, 154.28. TOF MS-ESI<sup>+</sup> *m/z*: 346.073, 100% (M+1)<sup>+</sup>. calculated for C<sub>15</sub>H<sub>9</sub>N<sub>3</sub>F<sub>6</sub>: C, 52.18; H, 2.63, N, 12.17%. Found: C, 51.94; H, 2.53, N, 11.96%.

## 2-[(3,5-bis(trifluoromethyl)pyrazol-1-ylmethyl)]pyridine (dCF<sub>3</sub>Py)

Yield = 1.02 g (61%). <sup>1</sup>H NMR (400 MHz: CDCl<sub>3</sub>): δ<sub>H</sub> (ppm); 5.68 (s, 2H, -CH<sub>2</sub>-), 6.95-6.97 (d, 1H, py), 7.00 (s, 1H, pz), 7.26-7.30 (t, 1H, py), 7.68- 7.73 (t, 1H, py), 8.61-8.62 (d, 1H, py). <sup>13</sup>C NMR (100 MHz: CDCl<sub>3</sub>): δ<sub>C</sub> (ppm); 57.08, 106.57, 117.73, 120.41, 120.97, 123.13, 133.91, 137.07, 142.64, 149.64, 154.35. TOF MS-ESI<sup>+</sup> *m/z*: 296.057, 100% (M+1). Anal. calculated for C<sub>11</sub>H<sub>7</sub>N<sub>3</sub>F<sub>6</sub>: C, 44.76; H, 2.39, N, 14.24%. Found: C, 44.42; H, 2.46; N, 14.41%.

### 5.2.3 Synthesis of the platinum complexes

The semi-flexible and versatile dichloro platinum(II) complexes, namely, [Pt{2-(pyrazol-1-ylmethyl)quinoline}Cl<sub>2</sub>], [Pt(H<sub>2</sub>Qn)Cl<sub>2</sub>], [Pt{2-(3,5-dimethylpyrazol-1-ylmethyl)quinoline}Cl<sub>2</sub>], [Pt(dCH<sub>3</sub>Qn)Cl<sub>2</sub>], [Pt{2-[(3,5-bis(trifluoromethyl)pyrazol-1-ylmethyl)]quinoline}Cl<sub>2</sub>], [Pt(dCF<sub>3</sub>Qn)Cl<sub>2</sub>], as well as [Pt{2-[(3,5-bis(trifluoromethyl)pyrazol-1-ylmethyl)]pyridine}Cl<sub>2</sub>], [Pt(dCF<sub>3</sub>Py)Cl<sub>2</sub>] were synthesised following the same procedure described for pyridine-bearing Pt(II) complexes in Chapter 4, section 4.2.3. For the formation of the complexes, [Pt(dCF<sub>3</sub>Qn)Cl<sub>2</sub>] and [Pt(dCF<sub>3</sub>Py)Cl<sub>2</sub>], 0.01 M HCl solution was used instead of ultrapure water to dissolve the platinum precursor, sodium tetrachloropalladate (K<sub>2</sub>PtCl<sub>4</sub>). All dichloro Pt(II) complexes were isolated as a yellow powders and their purity was confirmed by <sup>1</sup>H NMR, <sup>13</sup>C NMR, <sup>195</sup>Pt NMR, elemental analysis, TOF MS-ESI<sup>+</sup> and infrared (IR) spectroscopy.

[Pt(H<sub>2</sub>Qn)Cl<sub>2</sub>]. Yield: 187 mg (82%). <sup>1</sup>H NMR (400 MHz: DMSO-d<sub>6</sub>): δ<sub>H</sub> (ppm); 5.68 (s, 2H, -CH<sub>2</sub>-), 6.37-6.38 (t, 1H, pz), 7.13-7.16 (d, 1H, py), 7.53-7.57 (d, 1H, ph), 7.61- 7.64 (t, 1H, ph), 7.76-7.83 (t, 1H, ph), 7.96-8.04 (dd, 2H, pz), 8.06-8.13 (d, 1H, py), 8.34-8.38



(d, 1H, ph).  $^{13}\text{C}$  NMR (100 MHz: DMSO- $\text{d}_6$ ):  $\delta_{\text{C}}$  (ppm); 57.57, 106.22, 119.95, 127.05, 127.42, 128.35, 129.01, 130.40, 131.52, 137.61, 139.95, 147.36, 158.01.  $^{195}\text{Pt}$  NMR (107 MHz: DMSO- $\text{d}_6$ ):  $\delta_{\text{Pt}}$  (ppm); -2963.56. TOF MS-ES $^{+}$   $m/z$ : 440.056 (M-Cl) $^{+}$ . IR (KBr)  $\text{cm}^{-1}$ : 566, 607, 762, 820, 904, 1075, 1278, 1420, 1511, 1589, 2852, 2923, 3124. Anal. calculated for  $\text{C}_{13}\text{H}_{11}\text{N}_3\text{PtCl}_2$ : C, 32.86; H, 2.33, N, 8.84%. Found: C, 32.66; H, 2.81; N, 8.60%.

**[Pt(dCH<sub>3</sub>Qn)Cl<sub>2</sub>].** Yield: 175 mg (73 %).  $^1\text{H}$  NMR (400 MHz: DMSO- $\text{d}_6$ ):  $\delta_{\text{H}}$  (ppm); 2.41 (s, 3H, CH<sub>3</sub>), 2.45 (s, 3H, CH<sub>3</sub>), 5.87-5.91 (d, 1H, AB-spin system, -CH<sub>2</sub>-), 6.12 (s, 1H, pz), 6.36-6.40 (d, 1H, AB-spin system, CH<sub>2</sub>), 7.73-7.76 (d, 1H, py), 7.96-7.99 (d, 1H, ph), 8.06-8.11 (t, 2H, ph), 8.75-8.77 (d, 1H, py), 9.36-9.39 (d, 1H, ph).  $^{13}\text{C}$  NMR (100 MHz: DMSO- $\text{d}_6$ ):  $\delta_{\text{C}}$  (ppm); 11.65, 13.91, 54.7, 105.7, 119.7, 126.9, 127.4, 129.0, 130.4, 131.4, 141.9, 143.3, 147.5, 150.9, 156.7.  $^{195}\text{Pt}$  NMR (107 MHz: DMSO- $\text{d}_6$ ):  $\delta_{\text{Pt}}$  (ppm); -2991.37. TOF MS-ES $^{+}$   $m/z$ : 468.194 (M-Cl) $^{+}$ . IR (KBr)  $\text{cm}^{-1}$ : 412, 512, 702, 758, 780, 795, 818, 905, 1149, 1288, 1408, 1512, 1552, 1590, 2923, 2962, 3171. Anal. calculated for  $\text{C}_{15}\text{H}_{15}\text{N}_3\text{PtCl}_2$ : C, 35.80; H, 3.00, N, 8.35%. Found: C, 35.65; H, 2.86; N, 8.83%.

**[Pt(dCF<sub>3</sub>Qn)Cl<sub>2</sub>].** Yield: 164 mg (56%).  $^1\text{H}$  NMR (400 MHz: DMSO- $\text{d}_6$ ):  $\delta_{\text{H}}$  (ppm); 5.95 (s, 2H, -CH<sub>2</sub>-), 7.34-7.36 (d, 1H, py), 7.60-7.64 (t, 1H, ph), 7.74 (s, 1H, pz), 7.76-7.78 (t, 1H, ph), 7.86-7.88 (d, 1H, ph), 7.98-8.00-8.03 (d, 1H, py), 8.41-8.43 (d, 1H, ph).  $^{13}\text{C}$  NMR (100 MHz: DMSO- $\text{d}_6$ ):  $\delta_{\text{C}}$  (ppm); 57.64, 108.09, 119.63, 120.88, 122.34, 127.39, 127.57, 128.43, 129.00, 130.65, 133.95, 138.02, 143.28, 147.22, 155.20.  $^{195}\text{Pt}$  NMR (107 MHz: DMSO- $\text{d}_6$ ):  $\delta_{\text{Pt}}$  (ppm); -2962.18. TOF MS-ES $^{+}$   $m/z$ : 575.440 (M-Cl) $^{+}$ . IR (KBr)  $\text{cm}^{-1}$ : 467, 500, 641, 703, 775, 840, 997, 1056, 1143, 1200, 1269, 1428, 1572, 1610, 2930, 3090, 3115, 3149. Anal. calculated for  $\text{C}_{15}\text{H}_9\text{N}_3\text{PtCl}_2\text{F}_6$ : C, 29.47; H, 1.46, N, 6.87%. Found: C, 29.92, H, 1.19, N, 7.06%.

**[Pt(dCF<sub>3</sub>Py)Cl<sub>2</sub>].** Yield: 170 mg (63%).  $^1\text{H}$  NMR (400 MHz: DMSO- $\text{d}_6$ ):  $\delta_{\text{H}}$  (ppm); 5.89-5.93 (d, 1H, AB-spin system, -CH<sub>2</sub>-), 6.39 (s, 1H, pz), 6.49-6.53 (d, 1H, AB-spin system, -CH<sub>2</sub>-), 7.61-7.65 (d, 1H, py), 7.93-7.98 (t, 1H, py), 8.15-8.19 (t, 1H, py), 8.91-8.92 (d, 1H, py).  $^{13}\text{C}$  NMR (100 MHz: DMSO- $\text{d}_6$ ):  $\delta_{\text{C}}$  (ppm); 57.04, 107.93, 122.08, 123.76, 124.03, 137.73, 141.51, 149.86, 154.61, 154.92, 159.2.  $^{195}\text{Pt}$  NMR (107 MHz: DMSO- $\text{d}_6$ ):  $\delta_{\text{Pt}}$  (ppm); -2888.75. TOF MS-ES $^{+}$   $m/z$ : 525.979 (M-Cl) $^{+}$ . IR (KBr)  $\text{cm}^{-1}$ : 469,

778, 829, 976, 1045, 1095, 1129, 1227, 1275, 1384, 1599, 1643, 2741, 2922. Anal. calculated for  $C_{11}H_7N_3PtCl_2F_6$ : C, 23.54; H, 1.26, N, 7.49%. Found: C, 23.70; H, 1.30; N, 7.54%.

#### 5.2.4 Preparation of diaqua Pt(II) complex and nucleophile solutions

The solutions of diaqua Pt(II) complexes **Pt(H<sub>2</sub>Qn)**, **Pt(dCH<sub>3</sub>Qn)**, **Pt(dCF<sub>3</sub>Qn)** and **Pt(dCF<sub>3</sub>Py)** (**Figure 5.1**), were prepared following a literature procedure of Bugarčić *et al.*<sup>24</sup> A detailed procedure was described in Chapter 4, section 4.2.4. Solutions of the nucleophiles TU, DMTU and TMTU were prepared by dissolving known amounts of the nucleophile in 0.01 M HClO<sub>4</sub> solution of constant 0.10 M ionic strength. The adjustment of constant ionic strength was done to ensure a constant ionic strength throughout the kinetic measurements.

#### 5.2.5 Instrumentation and physical measurements

Bruker Avance DRX 400 or DRX 500 NMR spectrometer was used to record the NMR spectra of the ligands and complexes. All chemical shifts (proton and carbon) are quoted relative to the signals of relevant solvents. All data were recorded at 25 °C unless otherwise stated. The mass spectrometric data of the ligands and the complexes were acquired on the micromass spectrometer equipped with a positive electron-sprayer (ESI<sup>+</sup>) and a time of flight (TOF) analyser. The elementary compositions of all synthesised compounds were determined on a Thermo Scientific FLASH 2000 CHN Automatic Elemental Analyser. Infrared (IR) spectra were acquired using KBr discs on a Perkin Elmer Spectrum One FTIR spectrometer. Selected NMR and mass spectra of the synthesised compounds are represented as supplementary information in **Figure SI 5.1**. A Varian Cary 100 Bio UV-visible spectrophotometer, equipped with a thermostat which can accurately measure temperature within  $\pm 0.05$  °C was used for spectrophotometric titrations, preliminary wavelength searching experiments and kinetic measurements for slow reactions. Kinetic measurements of fast reactions were monitored using an Applied Photophysics (v4.33) SX.18 MV stopped-flow spectrophotometer coupled to an online data acquisition system. The temperature of the instrument was controlled to within  $\pm 0.1$  °C for all measurements. The  $pK_a$  measurements were determined on a

Jenway 4330 pH meter equipped with a 4.5  $\mu\text{m}$  glass electrode. The microelectrode was calibrated at 25  $^{\circ}\text{C}$  using the standard buffer solutions (Merck) at pH 4.0, 7.0 and 10.0.  $\text{p}K_a$  titration curve and time-dependent kinetic traces were graphically analysed using Origin 7.5<sup>®</sup> software package.<sup>25</sup>

### 5.2.6 Kinetic measurements

Prior to the kinetic measurements, preliminary experiments recording the spectral changes resulting from mixing the complex with the nucleophile were made to establish the appropriate wavelength at which the kinetics could be studied. A typical trial scan and suitable wavelengths chosen for studying the kinetic reactions are shown in **Figure SI 5.2** and **Table SI 5.1** (supporting information). All substitution kinetics reactions were performed under *pseudo* first-order conditions, as a function of nucleophile concentration and temperature, at constant temperature (298.1 K) and concentration respectively. The *pseudo* first-order conditions were achieved by providing the nucleophile concentration in at least 20-fold excess over that of a bifunctional Pt(II) complex. This afforded at least 10-fold excess of the nucleophile concentration for each of the two coordinated leaving group (after mixing), which is sufficient to force the reaction to go to completion. A pH of 2.0 was maintained throughout the kinetic runs to guarantee the presence of only diaqua complexes. Slow reactions were initiated by manually mixing equal volumes of the complex and the nucleophile solutions in a Suprasil tandem cuvette. For fast reactions, equal amounts of pre-equilibrated complex and nucleophile solutions were mixed through a pressure-driven cross-plunging technique in the chamber of the stopped-flow analyser.

### 5.2.7 Computational details

In order to gain an in depth understanding of structural and electronic differences that exist between the bifunctional Pt(II) complexes studied, computational calculations were performed. The ground state electronic structures of **Pt(H<sub>2</sub>Qn)**, **Pt(dCH<sub>3</sub>Qn)**, **Pt(dCF<sub>3</sub>Qn)** and **Pt(dCF<sub>3</sub>Py)** were optimized by Density Functional Theoretical (DFT) calculations using B3LYP/LanL2DZ level of theory.<sup>26</sup> This method is suitable for calculations of systems containing heavy atoms as in this

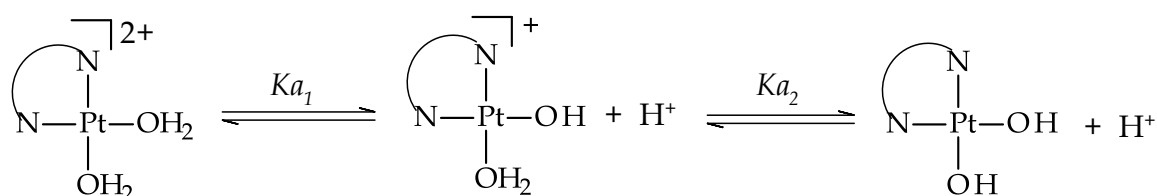
study (Pt atom).<sup>27</sup> The complexes were modelled as +2 gaseous ions. The singlet state was used due to the low electronic spin of Pt(II) complexes. Gaussian09 suite of programs was used for all computational analysis modelling and Gaussview5.0 was used to generate the frontier molecular orbitals of the modelled complexes at the same level of theory.<sup>28</sup>

## 5.3 Results

### 5.3.1 Acidity of diaqua Pt(II) complexes

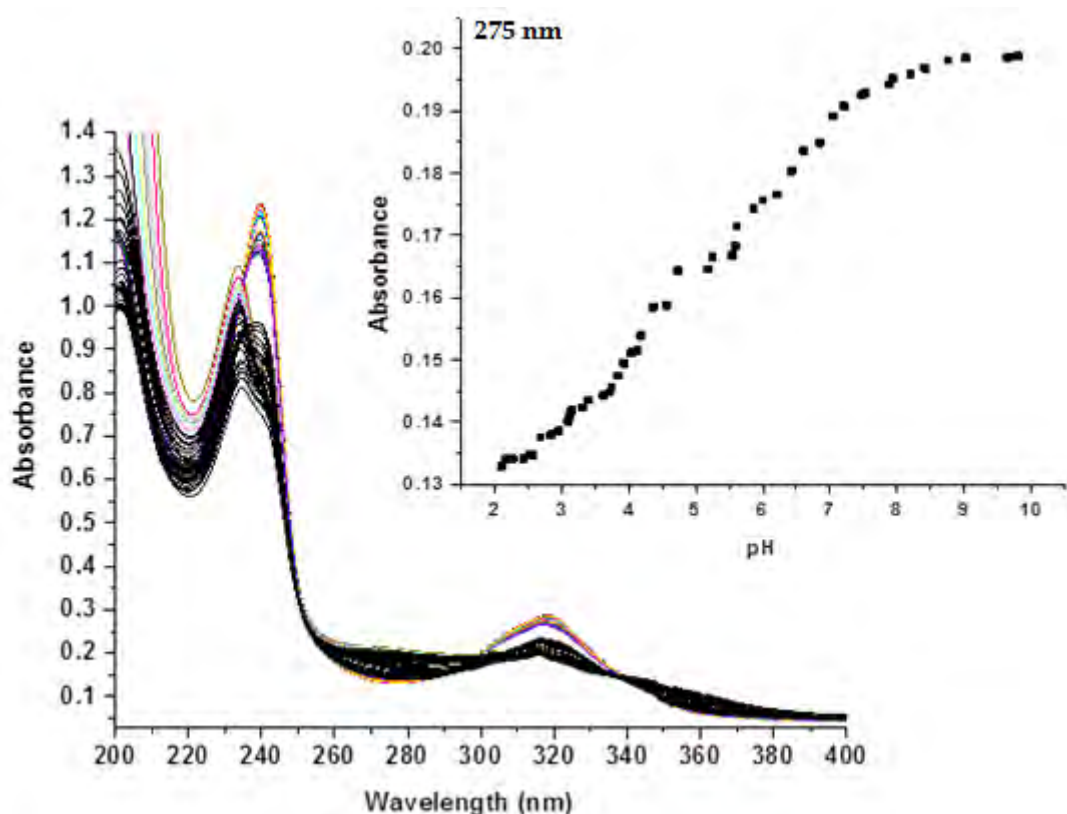
Spectrophotometric titrations of bifunctional Pt(II) complexes with NaOH show that the deprotonation of the two coordinated aqua ligands occurred in two successive steps. Therefore, the deprotonation steps for pH dependence can be represented by

**Scheme 5.1.**



**Scheme 5.1:** Proposed stepwise deprotonation for the pH dependence of mononuclear bifunctional Pt(II) system of complexes with different donors.

Typical UV/visible spectra obtained during the pH titration of **Pt(dCF<sub>3</sub>Qn)** with NaOH is shown in **Figure 5.2**.



**Figure 5.2:** UV/Visible spectra for the titration of 0.05 mM **Pt(dCF<sub>3</sub>Qn)** with NaOH in the pH range 2-9 at  $T = 298.15$  K. Inset: Absorbance *vs.* pH at 275 nm for **Pt(dCF<sub>3</sub>Qn)** complex.

The change in absorbance as a function of pH was fitted to two separate sigmoidal functions (Boltzmann) using Origin 7.5<sup>®</sup> software,<sup>25</sup> resulting in two  $pK_a$  values which are summarised in **Table 5.1**.

**Table 5.1.** Summary of  $pK_a$  values for the deprotonation of Pt-bound aqua ligands in bifunctional Pt(II) complexes studied.

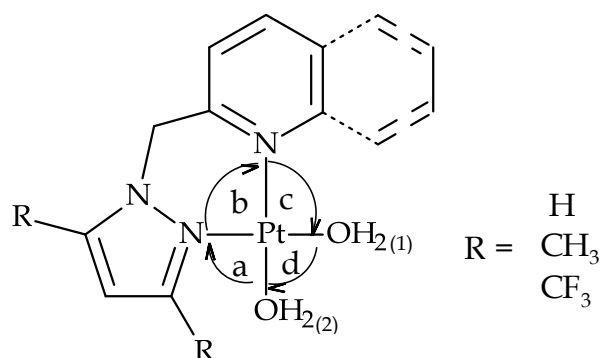
	<b>Pt(H<sub>2</sub>Qn)</b>	<b>Pt(dCH<sub>3</sub>Qn)</b>	<b>Pt(dCF<sub>3</sub>Qn)</b>	<b>Pt(dCF<sub>3</sub>Py)</b>
<b><math>pK_{a1}</math></b>	$4.56 \pm 0.02$	$4.88 \pm 0.10$	$4.07 \pm 0.08$	$4.76 \pm 0.05$
<b><math>pK_{a2}</math></b>	$6.32 \pm 0.05$	$6.31 \pm 0.05$	$6.35 \pm 0.07$	$6.27 \pm 0.02$

### 5.3.2 DFT-calculated optimised structures

Substituents of different electronic nature at the 3,5-positions of the pyrazole ring and the extended  $\pi$ -conjugation of a quinoline ligand are the two important structural parameters affecting the substitution chemistry of the Pt(II) complexes studied. Computational calculations were performed to simulate the structural and

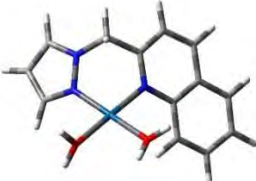
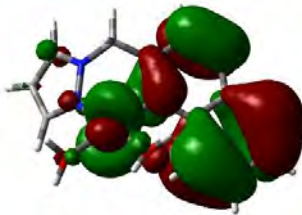
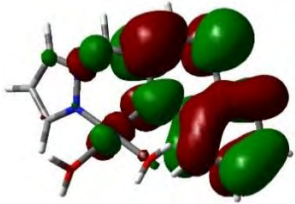
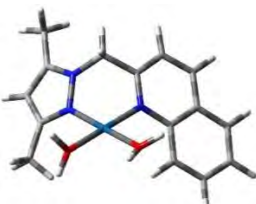
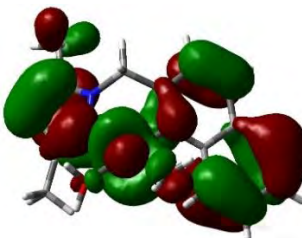
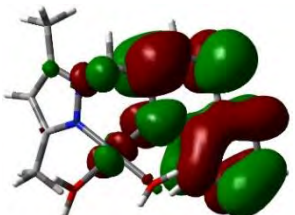

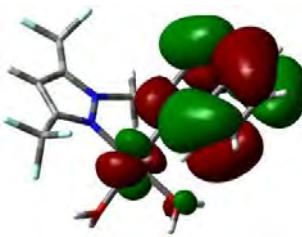
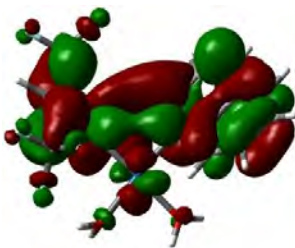
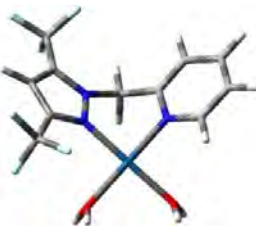
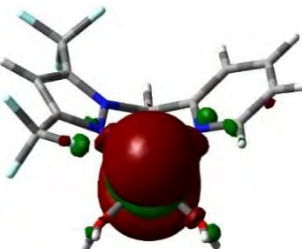
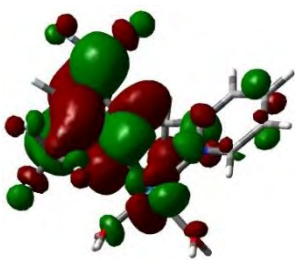
electronic properties of the bifunctional Pt(II) complexes in the ground state. A summary of the geometry-optimised data is presented in **Table 5.2** and **Figure 5.3**. Bond angles around each Pt(II) centre reflect a slightly distorted square-planar geometry (**Table 5.2**). Looking at the calculated NBO charges in **Table 5.2**, the effective charges on the Pt(II) centre increase in the order of **Pt(dCH<sub>3</sub>Qn)** (0.840) < **Pt(H<sub>2</sub>Qn)** (0.876) < **Pt(dCF<sub>3</sub>Qn)** (0.909) < **Pt(dCF<sub>3</sub>Py)** (0.991). Thus, the charges on the complexes are significantly affected not only by the electronic nature of the substituents in the 3,5-positions of the pyrazole ring but also by the replacement of the pyridine ring (a known strong  $\pi$ -acceptor moiety) with a quinoline ring in the *N,N*-bidentate ligand. The electron-donating methyl groups of **Pt(dCH<sub>3</sub>Qn)** decrease the charge on the Pt(II) ion relative to that of **Pt(H<sub>2</sub>Qn)**, while the electron-withdrawing trifluoromethyl substituents of **Pt(dCF<sub>3</sub>Qn)** increase the charge on Pt(II) ion. Despite the quinoline having delocalised  $\pi$ -molecular orbitals when compared to pyridine, this substructure decreases the charge on the Pt(II) metal centre when a comparison is made between the charges of **Pt(dCF<sub>3</sub>Qn)** and **Pt(dCF<sub>3</sub>Py)**.

**Table 5.2.** DFT-calculated data for bifunctional Pt(II) complexes.



Property	Pt(H <sub>2</sub> Qn)	Pt(dCH <sub>3</sub> Qn)	Pt(dCF <sub>3</sub> Qn)	Pt(dCF <sub>3</sub> Py)
<b>MO Energy (eV)</b>				
LUMO	-2.93	-2.91	-3.22	-3.06
HOMO	-7.21	-7.16	-7.34	-7.61
$\Delta E_{L-H}$	4.28	4.25	4.12	4.55
<b>NBO charges</b>				
Pt	0.876	0.840	0.909	0.991
<sup>1</sup> N <sub>qn/py</sub>	-0.406	-0.407	-0.410	-0.400
<sup>1</sup> N <sub>pz</sub>	-0.288	-0.373	-0.320	-0.337
<b>Bond lengths (Å)</b>				
<i>d</i> Pt–N <sub>py</sub>	2.034	2.032	2.033	2.018
<i>d</i> Pt–N <sub>pz</sub>	1.991	1.996	2.004	2.010
<i>d</i> Pt–OH <sub>2</sub> (1)	2.099	2.100	2.077	2.094
<i>d</i> Pt–OH <sub>2</sub> (2)	2.102	2.112	2.108	2.078
<b>Bond angles (°)</b>				
< N <sub>pz</sub> –Pt–OH <sub>2</sub> (1)	176.3	176.9	177.3	177.8
< N <sub>qn/py</sub> –Pt–OH <sub>2</sub> (2)	177.9	176.4	175.5	179.9
< <i>a</i>	94.5	86.8	97.0	91.1
< <i>b</i>	87.2	94.9	85.9	88.8
< <i>c</i>	94.7	82.0	94.0	90.2
< <i>d</i>	83.5	89.1	82.9	89.9

<sup>1</sup> N<sub>qn/py</sub> is the coordinated N-donor atom in the quinoline or pyridine head and N<sub>pz</sub> is the coordinated N-donor atom in the pyrazole ring

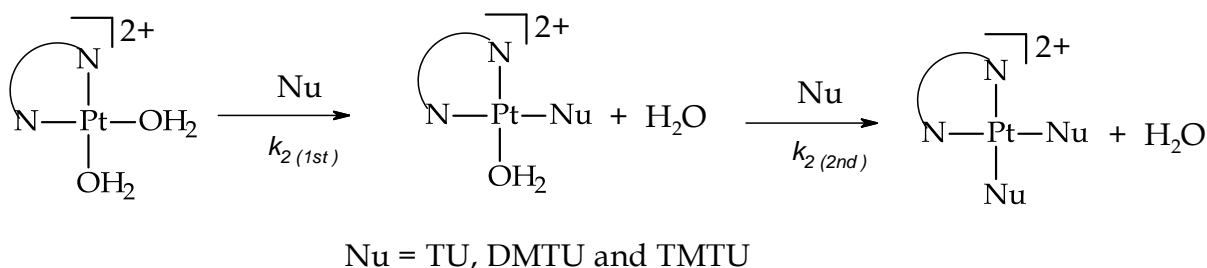
Complex	Structure	HOMO Map	LUMO Map
Pt(H <sub>2</sub> Qn)			
Pt(dCH <sub>3</sub> Qn)			
Pt(dCF <sub>3</sub> Qn)			
Pt(dCF <sub>3</sub> Py)			

**Figure 5.3:** DFT-calculated HOMO and LUMO frontier molecular orbitals of Pt(II) complexes.



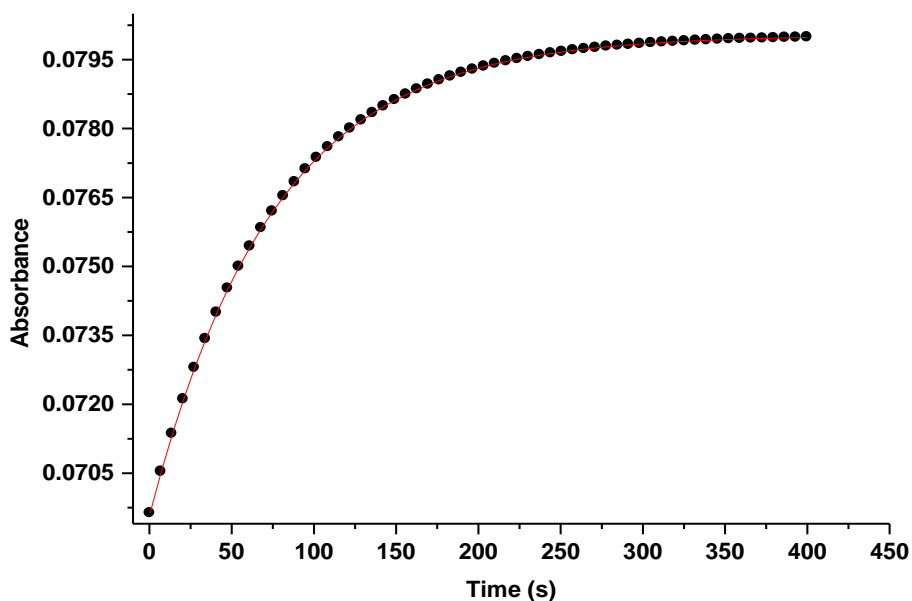
### 5.3.3 Kinetics of the substitution reactions with thiourea nucleophiles

Substitution of the labile aqua ligands from each of the bifunctional Pt(II) complexes (**Figure 5.1**) by thiourea nucleophiles i.e. TU, DMTU, and TMTU, occurred in two consecutive steps characterised by  $k_2$  (1st) and  $k_2$  (2nd) as shown in **Scheme 5.2**. Each step corresponds to the nucleophilic substitution of the coordinated aqua leaving groups, respectively.



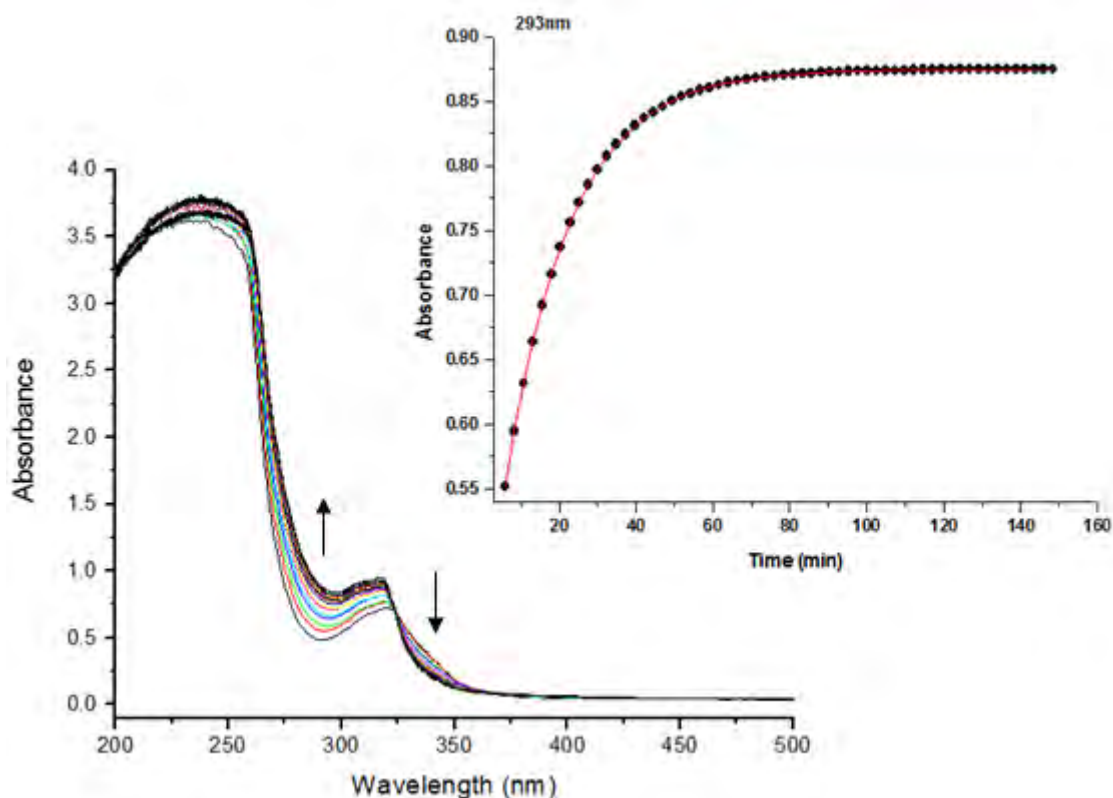
**Scheme 5.2:** The proposed stepwise substitution of diaqua ligand from bifunctional Pt(II) complexes by thiourea nucleophiles.

The substitution of the first aqua ligand was monitored by the stopped-flow technique while the slower and second substitution step was followed by the UV/visible spectrophotometry. The reduced reactivity of the Pt(II) metal centre in the second substitution step is ascribed to an increased steric hindrance around the metal centre upon the coordination of the first thiourea nucleophile as well as a decreased electrophilicity of the Pt(II) metal centre due to  $\sigma$ -donor capacity of the thioureas. These two factors retard the aerial approach of the nucleophile towards the Pt(II) centre, thereby decreasing the rate of substitution. An exemplary time-dependent kinetic trace for the first substitution step for the reaction of **Pt(dCH<sub>3</sub>Qn)** and 40-fold TU is shown in **Figure 5.4**.



**Figure 5.4:** A typical kinetic trace for the first substitution step in a two-step reaction between **Pt(dCH<sub>3</sub>Qn)** (0.15 mM) and TU (6.0 mM) recorded at 290 nm,  $T = 298$  K, pH = 2.0,  $I = 0.1$  M (HClO<sub>4</sub>/NaClO<sub>4</sub>) on the stopped-flow spectrophotometer.

The UV/visible spectral changes in absorbance resulting from the reaction of **Pt(H<sub>2</sub>Qn)** and 20-fold TU in the second substitution are shown in **Figure 5.5**. The appearance of an isosbestic point (325 nm) in the UV-visible spectra clearly indicates the conversion of reactants to products i.e. the conversion of **[Pt(H<sub>2</sub>Qn)(H<sub>2</sub>O)TU]<sup>2+</sup>** to **[Pt(H<sub>2</sub>Qn)(TU)<sub>2</sub>]<sup>2+</sup>** or indicates the presence of these two species in solution during the substitution reaction.<sup>29</sup> The time-dependent kinetic trace obtained for this reaction is shown as an insert in **Figure 5.5**.



**Figure 5.5:** UV/visible spectra recorded during a two-step reaction of 0.22 mM **Pt(H<sub>2</sub>Quin)** and 4.4 mM TU recorded at pH = 2,  $T = 298$  K and  $I = 0.1$  M (HClO<sub>4</sub>/NaClO<sub>4</sub>). Inset: Kinetic trace at 293 nm.

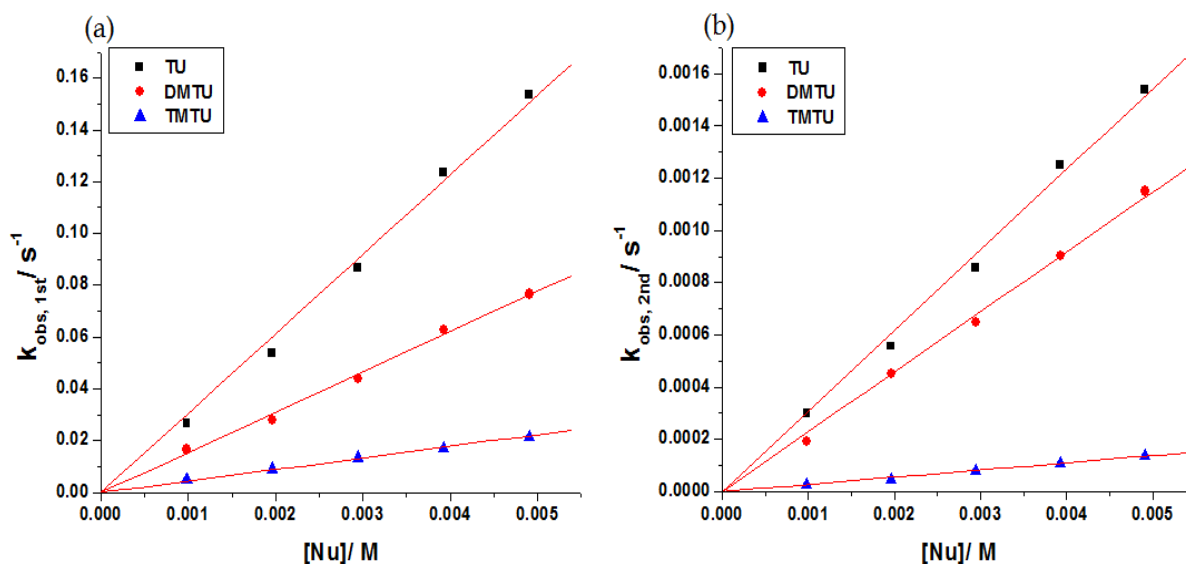
In both substitution steps, the kinetic traces fitted perfectly to a first-order exponential function to generate the observed *pseudo*-first-order rate constants,  $k_{obs(1/2)}$ , according to equation (5.1):<sup>30</sup>

$$A_t = A_o + (A_o - A_\infty)\exp[-k_{obs(1/2)}t] \quad (5.1)$$

where  $A_o$ ,  $A_t$  and  $A_\infty$  represent the absorbance of the reaction mixture at the onset of the reaction, at time ( $t$ ) and at the end of the reaction, respectively. The observed *pseudo*-first rate constants,  $k_{obs(1/2)}$ , at different nucleophile concentrations and temperatures were determined in the same manner. The second-order rate constants,  $k_{2(1st/2nd)}$ , for the first and second substitution steps were obtained from the slopes of the linear regression plots of  $k_{obs(1/2)}$  against the concentration of the entering nucleophile, according to the rate laws described in equation (5.2):<sup>31</sup>

$$k_{obs(1/2)} = k_{2(1st/2nd)} [Nu] + k_{-1(1st/2nd)} \cong k_{2(1st/2nd)} [Nu] \quad (5.2)$$

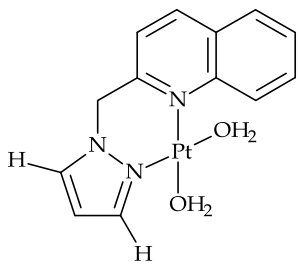
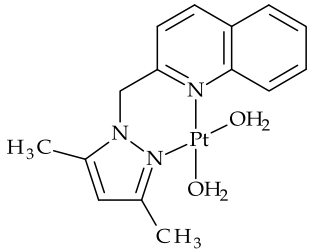
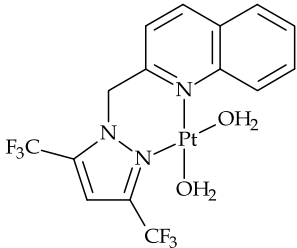
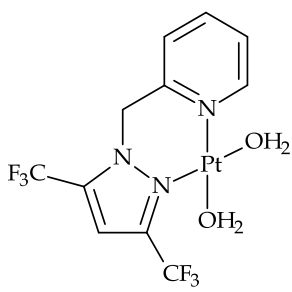
where Nu = TU, DMTU and TMTU. Representative plots displaying a linear dependence of  $k_{obs(1/2)}$  on the concentration of the entering nucleophiles are shown in **Figure 5.6** (also see **Figures SI 5.4**).



**Figure 5.6.** Pseudo-first-order rate constants,  $k_{obs(1/2)}$ , plotted as a function of nucleophile concentration for the substitution of the first (a) and second (b) labile aqua ligand from  $Pt(dCF_3Qn)$  at pH = 2.0,  $T = 298$  K and  $I = 0.1$  M ( $HClO_4/NaClO_4$ ).

No observable intercepts were recorded for all linear regression plots, suggesting the absence of the solvolytic pathway or insignificance of the reverse reaction. Thus, the first-order rate constant,  $k_{-1(1st/2nd)}$ , is too small to be measured accurately. The values of the second-order rate constants for the reactions of the complexes are summarised in **Table 5.3**.

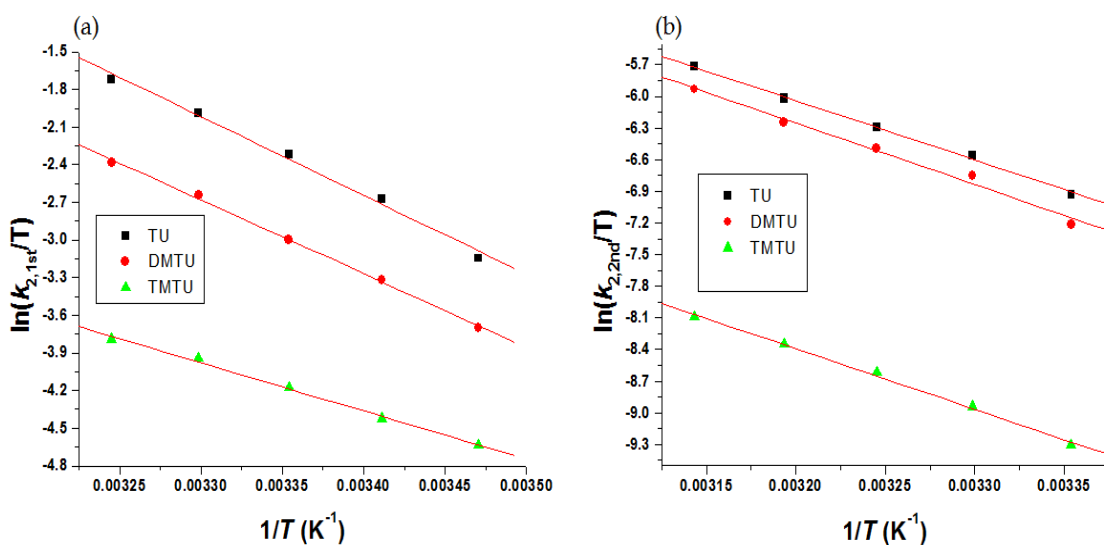
**Table 5.3.** Summary of the second-order rate constants for the stepwise substitution of labile aqua ligands by thiourea nucleophiles in diaqua Pt(II) complexes.

Complex	Nu	$k_2$ (1st) ( $\text{M}^{-1}\text{s}^{-1}$ )	$k_2$ (2nd) ( $10^{-1}\text{M}^{-1}\text{s}^{-1}$ )
<b>Pt(H<sub>2</sub>Qn)</b> 	TU	$100 \pm 1$	$4.74 \pm 0.02$
	DMTU	$72.6 \pm 0.7$	$4.72 \pm 0.05$
	TMTU	$20.2 \pm 0.2$	$0.266 \pm 0.01$
<b>Pt(dCH<sub>3</sub>Qn)</b> 	TU	$5.08 \pm 0.05$	$0.268 \pm 0.006$
	DMTU	$4.72 \pm 0.08$	$0.140 \pm 0.002$
	TMTU	$0.803 \pm 0.02$	$0.064 \pm 0.003$
<b>Pt(dCF<sub>3</sub>Qn)</b> 	TU	$30.7 \pm 0.6$	$0.309 \pm 0.006$
	DMTU	$15.5 \pm 0.3$	$0.230 \pm 0.003$
	TMTU	$4.46 \pm 0.06$	$0.028 \pm 0.001$
<b>Pt(dCF<sub>3</sub>Py)</b> 	TU	$147 \pm 1$	$2.520 \pm 0.05$
	DMTU	$87.9 \pm 2$	$1.510 \pm 0.02$
	TMTU	$18.8 \pm 0.1$	$0.259 \pm 0.003$

The temperature dependence of the second-order rate constants,  $k_{2(1st/2nd)}$ , was studied at a fixed nucleophile concentration, to determine the activation parameters of each substitution step. The enthalpy ( $\Delta H_{1/2}^\ddagger$ ) and entropy ( $\Delta S_{1/2}^\ddagger$ ) of activation were calculated using the Eyring equation:<sup>32</sup>

$$\ln[k_{2(1st/2nd)} / T] = -(\Delta H_{1/2}^\ddagger / R) \cdot 1/T + [23.8 + (\Delta S_{1/2}^\ddagger / R)] \quad (5.3)$$

where  $R$  and  $T$  represent the ideal gas constant and temperature, respectively. Typical Eyring plots are shown in **Figure 5.7** (also see **Figure SI 5.5**).



**Figure 5.7:** Plots of  $\ln(k_2/T)$  versus  $(1/T)$  for the substitution of the first (a) and second (b) aqua ligand from **Pt(dCF<sub>3</sub>Qn)** by thiourea nucleophiles at varying temperatures.

A summary of the activation parameters for the first ( $\Delta H_1^\ddagger$  and  $\Delta S_1^\ddagger$ ) and second ( $\Delta H_2^\ddagger$  and  $\Delta S_2^\ddagger$ ) substitution steps is presented in **Table 5.4**.

**Table 5.4.** Summary of the activation parameters for the stepwise substitution of labile aqua ligands by thioures from the diaqua Pt(II) complexes

Complex	Nu	$\Delta H_1^\ddagger$ (kJ mol <sup>-1</sup> )	$\Delta H_2^\ddagger$ (kJ mol <sup>-1</sup> )	$\Delta S_1^\ddagger$ (J mol <sup>-1</sup> K <sup>-1</sup> )	$\Delta S_2^\ddagger$ (J mol <sup>-1</sup> K <sup>-1</sup> )
<b>Pt(H<sub>2</sub>Qn)</b>	TU	42 ± 1	51 ± 4	- 66 ± 3	- 82 ± 2
	DMTU	41 ± 1	50 ± 2	- 72 ± 5	- 84 ± 7
	TMTU	42 ± 2	59 ± 3	-78 ± 8	- 79 ± 1
<b>Pt(dCH<sub>3</sub>Qn)</b>	TU	38 ± 1	51 ± 2	- 103 ± 5	- 131 ± 9
	DMTU	47 ± 2	54 ± 2	- 74 ± 1	- 97 ± 9
	TMTU	40 ± 1	57 ± 1	-111 ± 4	- 97 ± 1
<b>Pt(dCF<sub>3</sub>Qn)</b>	TU	52 ± 3	47 ± 1	- 42 ± 1	- 99 ± 5
	DMTU	49 ± 1	49 ± 3	- 59 ± 5	- 95 ± 1
	TMTU	32 ± 1	48 ± 4	-125 ± 4	- 115 ± 6
<b>Pt(dCF<sub>3</sub>Py)</b>	TU	41 ± 2	46 ± 2	- 67 ± 3	- 101 ± 7
	DMTU	45 ± 2	48 ± 2	- 58 ± 6	- 101 ± 7
	TMTU	36 ± 2	58 ± 3	- 101 ± 7	- 121 ± 1

## 5.4 Discussion

### 5.4.1 Acid-base equilibrium of diaqua Pt(II) complexes

By comparing the  $pK_a$  values in Table 5.1, an increasing order in the  $pK_{a1}$  values of: **Pt(dCH<sub>3</sub>Qn)** (4.88) < **Pt(H<sub>2</sub>Qn)** (4.56) < **Pt(dCF<sub>3</sub>Qn)** (4.07) is established for quinoline-bearing Pt(II) complexes. It is well-known that the  $pK_a$  values of the coordinated aqua ligands serve as an indicator of the electrophilicity of the metal centre.<sup>10,32,33</sup> The results clearly show a correlation between the  $pK_a$  values and the electrophilicity of the Pt(II) centre as already pointed in Section 5.3.2. The introduction of the electron-withdrawing trifluoromethyl (–CF<sub>3</sub>) substituents on the pyrazole ring decrease the electron density on the metal centre (*vide infra*). Consequently, the  $pK_{a1}$  value of **Pt(dCF<sub>3</sub>Qn)** is lower than that recorded for **Pt(H<sub>2</sub>Qn)**. As expected, **Pt(dCH<sub>3</sub>Qn)** a complex with electron donating substituents on the pyrazole ring records a higher  $pK_{a1}$  value due to  $\sigma$ -inductive donation of electron density towards the Pt centre.

The  $pK_{a2}$  values for the second deprotonation of the aqua ligand from aqua/hydroxo to dihydroxo species occurred at a higher pH than  $pK_{a1}$ . This is ascribed to a decrease in the overall charge of the Pt(II) complexes from +2 to +1 following the

deprotonation of the first aqua ligand to form aqua/hydroxo species. This decreases the electrophilicity and the acidity of the Pt(II) complex, leading to higher  $pK_a$  values.<sup>34,35</sup>

#### 5.4.2 DFT calculated optimised structures

In quinoline-bearing complexes, the HOMOs are located mainly on the quinoline ring and the metal centre, with an exception of **Pt(dCH<sub>3</sub>Qn)** which has an additional contribution from 3,5-dimethylpyrazole ring. This signifies that both quinoline and 3,5-dimethylpyrazole rings donate electron density on the metal centre thereby making it less electrophilic. However, in **Pt(dCF<sub>3</sub>Py)**, the HOMO is localised above and below the metal centre with no significant contribution from the pyridine and 3,5-bis(trifluoromethyl)pyridine rings. In all complexes, LUMOs are localised on the quinoline or pyridine rings with no significant contributions from either the 3,5-dimethylpyrazole or pyrazole rings. This is consistent with these rings, *viz.* pyridine or 3,5-bis(trifluoromethyl)pyridine being strong  $\pi$ -acceptor ligands. Importantly, the location of the HOMO and LUMO electron density maps on the quinoline ring indicates that this substructure of the *N,N*-bidentate has both  $\sigma$ -donor and  $\pi$ -acceptor properties, respectively. In addition, the ground state elongation of the Pt–OH<sub>2</sub> (2) bond length (**Table 5.2**) of the aqua leaving group *trans* to the quinoline ring, due to an increase in the electron density at the metal centre and along the *trans* axis, reflects an increase in the *trans*-influence as a result of its stronger  $\sigma$ -donor effect. The location of the LUMOs around the metal centre indicates that the  $\pi$ -acceptor ligands significantly reduce the electron density on the metal centre, rendering it more electrophilic. Furthermore, the location of the frontier molecular orbitals indicate that the  $\sigma$ -donor or  $\pi$ -acceptor strength of pyrazole can be controlled by introducing electron donating or withdrawing substituents on 3,5-positions of its ring.

#### 5.4.3 Kinetic studies

The substitution reactions were carried out at pH 2, where all the Pt(II) complexes predominantly existed in their diaqua forms and the protonation of the incoming thiourea nucleophiles can be neglected.<sup>7</sup> Two consecutive substitution steps were observed for all bifunctional Pt(II) complexes, indicating a difference in the *trans*-labilization effect of the coordinated rings of the flexible (pyrazolylmethyl)quinoline



bidendate ligand. The labilisation of two aqua ligands is distinct and therefore occurs at different rates. Similar to what was observed and described for the Pt(II) complexes of Chapter 4, the first observed reaction step is ascribed to the substitution of the aqua ligand *trans* to the quinoline ring, while the second corresponds to the substitution of the aqua ligand *trans* to pyrazole. This proposition is supported by the metrics of the Pt–OH<sub>2</sub> (2) bond *trans* to the quinoline ring bond which is marginally longer compared to the Pt–OH<sub>2</sub>(1) bond *trans* to pyrazole (see Table 5.2).

#### 5.4.3.1 First substitution step

A comparison of the  $k_{2(1st)}$  values shows a decreasing order in reactivity of **Pt(H<sub>2</sub>Qn)** > **Pt(dCF<sub>3</sub>Qn)** > **Pt(dCH<sub>3</sub>Qn)** for all the nucleophiles. When thiourea is the incoming nucleophile the rate of substitution decrease in the order: 100 M<sup>-1</sup> s<sup>-1</sup> **Pt(H<sub>2</sub>Qn)** > 30.7 M<sup>-1</sup> s<sup>-1</sup> **Pt(dCF<sub>3</sub>Qn)** > 5.08 M<sup>-1</sup> s<sup>-1</sup> **Pt(dCH<sub>3</sub>Qn)**. This trend indicates an interplay between steric and electronic effects, with the dominant factor controlling the rate. Since the substitution occurs first at the aqua ligands *cis* to the pyrazole ring carrying substituents of different electronic properties, the absence of steric influence at the 3,5-positions of pyrazole overrides the electronic effects of the ring leading to a fast rate of substitution in **Pt(H<sub>2</sub>Qn)** compared to its substituted analogues.

**Pt(dCF<sub>3</sub>Qn)** reacts about 6 times faster than **Pt(dCH<sub>3</sub>Qn)**. Considering the comparable spatial (steric) sizes of the –CF<sub>3</sub> and –CH<sub>3</sub> substituents, steric considerations alone cannot fully account for the observed large reactivity difference between the two complexes. Just as explained for their pyridine analogues (Chapter 4); a similar reason stands here to account for the observed differences in their reactivities. The electronic properties of the 3,5-substituents of pyrazole dominate the substitution of the aqua coordinated ligand from the complexes. The withdrawal of electron density from pyrazole by the –CF<sub>3</sub> groups reduces the  $\sigma$ -donation of the pyrazole ring towards the Pt centre leading to higher substitution rates. Alternatively, the withdrawal of electron density stabilises the  $\pi^*$ -molecular orbitals in the transition state switching 3,5-bis(trifluoromethyl)pyrazole into a good  $\pi$ -accepting ring for  $\pi$ -back-donation of electrons from the filled  $d\pi$ -orbitals of the

metal centre. This increases the electrophilicity of the metal centre, leading to an acceleration in the rate of substitution. Higher reactivity of **Pt(dCF<sub>3</sub>Qn)** compared to **Pt(dCH<sub>3</sub>Qn)** is also supported by relatively lower  $pK_{a1}$  value, smaller frontier orbitals energy gap and more positive NBO charge of the platinum atom.

The opposite is true for the 3,5-methyl groups of pyrazole in **Pt(dCH<sub>3</sub>Qn)** which strengthen electron donation at a *cis* position leading to a reduced rate of substitution. The 3,5-dimethylpyrazole ring donates the electron density inductively towards the metal centre leading to a decreased electrophilicity. This enhanced *cis*  $\sigma$ -donor effect destabilizes the electron-rich penta-coordinate transition state and repels the approach of an incoming nucleophile, leading to a retarded rate of substitution. Also important in slowing down the approach of the nucleophile to **Pt(dCH<sub>3</sub>Qn)**, is the steric effect due to a methyl (–CH<sub>3</sub>) group in the 3-position of the pyrazole ring. This steric effect and the electronic *cis*  $\sigma$ -donor effect of the two methyl groups are cooperative in retarding the rate of aqua ligand substitution. This explains why this complex has a significantly smaller second-order rate constant for the first substitution step ( $k_{2(1st)}$ ) compared to **Pt(dCF<sub>3</sub>Qn)**.

#### 5.4.3.2 Second substitution step

The second substitution step is significantly slower than the first one for all complexes. As already alluded (*vide supra*), this is due to a decrease in the electrophilicity of the metal centre upon the coordination of the first TU ligand which also confers steric hindrance to the second incoming nucleophile. For the substitution of the second aqua ligand (i.e. *trans* to the pyrazole ring), the same order of reactivity as reported for the first aqua leaving group: **Pt(H<sub>2</sub>Qn)** > **Pt(dCF<sub>3</sub>Qn)** > **Pt(dCH<sub>3</sub>Qn)** is observed. This order of reactivity is true for all the nucleophiles. Taking the reaction of **Pt(dCH<sub>3</sub>Qn)** and TU as a reference, the ratio of reactivity decreases in the ratio 18 : 1.2 : 1, respectively for **Pt(H<sub>2</sub>Qn)**: **Pt(dCF<sub>3</sub>Qn)**: **Pt(dCH<sub>3</sub>Qn)**. By making structural comparisons between the current complexes and those reported in Chapter 4, the lability of the aqua ligand *trans* to the pyrazole ring was expected to follow the order: **Pt(dCF<sub>3</sub>Qn)** > **Pt(H<sub>2</sub>Qn)** > **Pt(dCH<sub>3</sub>Qn)**. For this substitution step, the 3,5-susbtituents of pyrazole should impart a limited or no steric

effect since the aqua leaving ligand is at a *trans* position. The quinoline substructure being more steric-demanding than pyridine, the observed decrease in the rates of substitution of the second aqua ligand from both **Pt(dCF<sub>3</sub>Qn)** and **Pt(dCH<sub>3</sub>Qn)** relative to **Pt(H<sub>2</sub>Qn)** can possibly be due to an increase in the overall steric constraints at an already hindered Pt(II) centre in the transition states of the two substituted analogues. This destabilises the transition state leading to a decrease in their rates of substitution relative to **Pt(H<sub>2</sub>Qn)** as already stated. In this regard, the  $\pi$ -acceptor stabilising effect of the 3,5-bis(trifluoromethyl)pyrazole ring relative to 3,5-dimethylpyrazole ring leads to a slightly increased rate of substitution for the second aqua ligand in **Pt(dCF<sub>3</sub>Qn)** compared to **Pt(dCH<sub>3</sub>Qn)**. This is typical for substitution reactions proceeding *via* an associative mode of action that involves bond formation in the transition state. The increase in the reactivity of **Pt(dCF<sub>3</sub>Qn)** corroborates with the NBO charge on its platinum atom, HOMO-LUMO energy gap, and frontier molecular orbital diagrams which suggest an increase in the  $\pi$ -backbonding strength of the pyrazole ring upon the addition of -CF<sub>3</sub> substituents.

To pin down on the effect in the rate of substitution upon the replacement of a pyridine (which is known to be a strong  $\pi$ -acceptor ring) with a quinoline ring, the rate constants,  $k_2$  (1st/2nd), (Table 5.3) of **Pt(dCF<sub>3</sub>Py)** and **Pt(dCF<sub>3</sub>Qn)** were compared. In all cases, **Pt(dCF<sub>3</sub>Py)** reacts much faster than **Pt(dCF<sub>3</sub>Qn)**. The quinoline (benzopyridine) ring consists of a  $\sigma/\pi$ -donating phenyl ring fused to a  $\pi$ -accepting pyridine ring.<sup>7,36</sup> The coordinative character of the pyridyl ring of quinoline is therefore modulated by  $\sigma/\pi$ -donor of its phenyl ring. Its capacity to accept electrons from the  $d\pi$ -orbital of the metal to its  $\pi^*$ -molecular orbitals is weaker compared to pyridine which has lower and stabilised  $\pi^*$ -molecular orbitals. This leads to a less electrophilic Pt metal centre which repels the electron density of approaching nucleophiles. This reduces the rate of substitution.

The weaker  $\pi$ -accepting character of quinoline relative to pyridine is reflected by the relative magnitude of the NBO charges of the platinum atom which decreases from **Pt(dCF<sub>3</sub>Py)** (0.991) to **Pt(dCF<sub>3</sub>Qn)** (0.909). In addition, the LUMO energy in **Pt(dCF<sub>3</sub>Py)** (-7.61 eV) is significantly lower than the one for **Pt(dCF<sub>3</sub>Qn)** (-7.34 eV),

making quinoline a less  $\pi$ -acceptor than pyridine. The surprising and anomalous increase in the net  $\sigma$ -donor capacity of the quinoline as a substructure for a chelating polypyridyl nitrogen-donor ligand has been reported in the literature.<sup>6,7,37</sup> In all reported cases, the reduced electrophilicity of the metal centre is ascribed to the weakening of the  $\pi$ -acceptability of the coordinated pyridine ring of the benzopyridine (quinoline). This makes quinoline an apparent donor of electron density towards the metal centre rather than it being a  $\pi$ -acceptor if its extended molecular orbitals are taken into consideration.

#### 5.4.4 Activation parameters and reactivity of the nucleophiles

The data in **Table 5.3** show a clear dependence of second-order rate constants for the aqua substitutions on the steric hindrance of the incoming nucleophile. The rate of substitution decreases as the bulk size of the incoming nucleophiles increases. The sensitivity of the complexes on the structural size and hence steric effect of the incoming nucleophiles is characteristic of an associative mechanism. The small enthalpies of activation ( $\Delta H_{1/2}^\ddagger$ ) signify an ease in the formation of a bond in the transition state. The large and negative entropies of activation ( $\Delta S_{1/2}^\ddagger$ ) allude to a more ordered transition state. All these observations are in support of an associatively-activated mechanism of substitution, well documented for  $d^8$  square-planar Pt(II) complexes.<sup>10,13,21</sup>

#### 5.5 Conclusion

The 3,5-substituents on the pyrazole ring as well as the replacement of a pyridine with a quinoline ring in the *N,N*-bidentate chelate affects the electrophilicity of the Pt(II) centre, which in turn controls the lability of the coordinated aqua ligands. The complete order of reactivity for the first substitution was found to be **Pt(dCF<sub>3</sub>Py) > Pt(H<sub>2</sub>Qn) > Pt(dCF<sub>3</sub>Qn) > Pt(dCH<sub>3</sub>Qn)** and indicates an interplay between steric and electronic effects, with the dominant factor controlling the rate. Electron-withdrawing substituents on the pyrazole ring resulted in lower  $pK_a$  values while the opposite was true for electron-donating substituents. This study confirms that quinoline substructure in the (pyrazolylmethyl)quinoline ligands acts as an apparent

donor of electron density towards the metal centre rather than being a strong  $\pi$ -acceptor. This is contrary to what would be expected given its stabilized extended molecular orbitals, which should delocalise electrons better than those of pyridine. The mechanism of substitution remains associative throughout.

## 5.6 References

---

1. F. K. Keter, J. Darkwa, *Biometals*, 2012, **25**(9), 9.
2. (a) J. Reedijk, *Chem. Rev.*, 1999, **99**, 2499. (b) N. Fox, J. J. Roberts, *Cancer Metastasis Rev.*, 1987, **6**(3), 261.
3. C. Meljer, N. H. Mulder, H. Timmer-Bossch, W. J. Sluiter, G. J. Meersma, E. G. de Vries, *Cancer Res.*, 1992, **52**(24), 6885.
4. S. H. van Ritj, P.J. Sadler, *Drug Discovery Today*, 2009, **114**, 1089.
5. D. Reddy, D. Jaganyi, *Int. J. Chem. Kinet.*, 2011, **43**, 161.
6. P. O. Ongoma, D. Jaganyi, *Dalton Trans.*, 2013, **42**, 2724.
7. G. Kinunda, D. Jaganyi, *Transition Met. Chem.*, 2014, **39**, 939.
8. P. Sarmah and R. C. Deka, 2010, *J. Mol. Str.: THEOCHEM*, **955**, 53.
9. P. O. Ongoma, D. Jaganyi, *Int. J. Chem. Kinet.*, 2013, **45**, 676 (and references therein).
10. (a) A. Hofmann, D. Jaganyi, O. Q. Munro, G. Lier, R. van Eldik, *Inorg. Chem.*, 2003, **42**, 1688. (b) A. Hofmann, D. Jaganyi, O. Q. Munro, G. Lier, R. van Eldik, *Angrew. Chem. Int. Ed.*, 2001, **40**(2), 1680.
11. A. Hofmann, L. Dahlenburg, R. van Eldik, *Inorg. Chem.*, 2003, **42**, 6428.
12. P. D. Braddock, R. Romeo, M. L. Tobe, *J. Chem. Soc., Dalton Trans.*, 1993, 233.
13. M. L. Tobe, J. Burgess, *Inorganic Reaction Mechanisms*; Addison Wesley: London, 1999, p. 30- 39,73-94, 103-106 , 128.
14. M. Kotowski, R. van Eldik, *Inorganic High Pressure Chemistry*, Eds.; Elsevier Science Publisher: New York, 1986; Vol 7, p. 219.
15. R. Romeo, M. R. Plutino, L. Monsù Scolaro, S. Stoccoro, G. Minghetti, *Inorg. Chem.* 2000, **39**, 4749.
16. (a) D. Jaganyi, D. Reddy, J. Gertenbach, A. Hofmann, and R. van Eldik, *Dalton Trans.*, 2004, 299-304. (b) D. Jaganyi and D. Reddy, *Dalton Trans.*, 2008, 6724-6731.
17. P. Ongoma and D. Jaganyi, *Dalton Trans.*, 2012, **41**, 10724.
18. D. Jaganyi, K.-L. De Boer, J. Gertenbach, J. Perils, *Int. J. Chem. Kinet.*, 2008, 808.

19. A. Shaira, D. Reddy and D. Jaganyi, *Dalton Trans.*, 2013, **42**, 8426.
20. G. Kinunda and D. Jaganyi, *Transition Met. Chem.*, 2014, **39**, 451.
21. (a) D. Jaganyi, D. Reddy, J. Gertenbach, A. Hofmann, and R. van Eldik, *Dalton Trans.*, 2004, 299. (b) D. Jaganyi and D. Reddy, *Dalton Trans.*, 2008, 6724.
22. A. Hofmann, D. Jaganyi, O. Q. Munro, G. Liehr, and R. van Eldik, *Inorg. Chem.*, 2003, **42**, 1688.
23. T. V. Segapelo, I. A. Guzei, L. C. spencer, W. E. Van Zyl, J. Darkwa, *Inorganica Chimica Acta*, 2009, **362**, 3314.
24. Ž. D. Bugarčić, B. V. Petrović, R. Jelić, *Transition Met. Chem.*, 2001, **26**, 668.
25. Origin 7.5™ SRO, v7.5714 (B5714), Origin Lab Corporation, Northampton, One, Northampton, MA, 01060, USA, 2003.
26. (a) P. J. Hay and W. R. Wadt, *Chem. Phys.*, 1985, **82**, 270. (b) A. D. Becke, *Chem Phys.*, 1985, **82**, 270.
27. T. Shoeib and B. L. Sharp, *Metallomics*, 2012, **4**, 1308.
28. Gaussian 09, Revision A. I, M. J. Frisch, G. W. Trucks, H. B. Schlegel, G. E. Scuseria, M. A. Robb, J. R. Cheeseman, G. Scalmani, V. Barone, B. Mennucci, G. A. Petersson, H. Nakatsuji, M. Caricato, X. Li, H. P. Hratchian, A. F. Izmaylov, J. Bloino, G. zheng, J. L. Sonnenberg, M. Ehara, K. Toyota, R. Fukuda, J. Hasegawa, M. Ishida, T. Nakajima, Y. Honda, O. Kitao, H. Nakai, T. Vreven, J. A. Montgomery, Jr., J. E. Peralta, F. Ogliaro, M. Bearpark, J. J. Heyd, E. Brothers, K. N. Kudin, V. N. Staroverov, R. Kobayashi, J. Normand, K. Raghavachari, A. Rendell, J. C. Burant, S. S. Iyengar, J. Tomasi, M. Cossi, N. Rega, J. M. Millam, M. Klene, J. E. Knox, J. B. Cross, V. Bakken, C. Adamo, J. Jaramillo, R. Gomperts, R. E. Stratmann, O. Yazyvev, A. J. Austin, R. Cammi, C. Pomelli, J. W. Ochterski, R. L. Martin, K. Morokuma, V. G. Zakrzewski, G. A. Voth, P. Salvador, J. J. Dannenberg, S. Dapprich, A. D. Daniels, O. Farkas, J. B. Foesman, J. V. Ortiz, J. Cioslowski and D. J. Fox, Gaussian, Inc., Wallingford CT, 2009.
29. M. Ray, S. Bhattacharya, P. Banerjee, *Polyhedron*, 1999, **18**, 1569.
30. J.D. Atwood. *Inorganic and Organic Reaction Mechanisms*, pp. 32–34, 43–61, Wiley-VCH Inc., New York (1997).

31. R. B. Jordan, *Reaction Mechanisms of Inorganic and Organometallic Systems*, Oxford University Press Inc., New York, 1991.
32. A. Hofmann, R. van Eldik, *Dalton Trans.*, 2003, 2979.
33. H. Ertürk, J. Maigut, R. Putcha, R. van Eldik, *Dalton Trans.*, 2007, 2295.
34. N. Summa, W. Schiessl, R. Putcha, N. van Eikema Hommes, R. van Eldik, *Inorg. Chem.*, 2006, **45**, 2948.
35. S. Hochreuther, S. T. Nandibewoor, R. Putcha, R. van Eldik, *Dalton Trans.*, 2012, **40**, 512.
36. I. M. Wekesa, D. Jaganyi, *Dalton Trans.*, 2014, **43**, 2549.
37. P. K. Chattaraj, B. Maiti, *J. Am. Chem. Soc.*, 2003, **125**, 2705.



## 5.7 Supporting Information

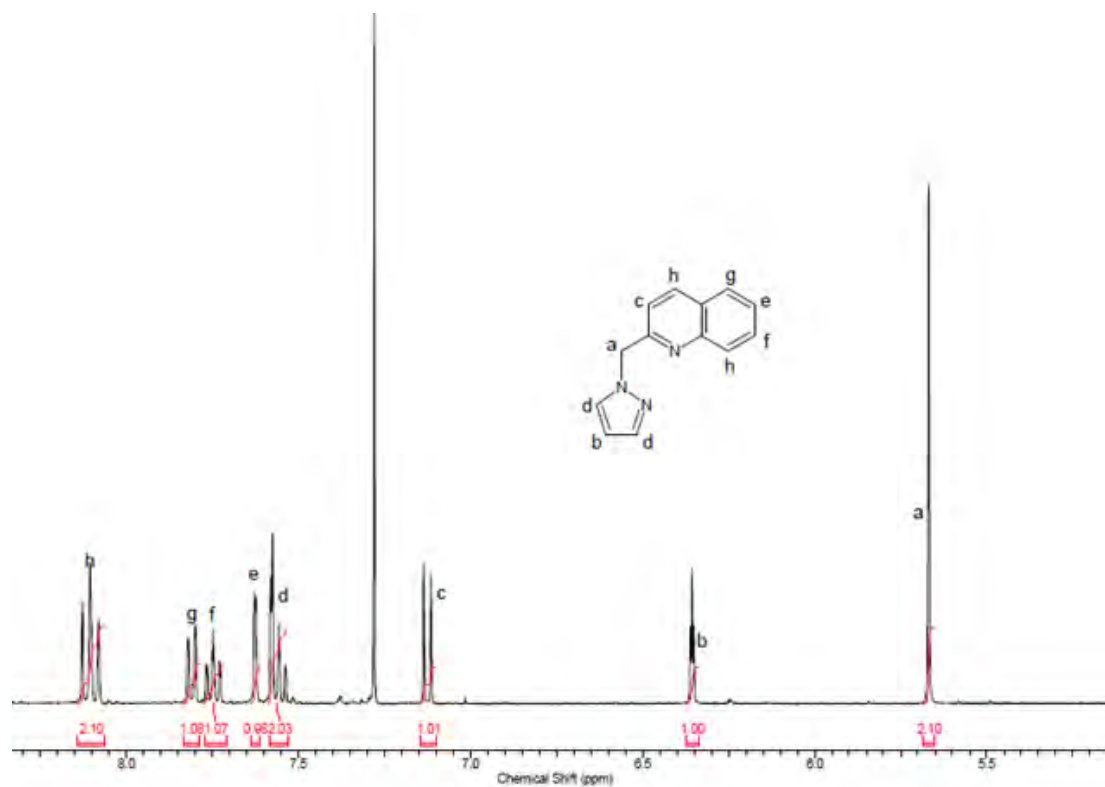
---

**Table SI 5.1a.** Summary of wavelength (nm) used for monitoring the first substitution reactions between a series of bifunctional Pt(II) complexes and thiourea nucleophiles.

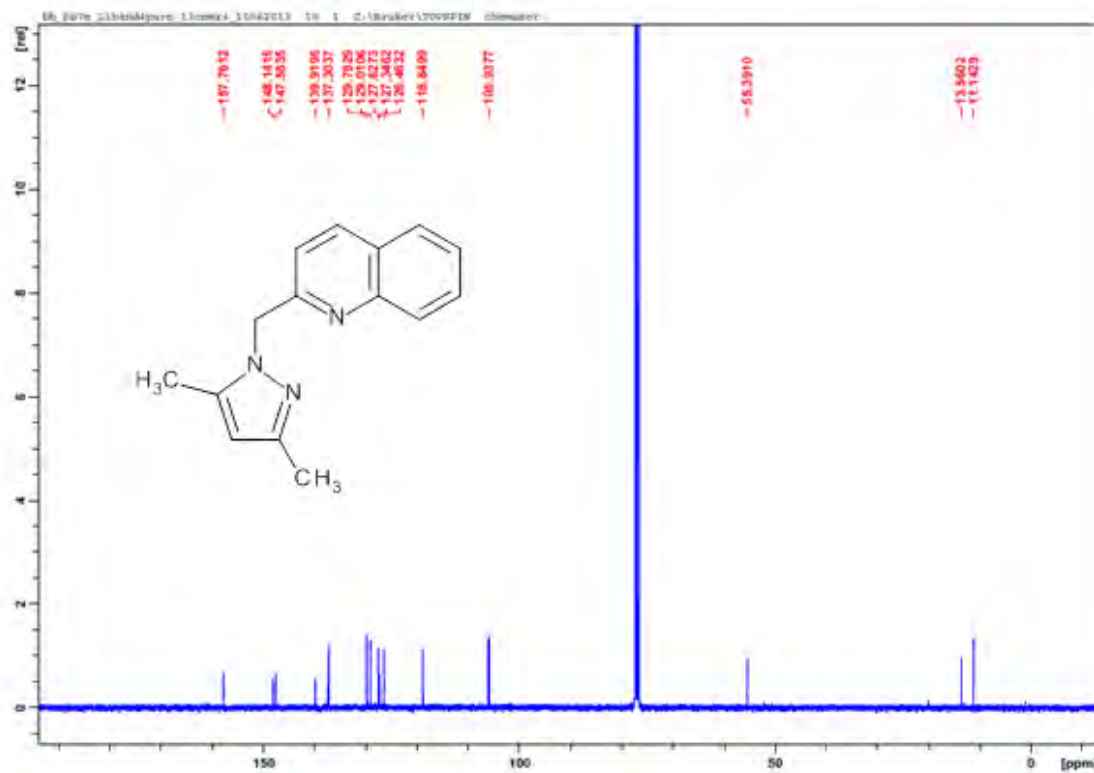
Complex	Nucleophile	Wavelength (nm)
Pt(H <sub>2</sub> Qn)	TU	284
	DMTU	286
	TMTU	340
Pt(dCH <sub>3</sub> Qn)	TU	298
	DMTU	290
	TMTU	300
Pt(dCF <sub>3</sub> Qn)	TU	295
	DMTU	295
	TMTU	300
Pt(dCH <sub>3</sub> Py)	TU	310
	DMTU	300
	TMTU	340

**Table SI 5.1b.** Summary of wavelength (nm) used for monitoring the second substitution reactions between a series of bifunctional Pt(II) complexes and thiourea nucleophiles

Complex	Nucleophile	Wavelength (nm)
Pt(H <sub>2</sub> Qn)	TU	293
	DMTU	290
	TMTU	385
Pt(dCH <sub>3</sub> Qn)	TU	290
	DMTU	285
	TMTU	385
Pt(dCF <sub>3</sub> Qn)	TU	270
	DMTU	275
	TMTU	310
Pt(dCF <sub>3</sub> Py)	TU	305
	DMTU	305
	TMTU	289



**Figure SI 5.1a:**  $^1\text{H}$  NMR spectrum of 2-(pyrazol-1-ylmethyl)quinoline (**H<sub>2</sub>Qn**) in  $\text{CDCl}_3$ .



**Figure SI 5.1b:**  $^{13}\text{C}$  NMR spectrum of 2-[3,5-bis(trifluoromethyl)pyrazol-1-ylmethyl]quinoline, **dCF<sub>3</sub>Qn** in  $\text{CDCl}_3$ .

## Single Mass Analysis

Tolerance = 50.0 PPM / DBE: min = -1.5, max = 50.0

Element prediction: Off

Number of isotope peaks used for i-FIT = 3

Monoisotopic Mass, Even Electron Ions

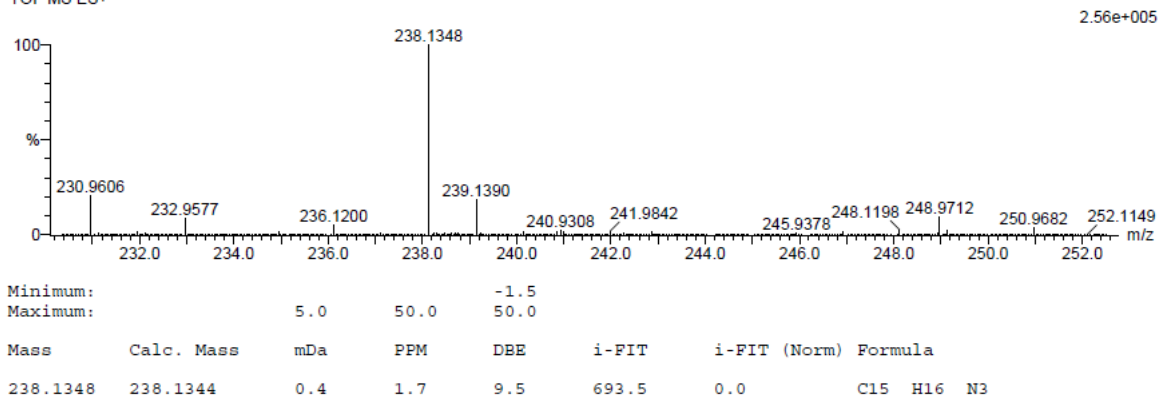
4 formula(e) evaluated with 1 results within limits (up to 50 best isotopic matches for each mass)

Elements Used:

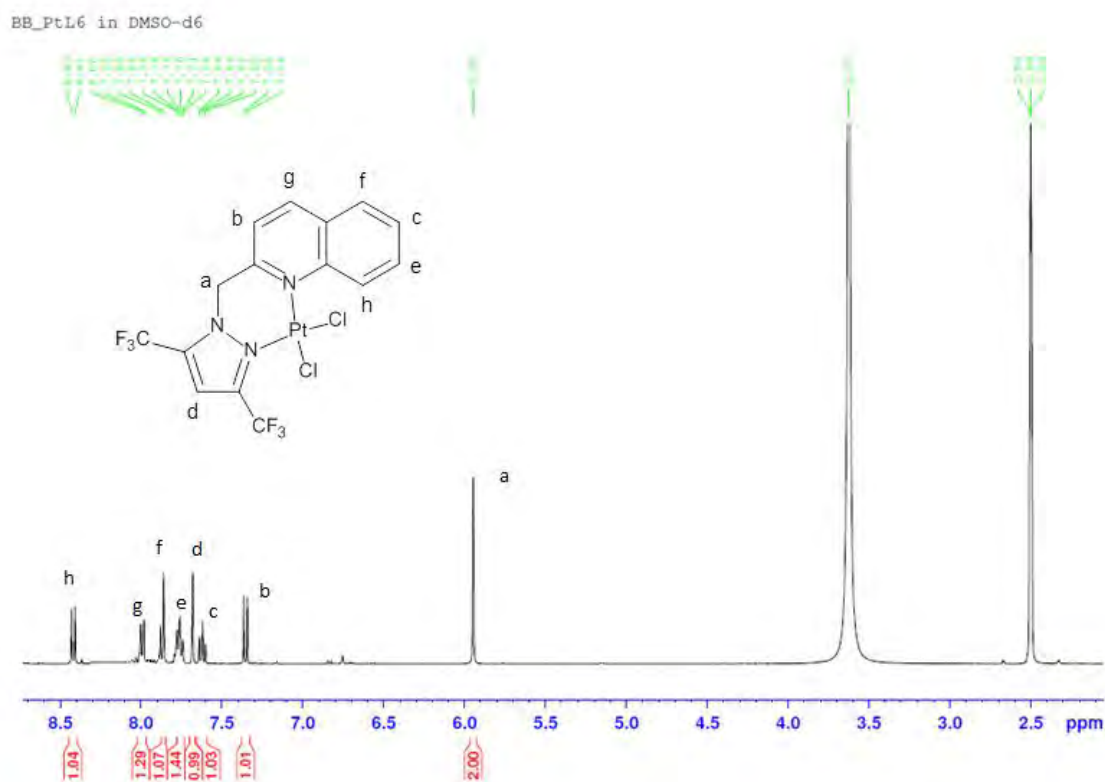
C: 10-15 H: 10-20 N: 0-5

Ligand 4 K 28 (0.459) Cm (1:30)

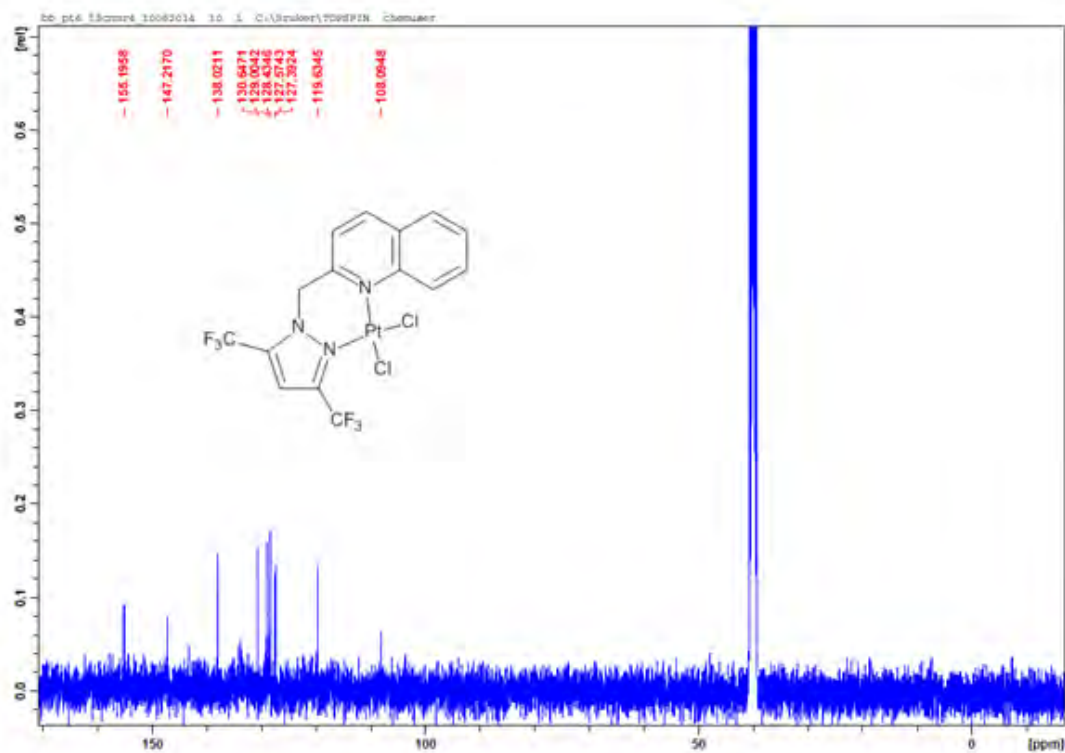
TOF MS ES+



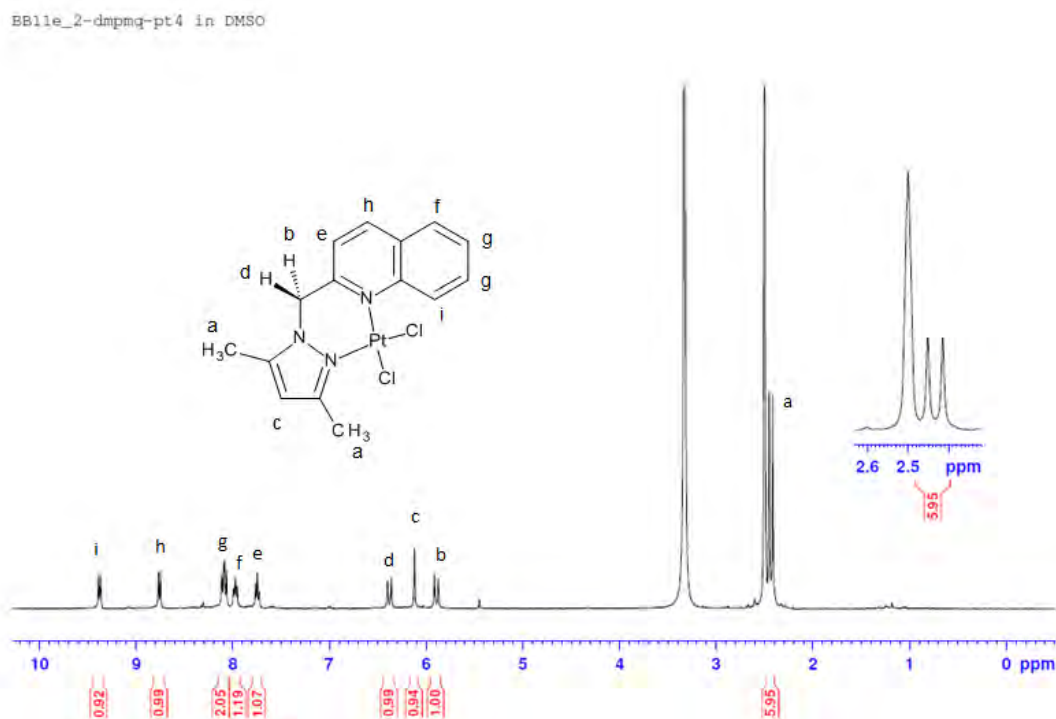
**Figure SI 5.1c:** Low resolution ESI<sup>+</sup> mass spectrum of 2-(pyrazol-1-ylmethyl)quinoline (H<sub>2</sub>Qn).



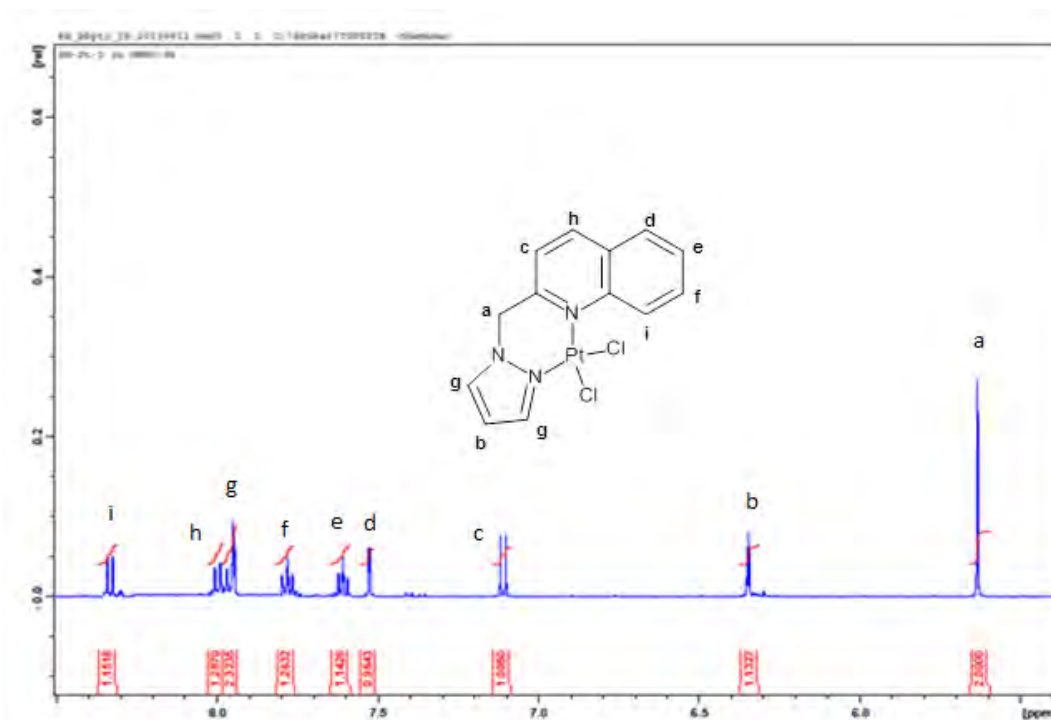
**Figure SI 5.1d:** <sup>1</sup>H NMR spectrum of [Pt{2-[(3,5-bis(trifluoromethyl)-pyrazol-1-ylmethyl]quinoline}Cl<sub>2</sub>], [Pt(dCF<sub>3</sub>Qn)Cl<sub>2</sub>] in DMSO-d<sub>6</sub>.



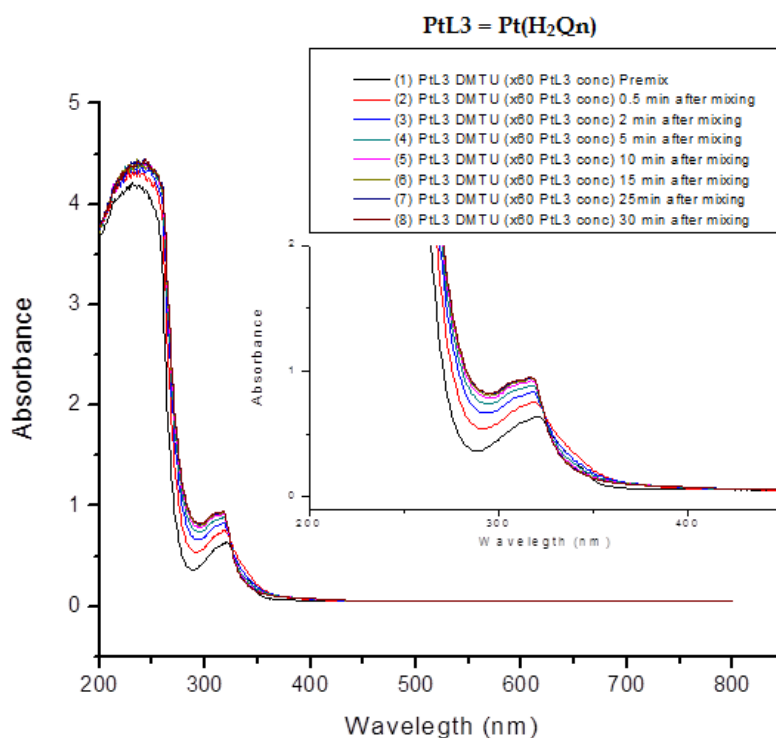
**Figure SI 5.1e:** <sup>13</sup>C NMR spectrum [Pt{2-[(3,5-bis(trifluoromethyl)pyrazol-1-yl)methyl]quinoline}Cl<sub>2</sub>], [Pt(dCF<sub>3</sub>Qn)Cl<sub>2</sub>] in DMSO-d<sub>6</sub>.



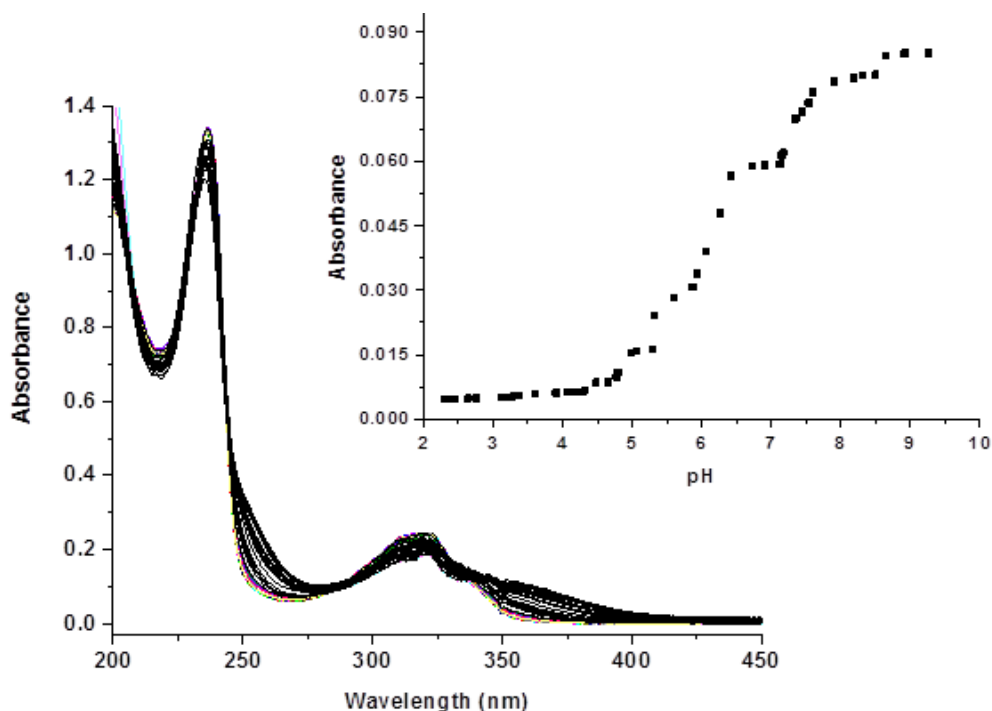
**Figure SI 5.1f:** <sup>1</sup>H NMR spectrum of [Pt{2-[(3,5-bis(trifluoromethyl)pyrazol-1-yl)methyl]quinoline}Cl<sub>2</sub>], [Pt(dCF<sub>3</sub>Qn)Cl<sub>2</sub>] in DMSO-d<sub>6</sub>.



**Figure SI 5.1g:**  $^1\text{H}$  NMR spectrum of  $[\text{Pt}\{(2\text{-pyrazoly-1-ylmethyl)quinoline}\}\text{Cl}_2]$ ,  $[\text{Pt}(\text{H}_2\text{Qn})\text{Cl}_2]$  in  $\text{DMSO-}d_6$ .



**Figure SI 5.2:** UV/visible scan for a trial run of the reaction between  $\text{Pt}(\text{H}_2\text{Qn})$  (written as PtL3) and 60-fold DMTU at different times.



**Figure SI 5.3:** UV/Visible spectra for the titration of 0.054 mM **Pt(dCH<sub>3</sub>Qn)** with NaOH in the pH range 2-10 at  $T = 298.15$  K. Insert: Absorbance versus pH plot at 295 nm for **Pt(dCF<sub>3</sub>Qn)** complex.

**Table SI 5.2a.** Average observed rate constants,  $k_{obs1}$ , for the displacement of the first aqua ligand in **Pt(H<sub>2</sub>Qn)** by thiourea nucleophiles, pH = 2.0,  $T = 298$  K,  $I = 0.1$  M (HClO<sub>4</sub>/NaClO<sub>4</sub>).

[TU]/ M	$k_{obs1}/ s^{-1}$	[DMTU]/ M	$k_{obs1}/ s^{-1}$	[TMTU]/ M	$k_{obs1}/ s^{-1}$
0.002186	0.23007	0.002186	0.1612133	0.002186	0.04969772
0.004372	0.39936	0.004372	0.3181796	0.004372	0.08848313
0.006558	0.64926	0.006558	0.4573171	0.006558	0.13115263
0.008744	0.86254	0.008744	0.6316229	0.008744	0.17503662
0.01093	1.12344	0.01093	0.8076081	0.01093	0.22193649

**Table SI 5.2b.** Average observed rate constants,  $k_{obs1}$ , for the displacement of the first aqua ligand in **Pt(dCH<sub>3</sub>Qn)** by thiourea nucleophiles, pH = 2.0,  $T = 298$  K,  $I = 0.1$  M (HClO<sub>4</sub>/NaClO<sub>4</sub>).

[TU]/ M	$k_{obs1}/ s^{-1}$	[DMTU]/ M	$k_{obs1}/ s^{-1}$	[TMTU]/ M	$k_{obs1}/ s^{-1}$
0.00149	0.0082105	0.00149	0.00586724	0.00149	0.002336462
0.00298	0.0155858	0.00298	0.01343998	0.00298	0.003320504
0.00447	0.0224411	0.00447	0.02044681	0.00447	0.004714193
0.00596	0.0297551	0.00596	0.02819208	0.00596	0.005895534
0.00745	0.0381513	0.00745	0.03596169	0.00745	0.007033142

**Table SI 5.2c.** Average observed rate constants,  $k_{obs1}$ , for the displacement of the first aqua ligand in **Pt(dCF<sub>3</sub>Qn)** by thiourea nucleophiles, pH = 2.0,  $T = 298$  K,  $I = 0.1$  M (HClO<sub>4</sub>/NaClO<sub>4</sub>).

[TU]/ M	$k_{obs1}/ s^{-1}$	[DMTU]/ M	$k_{obs1}/ s^{-1}$	[TMTU]/ M	$k_{obs1}/ s^{-1}$
0.0009816	0.026531867	0.0009816	0.016562318	0.0009816	0.005065183
0.0019632	0.053636887	0.0019632	0.027987854	0.0019632	0.009104683
0.0029448	0.086769674	0.0029448	0.043727462	0.0029448	0.013449955
0.0039264	0.123355366	0.0039264	0.062799493	0.0039264	0.017200094
0.004908	0.153634833	0.004908	0.076598717	0.004908	0.021662424

**Table SI 5.2d.** Average observed rate constants,  $k_{obs1}$ , for the displacement of the first aqua ligand in **Pt(dCF<sub>3</sub>Py)** by thiourea nucleophiles, pH = 2.0,  $T = 298$  K,  $I = 0.1$  M (HClO<sub>4</sub>/NaClO<sub>4</sub>).

[TU]/ M	$k_{obs1}/ s^{-1}$	[DMTU]/ M	$k_{obs1}/ s^{-1}$	[TMTU]/ M	$k_{obs1}/ s^{-1}$
0.0013365	0.209136	0.0013365	0.1062663	0.0013365	0.02589553
0.0026730	0.379717	0.0026730	0.2088192	0.0026730	0.05136792
0.0040095	0.584138	0.0040095	0.3379142	0.0040095	0.07594849
0.0053460	0.805353	0.0053460	0.4778034	0.0053460	0.09938629
0.0066825	0.975599	0.0066825	0.6032466	0.0066825	0.12552738

**Table SI 5.2e.** Average observed rate constants,  $k_{obs2}$ , for the displacement of the second aqua ligand in **Pt(H<sub>2</sub>Qn)** by thiourea nucleophiles, pH = 2.0,  $T = 298$  K,  $I = 0.1$  M (HClO<sub>4</sub>/NaClO<sub>4</sub>).

[TU]/ M	$k_{obs2}/ s^{-1}$	[DMTU]/ M	$k_{obs2}/ s^{-1}$	[TMTU]/ M	$k_{obs2}/ s^{-1}$
0.002186	0.001011554	0.002186	0.000931763	0.001093	1.84058E-05
0.004372	0.002071891	0.004372	0.002010494	0.002186	4.46553E-05
0.006558	0.00317183	0.006558	0.003097801	0.003279	7.75336E-05
0.008744	0.004149731	0.008744	0.004210897	0.004372	0.000106527
0.01093	0.005128	0.01093	0.005132675	0.005465	0.000132653

**Table SI 5.2f.** Average observed rate constants,  $k_{obs2}$ , for the displacement of the second aqua ligand in **Pt(dCH<sub>3</sub>Qn)** by thiourea nucleophiles, pH = 2.0,  $T = 298$  K,  $I = 0.1$  M (HClO<sub>4</sub>/NaClO<sub>4</sub>).

[TU]/ M	$k_{obs2}/ s^{-1}$	[DMTU]/ M	$k_{obs2}/ s^{-1}$	[TMTU]/ M	$k_{obs2}/ s^{-1}$
0.00149	3.6016E-05	0.00149	1.86322E-05	0.00149	1.29862E-05
0.00298	7.85319E-05	0.00298	3.84081E-05	0.00298	2.17823E-05
0.00447	0.000115767	0.00447	6.20721E-05	0.00447	2.89438E-05
0.00596	0.000162383	0.00596	8.34018E-05	0.00596	3.71296E-05
0.00745	0.000200962	0.00745	0.000106976	0.00745	4.69987E-05

**Table SI 5.2g.** Average observed rate constants,  $k_{obs2}$ , for the displacement of the second aqua ligand in **Pt(dCF<sub>3</sub>Qn)** by thiourea nucleophiles, pH = 2.0,  $T = 298$  K,  $I = 0.1$  M (HClO<sub>4</sub>/NaClO<sub>4</sub>).

[TU]/M	$k_{obs2}/s^{-1}$	[DMTU]/M	$k_{obs2}/s^{-1}$	[TMTU]/M	$k_{obs2}/s^{-1}$
0.0009816	0.000298646	0.0009816	0.00019207	0.0009816	2.58571E-05
0.0019632	0.000557257	0.0019632	0.000452216	0.0019632	4.76812E-05
0.0029448	0.000858948	0.0029448	0.000647351	0.0029448	7.98776E-05
0.0039264	0.001249669	0.0039264	0.000901553	0.0039264	0.000109918
0.004908	0.001537603	0.004908	0.001150635	0.004908	0.000137999

**Table SI 5.2h.** Average observed rate constants,  $k_{obs2}$ , for the displacement of the second aqua ligand in **Pt(dCF<sub>3</sub>Py)** by thiourea nucleophiles, pH = 2.0,  $T = 298$  K,  $I = 0.1$  M (HClO<sub>4</sub>/NaClO<sub>4</sub>).

[TU]/M	$k_{obs2}/s^{-1}$	[DMTU]/M	$k_{obs2}/s^{-1}$	[TMTU]/M	$k_{obs2}/s^{-1}$
0.0006833	0.000166531	0.0006833	8.56831E-05	0.0013665	3.1800E-05
0.0013666	0.000332366	0.0013666	0.000192329	0.0027330	7.3600E-05
0.0020499	0.000514252	0.0020499	0.000303338	0.0040995	1.0900E-04
0.0027332	0.000658979	0.0027332	0.000418477	0.0054660	1.4000E-04
0.0034165	0.000892367	0.0034165	0.000521954	0.0068325	1.7700E-04

**Table SI 5.3a.** Temperature dependence of the second-order rate constants,  $k_2$  (1<sup>st</sup>), M<sup>-1</sup> s<sup>-1</sup> for the displacement of the first aqua ligand in **Pt(H<sub>2</sub>Qn)** by thiourea nucleophiles, pH = 2.0,  $I = 0.1$  M (HClO<sub>4</sub>/NaClO<sub>4</sub>).

TU		DMTU		TMTU	
1/T, K <sup>-1</sup>	ln( $k_2/T$ )	1/T, K <sup>-1</sup>	ln( $k_2/T$ )	1/T, K <sup>-1</sup>	ln( $k_2/T$ )
0.003470415	-1.785334	0.003470415	-1.893185	0.003470415	-3.21812318
0.003411223	-1.492685	0.003411223	-1.627207	0.003411223	-2.98658428
0.003354016	-1.176108	0.003354016	-1.383966	0.003354016	-2.70192064
0.003298697	-0.935979	0.003298697	-1.055988	0.003298697	-2.40012973
0.003245173	-0.626953	0.003245173	-0.787489	0.003245173	-2.07924288

**Table SI 5.3b.** Temperature dependence of the second-order rate constants,  $k_2$  (1<sup>st</sup>), M<sup>-1</sup> s<sup>-1</sup> for the displacement of the first aqua ligand in **Pt(dCH<sub>3</sub>Qn)** by thiourea nucleophiles, pH = 2.0,  $I = 0.1$  M (HClO<sub>4</sub>/NaClO<sub>4</sub>).

TU		DMTU		TMTU	
1/T, K <sup>-1</sup>	ln( $k_2/T$ )	1/T, K <sup>-1</sup>	ln( $k_2/T$ )	1/T, K <sup>-1</sup>	ln( $k_2/T$ )
0.003470415	-4.56795	0.003470415	-4.933203	0.003470415	-6.16290124
0.003411223	-4.36015	0.003411223	-4.510882	0.003411223	-5.87139754
0.003354016	-4.08409	0.003354016	-4.177158	0.003354016	-5.64440739
0.003298697	-3.80833	0.003298697	-3.887616	0.003298697	-5.33277591



0.003245173	-3.54736	0.003245173	-3.645189	0.003245173	-5.08249946
-------------	----------	-------------	-----------	-------------	-------------

**Table SI 5.3c.** Temperature dependence of the second-order rate constants,  $k_{2(1^{st})}$ ,  $M^{-1} s^{-1}$  for the displacement of the first aqua ligand in **Pt(dCF<sub>3</sub>Qn)** by thiourea nucleophiles, pH = 2.0,  $I = 0.1$  M (HClO<sub>4</sub>/NaClO<sub>4</sub>).

TU		DMTU		TMTU	
$1/T, K^{-1}$	$\ln(k_2/T)$	$1/T, K^{-1}$	$\ln(k_2/T)$	$1/T, K^{-1}$	$\ln(k_2/T)$
0.003470415	-3.1449942	0.003470415	-3.70075165	0.003470415	-4.63628734
0.003411223	-2.6728291	0.003411223	-3.31899656	0.003411223	-4.42095143
0.003354016	-2.3148043	0.003354016	-2.99966134	0.003354016	-4.17866185
0.003298697	-1.9900971	0.003298697	-2.64452973	0.003298697	-3.94267414
0.003245173	-1.7210378	0.003245173	-2.38378940	0.003245173	-3.79296891

**Table SI 5.3d.** Temperature dependence of the second-order rate constants,  $k_{2(1^{st})}$ ,  $M^{-1} s^{-1}$  for the displacement of the first aqua ligand in **Pt(dCF<sub>3</sub>Py)** by thiourea nucleophiles, pH = 2.0,  $I = 0.1$  M (HClO<sub>4</sub>/NaClO<sub>4</sub>).

TU		DMTU		TMTU	
$1/T, K^{-1}$	$\ln(k_2/T)$	$1/T, K^{-1}$	$\ln(k_2/T)$	$1/T, K^{-1}$	$\ln(k_2/T)$
0.003470415	-1.94020813	0.003470415	-1.82993478	0.003470415	-3.33277200
0.003411223	-1.24929178	0.003411223	-1.52737825	0.003411223	-3.05254003
0.003354016	-0.71612601	0.003354016	-1.26347124	0.003354016	-2.75620791
0.003298697	-0.40161104	0.003298697	-0.93898081	0.003298697	-2.55663744
0.003245173	-0.14142259	0.003245173	-0.60713315	0.003245173	-2.36156920

**Table SI 5.3e.** Temperature dependence of the second-order rate constants,  $k_{2(2^{nd})}$ ,  $M^{-1} s^{-1}$  for the displacement of the first aqua ligand in **Pt(H<sub>2</sub>Qn)** by thiourea nucleophiles, pH = 2.0,  $I = 0.1$  M (HClO<sub>4</sub>/NaClO<sub>4</sub>).

TU		DMTU		TMTU	
$1/T, K^{-1}$	$\ln(k_2/T)$	$1/T, K^{-1}$	$\ln(k_2/T)$	$1/T, K^{-1}$	$\ln(k_2/T)$
0.003470415	-7.1529987	0.003470415	-7.15267548	0.003354016	-9.44217912
0.003411223	-6.7793919	0.003411223	-6.84922886	0.003298697	-9.15832684
0.003354016	-6.4239739	0.003354016	-6.44758989	0.003245173	-8.76711074
0.003298697	-6.0971896	0.003298697	-6.17109038	0.003193358	-8.30233588
0.003245173	-5.7784728	0.003245173	-5.79459433	0.003143171	-7.99590252

**Table SI 5.3f.** Temperature dependence of the second-order rate constants,  $k_{2(2^{nd})}$ ,  $M^{-1} s^{-1}$  for the displacement of the first aqua ligand in **Pt(dCH<sub>3</sub>Qn)** by thiourea nucleophiles, pH = 2.0,  $I = 0.1$  M (HClO<sub>4</sub>/NaClO<sub>4</sub>).

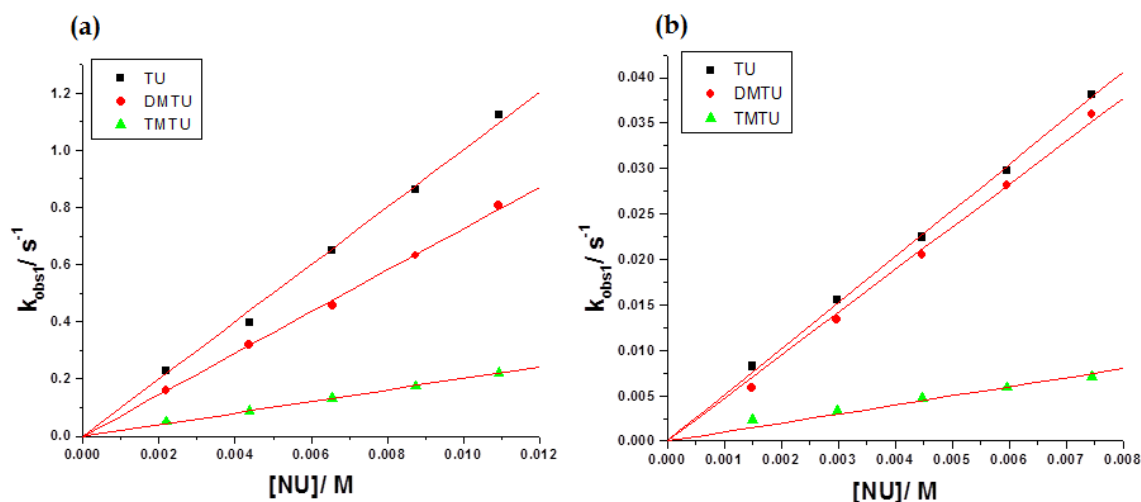
TU		DMTU		TMTU	
$1/T, K^{-1}$	$\ln(k_2/T)$	$1/T, K^{-1}$	$\ln(k_2/T)$	$1/T, K^{-1}$	$\ln(k_2/T)$
0.003411223	-9.18549	0.003411223	-10.24122	0.003354016	-10.7373829
0.003354016	-8.64131	0.003354016	-9.97444	0.003298697	-10.3737568
0.003298697	-8.01717	0.003298697	-9.56704	0.003245173	-9.92393518
0.003245173	-7.35479	0.003245173	-9.17496	0.003193358	-9.69017133
0.003193358	-6.85434	0.003193358	-8.85581	0.003143171	-9.28191049

**Table SI 5.3g.** Temperature dependence of the second-order rate constants,  $k_{2(2^{nd})}$ ,  $M^{-1} s^{-1}$  for the displacement of the first aqua ligand in **Pt(dCF<sub>3</sub>Qn)** by thiourea nucleophiles, pH = 2.0,  $I = 0.1$  M (HClO<sub>4</sub>/NaClO<sub>4</sub>).

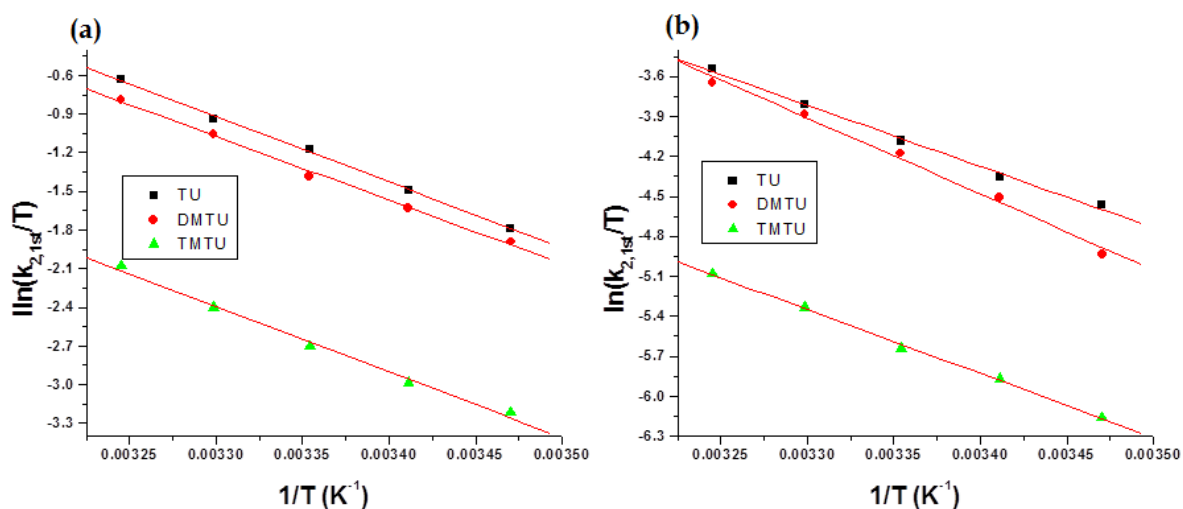
TU		DMTU		TMTU	
$1/T, K^{-1}$	$\ln(k_2/T)$	$1/T, K^{-1}$	$\ln(k_2/T)$	$1/T, K^{-1}$	$\ln(k_2/T)$
0.003354016	-6.92968499	0.003354016	-7.21250349	0.003354016	-9.3048933
0.003298697	-6.55842464	0.003298697	-6.75307388	0.003298697	-8.94371596
0.003245173	-6.29268965	0.003245173	-6.49021734	0.003245173	-8.61731744
0.003193358	-6.01963565	0.003193358	-6.24274166	0.003193358	-8.34847626
0.003143171	-5.72083729	0.003143171	-5.93159127	0.003143171	-8.09089331

**Table SI 5.3h.** Temperature dependence of the second-order rate constants,  $k_{2(2^{nd})}$ ,  $M^{-1} s^{-1}$  for the displacement of the first aqua ligand in **Pt(dCF<sub>3</sub>Py)** by thiourea nucleophiles, pH = 2.0,  $I = 0.1$  M (HClO<sub>4</sub>/NaClO<sub>4</sub>).

TU		DMTU		TMTU	
$1/T, K^{-1}$	$\ln(k_2/T)$	$1/T, K^{-1}$	$\ln(k_2/T)$	$1/T, K^{-1}$	$\ln(k_2/T)$
0.003354016	-7.08042913	0.003354016	-7.60829774	0.003354016	-9.32225342
0.003298697	-6.82076324	0.003298697	-7.22648780	0.003298697	-8.89819742
0.003245173	-6.45131890	0.003245173	-6.91286531	0.003245173	-8.57414989
0.003193358	-6.16827619	0.003193358	-6.65181158	0.003193358	-8.28614497
0.003143171	-5.93919625	0.003143171	-6.38318238	0.003143171	-7.99989456



**Figure SI 5.4:** Concentration dependence plots of  $k_{obs1}$ ,  $s^{-1}$ , for the displacement of the first aqua ligand of  $Pt(H_2Qn)$  (a) and  $Pt(dCH_3Qn)$  (b) by thiourea nucleophiles, pH = 2.0, T = 298 K, and  $I = 0.1$  M ( $HClO_4/NaClO_4$ ).



**Figure SI 5.5:** Eyring plot for the substitution of the first aqua ligand of  $Pt(H_2Qn)$  (a) and  $Pt(dCH_3Qn)$  (b) by thiourea nucleophiles, pH = 2.0, and  $I = 0.1$  M ( $HClO_4/NaClO_4$ ).